ANALYSIS OF PRE-MAIN-SEQUENCE δ-SCUTI STARS.

by

Michael Patrick Casey

A thesis submitted to the faculty of
Saint Mary's University,
Halifax, Nova Scotia, Canada
in partial fulfillment of the requirements for the degree of

Doctor of Philosophy in Astronomy

Approved: Dr. David B. Guenther, Advisor

Approved: Dr. C. Ian Short, Reader

Approved: Dr. Robert G. Deupree, Reader

Approved: Dr. Konstanze Zwintz, External Examiner

Department of Astronomy and Physics
Saint Mary's University
September 13, 2011

Your file Votre référence
ISBN: 978-0-494-82337-8
Our file Notre référence
ISBN: 978-0-494-82337-8

SAINT MARY'S UNIVERSITY

GRADUATE COMMITTEE APPROVAL

ANALYSIS OF PRE-MAIN-SEQUENCE δ-SCUTI STARS.

by

Michael Patrick Casey

A thesis submitted to
Saint Mary's University
Halifax, Nova Scotia, Canada
in partial fulfilment of the requirements for the degree of

Doctor of Philosophy in Astronomy.

This thesis has been read by each member of the following graduate committee and by majority vote has been found to be satisfactory.

Date	David B. Guenther, Advisor
Date	C. Ian Short, Reader
Date	Robert G. Deupree, Reader
Date	Konstanze Zwintz, External Examiner

ABSTRACT

ANALYSIS OF PRE-MAIN-SEQUENCE δ-SCUTI STARS.

by Michael Patrick Casey

September 13, 2011

Information on 72 confirmed or candidate pre-main-sequence δ-Scuti stars is collected and analysed to varying degree of sophistication and completeness. A systematic asteroseismic analysis of around 40 of these stars is performed, putting significant luminosity constraints on many of them simply by comparing the pulsation spectra of the stars to the fundamental and acoustic cut-off frequencies of a dense grid of stellar models. One star in particular, V1366 Ori, appears to be pulsating at or near the acoustic cut-off frequency. Many stars are found to otherwise defy proper asteroseismic analysis, in that matches between observed pulsation spectra and computed values are not able to be found. A simple test reveals that the most likely cause for these problems are the high stellar-rotation rates typically found in this class of star, with $v \sin i$ most typically between 60 and 200 km/s. The high rotation rates are found to significantly modify the pulsation spectrum of a star compared to a non-rotating star. These collective results reveal the richness and variety of phenomena within this group of stars, with stars pulsating anywhere from the lowest to the highest possible radial orders, including radial orders just below the acoustic cut-off frequency of some stars. Pulsation in non-radial orders is the normal case, not the exception to the rule, with all stars displaying low-amplitude δ-Scuti variability only.

ACKNOWLEDGMENTS

This thesis would not have been possible without the Saint Mary's Astronomy and Physics Department giving me the opportunity to pursue my Ph. D. after my long absence from the field. The Department's overall support and enthusiasm for my return, particularly when I made my first preliminary enquiries, made the process much easier and enjoyable than anticipated. I'm not sure where the four years went, but they have been fun, and I've learned a lot!

I wish to thank my supervisor, David Guenther, for the direction and structure that has essentially got this thesis done more-or-less on schedule, and provided me with the opportunity to interact with all the people in the *MOST* community. Thanks also to Konstanze Zwintz and all the people associated with the *MOST* team, for the opportunities to meet and interact in ways that really helped focus the the final results of this thesis.

My fellow students, both graduate and (in one-or-two cases) undergraduate also deserve mention for providing such diverse things as friendship, entertainment, and technical support, all of which could be useful at times when sanity was needed, or difficulties had to be overcome! That last is directed at the old Dal Oceanography crew as well.

Thanks everyone, I do appreciate it!

Contents

List of Tables

List of Figures

Chapter 1

Introduction

Stars vibrate. The study of how stars vibrate is known as asteroseismology. How a star vibrates is determined by the star's internal structure and the physical processes taking place within the star. These vibrations manifest themselves in both the light curves and spectral-line profiles measured for the star, and therefore astronomers can observe these vibrations, called pulsations, from afar, providing vital information on the interior of the star, where otherwise only bulk surface properties (*e.g.* effective temperature, luminosity) are observable. Not all stars pulsate at observable amplitudes, and so the discovery of pulsations in any star is useful, for it allows a probe into the interior of the star. Specifically, it provides a way of comparing observations to stellar-evolution and structure models. In the case of the Sun, in which information on many of modes of oscillation are available, it has been a key ingredient in fine-tuning models of the Sun, and has significantly improved our understanding of some of the fine details of stellar structure, such as differential internal rotation, and chemical composition gradients.

Pre-main-sequence (PMS) stars, stars that have recently emerged from the stellar nebulae from which they were born, shine mainly from the conversion of gravitational potential energy into heat energy. Aside from relatively small contributions during various parts of this phase from deuterium burning, nuclear fusion at the core of the star has yet to begin; the star has yet to reach the zero-age main sequence (ZAMS) of core hydrogen burning.

Prior to the PMS stage of evolution is the protostar phase, in which the star is undergoing active accretion, and is growing in mass with time. The star is embedded in an optically-thick dust-and-gas cloud. Because of the surrounding cloud, the star during these formative years cannot be directly observed, and thus the details of

its formation remain in the realm of educated guesswork much of the time, even though significant progress is being made over the years. These formative processes may leave imprints on the structure of the star, as can be seen by comparing the core-accretion/birthline models of Palla & Stahler (1990, 1992) to the contracting polytrope models of Iben (1965), and thus have asteroseismic consequences that could be measured in any cooperating star that may be pulsating at sufficient amplitudes to be detected. Discovering and analysing these pulsations have the potential to unravel the recent history and current condition of the star for comparison to observations, providing key information on the accuracy of our stellar models in this phase of stellar evolution. For this to work, the pulsations must first be discovered. The study of PMS pulsating stars is fairly new, and because they are hard to distinguish from their more-evolved counterparts, to date only ~ 50 such stars have been discovered. Some of these stars have been found in young open clusters, others as Herbig Ae field stars associated with various star-formation regions (SFRs) and OB associations scattered throughout the local disc of the galaxy. Only within the last ten years has this class of star been truly accepted as a subclass of what are known as δ-Scuti stars. The majority of δ-Scuti stars are in more evolved stages of evolution than the PMS phase (main sequence or shell hydrogen-burning stars), but determining the difference between one subclass and other can be difficult. PMS or otherwise, all δ-Scuti stars generally pulsate in pressure modes (pressure is the main restoring force), with frequencies of between 5 and 80 cycles/day (c/d). Collectively, aside from their similarity to post-ZAMS δ-Scutis, little is known about their characteristics.

In the course of previous work, there have been successes in modelling the pulsation spectra some of stars (Zwintz, Guenther & Weiss 2007; Guenther et al. 2007), and there have been failures or ambiguous results with others (Zwintz et al. 2009b; Guenther et al. 2009). The purpose of this thesis is to discover the collective properties of these stars, provide asteroseismic analysis of these stars, and perhaps discover why the pulsation spectra of some stars can be successfully modelled, while others

cannot. In this way, suggestions for the improvement of stellar models, and the direction of future observations can be made. This should lead to a better understanding of this phase of stellar evolution.

In the course of this work, in no particular order, the following advances have been made:

1. Identification of previously-ignored candidate PMS δ-Scuti stars from literature.
2. Production of a revised Hertzsprung-Russell Diagram (HRD) for PMS δ-Scutis, further advancing the work of Zwintz (2008).
3. Approximate identification of the radial order of pulsation for various members of the class.
4. Inadequacy of stellar asteroseismic analysis in certain cases, and speculation as to why these inadequacies exist (*e.g.* stellar rotation).
5. Use of both the fundamental and acoustic-cut-off frequencies in stellar models for putting constraints on the maximum and minimum luminosities a star can have, given an observed pulsation spectrum.
6. Identification, of one star (V1366 Ori) as pulsating in very-high radial orders, probably hitting the acoustic cut-off frequency in the process.
7. Suggestions of targets for the MOST space telescope (joint effort with Konstanze Zwintz and David Guenther), analysis of these targets, and removal of three of them from the PMS δ-Scuti list (UX Ori, HD 35929 and BF Ori), along with the serendipitous discovery of another in the course of MOST observations (HD 37357).
8. Identification of future work, both theoretical, numerical and observational.

Overall, the most important result of this thesis is that the detailed collective analysis of PMS δ-Scuti stars is not straight forward, with the identification of stellar

rotation as the probable most-important element missing from the models of the stars (*e.g.* see Figure 2.3). Nevertheless, even with rotation missing, a few very basic, but powerful tests can be performed, in which comparisons of observations to models put useful constraints on PMS δ-Scuti stars, identifying where future research efforts should be directed.

I will now provide a more detailed description of PMS δ-Scuti stars, and the relevant work that has lead to the current level of understanding.

1.1 δ-Scuti stars - general properties

δ-Scuti stars are pulsating variable stars that inhabit the lower part of the classical Cepheid instability strip, specifically the area from the ZAMS to about 2 magnitudes brighter than the ZAMS itself. Spectral classes range approximately from F0 through to A0 (effective temperature, $T_{eff} \sim$ 7200 K to 10000 K), although cooler members of the class do exist. Pulsation frequencies are typically 5 to 80 cycles/day (c/d; 55 to 925 μHz), although the high end of this range is rare. Pulsation modes may be radial or non-radial in nature (see Section 2.1). Amplitudes range from several tenths of magnitudes down to at least the millimagnitude (mmag) level. δ-Scutis with amplitudes $> 0.^{\mathrm{m}}3$ are known as high-amplitude δ-Scutis (HADS). At least in part, maximum pulsation amplitudes for a given star appear to be tied to surface rotation velocity (*e.g.* Breger 2007) – all HADS appear to be slow rotators with $v \sin i \leq 30$ km/s projected surface equatorial velocity.[1] High-amplitude frequencies appear to be those of radial pulsations, whereas low amplitude frequencies may correspond to radial or non-radial modes. The light curves of HADS generally exhibit linear-combination frequencies of the highest-amplitude frequencies in the spectrum, a result of the star pulsating at amplitudes in the non-linear regime. These combination frequencies are not considered independent frequencies for the purposes of

[1]Here, v is the surface equatorial velocity of the star, i the angle the rotation axis of the star makes with the line of sight, and $v \sin i$ is the projection of v onto the line of sight, and is the quantity typically measured by astronomers.

asteroseismic analysis. Generally low-amplitude frequencies do not cause linear combinations, with many independent frequencies potentially appearing in the spectrum of a low-amplitude δ-Scuti.

δ-Scutis can be in one of a number of different evolutionary states: 1) pre-main sequence; 2) main sequence of core-hydrogen burning; 3) post main sequence hydrogen-shell burning. Masses range from $\sim$ 1.3 $M_{\odot}$ to 4 $M_{\odot}$. δ-Scuti stars in the upper part of this mass range are rare as these stars are rapidly evolving when in the instability strip, and thus spend little time there, reducing the likelihood of their discovery. Lower-mass stars ($<$ 2.0 $M_{\odot}$) spend the main sequence in the instability strip, and given the extended nature of time spent in this evolutionary state compared to the other states, are the most likely to be discovered.

1.2 PMS δ Scuti stars

PMS stars are stars that have recently formed, and have yet to start core hydrogen burning on the main sequence. They derive most of their luminous energy from the conversion of gravitational potential energy into heat. Stars between about 1.3 $M_{\odot}$ and 5.0 $M_{\odot}$ spend part of this evolutionary phase in or near the instability strip, and thus have the potential to pulsate with δ-Scuti characteristics. Breger (1972) made the first discoveries of this subclass of δ-Scuti star, that of V588 Mon and V589 Mon, two δ-Scutis in the young open cluster NGC 2264, age $<$ 10 Myr. Given the youth of the cluster, and the position of the δ-Scutis in the HRD, as long as the two stars are truly members of the cluster, PMS status is reasonably assured. The difficulty with such discoveries is in positively determining the membership status of the stars in the cluster; if the star is not a member, but merely a field star projected on to the cluster, the star could be an evolved δ-Scuti star, not a PMS δ-Scuti star. These uncertainties early on allowed for reasonable scepticism as to whether or not PMS δ-Scutis existed as a class, especially since there was a long gap until the next discovery, that of V856 Sco (HR 5999) by Kurtz & Marang (1995), an HAe star associated with the Lupus 3 dark cloud. By the year 2000 a few more stars had been

added to the list, the Herbig Ae stars DX Cha (Donati et al, 1997), and HD 35929[2] and V351 Ori (both by Marconi et al. 2000).

In particular, searches for more class members were spurred on by the analysis of Marconi & Palla (1998), who performed an asteroseismic analysis of the first three radial modes in these stars. Here, Marconi & Palla determined from a theoretical standpoint that these stars could pulsate, and furthermore, they would be subject to pulsations in approximately the same region of the HRD as classical δ-Scuti stars are, *i.e.* they would also be located within the traditional instability strip of the HRD.

Spectroscopically, δ-Scutis range from approximately A0 through to early-to-mid F-Class stars, with luminosity classes ranges from III to V.

With one or two known exceptions, it has been found that PMS pulsators tend to divide into two subclasses:

1. field Herbig Ae stars (see Section 1.3) usually associated with some nearby star-formation region.

2. young open clusters members (see Section 1.4), with cluster ages $<\sim$ 10 Myr.

One notable exception to this classification is RS Cha, a double-lined eclipsing-binary system in the very sparse open cluster, ϵ Cha. Both RS Cha A and B are PMS δ-Scutis. This could perhaps be a transition case between the above two classes, reflecting the nature of the stellar environment needed to generate Herbig Ae characteristics. There is, perhaps, a selection mechanism at work here, a star of subclass 2 above could be ejected from the birth cluster, and thus be hard to distinguish as either a classical δ-Scuti or a PMS δ-Scuti without the identifying HAe characteristics. A case in point are the two PMS δ-Scutis, EE Cha and EF Cha, originally thought to be two evolved field δ-Scutis, but since determined to be members of a very-sparse moving group of young stars (see Section 3.3.1, and references therein). My own speculation is the following: it might be possible that a star needs to be ejected from its birth cloud (and thus become visible) while still undergoing active

[2]Since removed from the list. See Section 3.1.5.2.

accretion for HAe characteristics to exhibit, *i.e.* the star leaves the cluster with an accretion disk still gravitationally bound to the star. Otherwise, a star that remains in a sufficiently-dense open cluster would then be subjected to gravitational or radiative interactions with other cluster members that would then remove the dust and gas from the system that would otherwise be responsible for the HAe phenomenon.

To date, published results list about 50 objects that have been discovered, some through ground-based observations (*e.g.* Pinheiro et al. 2003; Zwintz & Weiss 2006), others through satellite-based measurements (*e.g.* Zwintz et al. 2009a). Asteroseismic analysis has confirmed that pulsations can be both radial and non-radial in nature (Zwintz, Guenther, & Weiss 2007), and further analysis has shown that the pulsation frequencies of some stars are consistent with models, but others are not (Guenther et al. 2009).

The last comprehensive review was by Zwintz (2008), a paper that explored and compared the observational colour-magnitude diagram (CMD) of classical δ-Scuti stars and their PMS δ-Scuti counterparts, finding the two classes more or less coincident with one another. At the time of writing, about 36 PMS δ-Scuti stars were suspected or confirmed.

Since then, approximately 40 stars have been added to the list, and three candidate variables removed from the list (UX Ori, HD 35929, and BF Ori, all through observations of the MOST space telescope; see Section 3.1.5 for more details). The additions and deletions have, in part, been related to the work of this thesis.

A comprehensive list of stars is available in Tables 4.1 and 4.2.

1.3 Herbig AeBe stars

Herbig Ae stars are A-through-early-F stars exhibiting emission lines in Hydrogen (particularly Balmer lines) and Calcium, hence the Ae designation. PMS evolutionary status is deduced from such things as observed infrared excesses (above the level normally associated with the spectral energy of an isolated star) that is thought to originate from circumstellar material left over from the star's formation.

Originally, association with a star-formation region, or a reflection nebula, was required, although isolated stars are now recognized as members of the class. Even so, isolated HAe stars should be traceable back to a birth star-formation region (SFR). Tracing, however, may be difficult if, for example, the star is from a sparse open cluster that is in the process of evaporating into the field, as the cluster itself may be hard to identify separately from the background galactic field. This, for example, was the case with the HAe star, DX Cha (Mamajek, Lawson & Feigelson 1999, and also Section 3.3.1.2).

HAe stars are a subgroup of the more general Herbig AeBe (HAeBe) stars, which include the more massive Herbig Be stars ($\sim 5.0\ M_\odot < M < 8.0\ M_\odot$), stars that may or may not have already reached the main-sequence. Herbig Be stars differ from traditional Be stars in that the latter are main-sequence-or-older stars, that are *loosing* stellar material as the star is evolves, whereas the former are possibly gaining small amounts of material from the remnants of an accretion disk left over from the star's formation. In both cases the emission is from the circumstellar material, not the photosphere of the star. HAe stars are probably in a stage of evolution that is between the phase of *substantial* active accretion (the protostar phase, during which the star optical radiation is completely obscured by the cloud from which it was formed), and before the star reaches the main sequence. As an HAe star ages and reaches the main sequence it may evolve into β-Pictoris-like star with a surrounding debris disk. Indeed, β Pic exhibits δ-Scuti behaviour, and is perhaps a transition object between PMS δ-Scutis and main-sequence δ-Scutis, given the uncertainty in its exact evolutionary state. Indeed, because of this ambiguous status, β Pic is often included within the list of PMS δ-Scuti stars.

Since HAe stars are young stars, they are usually rotating rather rapidly, with typical $v \sin i$ values ranging from 60 km/s to 250 km/s, with the most common values between about 75 and 150 km/s (see Table 4.1 for examples). Many studies have looked at the collective properties of these stars. Studies that were particularly useful to this thesis include Herbig (1960b); Thé, de Winter & Perez (1994); Malfait, Bogaert

& Waelkens (1998); Mora et al. (2001); de Winter et al. (2001); Vieira et al. (2003); Hernández et al. (2004). Many others were employed, and they will be referenced in due course as individual stars are investigated.

Some HAe objects exhibit UX Ori-type variability, in which the aforementioned circumstellar material aperiodically partially eclipses the host star, causing dips in brightness of up to 2.5 magnitudes, although the depth of the individual eclipses can vary considerably from one eclipse to the next. UX Ori variability in some stars has sometimes been initially misidentified as being caused by an Algol-type eclipsing binary system until the eclipses where shown to be aperiodic in nature. When observing an HAe star for δ-Scuti pulsations, if the star should also exhibit UX Ori variability, then care must be taken with the analysis. Fortunately, UX Ori variability is usually on a much larger time scale than δ-Scuti pulsations (days to weeks versus tens of minutes to hours), but given the irregularity, still needs to be subtracted from the light curve of the star before the δ-Scuti analysis of the star can proceed.

1.4 Cluster stars

Some PMS δ-Scuti stars are found as members of open clusters. These stars generally do not show HAe characteristics, and so if a δ-Scuti is located within the field of a sufficiently-young cluster (generally less than about 10 Myr), youth must be inferred by other means, primarily, the star needs cluster membership confirmed through such means as proper-motion studies, and an appropriate position in the colour-magnitude diagram for the open cluster. However, if cluster membership is confirmed, then other tools become available: the star must have an evolutionary age compatible with the rest of the stars in the cluster, against which asteroseismic conclusions must be consistent. Also, collectively, if multiple δ-Scutis are located within the cluster, they must (hopefully!) be in agreement with one another, matching age range, and other group properties of the cluster. A number of δ-Scuti stars in

young open clusters will be investigated in this thesis, such as the stars in NGC 2244 and NGC 2264.

1.5 The role of asteroseismology

Pulsations represent travelling or standing waves of particular harmonics that have been set up by various physical processes within a star. Solar-like pulsations are stochastically-driven modes induced by near-surface convective motion. However, in the case of stars in the instability strip, including δ-Scuti stars, pulsations are driven by the κ opacity mechanism in the near-surface He II ionization regions of stars of the correct surface-temperature range. In this case, pressure (essentially sound) waves are the result, in which pressure is the main restoring force. Signals travel throughout the star, reflecting off layers within the interior and atmosphere of the star, setting up overall wave patterns that constructively interfere at particular frequencies, and with particular waveforms on the surface of the star. These waveforms manifest themselves as temperature and velocity variations across the surface of the star, and cause periodic changes in the integrated light and spectral line profiles coming from the star, thus making them detectable by an a distant observer.

The frequencies $\nu_{n\ell m}$ are quantified by the patterns set up in the star, with n indicating the number of radial nodes of oscillation in the interior of the star, ℓ indicating the number of great circles of nodes on the surface of the star, and with $|m|$ indicating the number of longitudinal lines of nodes on the star. Here m is limited to the range $-\ell \leq m \leq \ell$, and only manifests when some physical process such as rotation breaks spherical symmetry.

The frequencies associated with any particular mode of oscillation are governed by the internal structure of the star, such things as density, temperature, and chemical composition, all of which influence the local sound speed in the star, and thus the speed at which perturbations are transmitted. Therefore, detection of any pulsation frequencies in the light curve of a star gives insight into the internal structure of the star. Part of the goal of this thesis is to use asteroseismology as a tool in the analysis

of PMS pulsators as a way of evaluating the current models of stellar evolution in the PMS phase. One reason PMS stars have been targeted is that it has generally been thought that since PMS stars have simpler structures than older stars (they do not contain the central cores that all other older stars have), then they might be easier to analyse astroseismically. Analysis of post-MS low-amplitude δ-Scutis has proved difficult to date, and so concentrating on theoretically simpler PMS δ-Scutis may be a more tractable problem. Hence, any insight gained might not only enhance our understanding of the structure of PMS stars, but also enhance our understanding of δ-Scuti astroseismology as a whole from the development of useful techniques of analysis.

1.5.1 Other types of variability in A-type stars

Besides UX Ori variability mentioned above, in the search for δ-Scuti pulsations in A-type stars, a number of other causes of variability might be encountered that need to be distinguished from the κ-mechanism-driven pressure modes that characterise δ-Scuti stars.

As indicated in Aerts, Christensen-Dalsgaard & Kurtz (2010, page 64), rapidly rotating late-B and early-A stars may exhibit slowly-pulsating-B (SPB) star characteristics in a region of the HRD coincident with the highest-temperature δ-Scuti pulsators. The pulsations are thought to be rotationally-shifted κ-driven, non-radial, g-mode frequencies, with frequency values lower than δ-Scuti values. Regular (not-so-quickly rotating) SPBs generally inhabit a region of the HRD slightly hotter than the δ-Scuti region, and don't overlap with δ-Scutis, however with the former being discovered, care must be taken when analysing the pulsation spectrum of particularly hot candidate δ-Scuti stars, lest one be misidentified as the other. Likewise, γ-Doradus (γ Dor) pulsators are cool A-range stars that exhibit g-modes and overlap in the HRD with δ-Scuti pulsators at the cool side of the instability strip (Kaye 2007). These g-mode frequencies are lower than the δ-Scuti frequencies (a few cycles/day and lower), and can be difficult to confirm. For example, sunspot-induced

variability can produce similar frequencies to that of g-mode pulsations — as the star rotates the sunspot is not necessarily always pointed towards the observer, causing changes in apparent magnitude of the star concident with the rotational period of the star, which may be on the order of a few cycles/day. If a g-mode from an SPB or γ Dor star is mistaken for a p-mode, the asteroseismic analysis will be in error.

Rapidly-oscillating, chemically-peculiar A stars (roAp stars) are stars that oscillate with periods ranging from about 5 to 21 minutes, *i.e.* with frequencies of about 800 to 3300 μHz. They inhabit the cool, lower part of the instability strip nearest the ZAMS with the lowest part of the frequency range coincident with the highest part of the δ-Scuti pulsation spectrum (see *e.g.* Cunha 2002). The pulsation spectra, chemical abundance anomalies, and strong magnetic fields measured within these stars appear to be linked, and so to distinguish them from δ-Scuti stars spectroscopic measurements of the relevant quantities might be required, particularly in the frequency regimes where the two classes of star overlap.

For high-precision light curves of A stars collected by such instruments as *CoRoT*, granulation signals may also be detected and confused with the pulsation spectrum of a δ-Scuti star (Kallinger & Matthews 2010; Zwintz et al. 2011). However, granulation produces random, frequency-independent (essentially white noise), non-repeatable (except by coincidence) frequencies from one observing session to the next, whereas the pulsation signals should be repeatable. Therefore, by observing a target in multiple epochs, an observer should be able to distinguish a pulsation signal from granulation noise.

The rest of this thesis analyses asteroseismically and otherwise, the majority of the PMS δ-Scuti stars already known, looking for patterns, and insights for the group of star as a whole. Chapter 2 provides an outline of the techniques and tools used in the analysis. Chapter 3 gives a star-by-star analysis of most known PMS δ-Scuti stars. Chapter 4 looks at the collective results of Chapter 3, and Chapter 5 gives final summaries, discussions, and conclusions.

Chapter 2

Procedures, techniques and tools

I now present a review of the various procedures, techniques and tools that were either used and developed in the course of this thesis, including the very basics of how asteroseismology is used to probe the interior of a star. I also briefly explain the modelling tools, on-line resources, and observational resources used in the completion of this thesis. Finally, I look at how all of these tools are brought together to form an asteroseismic analysis of a star, outlining the basic procedures that are used in analysing the individual stars in Chapter 3.

2.1 Asteroseismology

In a spherically symmetric star, perturbation theory is used to describe the deviations from equilibrium for various quantities within the star. The spatial perturbations can be described using the following expressions, $\xi_{nm\ell}(r,\theta,\phi,t)$, separable into expressions describing the radial and non-radial components individually,

$$\xi_{nm\ell}(r,\theta,\phi,t) = \xi_{n\ell}(r)Y_n^m(\theta,\phi)e^{i\omega_{nm\ell}t}. \tag{2.1}$$

The angular components are given by the spherical harmonics,

$$Y_l^m(\theta,\phi) = (-1)^m C_{\ell m} P_l^m(\cos\theta)e^{im\phi}. \tag{2.2}$$

P_l^m are the Legendre polynomials of order ℓ and m, with $C_{\ell m}$ the normalization constant for integration over the unit sphere. (Spherical-polar coordinates r, θ and ϕ, are used.) The radial components, $\xi_{n\ell}(r)$, are determined by the internal structure of the star. Angular frequencies, $\omega_{n\ell m}$, are related to observed frequencies, $\nu_{n\ell m}$, via

the definition

$$\omega_{n\ell m} \equiv 2\pi\nu_{n\ell m}. \tag{2.3}$$

For p-mode frequencies for which $n \gg \ell$, known as the asymptotic regime, an approximation of the frequencies has been made by Tassoul (1980)

$$\nu_{n\ell} \simeq \left(n + \frac{\ell}{2} + \frac{1}{4} + \alpha\right)\Delta\nu - (AL^2 - \delta)\frac{\Delta\nu^2}{\nu_{n\ell}} \tag{2.4}$$

where

$$A = \frac{1}{4\pi^2\Delta\nu}\left[\frac{c(R)}{R} - \int_0^R \frac{dc}{dr}\frac{dr}{r}\right] \tag{2.5}$$

and

$$\Delta\nu = \left[2\int_0^R \frac{dr}{c}\right]^{-1}. \tag{2.6}$$

Here c is the sound speed, and α, δ are quantities dependent upon the radial stellar structure, but are independent of l. $L = \ell + \frac{1}{2}$. $\Delta\nu$ is referred to as the large frequency spacing, and is a measure of the inverse of twice the sound travel time between the centre ($r = 0$) and the surface ($r = R$) of the star, or in other words a measure of the frequency of a signal travelling from one side of the star to the other via the centre of the star. A consequence of the above is that regular spacings exist between frequencies of particular n and ℓ values.

One of these differences, Δn is

$$\Delta n = \nu_{n\ell} - \nu_{(n-1)\ell} \tag{2.7}$$

is related to the large spacing, and measures the difference between two successive radial orders of the same non-radial order; the same surface pattern is observed, but the frequency and amplitude would be different between the two modes. Ignoring terms of $\Delta\nu^2$, Equation 2.4 can be used in Equation 2.7 to find

$$\Delta n \simeq \Delta\nu, \tag{2.8}$$

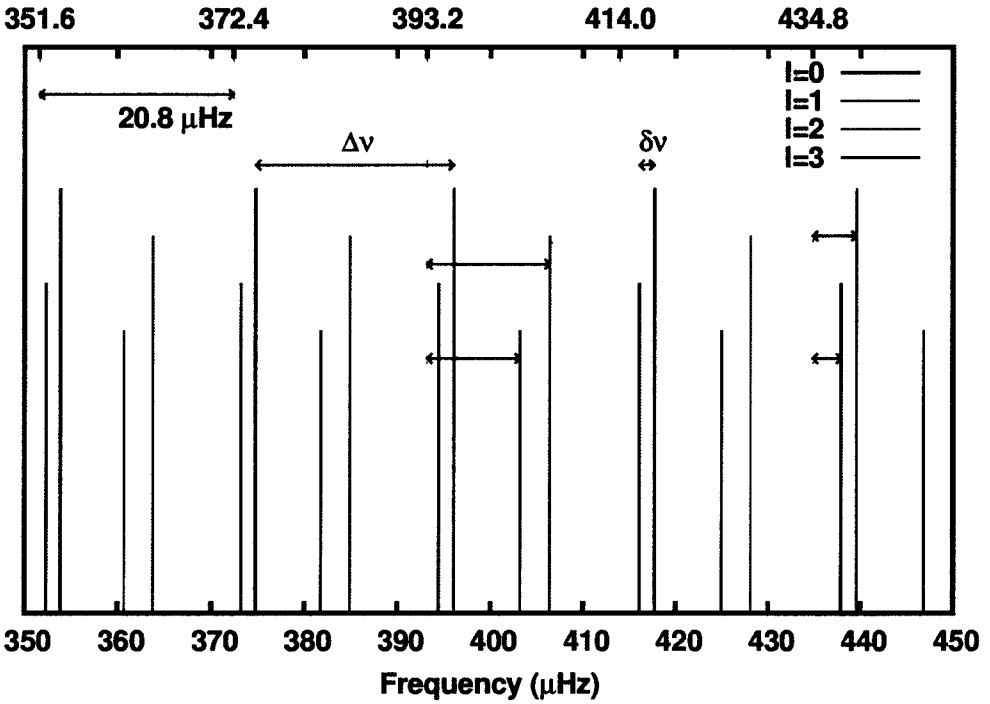

Figure 2.1: Sample pulsation frequency spectrum from a stellar model showing large ($\Delta\nu$) and small ($\delta\nu$) spacings between sample frequencies. Also indicated are the frequencies at which the spectrum is "chopped" (20.8 μHz intervals in this case) to produce an echelle diagram, and a number of sample folded frequencies (unlabelled arrows) for individual modes of pulsation.

showing that at large n the indicated modes are evenly spaced. The phenomenon is not entirely unlike the regular spacings in frequency space of successive harmonics of standing waves on a string.

Frequency differences of the following n and ℓ combinations are expected to have small, but non-zero values (*i.e.* they are almost, but not quite, degenerate modes)

$$\delta\nu_{n\ell} \equiv \nu_{n\ell} - \nu_{(n-1)(\ell+2)}. \tag{2.9}$$

$\delta\nu_{n\ell}$ are known as the small spacing, and using Equation 2.4, but this time neglecting the term containing the surface sound speed, $\frac{c(R)}{R}$ (small compared to interior sound speed), gives results sensitive to the internal sound speed, and thus structure of the

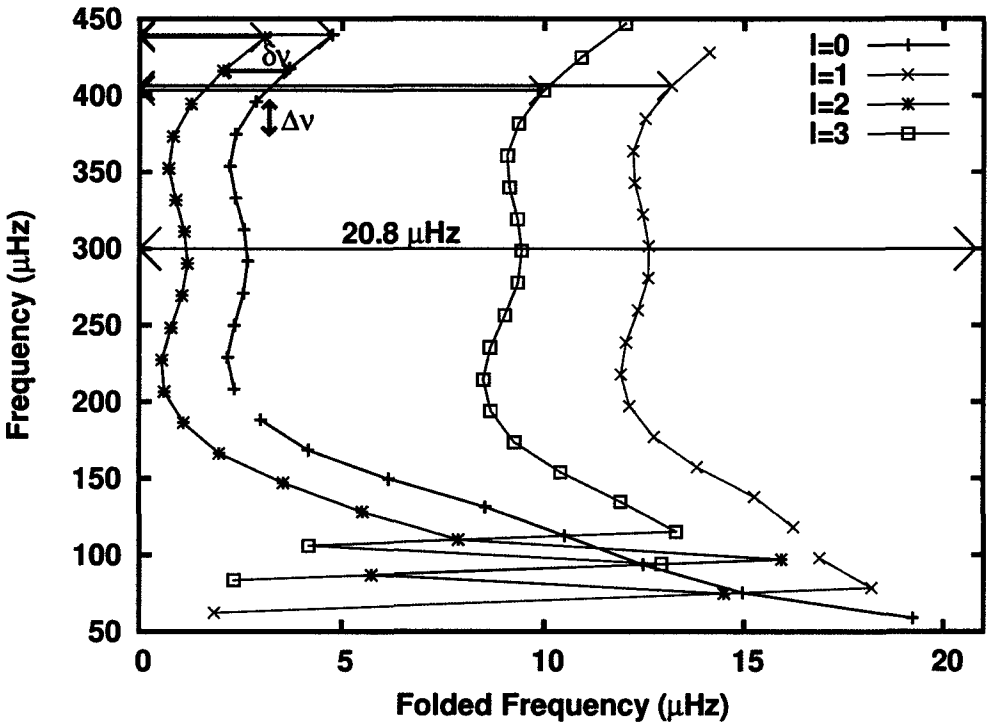

Figure 2.2: Sample pulsation frequency spectrum from a stellar model in echelle-diagram format showing large ($\Delta\nu$) and small ($\delta\nu$) spacings between sample frequencies. Also indicated are the frequencies at which the spectrum is "chopped" (20.8 μHz intervals in this case) to produce the echelle diagram, and the same sample folded frequencies (unlabelled arrows) for individual modes of pulsation depicted in Figure 2.1. Note how the frequencies of similar ℓ stack atop one another in the asympotic (high n) regime.

star, more so than Δn:

$$\delta\nu_{n\ell} \simeq -(4\ell+6)\frac{\Delta\nu}{4\pi^2\nu_{n\ell}}\int_0^R \frac{dc}{dr}\frac{dr}{r} \tag{2.10}$$

With this, $\delta\nu_{n\ell}$ is often used as a diagnostic between models of stars of otherwise similar surface properties (effective temperature and luminosity), but differing internal structure.

Pulsation-frequency spectra from a particular stellar model will look like Figure 2.1, with large and small spacings indicated. In Figure 2.1 a number of radial orders of modes, from $\ell = 0$ to $\ell = 3$ are plotted. Modes of similar ℓ, but differing n

are plotted with similar colour and amplitude for clarity. Within a particular ℓ series, n increases with increasing frequency.

After a suitable offset, ν_o, is chosen, it is often useful for reasons of clarity to "chop" the frequency space into chunks of approximately $\Delta\nu$, thus isolating a particular set of frequencies within the overall spectrum. The frequency of pulsation is then plotted against that frequency's position within its individual "chunk" (known as the folded frequency, ν_{fold}). With this visualization, modes of similar ℓ and m, but increasing n conveniently line up vertically in a ladder-like fashion. Such a graph is known as an *echelle diagram*, coming from the French word for ladder, *echelle*. Mathematically

$$\nu_{fold} = \mathrm{MOD}(\nu + \nu_o, \Delta\nu) \tag{2.11}$$

where MOD is the modulus function, a function that retains only the remainder of the division $(\nu + \nu_o)/\Delta\nu$. Figure 2.2 show the same pulsation spectrum displayed in Figure 2.1, but displayed as an echelle diagram.

2.2 Modelling tools

Calculations were performed using the facilities of the Atlantic Computational Excellence Network (ACEnet), the Institute for Computational Astrophysics (ICA) at Saint Mary's University, Halifax, and the Department of Astronomy and Physics, Saint Mary's University.

2.2.1 YREC and JIG — Stellar-evolution and stellar-pulsation codes

2.2.1.1 YREC

To study the astroseismic properties of PMS stars, a dense grid of stellar evolutionary tracks was computed using the one-dimensional YREC stellar-evolution code (Demarque et al. 2008). Some of the calculations had been previously performed by D. Guenther and J. Tanner, while others were performed by me. Stellar masses between 0.8 and 5.0 $M_\odot$ in increments of 0.01 $M_\odot$ with up to 1000 models per track

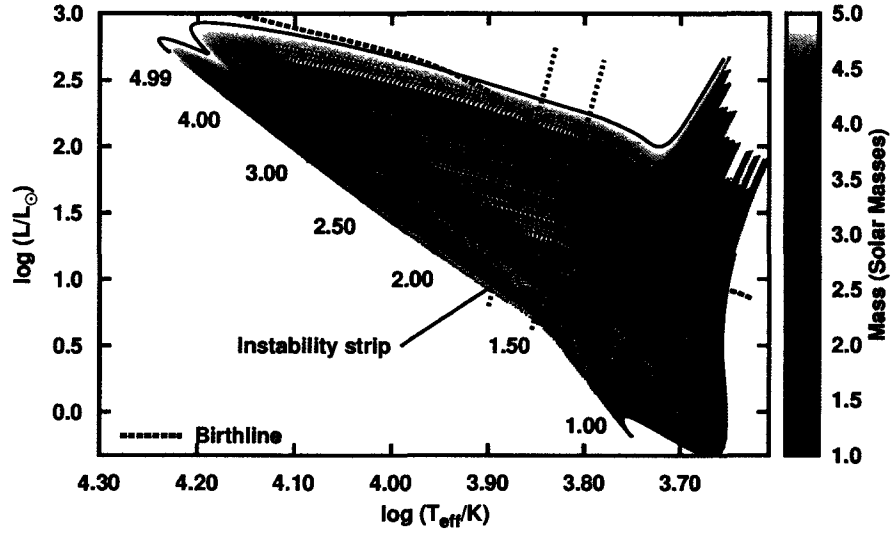

Figure 2.3: The grid of PMS models as used in this thesis. The "Birthline" refers to the line in the HRD, as defined by Palla & Stahler (1990), above which very few PMS stars are expected to be directly observed as they are otherwise still obscured by the cloud from which the star formed. The instability strip is as calculated by Marconi & Palla (1998) for the first three radial modes of PMS stars.

were computed. With such a dense grid of models, interpolation between models is generally not required in order to find a model that sufficiently matches a set of observables. A representative grid is shown in Figure 2.3. Note that Figure 2.3 is not a contour plot, a dot is plotted for only one in four models in the grid, and interpolation is not required to see the smooth variation of various physical quantities across such a diagram.

The PMS models are initiated as polytropes on the convective Hayashi track (Hayashi 1961) in the general style of Iben (1965) PMS evolutionary tracks, and evolved to the ZAMS. Neither mass accretion nor mass loss are included, i.e. the protostar (mass accretion) phase of evolution as investigated *e.g.* by Palla & Stahler (1991, 1992) and more recently by Hosokawa, Offner & Krumholz (2011), is not included. Depending upon the mass of the star in question, this may or may not have a significant impact on the astroseismology of the star, as suggested by this research group in Guenther et al. (2009). This is an area for future investigation.

The instability strip in Figure 2.3 is as calculated by Marconi & Palla (1998) for the first three radial modes of PMS stars, the first such calculation of pulsation in PMS stars. This is the instability strip used in all future figures that contain an instability strip. The theoretical birthline of Palla & Stahler (1990) is also indicated. At optical wavelengths in particular, stars above the birthline are obscured within their birth cloud, and are still experiencing mass accretion at high enough rates, $\dot{M}$, to substantially affect the mass on evolutionary time scales, affecting the structure of the star ($\dot{M}$ up to 10^{-5} $M_{\odot}$/year would not be uncommon). This curve was calculated by Palla & Stahler based upon models of the optical depth of the material surrounding the protostar. The birthline has a minor sensitivity to model parameters, but is reasonably consistent with observed positions of PMS stars in the HRD. PMS stars above the birthline are rarely observed, with none substantially more luminous than the birthline, with many PMS stars otherwise found in the region in the HRD between the birthline and the ZAMS. Thus, the birthline effectively acts as an upper limit on the luminosity of a PMS star of a given effective temperature, and is used as such in this thesis.

Except for the star V1366 Ori, in which low-metallicity (Z=0.004) models were also employed, all stars were compared to solar metallicity (Z=0.02) models. Models used both the OPAL98 (Iglesias & Rogers 1996) opacity tables for temperatures greater than 6000 K and the Alexander & Ferguson (1994) opacity tables for temperatures below 15,000 K. For the equation of state, the Lawrence Livermore tables were used (Rogers 1986; Rogers, Swenson & Iglesias 1996).

To parametrize convection, the code used the mixing-length theory of Böhm-Vitense (1958), with mixing-length parameter, $\alpha = 1.8$, calibrated against a solar model that used the same parameters as for the PMS grid. A gray atmosphere in the Eddington approximation supplied the outer boundary conditions for the models. Nuclear cross-sections for fusion reactions were from Bahcall, Pinsonneault & Basu (2001). For simplicity, convective overshoot and elemental diffusion were not included; inclusion of these affects would change the details of the results, but not the overall

qualitative conclusions of this work, as the effects are relatively minor compared to the exclusion of stellar rotation.

A typical model has approximately 1800 to 2000 radial shells, with approximately one third covering the interior of the star (about 95% by radius), one third in the outer envelope (about the outer 5% by radius), and the last third the atmosphere of the star. The latter is needed in order to properly calculate the pulsation frequencies of the star where the outer boundary conditions for the pulsations are set, whereas the inner two thirds are needed to properly calculate the evolution and structure of the star.

Most significantly, stellar rotation was not included. At the outset of this work the effects of stellar rotation on the pulsation spectrum of a PMS star were not fully appreciated. One of the major outcomes of this work is a fuller appreciation of the effects that rotation must have on the pulsation spectra of PMS δ-Scuti stars, as will be outlined in Section 2.6.3, and Chapter 3.

2.2.1.2 JIG

Adiabatic and non-adiabatic pulsation frequencies from azimuthal orders $\ell =$ 0 through 3 and and radial orders $n = 0$ through 35 were calculated for each stellar model using JIG, an in-house stellar-pulsation code originally outlined in Guenther (1994). JIG solves the linearized non-radial adiabatic and non-adiabatic stellar pulsation equations via the Henyey relaxation technique. For simplicity, in this analysis the adiabatic frequencies are used. As with such things as convective overshoot and elemental diffusion, including non-adiabatic effects would change the details of the analysis in this thesis, but not the qualitative results, as will be seen in Chapters 3 and 4.

2.2.2 χ^2 fitting routines and plots

Upon obtaining a pulsation spectrum the observations are compared to the model frequencies using the χ^2 relation:

$$\chi^2 = \frac{1}{N}\sum_{i=1}^{N}\frac{(\nu_{obs,i} - \nu_{mod,i})^2}{\sigma^2_{obs,i} + \sigma^2_{mod,i}}, \tag{2.12}$$

where N is the number of observed frequencies, $\nu_{obs,i}$ and $\nu_{mod,i}$ are the i^{th} observed and model frequencies respectively, and $\sigma^2_{obs,i}$ and $\sigma^2_{mod,i}$ are the i^{th} observed- and model-frequency uncertainties respectively. The $\sigma^2_{mod,i}$ are estimated from comparisons of model frequencies to observed solar frequencies. The results of Guenther & Brown (2004) are used, in which discrepancies of 0.008% for radial orders, $n < 20$, rising to 0.3% for $n > 30$ are found. As in Guenther et al. (2009), $\sigma^2_{mod,i}$ tend to be small compared to $\sigma^2_{obs,i}$ and are therefore ignored for the purposes of these calculations. For the purposes of χ^2 calculations, for all stars σ_{obs} are taken as $1/T$ where T is the observation period for the frequency determinations. As explained in Breger (2007), σ_{obs} can often be much better than this, depending upon the method used to determine the frequencies (such as via sine-curve fitting), however the frequencies for this project have been collected from many different sources, many of which cite $1/T$ as σ_{obs}. Without further information on how their data was collected, and frequencies determined, $1/T$ cannot realistically be improved upon. Therefore, for consistency of analysis across many stars, $1/T$ is always used. For some stars, particularly for those in which such packages as Period04 (Lenz & Breger 2005) or Sigspec (Reegen 2007) were used for frequency determinations, the more precise values for σ_{obs} are also reported, but not used in the χ^2 calculations.

For an individual model, χ^2 is minimized; an observed frequency is matched to the closest model frequency in value, and the resultant χ^2 value calculated from the sum of all such pairings. It is possible that multiple observed frequencies might map to the same model frequency, *i.e.* the model frequency is the closest match for multiple observed frequencies. In the case of small rotational splitting this might be

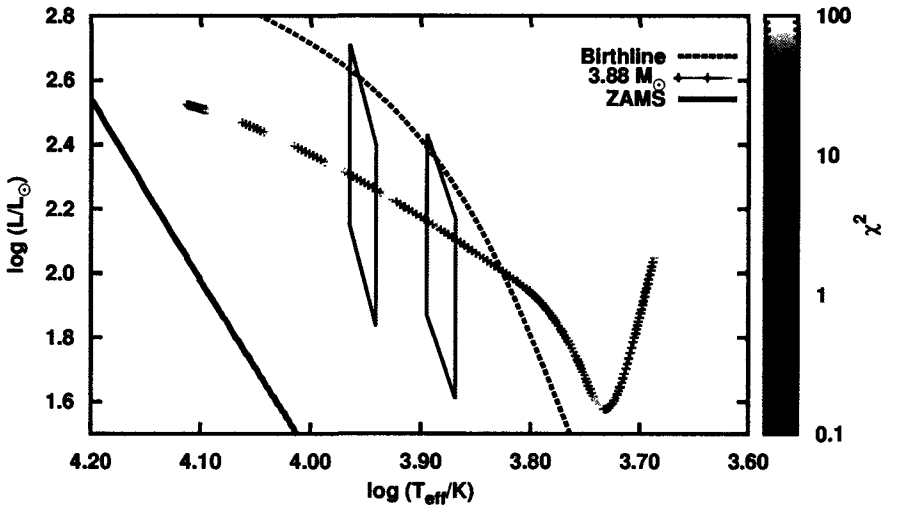

Figure 2.4: χ^2 fits to all three frequencies observed by *MOST* of NGC 2244 183, $\ell = 0$ to 1 modes, mass = 3.88 $M_\odot$ evolutionary track only. All models with $\chi^2 > 100$ default to the $\chi^2 = 100$ colour. The two error boxes indicate two different possible positions for the star in the HRD, a result of two very different spectral classifications available in the literature.

desirable, however as a result of this work, small rotational splittings are not generally expected for PMS δ-Scuti stars (see Section 2.6.3), and so multiple mappings to a single model frequency are not permitted. In this case, the frequency closest to the model frequency is mapped to ν_{obs}, and the second observed frequency is fit to the next closest ν_{mod} for the χ^2 calculation.

2.2.2.1 Families of solutions: Interpreting χ^2 results

A brief introduction to interpreting χ^2 tests in the context of a grid of models is useful. Figure 2.4 shows a typical result for fitting three observed frequencies to model pulsation spectra. In this case the data is from *MOST* observations of NGC 2244 183, and the full analysis is available in Section 3.2.2.4. The single evolutionary track for a 3.88 $M_\odot$ star shows a number of χ^2 minima, any of which could be considered a theoretical asteroseismic solution to the observed frequencies. If such a fit is done to all other evolutionary tracks of the grid, and for clarity, the bad fits (high χ^2 values) removed from the plot, the results for the grid are as shown in Figure 2.5. The error box indicates the star's position in the HRD as determined from observations outlined

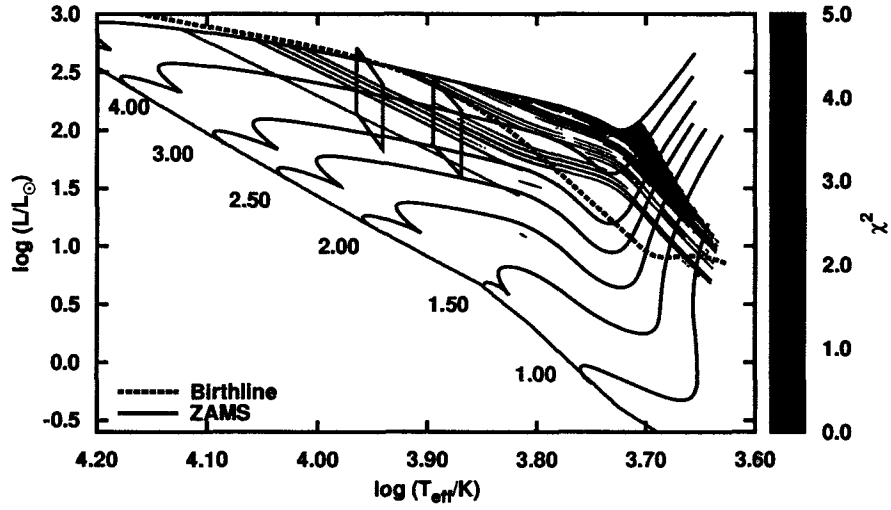

Figure 2.5: χ^2 fits to all three frequencies observed by *MOST* of NGC 2244 183, $\ell = 0$ to 1 modes. Given different spectral classifications of A2 and A7, both possible positions for the star in the HRD are shown.

in Section 2.5. In this case, there are two different error boxes, the result of two very different spectral classifications available for the star in the literature.

The important thing to note is the diagonal lines of good fits running approximately parallel to the ZAMS. Each line of good fits I call a *family of solutions.* Each model within a family of solutions has identical mode identification, (n, ℓ), for a particular observed frequency. The main similarity along a family of solutions is stellar density, with stars of slightly different mass evolving to a slightly different point in the HRD diagram but still having approximately the same mean density as another star in the family of solutions. The mean stellar density determines the approximate sound-travel times for a pulsation signal to travel throughout the star, a quality that helps set the regular spacings between frequencies in a pulsation spectrum, as outlined in Section 2.1. The result is that a star with a slightly different mass from another star will require a slightly different radius from the comparison star to achieve the same sound travel time. This, combined with slightly different stellar luminosities between the two stars, gives these diagonal patterns that we see. Note that one star can match the observations at multiple times in its evolution, but

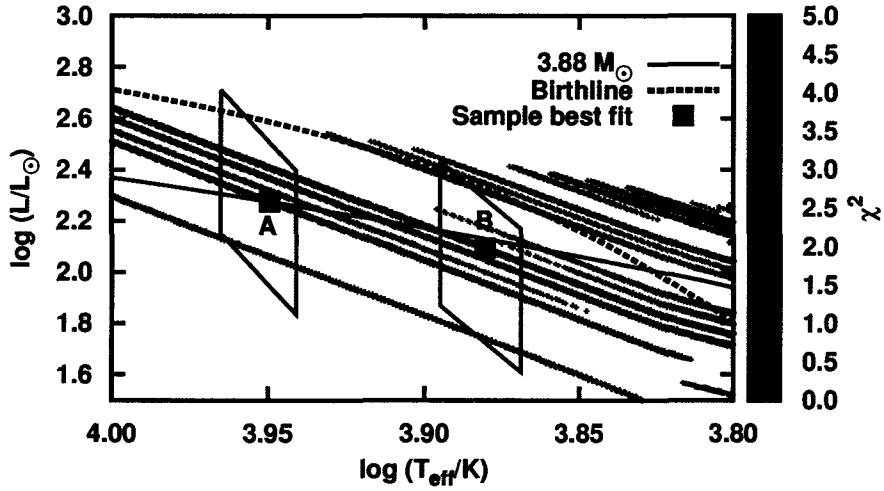

Figure 2.6: χ^2 fits to all three frequencies observed by *MOST* of NGC 2244 183, $\ell = 0$ to 1 modes, demonstrating the resulting families of solutions.

with different mode identification, so in this case, other observations are needed to rule out different models: each good fit in a family of solutions is probing not only the individual frequencies, but the *differences* between the observed frequencies.

To demonstrate the differences between two different families of solutions, Figure 2.7 shows the corresponding echelle diagrams to the two sample fits labelled "A" and "B" in Figure 2.6 (a zoomed-in version of Figure 2.5) each one belonging to a different family of solutions. In the model marked "A", mode identification is as shown the left-hand side of Figure 2.7: two consecutive non-radial $\ell = 1$ modes for f_1 and f_3, with f_2 identified as a radial mode. All members of this family of solutions would have this mode identification, and given the $\chi^2 < 1$ fits all along the family, there is no reason to prefer one solution over the other based upon χ^2 values alone. The model marked "B" has different mode identification, as shown in the right-hand side of Figure 2.7. Now f_1 and f_3 are identified as two consecutive radial modes, while f_2 is identified as an $\ell = 1$ non-radial mode. In this particular case, there were no models with good fits within the star's position in the HRD in which purely radial modes could explain the observed pulsation spectrum, meaning that non-radial modes have been detected in the star.

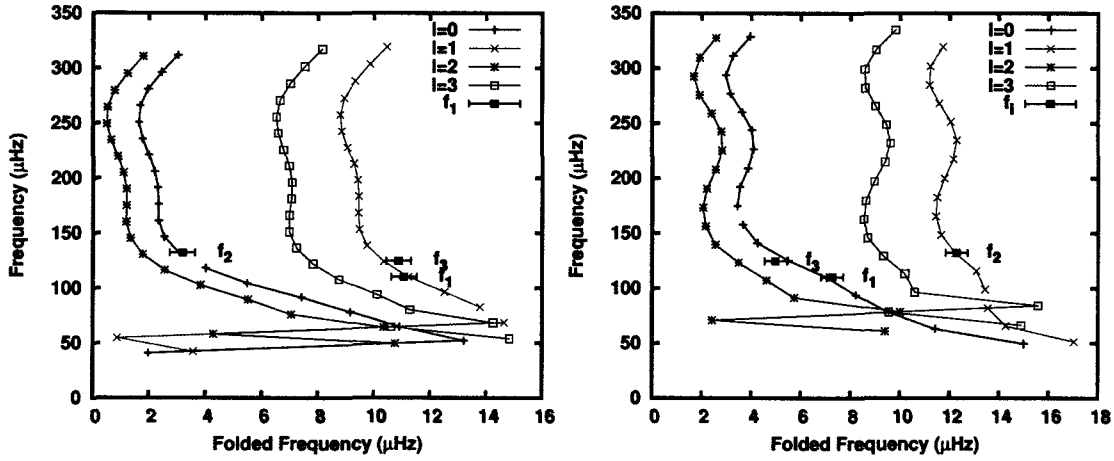

Figure 2.7: Sample echelle diagrams demonstrating the two different families of solutions of Figure 2.6 to the observations frequencies of NGC 2244 183. Left: Model A with specs $\chi^2 = 0.52$, mass = 3.88 $M_\odot$, $\log(T_{eff}/K) = 3.95$, $\log(L/L_\odot) = 2.28$. Right: Model B with specs $\chi^2 = 0.51$, mass = 3.76 $M_\odot$, $\log(T_{eff}/K) = 3.88$, $\log(L/L_\odot) = 2.09$.

Note that as the number of observed frequencies increases, the number of families of solutions is expected to decrease, as well as the diagonal extent of each family. With sufficient number of observed frequencies, fits become less ambiguous, and hopefully lead to solutions that are in agreement with the star's position in the HRD. Unfortunately, this is often not the case, at which point further investigation is needed to discover whether the problems are with the models or the observations. Section 2.6 below will outline some basic tests that can be performed to help discover where the discrepancies might lie.

2.3 On-line tools and databases

In the course of this research a number of on-line databases and systems were utilized, and need to be acknowledged. For open-cluster information WEBDA provides an excellent database of observations and references, invaluable for evaluating potential targets for observation, or for investigating the observational history of a particular cluster (Paunzen 2008).

Simbad (Wenger et al. 2007), coupled with the NASA Astrophysics Data System (better known as ADS; Eichhorn et al. 2002) and VizieR electronic catalogues (Ochsenbein, Bauer & Marcout 2000) allowed for extensive literature searches on individual stars, allowing data to be used that would have otherwise been inaccessible. Simbad is a database that cross references data sources with astronomical targets, often linking to ADS, a cross-linked database of journal papers and references therein. VizieR is a database of catalogues, ranging from the very large (*e.g.* the Two-Micron All-Sky Survey, 2MASS, Skrutskie et al. 2006) to the small (*e.g.* list of targets and observations from individual papers).

These services were useful for such things as determining the position of stars in the HRD by allowing the compilation of an extensive list of relevant information on individual stars (spectral classes, apparent magnitudes, *etc.*) from a collection of very disparate sources.

2.4 Observational tools

2.4.1 Microvariability and Oscillations of STars (MOST) satellite

The Microvariability and Oscillations of STars (MOST) satellite is a microsatellite of the Canadian Space Agency (CSA) of mass 53 kg in a sun-synchronous polar orbit of about 100 minutes in duration (Walker et al. 2003). *MOST* contains a 15 cm Maksutov telescope with a custom broad-band filter, approximately 300 nm wide, centred at 525 nm, *i.e.* the filter covers most of the visual spectrum. Currently there are no calibrations of various stellar classes of the *MOST* filter against standard photometric systems, such as Johnson V-band. The satellite is specifically designed for continuous observations of up to eight weeks for stars that fall within the satellite's continuous-viewing zone (CVZ), roughly -19° through +36° in declination.

The satellite provides photometry of very high precision (up to micromagnitudes) and high cadence. For example, for V1366 Ori each measurement was about 3 seconds long, with 20 consecutive images stacked for a total integration time of about 60 s per co-added measurement. An image could be taken approximately every 11

seconds. Three different methods of observation are available, depending upon the brightness of the star, and whether the star is a primary target, or used as a guide star. For bright stars (about $V < 6.5$ mag) a Fabry lens is used to spread the light out over the CCD. Two other modes are useful for dimmer stars, and are akin to standard CCD photometry, and are used for stars of apparent magnitude down to about 11^{th} magnitude (Rowe et al. 2006b). By carefully selecting fields and targets, particularly for star-cluster fields, multiple targets can be observed with one pointing of the telescope. Often observations for the PMS δ-Scuti stars in this project were collected as data from secondary targets that happened to be in the field of the primary target for that particular pointing of the telescope (*e.g.* the primary targets in NGC 2244 were the O and B stars, but A stars were also selected in search of δ-Scuti pulsations and other types of variability).

With these types of observations, precision light curves are obtained, the results considerably superior to that of most ground based observations. Very small amplitude pulsations of tenths of millimagnitudes can be detected, with rich pulsation spectra often the result, rich enough for details comparisons between observed and theoretical pulsation spectra to be made. In general, light-curve analysis for *MOST* targets were performed by other members of the *MOST* team, with the pulsation spectra passed on to me for analysis.

2.4.2 Ground-based observations

With the exception of multi-site campaigns, ground-based observations of the light curves of δ-Scuti stars in general are of insufficient quality for detailed asteroseismic analysis. Generally the pulsation spectra are not rich enough to provide more than a very basic understanding of the star (pulsating in low or high overtones for example). As such, except for observations of EE Cha and EF Cha (too far south for *MOST*), no ground-based light-curve observations were proposed specifically for this

project.[1] Nevertheless, ground-based results, as presented in the literature were used for pulsation analysis of as many stars as possible.

Multi-site campaigns provide reasonable-quality data (such as for IP Per; Ripepi et al. 2006), often good enough for a more detailed analysis of the star, particularly if several frequencies have been detected. Single-site observations generally only detect one or two pulsation frequencies, subject to integer cycle/day aliases, and often only good enough for identifying candidate δ-Scuti star for future targeting by other, more extensive, observing campaigns. It should be noted that UX Ori variability from single-site observations, at least on the short term of a night or two, may mimic δ-Scuti pulsations, and so any potential detection from such observations of δ-Scuti characteristics must be treated as tentative until more extensive observations of the target can be obtained. To date three such stars have been removed from the list of candidate PMSDSS through *MOST* observations (UX Ori, BF Ori, HD 35929; see Section 3.1.5).

2.5 Determining a star's position in the HRD

Determining a star's position in a theoretical HRD from observations is one of the most basic and oldest problems in modern astronomy. The intrinsic properties of a star are difficult to determine due to intervening material between the target and the observer, and of course the flux seen by an observer is proportional to the inverse square of the distance between the target and the observer. Compensating for these effects, and turning basic observations into effective temperatures and luminosities for comparison to models was essential for this work, and so a brief overview of how this is done is provided.

If available, parallax measurements, such as those made by the Hipparcos mission were used to determine a distance to an object, establishing minimum and

[1]Unfortunately observations in March 2010 (14 nights) of EE Cha and EF Cha, the result of a proposal by K. Zwintz and myself, from the South African Astronomical Observatory 0.5 m telescope were unusable due to bad weather.

maximum distances from the 1 σ uncertainties quoted for the parallaxes in the most-recent reductions from van Leeuwen (2007). If the star is too far away for effective parallax measurements, then estimates were made by assuming association with either an open cluster or star-formation region in the vicinity of the star, to which distance estimates would have been made by other means, such as colour-magnitude diagram cluster-main-sequence fitting. It is important to note that if the assumption of association is wrong, then the distance estimate could be wrong, with any derived position in the HRD likewise misplaced.

Temperature determinations largely depended upon spectral classifications and spectral-line modelling done by other researchers and extracted from the literature. Generally, if multiple determinations were available, the results were taken as an ensemble, with a reasonable range of temperatures extracted from the group, *e.g.* if a number of spectral classes ranging continuously from A0 to A2 were found, with no reason to prefer one type over the other, T_{eff} was set as a range that encompassed all of these spectral types. Effective temperature and bolometric correction (BC) values were extracted from spectral types by comparison in the tables published in Ostlie & Carroll (1996), based upon the work of Schmidt-Kaler (1982).

From these tables, intrinsic $(B-V)_0$ colours were compared to observations, $B-V$, thus determining the amount of reddening, $\mathrm{E}(B-V) = (B-V)-(B-V)_0$ for a given star. The observed $B-V$ are from various sources, and the relevant data will be referenced within the sections on each individual star. From this, overall extinction in V, A_V, was determined, assuming

$$A_V = R_V \mathrm{E}(B-V) \tag{2.13}$$

where R_V is the empirically-determined ratio of selective-to-overall extinction, as measured by such researches as Turner (1994). Given the often large uncertainties otherwise associated with the observations, the Schmidt-Kaler (1982) tables were

deemed to be of sufficient accuracy for the job at hand, recognizing that the temperature determinations might eventually be supplanted by more modern determinations. Note that for the spectral types in question here (not necessarily true for other spectral classes), the difference between T_{eff} and BC for different luminosity classes of the same spectral class (*e.g.* A2 V versus A2 III) in the tables used are small, if they exist at all, and so an error in luminosity-class determination by a researcher does not have a significant effect on the $(B-V)$ and BC calculations as performed here. Such an error might otherwise result in disagreement between the luminosity class and the asteroseimic or distance-corrected luminosities for the star.

It is important to note that for a HAe star, depending upon A_V, R_V might be wrong. At high levels of A_V (more than 1.5 magnitudes or so), stars may start to appear bluer instead of redder with increased A_V, a result of the star's surrounding dust clouds reflecting light into the line of sight of the observer, causing a bluing effect. Curiously, not all stars deviate from $R_V = 3.1$ at high values of A_V (Bibo & The 1991), suggesting that perhaps there is a difference in composition of the obscuring material from star to star. Multi-filter observations of V351 Ori by van den Ancker, Thé & de Winter (1996) dramatically demonstrate the bluing phenomenon. V351 Ori is an HAe star that displays UX Ori-type variability, in this case dramatic non-periodic dimming by eclipsing dust and gas clouds of up to 2.5 magnitudes in V. Statistically, up to about $\Delta V = 1.5$, A_V versus E(B–V) follows the standard slope of $R_V = 3.1$. Above $A_V = 1.5$ the star becomes bluer with increased extinction. Without detailed multi-filter observations so that time-dependent colour information can be extracted for the star, a correction for reddening and extinction might be in error, and this must be kept in mind when calculating A_V. This phenomenon could explain why some stars appear anomalously dim in the HRD compared to the determinations of, for example, asteroseismology.

The luminosity, L, of a star is related to its absolute bolometric magnitude, M_{bol}, via

$$\frac{L}{L_\odot} = 100^{(M_{bol,\odot} - M_{bol})/5} \tag{2.14}$$

where $L_\odot$ and $M_{bol,\odot}$ are the luminosity and absolute bolometric magnitude of the sun respectively. Also,

$$M_{bol} = V_0 + BC \tag{2.15}$$

where V_0 is the absolute V-band Johnson magnitude of the star, and BC is the bolometric correction of the star, estimated from tabulated values for a star of a given spectral class. V_0 is related to the apparent V magnitude, the distance, d (in parsecs), and A_V via

$$V_0 = V - A_V - 5\log_{10}\left(\frac{d}{10\text{pc}}\right). \tag{2.16}$$

Given the above equations, estimates of L and T_{eff} for a star are made, and thus the position of the star in the HRD is determined. However, there are uncertainties in all the input quantities, particularly the distance and spectral class/effective temperature of the star. The calculation of E(B–V) (and therefore A_V) is dependent upon the spectral class of the star (generally a red star of magnitude V has undergone less extinction than a blue star of similar V), and therefore a star's luminosity at the cool edge of its temperature-uncertainty range must be calculated separately from the luminosity at the hot edge. Given uncertainties in the distances estimates to the star, the star's position in the HRD is therefore approximated as a trapezoid. A sample of this was seen in Figure 2.6. It is usually this trapezoid area in the HRD to which stellar models of the correct luminosity/temperature range are compared.

2.6 Practical application of asteroseismology to observed frequencies

Upon obtaining the pulsation spectrum of a star there are a few basic calculations that can be made that may eliminate a significant number of candidate models from consideration, and enhance our understanding of the star.

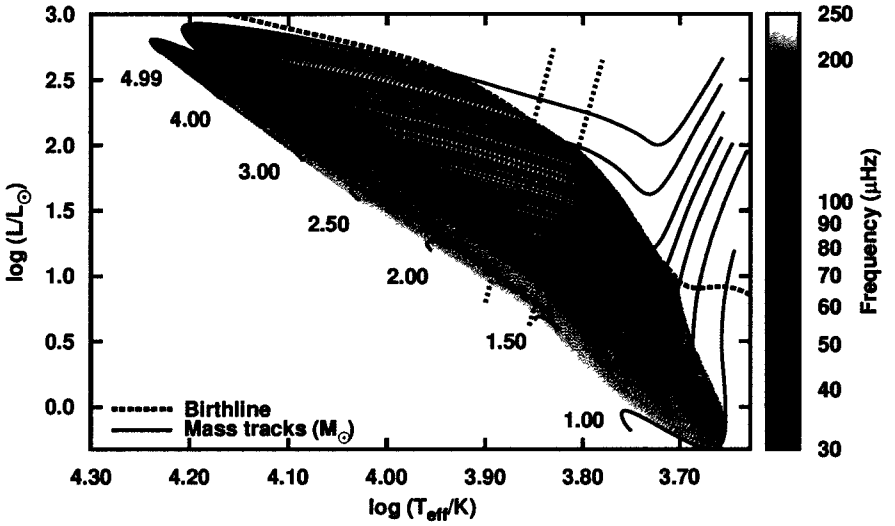

Figure 2.8: Fundamental frequencies of the PMS models under consideration.

2.6.1 Fundamental mode

Any star with a particularly low frequency should be checked against a model's fundamental frequency, the lowest frequency the star can support that is not a gravity mode. This frequency is given approximately by the following expression:

$$f \simeq \frac{1}{t_{dyn}} \simeq \left(\frac{GM}{R^3}\right)^{\frac{1}{2}} \propto (\overline{\rho})^{\frac{1}{2}} \tag{2.17}$$

where t_{dyn} is the dynamical timescale, the time it would take for a star to recover hydrostatic equilibrium if some physical process should disturb the balance between gravitational forces and internal pressures (Aerts, Christensen-Dalsgaard & Kurtz 2010). Here M and R are the mass and radius of the star and G is the gravitational constant. The fundamental frequency mainly depends upon the overall average density of the star, $\overline{\rho} = 3M/4\pi R^3$, and is therefore not sensitive to the internal structure of the star.

Figure 2.8 shows the fundamental frequencies of the PMS models under consideration. In the region of the instability strip, lines of constant fundamental frequency run approximately parallel to the ZAMS. Consequently a sufficiently low frequency

detected within a pulsation spectrum implies a *minimum* luminosity above the ZAMS that the star need to have in order to support this p-mode frequency, and a useful constraint is placed upon the star's position in the HRD, independent of other means. This does *not* imply that the detected frequency *is* the fundamental mode, merely that the fundamental mode must have a frequency *lower* than the observed frequency in order for it to be supported. As will become evident in Chapter 3, this consideration is important for a number of stars. However, it is also important to note that if a gravity-mode (g-mode) should be mistaken for a p-mode (g-modes have lower frequencies than p-modes), then this test will yield incorrect results, implying a higher luminosity for the star than would otherwise be needed for the star to support the g-mode. Stars pulsating in g-modes overlap the position of δ-Scuti stars at the low-luminosity, cool edge of the instability strip (γ-Doradus pulsators), as well as at the low-luminosity blue edge (rapidly-rotating slowly-pulsating-B stars — see Section 3.1.3.3 on VV Ser), and so in these regions of the HRD particular care must be exercised in applying the fundamental-mode test. Even if a g-mode is mistakenly labelled a p-mode, this test may still yield a useful result, for in such a star the asteroseismic HRD position might not agree with the position determined via broad-band photometry and spectroscopy, as outlined in Section 2.5, and would suggest that perhaps g-modes should be calculated for the star as a means of reconciling the positions, particularly if the star's position in the HRD is otherwise fairly well established.

2.6.2 Acoustic cut-off frequency

The acoustic cut-off frequency (ACF) is the highest p-mode frequency that can be trapped by the star, thus setting up a pulsation that can be observed; signals that would otherwise produce p-mode pulsation frequencies higher than this are transmitted into the outer atmosphere of the star, do not reflect off the atmosphere, and thus have have no outer boundary condition upon which the pulsation can be established. Reflection of the signal is necessary for an observable regular wave pattern to be set up in the star, thus eliminating the possibility of seeing these very high

frequencies. As outlined in (Aerts, Christensen-Dalsgaard & Kurtz 2010) the *lowest* frequency that can be transmitted at any point *locally* in a star, ν_c, is given by

$$\nu_c^2 = \frac{c^2}{16\pi^2 H^2}\left(1 - 2\frac{\mathrm{d}H}{\mathrm{d}r}\right), \tag{2.18}$$

where c is the local sound speed, and H is the density scale height given by

$$H^{-1} = \left|\frac{\mathrm{d}\ \ln\rho}{\mathrm{d}r}\right|, \tag{2.19}$$

in which r is the radial coordinate measured from the centre of the star. All signals of higher frequency can propagate in these regions, lower frequencies will not. The higher the rate of change of the density scale height, the higher the lowest-permissible frequencies will be. For stars, $\mathrm{d}H/\mathrm{d}r$ is largest in the outer atmosphere, but lower within the interior, *i.e.* lower frequencies can only propagate in the interior. Therefore, a signal *between* the fundamental frequency and the highest ν_c in the outer atmosphere, ν_{ACF} can be generated in the the *interior* of the star, will be forced to reflect off the outer atmosphere (the signal cannot propagate there, so the region acts as a node), back toward the interior, potentially setting up the wave patterns that can be observed as pulsations. Frequencies above ν_{ACF} can essentially be transmitted to "infinity" by the atmosphere of the star; reflection does not occur, and therefore pulsation cannot be set up above ν_{ACF}. The acoustic cut-off frequency is significant for a number of stars under consideration in this study, but it is absolutely crucial for understanding the pulsation spectrum of one star in particular, V1366 Ori, as will be shown in Section 3.1.1.4. Values for the acoustic cut-off frequency of PMS models are given in Figure 2.9. What is crucial to note about this plot is that at any given temperature, the higher the luminosity of the star, the lower the acoustic cut-off frequency is. Therefore, the highest frequency observed within a pulsation spectrum of a star puts a maximum luminosity constraint on the star: a higher-luminosity star would have a lower ν_{ACF}, and that frequency would not be able to propagate in that star. Generally PMS δ-Scuti stars with pulsation frequencies of 350 μHz and higher

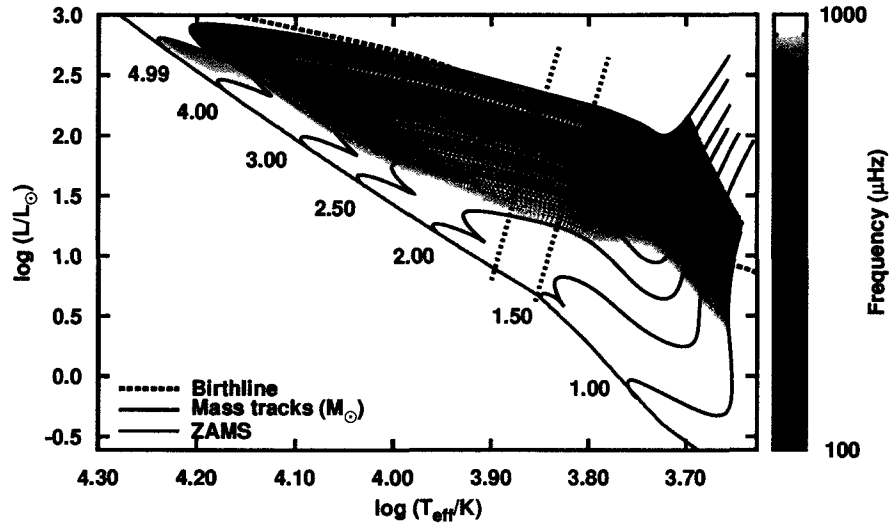

Figure 2.9: Acoustic cut-off frequencies of the PMS models under consideration. Models with ACF less than 100 μHz and greater than 1000 μHz are not shown. All models in the instability strip that are close to the ZAMS would have ACF $>$ 1000 μHz, out of δ-Scuti pulsation range, and are unlikely to play a part in PMS δ-Scuti stars.

must have reduced luminosities from those maxima otherwise imposed by the stellar birthline, and so these frequencies can be used to constrain the star's position in the HRD. If the star's pulsation spectrum spans a large range, as it does with V346 Ori (Section 3.1.2.3), and IP Per (Section 3.1.2.1), then maximum *and* minimum luminosity constraints can be put on the star by considering both the required ACF and fundamental frequency of the star. As will be seen, this is somewhat rare. Constraints on the minimum, or the maximum luminosities are not uncommon, but both at the same time are less common.

It is important to note that there are unusual physical phenomena, such as strong magnetic fields, that can alter the density scale height enough in the atmosphere of a star to significantly alter the ACF over what is normally encountered. In such a case, if independent measurements otherwise placed a star specifically in one spot of the HRD, but the star was found to be oscillating above the ACF consistent with this position, this would be an indication of such additional phenomena. This

appears to be the case with some rapidly-oscillating Ap stars (commonly known as roAp stars), see *e.g.* Audard et al. (1998).

2.6.3 Rotational splitting

A third basic consideration is the effects of rotation on the pulsation spectrum of a star. Rotation breaks the degeneracy imposed upon an otherwise spherically symmetric star, resulting in rotational splittings of ℓ modes into individual m modes. The component m modes of a particular (n, ℓ) are collectively known as a multiplet. For small rotational velocities, v_{rot}, the difference in frequency between two adjacent members of a multiplet, $\Delta f = \nu_{n\ell m} - \nu_{n\ell(m-1)} = 1/\Omega$ where $\Omega = 2\pi R/v_{rot}$ is the rotational period of the star. Therefore

$$\Delta f = \nu_{n\ell m} - \nu_{n\ell(m-1)} = \frac{v_{rot}}{2\pi R}. \tag{2.20}$$

An important consequence of this relationship is that for a given rotational velocity a physically smaller star has a larger Δf. For a PMS star that is physically shrinking as it undergoes gravitational collapse (until it reaches the ZAMS) conservation of angular momentum dictates that v_{rot} will increase with time, and rotational splitting will be become more and more important as the star ages. Note that this assumes that the star is not loosing significant amounts of angular momentum through either magnetic braking or mass loss, nor that the evolution of the star is significantly redistributing the angular momentum throughout the star such that the surface rotational velocity is modified in unexpected ways. These are processes that are thought to act upon much longer time scales than that contained within the PMS phase of evolution.

Generally, a projected rotational velocity, $v_{proj} = v_{rot} \sin i$ (hereafter simply $v \sin i$), is what is measured for a star, and so this is a *minimum* value for the true rotational velocity of the star. Using $v \sin i$ in Equation 2.20 instead of v_{rot} then gives a minimum estimate of the expected Δf. For large rotational velocities, Equation 2.20 does not apply in detail, however it does provide an order-of-magnitude estimate of

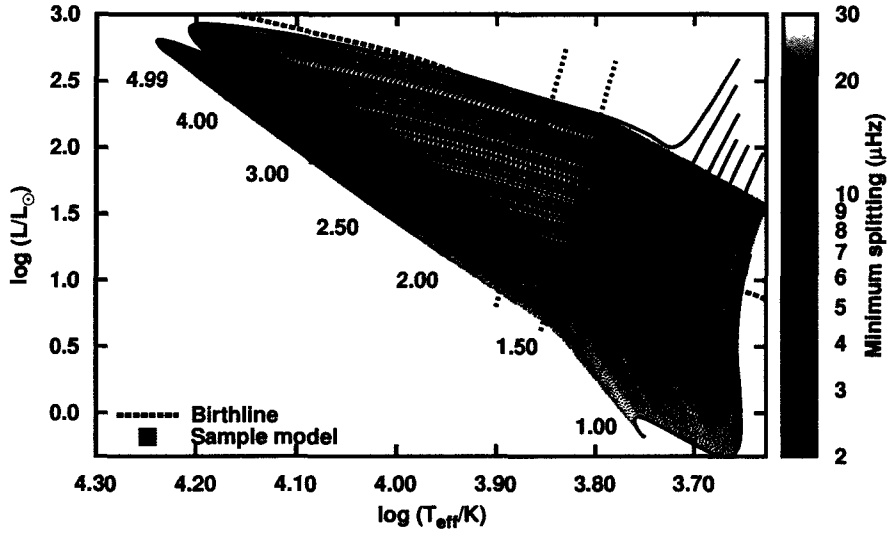

Figure 2.10: Approximate minimum rotational splitting that can be expected from $v \sin i =$ 100 km/s. The sample model indicated by the black square is the model used in Figure 2.11.

the expected level of splitting. Detailed calculations for high velocities require 2D calculations, such as those outlined in Lovekin & Deupree (2008) and Deupree & Beslin (2010). In this regime, the star becomes oblate, the Δf become asymmetric, sometimes dramatically so, and so Equation 2.20 is only a rough estimate of the *average* splitting to be expected over a full multiplet (Deupree 2011). In particular, at smaller rotational velocities than those stars studied here, rotational splittings can can very quickly match the small separations calculated in non-rotating models, causing potential confusion. The implication of Equation 2.20 is that what looks to be a rotationally-split multiplet of what would otherwise be a single non-radial mode in the non-rotating case, might be multiple multiplets overlapping one another if the rotation of the star is large enough. If $v \sin i$ has been measured for a star, Δf can be calculated for each model under consideration since one knows the stellar radius for each model. This can be compared to the potential multiplet observed in the pulsation spectrum. If the minimum splitting is significantly larger than the differences between the frequencies under question, there is a high probability that these are not frequencies from a single multiplet, but are the result of very large splitting, so

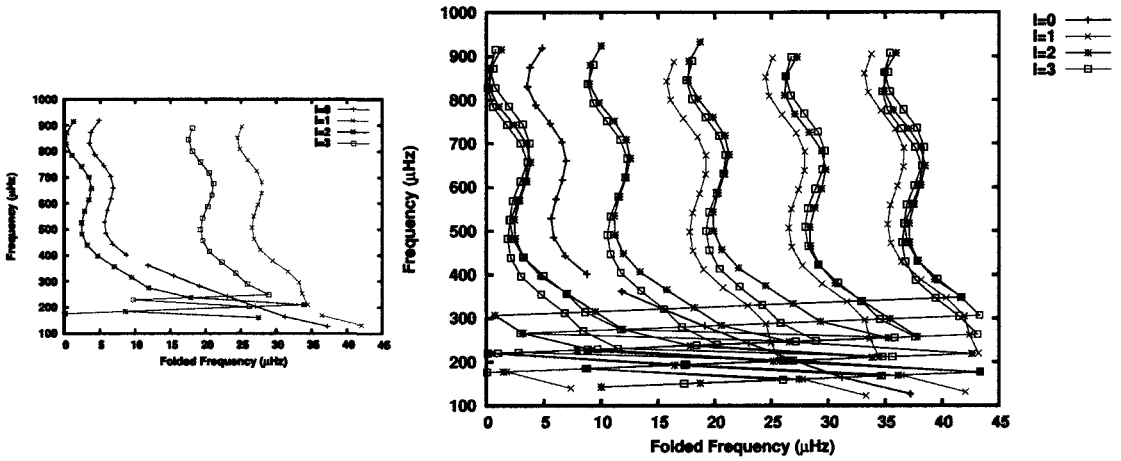

Figure 2.11: Left-hand side: Echelle diagram of a 2.30 $M_\odot$ star, radius = 2.62 $R_\odot$ without rotation. Right-hand side: same star with $v \sin i$ = 100 km/s, minimum rotational splitting about 8.7 μHz.

large that the different multiplets are overlapping one another, making any pattern extremely hard to identify. Note that the test does *not* firmly conclude that even at high rotational velocities that two (or more) nearby frequencies *cannot* be members of the same multiplet, as the asymmetries in the splittings can bring two modes back into close proximity to one another in frequency space, as demonstrated by *e.g.* by Deupree & Beslin (2010). The test merely indicates whether a high rotational velocity might make this less likely to be the case.

Prior to this work this was an effect not entirely appreciated when applied to PMS δ-Scuti stars, it was thought that rotational splittings might be easy to identify. Typical $v \sin i$ (50 to 150 km/s) and radius values for this class of object however generally conspire to make Δf values large enough for multiplet contamination to be the norm, rather than the exception. As an example, Figure 2.10 shows an HRD of the Δf that might approximately be expected for each model for stars with $v \sin i$ = 100 km/s. The Δf range from a few to tens of microHertz in the part of the HRD relevant to δ-Scutis. Figure 2.11 is a typical echelle diagram for a PMS star (relevant model indicated by the black square in Figure 2.10), first the non-rotating spectrum on the left, and then the rotating spectrum calculated from Equation 2.20 on the

right. Here, I do not claim that Figure 2.11 is accurate numerically, but it gives a reasonable qualitative picture of the confusion that befalls an echelle diagram once a star becomes rapidly rotating. As one can see, multiplets are thoroughly mixed together, however at first glance there are several spots in the echelle diagram that produce a series of frequencies that *look* like a single multiplet from a minimally-split ℓ mode, hence the confusion that can abound.

With the above tests and techniques in place, analysis of individual stars can now proceed.

Chapter 3

Results for individual stars

The results for individual stars are divided up into two major sections, Herbig Ae stars, and Open Cluster stars, each one of which is further divided into stars or clusters observed by *MOST*, and those observed by ground-based observations. These subdivisions allow the observations to be divided by the quality of the observations for ease of comparison of the results between various objects, *MOST* observations being of the highest quality, followed by multi-site ground-based observations, and then by single-site ground-based observations. Except in a few select cases, detailed asteroseimic analysis has been limited to those stars for which *MOST* or multi-site ground-based observations have been obtained. However, even for the lower-quality data, often the basic tests outlined in Section 2.6 (fundamental and acoustic cut-off frequencies, and minimum rotational splittings) can bring significant insight into the physical situation for the corresponding stars.

The Herbig Ae section also contains a subsection on stars for which *MOST* observations are scheduled, but for which observations have yet to be collected, and a subsection on stars for which *MOST* observations have ruled out δ-Scuti pulsations in stars for which pulsations had previously been suspected, but not confirmed.

The Open Cluster section also contains a list of clusters and stars for which pulsations have been identified in the literature, and for which the cluster's age suggest PMS status for any pulsating stars, yet before this study, these stars had not previously been included in the list of candidate PMS δ-Scuti stars. Further observations will be needed to confirm or refute the PMS δ-Scuti status of these stars.

3.1 Herbig Ae stars

3.1.1 *MOST* observations

3.1.1.1 V856 Sco (HR 5999)

V856 Sco, more popularly known as HR 5999, is one of the most studied HAe stars in the literature. It is associated with the Lupus 3 dark cloud star-formation region. It has been classified as an A7e III/IV (Herbig & Bell 1988) to an A8/A9 star (Royer et al. 2002b). In the 1970s, during early investigations of the star, HR 5999 was often confused with HR 6000, a star with which it forms a visual binary (Bessell & Eggen 1972; Kukarkin et al. 1972). It is thought that the two stars are approximately coeval and cospatial, and share a common history, but are not two parts of a bound binary system.

V856 Sco displays UX Ori irregular variability of up to $1.^{m}5$ in the V-band from circumstellar material obscuring the star, with most variations between about 6.7 and 7.1 in V (*e.g.* Thé et al. 1996). It was the first HAe star, and only the third PMS star for which δ-Scuti variability was discovered (Kurtz & Marang 1995). The latest Hipparcos reductions of van Leeuwen (2007) report a parallax of 6.14±0.57 mas, corresponding to a distance range of 149 to 180 pc. Royer et al. (2002b) report a

Label	Frequency (c/d)	Err Freq (c/d)	Frequency (μHz)	Err Freq (μHz)	Amplitude (mmag)
f_1	2 845	0 006	32 93	0 07	3 1
f_2	4 347	0 006	50 32	0 07	2 1
f_3	5 733	0 006	66 36	0 07	2 3
f_4	4 828	0 007	55 88	0 08	1 8
f_5	6 607	0 010	76 50	0 10	1 3

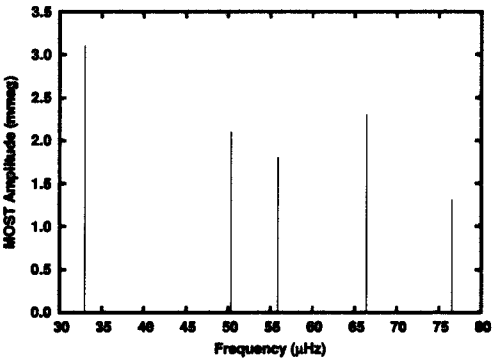

Figure 3.1: Frequencies of V856 Sco as observed by *MOST*. f_1 is probably too small to be a p-mode pulsation frequency, and may be a signature of rotation.

large $v \sin i$ = 204 km/s, Boehm & Catala (1995) a lower (but still large) value of 180±50 km/s.

V856 Sco was observed by *MOST* for 12 days in April 2009, corresponding to a 0.083 c/d or 0.97 μHz frequency resolution.[1] Besides δ-Scuti variability, the star showed irregular variability during the observation period, a signal that needed to be removed from the light curve before analysis for pulsations signals could be performed. Frequency analysis of the light curve was performed by K. Zwintz and passed on to me; it appears in this work in written form for the first time. Five frequencies were found (Figure 3.1), one of which (f_1) is too low to be δ-Scuti pulsation, and could be a signal of rotation (*e.g.*sunspots). The errors are as determined by the light-curve analysis software. Note that if f_2 is a p-mode pulsation frequency, then this would indicate minimum luminosities coincident approximately with the birthline. The rest of the frequencies are also rather low, ranging from $\sim$ 50 through 77 μHz, but are high enough to be δ-Scuti pulsations.

[1]V856 Sco was further observed by *MOST* in May 2010 for 21 consecutive days, however the light-curve analysis is not currently available.

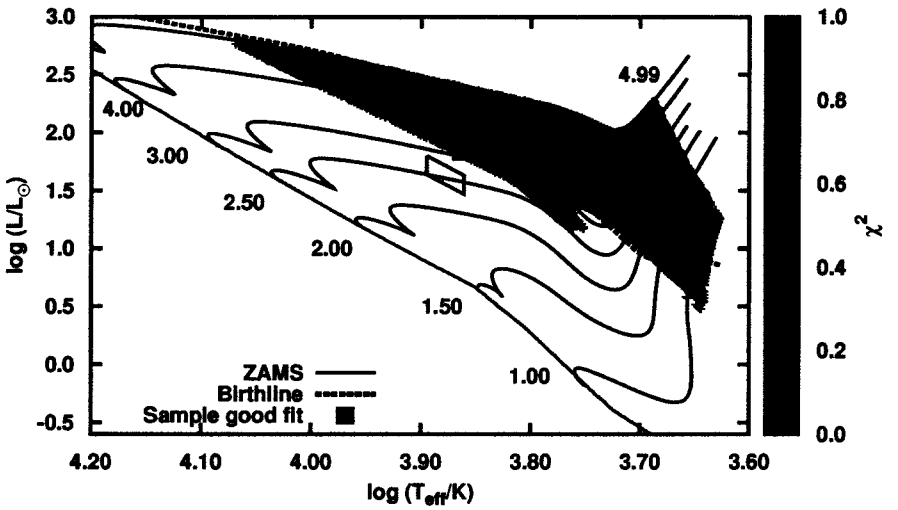

Figure 3.2: Simultaneous χ^2 fit to f_2 through f_5 of V856 Sco, ℓ= 0 to 3 modes, along with the star's position in the HRD, indicated by the error box.

In Figure 3.2 appear χ^2 fits to f_2 through f_5 for ℓ=0 to 3 modes. The large uncertainties associated with each frequency preclude firm conclusions, however, the only simultaneous good fits to all frequencies appear above the star's position in the HRD. The reason for this is demonstrated by the low value of f_2 =4.347 c/d (50.32 μHz), at the low end of frequencies expected for DS pulsations; Figure 3.3 shows the models in which the fundamental frequency is lower than f_2, and could thus support that frequency, and all of them are more luminous than the star's position in the HRD. Indeed, although not shown, a similar analysis for all the other frequencies finds that only the highest frequency, f_5, can be supported by the star's position in the HRD, and in that case, only the upper half of the range of the error box at any given temperature. The next-highest frequency, f_3, requires luminosities as high as the upper boundary of the error box. These results collectively support the idea that V856 Sco's luminosity has been underestimated by the dereddening solution using broad-band photometry, and is perhaps suffering from a bluing effect.

Figure 3.4 shows a sample echelle diagram for the family of solutions closest to the upper edge of the error box. This family of solutions is slightly below the

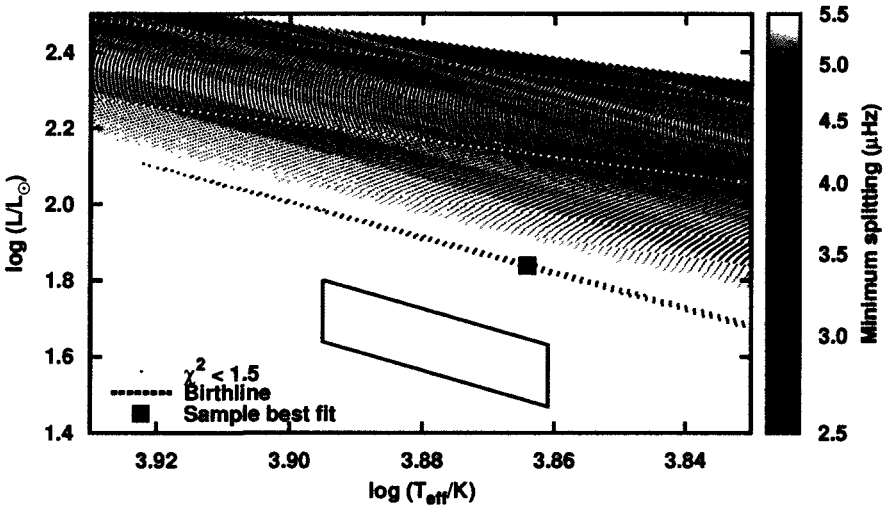

Figure 3.3: Models that can support f_2 of V856 Sco, along with the expected minimum rotational splitting expected for each such model. Note the high luminosity needed to support such pulsations. Also indicated are the models from Figure 3.2 with $\chi^2 < 1.5$ (dark blue dots), and the sample best fit of Figure 3.4.

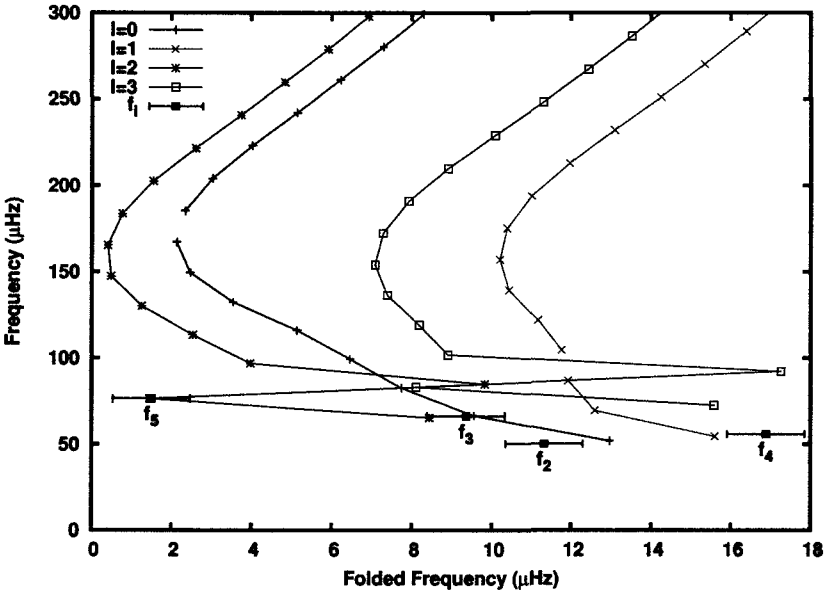

Figure 3.4: Sample echelle diagram for f_2 through f_5 observed frequencies of V856 Sco. Model parameters: $\chi^2 = 1.15$, mass = 3.12 $M_\odot$, log (T_{eff}/K) = 3.864, log $(L/L_\odot)$ = 1.839, log g = 3.71.

models for which f_2 is less than or equal to the fundamental frequency, but still, f_2 is lower than the fundamental mode by less than 2σ, indicating that no solutions dimmer than this are possible if f_2 is indeed from pulsation. Note that the pulsation frequencies in this case are not in the asymptotic regime. Also, note that Figure 3.3 also indicates the minimum expected rotational splitting, corresponding to the lowest values from the literature of 130 km/s from $v \sin i$ = 180±50 km/s of (Boehm & Catala 1995). The values are comparable to, or larger than, the differences between different ℓ orders, making any signature of rotational splitting difficult to identify without more rigorous techniques.

In summary, the asteroseimic analysis would suggest that V856 Sco's luminosity has been underestimated by a small amount, either through underestimating the extinction that the star is experiencing, or by the Hipparcos measurements being not quite correct. The former is probably the most likely, given the UX Ori variability that the star exhibits.

label	frequency (c/d)	err freq. (c/d)	frequency (μHz)	err freq. (μHz)	Amplitude (mmag)
f_1	10.313	0.001	119.37	0.01	11.2
f_2	12.463	0.004	144.25	0.04	2.5
f_3	10.842	0.004	125.48	0.05	2.5
f_4	10.487	0.005	121.38	0.05	2.3
f_5	16.053	0.006	185.79	0.07	1.8
f_6	20.473	0.006	236.95	0.07	1.6
f_7	19.522	0.007	225.95	0.08	1.3
f_8	13.492	0.007	156.16	0.08	0.9

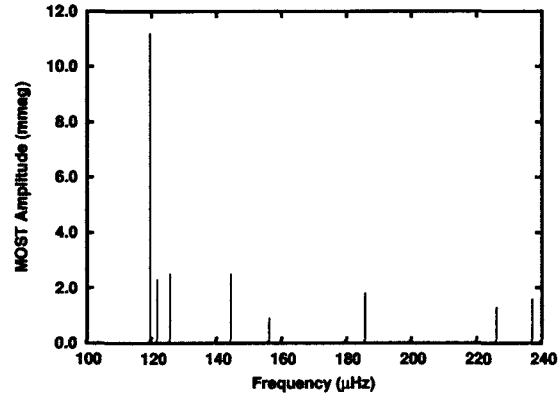

Figure 3.5: V1247 Ori: frequencies observed by *MOST*.

3.1.1.2 V1247 Ori

V1247 Ori (HD 290764) is a HAe star associated with the Orion OB1b association, apparent V magnitude 9.$^{\rm m}$8. Schild & Cowley (1971) classified it as A5 III, Vieira et al. (2003) as F0 V. V1247 Ori does not display variability associated with CS extinction that is typical of many HAe stars, and as such was first identified as variable by Lampens & Rufener (1990) when they detected δ-Scuti variations with a frequency of about 10.31 c/d. It was not identified as a probable PMS star until it was studied by Fujii, Nakada & Parthasarathy (2002) as a potential post-asymptotic-giant-branch (post-AGB) star; the stars characteristics were more indicative of the former rather than the latter. Vieira et al. (2003) then included it within their study of 131 HAeBe candidates, in which Hα was observed in emission.

Unfortunately, V1247 Ori does not have a usable parallax: Hipparcos reductions as reported in Perryman & ESA (1997) give -32.40±9.20 mas; Kharchenko (2001) reported -32.40 ±35.10 mas. The unphysical -*ve* sign in the parallax indicates significant problems with the data for this star, rendering the parallaxes unusable. Hence, a distance to the star is estimated from its potential membership in the Orion OB1a association (Vieira et al. 2003), with an estimated distance between 270 and 640 pc. Estimates from spectral class and $B-V$ colours indicate $E(B-V)$ between 0.$^{\rm m}$00 and 0.$^{\rm m}$20, and $A_{\rm v}$ between 0$^{\rm m}$ and 0.$^{\rm m}$62. Temperatures are between 8100

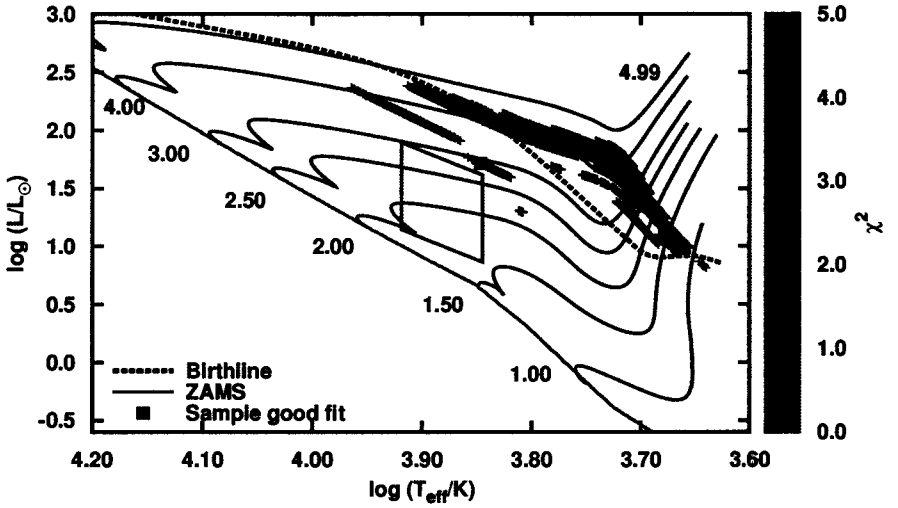

Figure 3.6: χ^2 fit to all eight significant frequencies in V1247 Ori detected by *MOST*, ℓ=0 to 3 modes.

K (for an A5 III star) and 7150 K (for an F0 III star, slightly cooler than for an F0 V star at 7200 K). Correcting for extinction, and converting to luminosity gives $\log L/L_\odot$ between 0.867 and 1.896, just clearing the ZAMS on the low end of the luminosity range. Currently there is no reported value for $v \sin i$ in the literature.

V1247 Ori was observed by MOST in 2009 for 31.09 days, indicating frequency resolution of 0.03 c/d or 0.36 μHz. It is upon these observations that the asteroseismic analysis for this star are based, and the results are reported here in written form for the first time. Analysis of the light curve was performed by K. Zwintz using SigSpec and Period04, and the results were communicated to me. The light curve was not affected by CS variability. Eight frequencies of high significance are reported, and appear in tabular and graphical form in Figure 3.5.

Asteroseismic analysis of all 8 frequencies yields the following results: a reasonable family of solutions exist just to the right of the upper part of the error box for V1247 Ori in the HR diagram for fits with ℓ= 0 to 3 modes (Figure 3.6). Good solutions for modes $\ell < 3$ were not found. Figure 3.7 shows an echelle diagram of a typical fit with mass 2.90 $M_\odot$, χ^2 =3.6. Radial orders vary from $n = 4$ through to $n = 11$. As an experiment, tests were made by successively eliminating one frequency

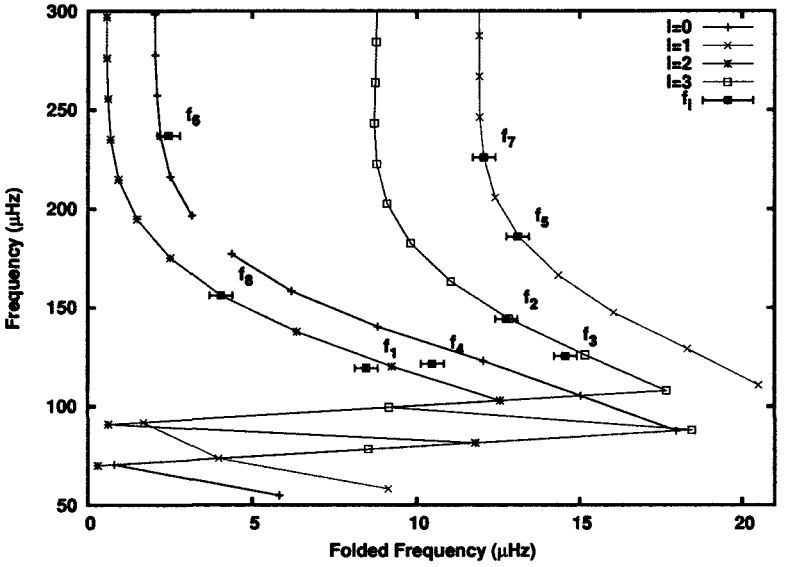

Figure 3.7: Simultaneous χ^2 fit to all frequencies of V1247 Ori found by *MOST*, ℓ= 0 to 3 modes. χ^2 = 3.6, mass = 2.90 $M_\odot$, $\log(T_{eff}/K)$=3.847, $\log(L/L_\odot)$=1.72.

from the fit after another to see if a better fit could be found. The best results were found by eliminating f_4, with the best solution very similar to the above solution in which all frequencies were included in the fit. The echelle and HRD are shown in Figure 3.8, and a representative fit is for mass = 2.91 $M_\odot$, χ^2 =1.32. Identifications for each frequency remain the same as above.

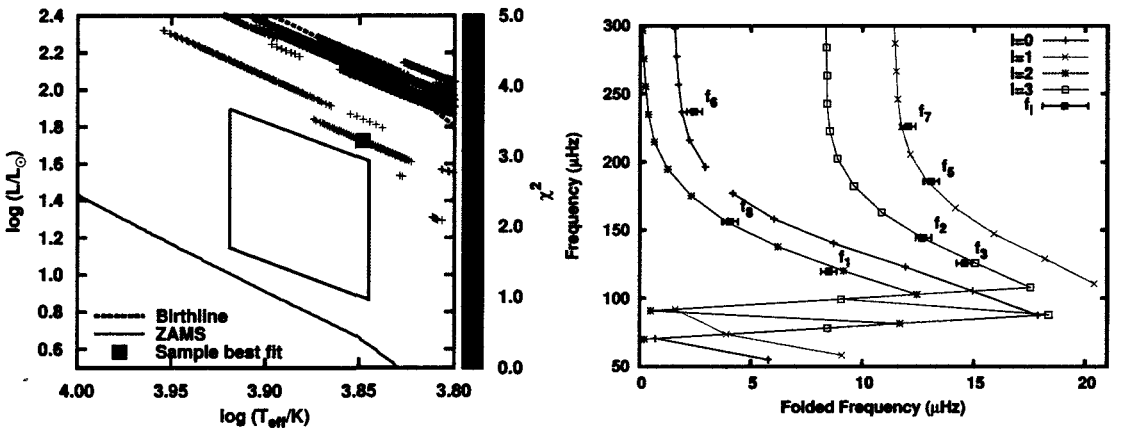

Figure 3.8: Simultaneous χ^2 fit to all frequencies, excluding f_4 in V1247 Ori, ℓ= 0 to 3 modes. χ^2 = 1.33, mass = 2.91 $M_\odot$, $\log(T_{eff}/K)$=3.848, $\log(L/L_\odot)$=1.723.

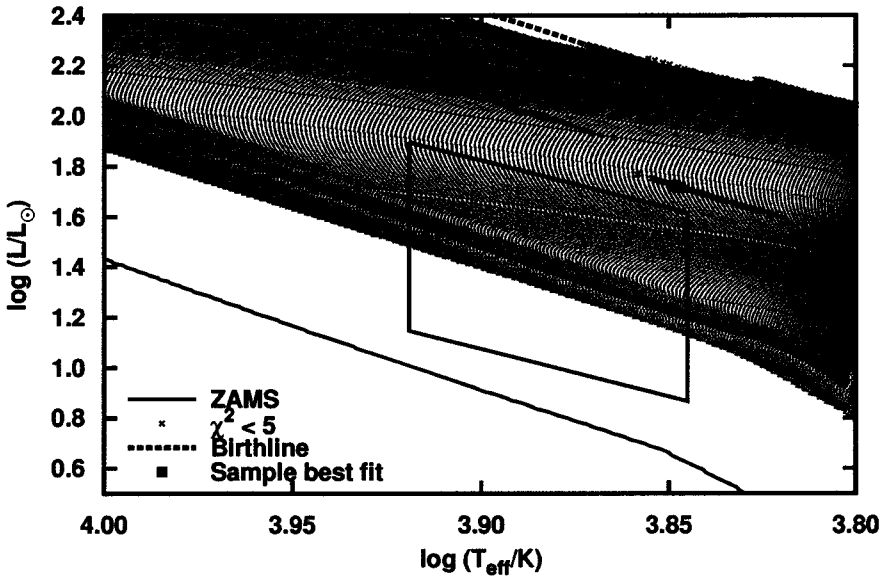

Figure 3.9: V1247 Ori: models with fundamental frequency less than f_1= 119.37.

This seems to be a rare case in which an analysis seems to be straight forward, as will become apparent as more stars are discussed, however whether this is a false positive remains to be seen, and could be an indication of slow rotation in the absence of information on $v \sin i$ for the star, however unlikely this may be. Note that the lowest frequency, f_1 =119.37 μHz, is low enough to put a constraint on the minimum-allowed luminosity for the star, as shown in Figure 3.9, including about half of the lower range of the error box. Interestingly, none of the good fits are near the lower range of acceptable luminosities, as often happens when one of the frequencies is limiting either the minimum or maximum allowed luminosities.

In summary, for V1247 Ori, asteroseismicly-reasonable fits just outside the star's position in the HRD diagram were found, suggesting a potential solution, although the possibility remains that this is a false positive solution. Measurements of $v \sin i$ will be required to determine how much a role rotation may play in modifying the pulsation spectrum of the star. The lowest-valued frequency, f_1, if a pulsation frequency, eliminates about half of the luminosity range for this star's rather ill-determined position in the HRD.

ID	freq. (c/d)	err freq. (c/d)	freq (μHz)	err freq. (μHz)	Amp (mmag)	sig
f_1	22.008	0.001	254.64	0.01	2.557	400.2
f_2	21.252	0.001	245.89	0.01	2.535	384.3
f_3	17.979	0.002	208.02	0.02	0.748	136.6
f_4	6.17	0.01	71.4	0.1	0.22	15.1
f_5	28.04	0.01	324.4	0.1	0.193	14.7
f_6	7.11	0.01	82.3	0.1	0.205	11.3
f_7	11.65	0.01	134.8	0.1	0.15	10.2
f_8	11.86	0.01	137.2	0.1	0.131	11.1
f_9	27.88	0.01	322.6	0.1	0.156	10.7
f_{10}	9.79	0.01	113.3	0.1	0.128	7.7
f_{11}	5.78	0.01	66.8	0.1	0.123	6.8
f_{12}	27.72	0.01	320.8	0.1	0.116	6.2

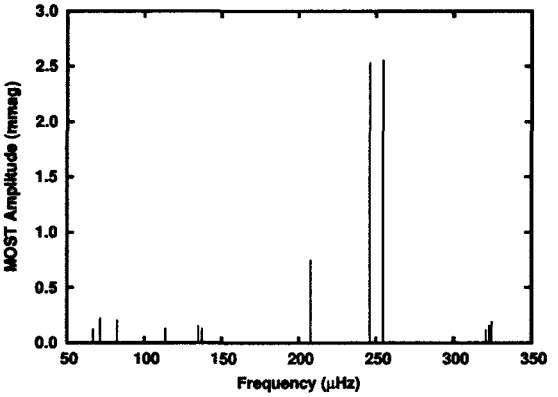

Figure 3.10: Frequencies of V1026 Sco as observed by *MOST*.

3.1.1.3 V1026 Sco (HD 142666)

V1026 Sco, more popularly known in the literature as HD 142666, is a UX-Ori-type HAe star exhibiting changes of brightness of up to $1.^{\mathrm{m}}8$ in V. First identified as a potential variable star by Strohmeier, Knigge & Ott (1964), its variability was finally confirmed by Makarov et al. (1994) using Tycho data. It is generally associated with the Sco R1 star-formation region (Vieira et al. 2003), and upon identification as an IRAS point source with the correct IR spectrum, a PMS star (*e.g.* Gregorio-Hetem et al. 1992). It was then added to the list of HAeBe objects by Thé, de Winter & Perez (1994), and only given its General Catalogue of Variable Stars (GCVS) designation shortly thereafter (Kazarovets & Samus 1997). Most researchers have found spectral class A8 Ve $\pm$ one spectral class, corresponding approximately to $T_{eff} \sim 7200$ K to 7850 K (Thé, de Winter & Perez 1994; Dunkin, Barlow & Ryan 1997; Mora et al. 2001). Dunkin, Barlow & Ryan (1997) found $v \sin i = 70 \pm 2$ km/s, and Mora et al. (2001) 72 ± 2 km/s.

The distance to V1026 Sco is not well known, the parallax from Tycho data is unphysical (-3.30 ± 10.90 mas; Hoeg et al. 1997). Vieira et al. (2003) use a distance to V1026 Sco of 100 to 160 pc based upon its association with the Sco R1 star-formation region. (Note they also report slightly different results for spectral class, F0 V, and projected rotational velocity, $v \sin i = 97$ km/s.) In addition to the uncertainty over

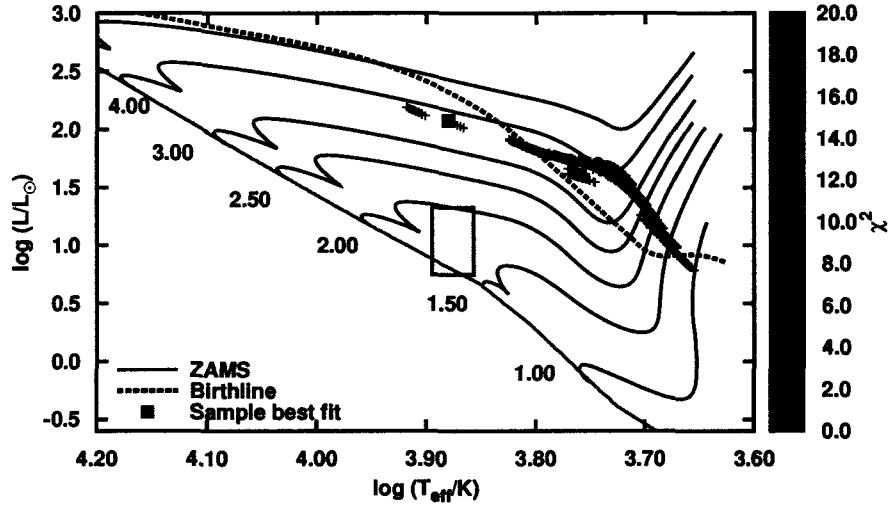

Figure 3.11: χ^2 fit to all frequencies of V1026 Sco detected by *MOST*, ℓ= 0 to 3 modes. Best fits are of very high luminosity. HRD position of the star is indicated by the error box.

the distance, extensive simultaneous multi-broad-band observations have not been performed, as was done for V351 Ori (van den Ancker, Thé & de Winter 1996), so the level of obscuration is unknown. The end result is that the true luminosity remains quite uncertain, except for the fact that it should be consistent with luminosity class V found by observers. Here I use the luminosity found by Monnier et al. (2005) through fitting of the SED, $L = 8.8 \pm 2.5$ $L_\odot$. However, Monnier et al. (2005) used a very precise distance of 116 pc. To better reflect the uncertainty in the distance, this luminosity range was expanded to reflect the uncertain distance to the Sco R1 star-formation region; this gives $\log(L/L_\odot) = 0.75$ to 1.33.

δ-Scuti pulsation in V1026 Sco was first detected by Kurtz & Müller (2001), in which a frequency peak of 23.4 $\pm$ 3.6 c/d was found in the Fourier analysis of the light curve of the star. This frequency was based upon only 6.6 hours (one night) of ground-based broad-band observations. Further observations were undertaken in 2006 and 2007 by *MOST* in which 12 significant frequencies not thought to be instrumental were detected in both data sets, the results reported by this research group in Zwintz et al. (2009b). Asteroseismological analysis proved to be quite unsatisfactory, with rotation thought to be the main quantity not included within the models that could

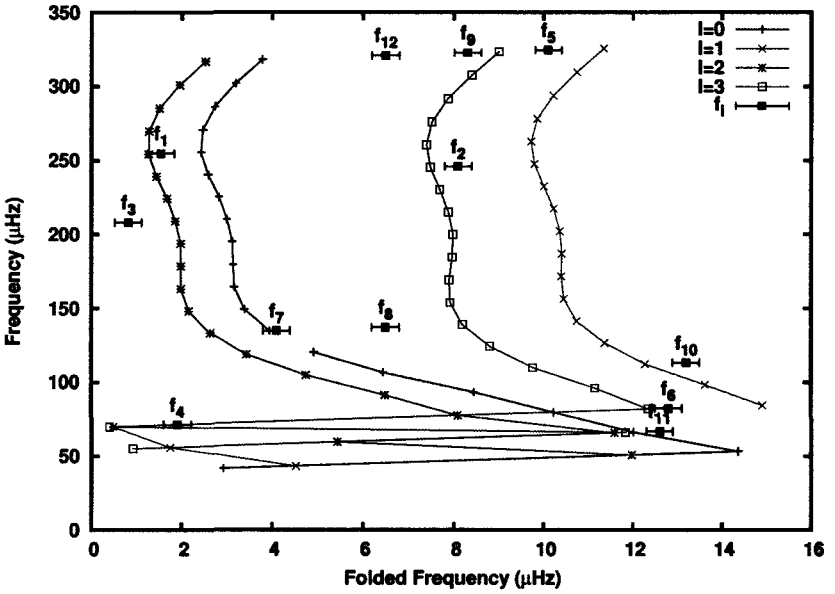

Figure 3.12: Sample echelle diagram for all frequencies observed by *MOST* of V1026 Sco. Model parameters: $\chi^2 = 16.0$, mass = 3.71 $M_\odot$, $\log(T_{eff}/K) = 3.88$, $\log(L/L_\odot) = 2.08$.

be leading to unsatisfactory fits to the data. The results of that analysis are repeated here, with some additional insight added since the initial paper was published. The frequencies for the 2007 season are used in the analysis, as these observations had a longer time base ($\sim$ two weeks) compared to the 2006 observations ($\sim$ one week). The frequencies are shown in tabular and graphical form in Figure 3.10, and show two dominant peaks straddling 250 μHz, with the overall maximum amplitude of order 2.5 mmag, but most frequency amplitudes are significantly smaller than this. Note that in the original observations of Kurtz & Müller (2001) their single frequency would have been an unresolved blend of f_1 and f_2, and perhaps even of f_3.

χ^2 fits to all frequencies reveal the best fits at much higher luminosities than the position in the HR diagram, but these values, even so, are not very satisfactory, with $\chi^2 \sim 15.9$ (Figure 3.11). An echelle diagram (Figure 3.12) reveals some of the potential problems: the frequencies f_5, f_9 and f_{12} could be part or all of a rotational splitting of a given (n, ℓ) mode, with perhaps f_7 and f_8 another such splitting. However, the differences between modes with different ℓ values (such as the small spacing) are of

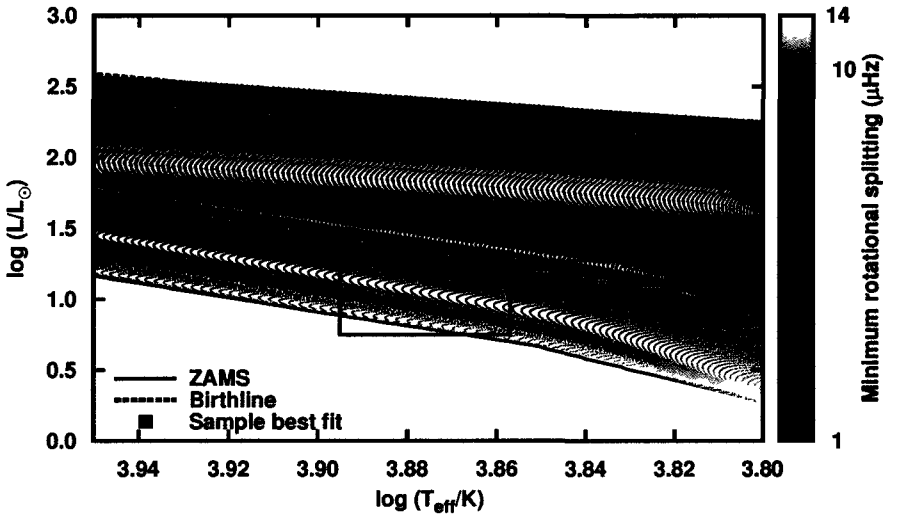

Figure 3.13: Estimated value of minimum rotational splittings for V1026 Sco based upon $v \sin i = 70$ km/s.

the same order, considerably confusing the matter. Using the value $v \sin i = 70$ km/s, one can make a lowest-order prediction of the expected minimum magnitude of the splittings for this star. Figure 3.13 shows these calculations. For the high luminosities the differences between f_5, f_9, and f_{12} could be from successive m values, but for lower luminosity values the frequency splittings are much larger, ranging from ~ 7 through 11 μHz, far larger than the ~ 2 μHz between the various close pairs, and making it far less likely that these frequencies are from a single, rotationally-split multiplet.

Looking at the frequencies as a whole, there are two useful constraints the observed frequencies put on the stellar models: 1) the fundamental frequency of the star needs to be lower than $f_{11} = 66.8$ μHz, the lowest observed frequency, otherwise f_{11} cannot be a p mode; 2) the acoustic-cut-off frequency must be higher than f_5, the highest frequency, otherwise it, too, could not be a p mode. In both cases we are assuming that these frequencies are p-mode pulsation frequencies despite the low amplitudes associated with each. Together, these two constraints significantly limit the luminosity to between approximately $\log(L/L_\odot) = 1.6$ and 2.1 (Figure 3.14), with the best-fit models from Figure 3.11 appearing at the very top of this range.

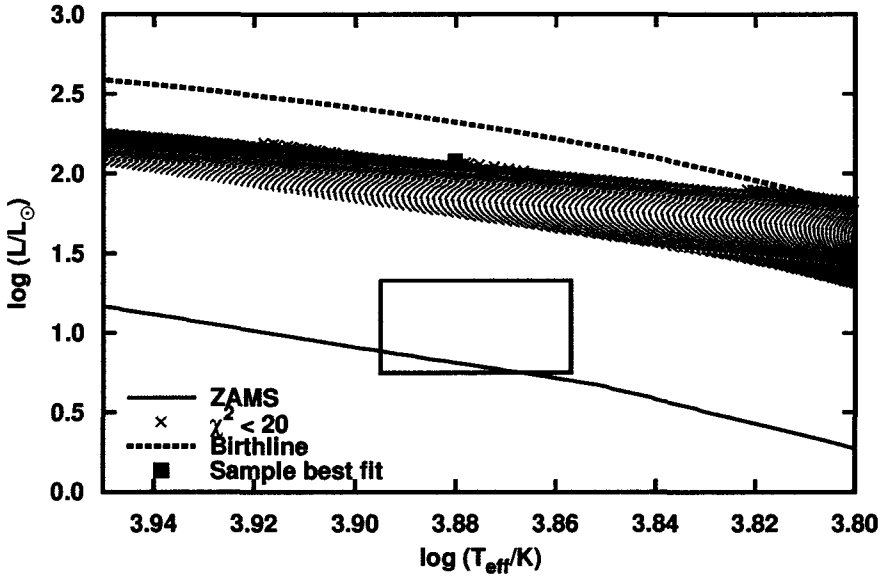

Figure 3.14: Stellar models that can support all the frequencies of V1026 Sco that were observed by *MOST* considering the fundamental and acoustic-cut-off frequencies of each model. Blue "×" indicate models with $\chi^2 < 20$. The filled square indicates the position of the best-fit model of Figure 3.12 ($\chi^2 = 16.0$).

Unfortunately, these luminosities are *not* consistent with the luminosity class agreed upon by observers (class V), with the luminosities more consistent with bright class III objects. Here I now provide a demonstration of what an asteroseismic analysis would have produced had results from less-precise instrumentation been obtained, yielding only the the three highest-amplitude frequencies, f_1 through f_3. Here, f_1 = 254.64 μHz and f_3 = 208.02 μHz are the highest and lowest frequencies, respectively. These frequencies can be supported by models consistent with the luminosity class for the star. As in Zwintz et al. (2009b), fits to only $\ell = 0$ and 1 modes produce only high-luminosity solutions with low χ^2 values (not shown). Expanding fits to $\ell = 3$ modes produces good fits at the correct luminosity range (Figure 3.15), with a mass of around 1.73 $M_\odot$. Mode identification is: f_1 = (n=3, ℓ=1), f_2 = (2,0) and f_3 = (0,3). (Note that a slightly different model on the same evolutionary track produced mode identification: f_1=(2,2), f_2=(1,3) and f_3=(0,3).) In both cases the frequencies are of low radial order, *i.e.* not in the asymptotic regime. The difference between

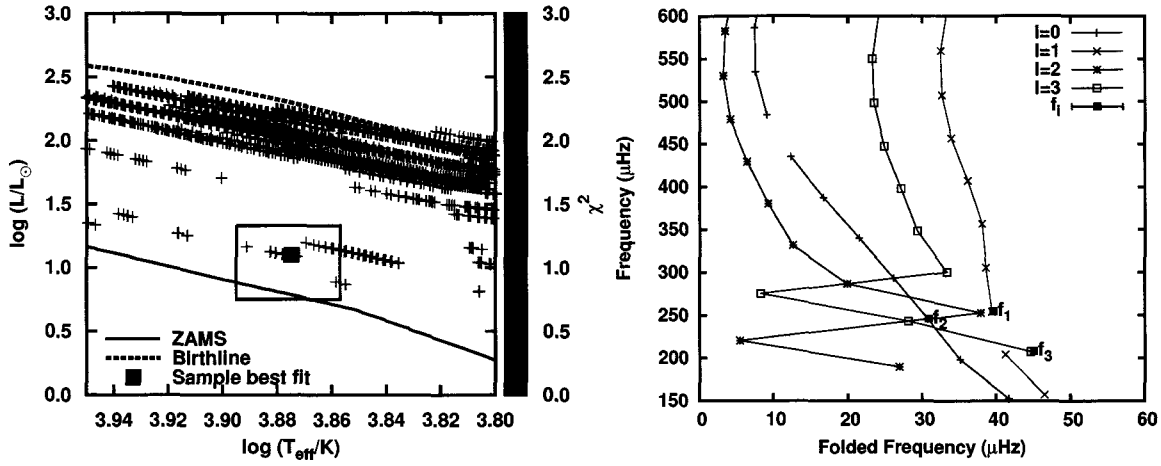

Figure 3.15: χ^2 fit to f_1 through f_3 of V1026 Sco detected by *MOST*, ℓ= 0 to 3 modes. In this case a number of good fits are obtained that agree with the observed luminosity class of the star. Model parameters: $\chi^2 = 0.84$, mass = 1.73 $M_\odot$, log (T_{eff}/K) = 3.87, log $(L/L_\odot)$ = 1.10

this latter result and the original that included all of the frequencies is striking, and demonstrates how much the quality of the observations can impact the results of an asteroseismic analysis of a star.

In summary, this star still remains a problem, but the problem has been quantified to a higher degree of precision than before. The luminosity class of the star, the independently-determined HRD position from broad-band photometry and spectroscopy, and the asteroseismic HRD position do not agree with one another. If the low-amplitude frequencies are not pulsation frequencies, then these need to be explained, either as an instrumental effect, or as a signature of some other stellar process, a problem that does not fall within the realm of this thesis. If the observed pulsation frequencies hold up to future results, then more spectroscopy and better distance estimates to the star will be needed to reconcile the the star's position in the HRD.

3.1.1.4 V1366 Ori (HD 34282)

V1366 Ori is a $V = 7.84$ magnitude-bright Herbig Ae star, first identified as a HAe star by Thé, de Winter & Perez (1994), variously classified in the past between

ID	freq (c/d)	err freq. (c/d)	freq (μHz)	err freq. (μHz)	Amp. (mmag)	A06 ID
f_1	79.423	0.001	919.24	0.01	6.344	A10
f_2	79.252	0.002	917.27	0.02	3.523	A9
f_3	75.416	0.002	872.87	0.02	3.339	A7
f_4	75.864	0.002	878.05	0.03	2.427	A8
f_5	75.356	0.002	872.18	0.03	2.205	A6
f_6	71.589	0.003	828.58	0.03	2.075	A4
f_7	71.525	0.003	827.84	0.03	1.862	A3
f_8	57.060	0.003	660.42	0.03	1.681	A1
f_9	71.972	0.002	833.01	0.03	1.630	A5
f_{10}	68.152	0.003	788.80	0.03	1.475	A2
f_{11}	64.695	0.003	748.79	0.04	1.245	-
f_{12}	61.053	0.004	706.63	0.05	0.754	-
f_{13}	67.787	0.005	784.58	0.05	0.714	-
f_{14}	71.043	0.005	822.26	0.05	0.707	-
f_{15}	75.402	0.004	872.70	0.05	0.658	-
f_{16}	53.427	0.005	618.37	0.06	0.553	-
f_{17}	67.534	0.005	781.65	0.06	0.524	-
f_{18}	75.448	0.006	873.24	0.07	0.492	-
f_{19}	68.669	0.006	794.78	0.07	0.448	-
f_{20}	72.319	0.006	837.03	0.07	0.418	-
f_{21}	60.353	0.006	698.53	0.07	0.377	-
f_{22}	67.465	0.007	780.84	0.08	0.345	-

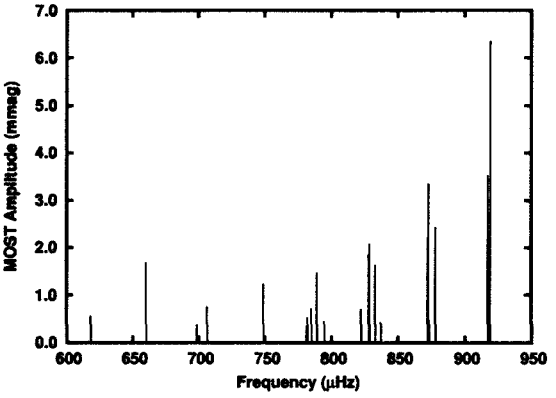

Figure 3.16: Pulsation frequencies for V1366 Ori as observed by *MOST*. The last column (A06 ID) cross references frequencies to those reported by Amado et al. (2006).

spectral types A0 and A3 (*e.g.* Vieira et al. 2003; Mora et al. 2001; Merín et al. 2004). Mora et al. (2001) report $v \sin i = 129 \pm 11$ km/s. The latest Hipparcos reductions report a parallax of 5.2 ± 1.7 mas, corresponding to a distance of 145 to 280 pc (van Leeuwen 2007). With temperature estimates as high as $T_{eff} \sim 9530$ K (Vieira et al. 2003), past analysis has placed V1366 Ori at the blue border of the classical instability strip, either just above or on the ZAMS, and sometimes anomalously below the ZAMS (Vieira et al. 2003). At this position in the HRD, the star's PMS nature is particularly ambiguous - it would appear that V1366 Ori has almost reached the ZAMS, or has only recently done so, and has thus just started to burn hydrogen in its core. It is possible that past reddening/extinction calculations for this star have underestimated the dust and gas obscuration for this star, and is thus intrinsically more luminous than previously thought. However, using standard de-reddening/extinction calculations, I find the HRD position is *not* anomalous, with the star's minimum luminosity about 0.1 dex in luminosity above the ZAMS (Figure 3.18).

Merín et al. (2004) found V1366 Ori has an anomalously low metallicity, [Fe/H] = -0.8 (fractional metal content by mass, Z=0.004). Such a low metallicity for a supposedly PMS star in the disk of the Milky Way poses questions regarding the true evolutionary status of the star; unless there are patches of low-metallicity material within the ISM from which the star could form, a newly-formed star should not otherwise have such low metal content. One solution is that perhaps this star is also a λ-Bootis star, with depressed levels of heavier metals at the surface, but near-solar values for carbon, nitrogen, and oxygen (CNO) throughout, and near-solar values for heavy metals below the surface layers of the star as well. The λ-Bootis characteristics could be the result of recent preferential accretion of metal-depleted gas over metal-rich dust, *e.g.* as outlined in Kamp & Paunzen (2002). In this case V1366 Ori could consistently be a PMS (or new MS star) without otherwise needing to question the low metal abundance of the star. In the past, Gray & Corbally (1998) observed this star as part of a systematic campaign to identify λ-Bootis characteristics in young A-type stars, in which they classified V1366 Ori as *A0.5 Vb (shell)r* in their extended Morgan-Keenan classification system, but failed to detect λ-Bootis characteristics. On the other hand Gray & Corbally (1998) did *not* report an anomalously low Z for the star, as later found by Merín et al. (2004). The source of this discrepancy is unknown. Low metallicity and high $v \sin i$ is confirmed by P. Amado (personal communication) for heavier metals, but so far analysis of the required lighter metals (CNO plus S) is not complete — blending of the relevant spectral lines with other lines caused by the high $v \sin i$ of the star make these determinations difficult, and final results are pending.

If V1366 Ori has indeed [Fe/H]=-0.8 throughout the star, not just in the upper layers, then this star could be a Population II star, and therefore an SX Phe star, the Pop. II equivalent of a δ-Scuti star. Explaining the disc material surrounding the star then becomes a problem, as unless something drastic has happened in the star's recent past, such an evolved system is not expected to contain obscuring circumstellar material. Note, however, that SX Phe stars tend to be blue stragglers, stars that are

supposedly too old to be located in their current observed place in the HRD; if a blue straggler spent its entire evolutionary history as a single star, then it should have evolved to another part of the HRD by now. Blue stragglers are thought to be the result of mass transfer in a binary system, or the product of the merger of two smaller stars. If such an event happened in the near past, then perhaps this is the source of the disk of material in V1366 Ori, and the system becomes interesting for reasons other than its (then) misidentification as a PMS star. However unlikely this scenario, it is a possibility that must be kept in mind, although it is not considered in this analysis, as modelling the product of a stellar merger is beyond the scope of this thesis. In this analysis I will use low-metallicity (Z = 0.004) as well as solar metallicity (Z = 0.02) PMS evolutionary tracks and compare the results.

Amado et al. (2004) discovered high-frequency δ-Scuti-type pulsations in V1366 Ori. A multi-site ground-based observation campaign then discovered ten frequencies with values ranging from 64.7 to 79.4 c/d (Amado et al. 2006). Significantly, these are the highest published frequencies for a δ-Scuti star of any type to date, and so regardless of PMS status, V1366 Ori is a star particularly worthy of asteroseismic analysis. V1366 Ori was therefore observed by *MOST* for 31 consecutive days in December 2007/January 2008, the results are reported here for the first time in written form, with a paper on the results currently in preparation (Casey et al. 2011).

During the observations V1366 Ori showed only moderate peak-to-peak irregular variability in the integrated light of less than 0.1 magnitude from circumstellar gas and dust. Significantly, this is in contrast to observations of V1366 Ori made by Malfait, Bogaert & Waelkens (1998), in which they report variations of ~ 2.5 V magnitudes over the course of their study, and so the MOST observations seemed to have been fortuitously taken during a period of relative quiescence, with no large changes in the amount of obscuring CS material.[2] K. Zwintz and I independently carried out the frequency analysis of V1366 Ori, and the results compared. 22 independent

[2]HAe stars that undergo UX Ori can have these periods of relative quiescence, followed by periods of large peak-to-peak variability, and so capturing the star in a period of quiescence is a matter of luck, but is not necessarily surprising.

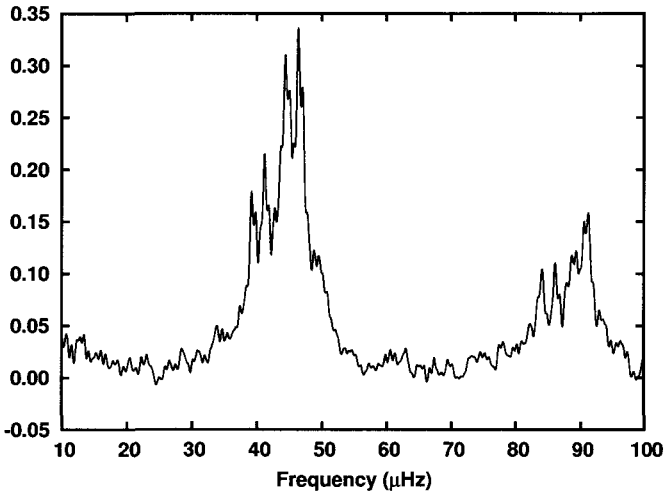

Figure 3.17: Autocorrelation function performed on the scrubbed V1366 Ori light curve from MOST

frequencies were detected, concentrated in a region between $\sim$ 50 and 80 c/d (or 575 and 925 μHz). The results are displayed in tabular and graphical form in Figure 3.16.

Collectively the pulsation spectrum is quite striking, with distinct groupings of frequencies approximately every 45 μHz with an abrupt cut off in power above the highest frequency where one might otherwise expect the pattern to drop off in amplitude if it should continue to higher frequencies. Using a self-written computer code, an auto-correlation function was performed on the light curve (removed of all other known signals other than the pulsations) and reveals a distinct peak of 46.4 μHz (Figure 3.17). This is part of a broad band running from approximately 40 to 50 μHz. Unsurprisingly, χ^2 fits to models yield no good fits to $\ell = 0$ to 3 modes (not shown; best χ^2 value was around 915 within the error box). The cause of this distinct pattern is unknown, however it may be related to the large spacing of the star, in which case from visual inspection alone one might surmise that the detected frequencies range over 8 radial orders. Why subsequent frequencies of lesser amplitudes in a particular group would be clustered about a central mode is unknown. Figure 3.18 shows the average large spacings expected, and therefore where one might

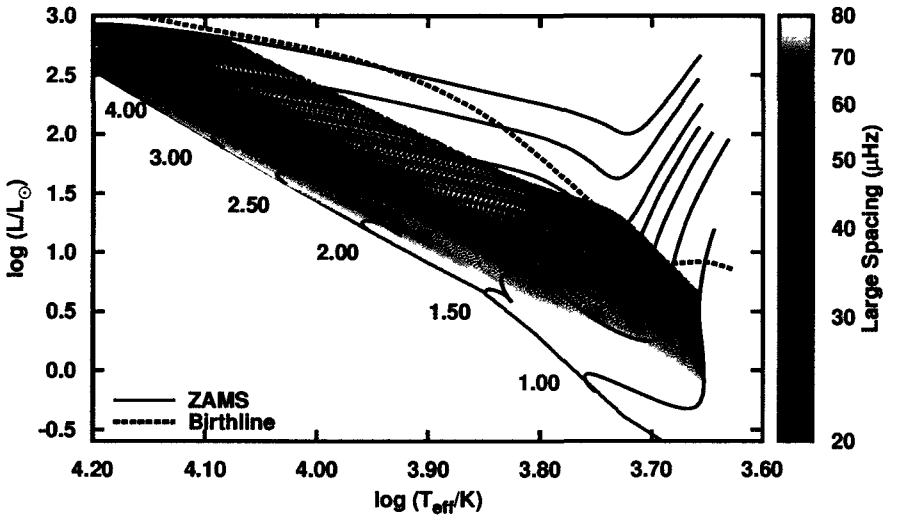

Figure 3.18: Large spacing of models that fall within the observational range of V1366 Ori, as well as the star's position in the HRD (error box).

expect to find a solution if the pattern is related to the large spacing. In this case, a large spacing of 40 to 50 passes through the approximate middle of the observational error box. Further evidence, examined below, also supports these luminosities for this star. Figure 3.19 demonstrates how a folding frequency of 43 μHz in this case causes the groupings to stack on one side of an echelle diagram. Some of the groupings are spread out by as much as $\sim$ 15 μHz, but none of the frequencies appear in the right hand side of the echelle diagram — with this many frequencies in play, one might expect frequencies to appear in the right-hand side of the diagram if either the folding frequency was ill chosen, or there was no obvious regular spacing evident in the data.

Note that some of the frequencies seem to have differences of about 2 to 4 μHz, which one might identify as multiplets of a rotationally-split non-radial mode. Figure 3.20 demonstrates that this is unlikely; a lowest-order estimate of the *minimum* rotational splitting between two successive m modes for a given ℓ mode based upon $v \sin i = 129 \pm 11$ km/s of Mora et al. (2001) is too large, particularly when limited to models for which the acoustic-cut-off frequency is higher than f_1, otherwise this star could not support f_1 as a p-mode frequency. Here, the minimum average split-

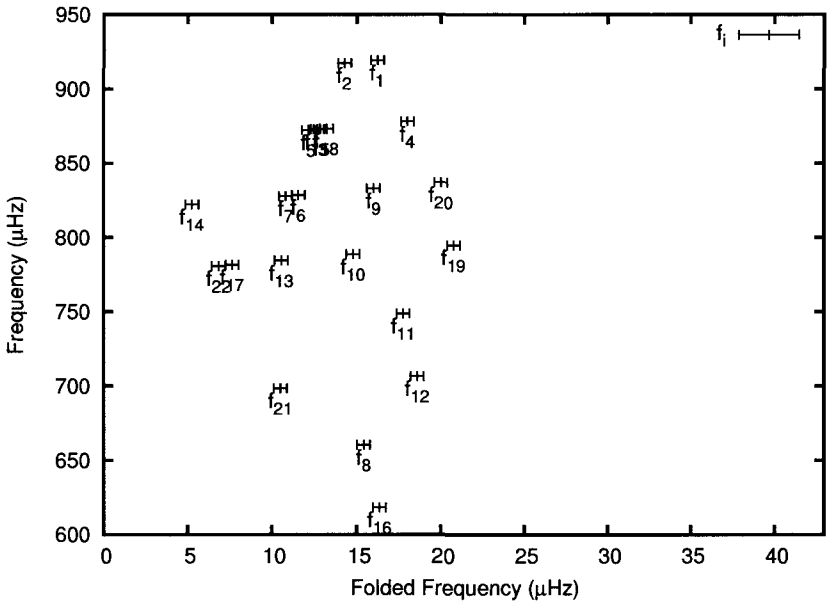

Figure 3.19: Sample echelle diagram for all frequencies of V1366 Ori observed by *MOST*. A folding frequency of 43 μHz is used to show how the frequencies fall into groups separated approximately by 40 to 46 μHz.

ting is around 10 μHz, and so these frequencies are unlikely to be part of a single, rotationally-split multiplet.

It is probable that some physical phenomenon is driving the frequencies in this regular pattern, but the mechanism is not known. As speculated above, these spacings of 40 to 50 μHz could be related to the large spacing between successive radial orders of a given azimuthal order, ℓ. As an experiment, weighted means of each "grouping" were calculated according to two different schemes, the first one takes the weighted mean using the sum of the amplitudes and frequencies in each group:

$$H_j = \frac{\sum_{i=1}^{N_j} f_{ji} a_{ij}}{\sum_{i=1}^{N_j} a_{ji}}, \tag{3.1}$$

where a_{ji} and f_{ji} are the i^{th} constituent amplitudes and frequencies of the j^{th} grouping, with resultant weighted frequency, H_j. N_j is the number of frequencies included in

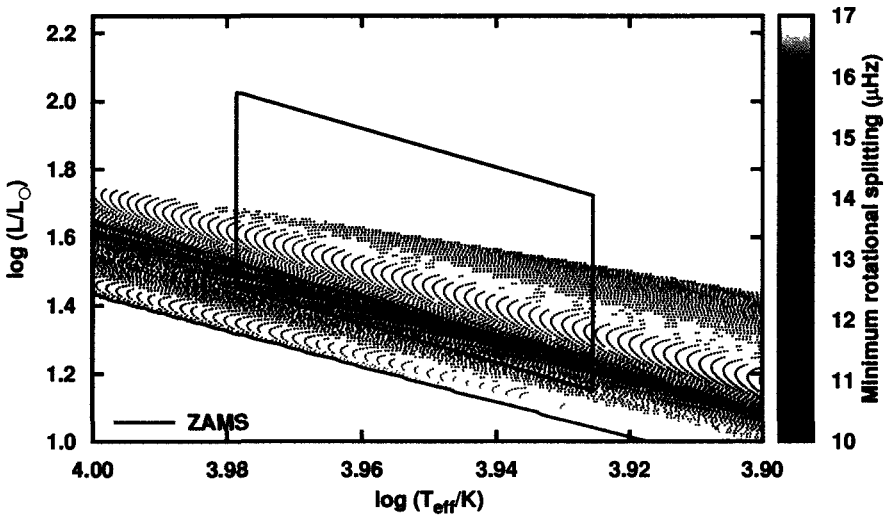

Figure 3.20: Estimated value of the minimum rotational splittings of 118 km/s for V1366 Ori (based upon $v \sin i = 129 \pm 11$ km/s of Mora et al. 2001), limited to those models for which the acoustic cut-off frequency is greater than $f_1 = 919.24$ μHz.

the j_{th} group. The second scheme uses squared amplitudes in the sums,

$$H_j = \frac{\sum_{i=1}^{N_j} f_{ji} a_{ji}^2}{\sum_{i=1}^{N_j} a_{ji}^2}. \tag{3.2}$$

The results are listed in Figure 3.21 in both graphical and tabular format. The results are listed in the order of increasing frequency. Note that the low amplitudes and small number of component frequencies for some groups such as H_1, H_2 means the results of these calculations should be viewed with caution. Both schemes yield similar results, with maximum differences between the two cases of about 1 μHz. More rigorous analysis of the potential errors could be performed, however even this simple calculation yields interesting results.

The weighted frequencies can then be compared to either strictly $l = 0$ or $l = 1$ modes to match up the large spacings between consecutive radial orders of pulsation. Given the differences between the a and a^2 cases are at most 1 μHz, 1 μHz errors are assigned to the H_j for the purposes of χ^2 fits. This is merely to allow χ^2 values

H_j ID	Orig ID	j,i	f_{ji} (μHz)	a_{ji} (rel amp)	$\sum a_{ji}$ (rel amp)	$\sum a_{ji}^2$ (rel amp^2)	$H_{j,a}$ (μHz)	H_{j,a^2} (μHz)
H_1	f_{16}	1,1	618 37	0 510	0 510	0 260	618 37	618 37
H_2	f_8	2,1	660 42	1 549	1 549	2 400	660 42	660 42
H_3	f_{21}	3,1	698 53	0 348	1 043	0 604	703 93	705 01
	f_{12}	3,2	706 63	0 695				
H_4	f_{11}	4,1	748 79	1 148	1 148	1 317	748 79	748 79
H_5	f_{22}	5,1	780 84	0 317	3 321	2 786	786 85	787 62
	f_{17}	5,2	781 65	0 483				
	f_{13}	5,3	784 58	0 658				
	f_{10}	5,4	788 80	1 360				
	f_{19}	5,5	794 78	0 413				
H_6	f_{14}	6,1	822 26	0 651	6 168	9 434	829 31	829 26
	f_7	6,2	827 84	1 716				
	f_6	6,3	828 58	1 913				
	f_9	6,4	833 01	1 502				
	f_{20}	6,5	837 03	0 385				
H_7	f_5	7,1	872 18	2 033	8 410	19 198	874 09	874 07
	f_{15}	7,2	872 70	0 606				
	f_3	7,3	872 87	3 080				
	f_{18}	7,4	873 24	0 453				
	f_4	7,5	878 05	2 237				
H_8	f_2	8,1	917 27	3 250	9 110	44 903	918 54	918 78
	f_1	8,2	919 24	5 860				

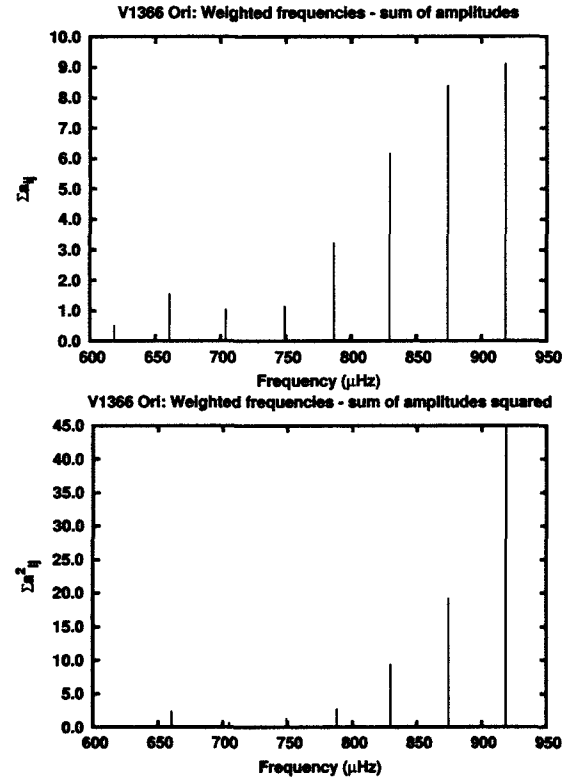

Figure 3.21: Weighted frequencies for V1366 Ori.

to be calculated, recognizing that the results are relative in this case, with absolute numbers not to be interpreted with rigour. H_j values for the a case are used in χ^2 fits.

The top row of Figure 3.22 shows the results of the purely-radial ($\ell = 0$) modes, along with a sample echelle diagram. There is a group of very reasonable fits (particularly considering the ad-hoc nature of the weighted-frequency calculations) that falls in the middle of the star's HRD uncertainty box. There are also some good fits at lower temperatures. The echelle diagram reveals some very interesting results: the weighted frequencies simultaneously fit the very highest eight radial-order modes the star can support (n = 13 through 20) with no calculated, nor observed frequencies above H_8, implying that the star is pulsating at the frequencies just below the acoustic cut-off frequency. The red series of dots through the middle of the HRD position also indicate the models with an acoustic cut-off frequency within one large spacing of the highest frequency of pulsation. Simultaneously, the large spacing has

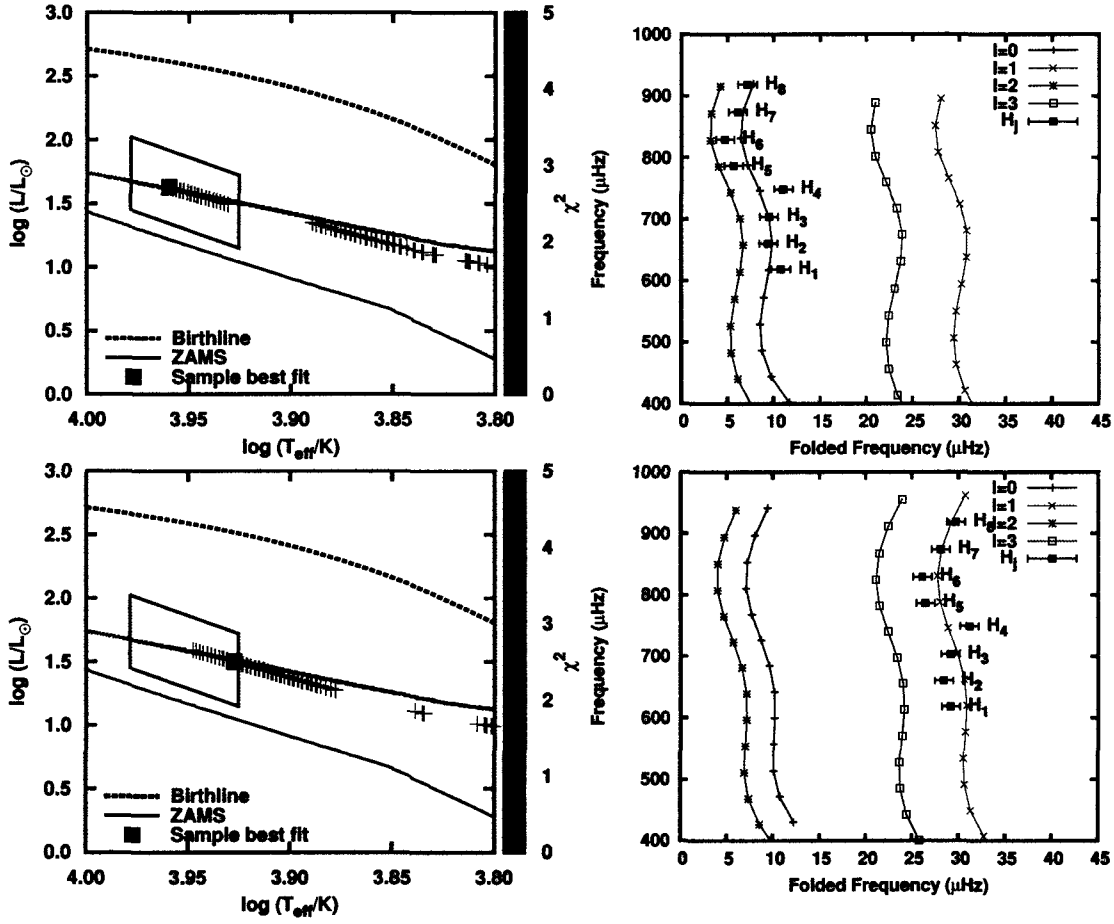

Figure 3.22: χ^2 fits to weighted frequencies for V1366 Ori. Top row: $\ell = 0$ models only. Red dots through the middle indicate models with acoustic-cutoff frequencies that fall within one large spacing of H_8, the highest-valued frequency group. Model parameters: $\chi^2 = 1.79$, M = 2.30 $M_\odot$, $\log(T_{eff}/K) = 3.960$, $\log(L/L_\odot) = 1.629$. Bottom row: $\ell = 1$ models only, model parameters: $\chi^2 = 2.42$, M = 2.15 $M_\odot$, $\log(T_{eff}/K) = 3.927$, $\log(L/L_\odot) = 1.498$.

been fit by successive groups of frequencies, which then show that the best fit to those frequencies predicts that the top frequency group is within one large spacing of the acoustic cut-off frequency. Collectively this provides an explanation for the abrupt cut off in amplitude above H_8 even though amplitudes were rising with each consecutive frequency grouping up to H_8: the acoustic cut-off frequency has been reached for this star. If this analysis is correct, this is the first δ-Scuti star of any evolutionary status found to be pulsating at the acoustic cut-off frequency, and is therefore an important discovery.

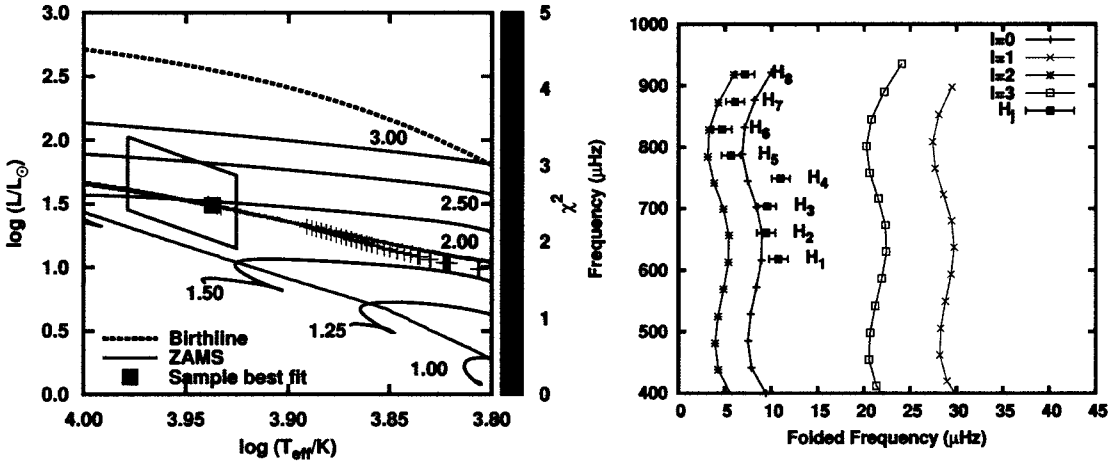

Figure 3.23: χ^2 fits to weighted frequencies for V1366 Ori, $\ell = 0$ models only, low metallicity (Z = 0.004). The series of red dots is as in Figure 3.22. Sample echelle is for $\chi^2 = 1.62$, M = 1.96 $M_\odot$, $\log(T_{eff}/K) = 3.937$, $\log(L/L_\odot) = 1.489$.

Further χ^2 fits were performed to $\ell = 1$ modes only, the results shown in the bottom row of Figure 3.22. The results are similar in quality, with a line of good fits that are a bit cooler than those of the $\ell = 1$ case. The echelle diagram for a sample best fit for a model in agreement with the star's position in the HRD shows one frequency exists above H_8, indicating that H_8 is not within one large spacing of the acoustic cut-off frequency. However, given that certain physics (such as rotation) are missing from the stellar models (and hence change some of the relevant quantities, such as the acoustic cut-off frequency, itself), the values are perhaps close enough that the acoustic cut-off frequency could be responsible for the abrupt cut off in power on the high end of the frequency spectrum.

Weighted frequencies were also compared to low-metallicity (Z = 0.004) PMS evolutionary models between 1.00 and 3.00 $M_\odot$, specially computed for this star. The results are shown in Figure 3.23. The evolutionary tracks shown are low-Z tracks. For comparison, the ZAMS shown is for the Z = 0.02 case, indicating that the ZAMS for the low-Z case (outlined by the lowest points of each evolutionary track) is of lower luminosity at a given temperature than for the high-Z case. Quantitatively, the results are not as good as for the Z = 0.02 case, but qualitatively give the same

result: a star pulsating in high radial orders (n = 13 though 20) up to the acoustic cut-off frequency (note the models with $\chi^2 < 5$ that fall within the HRD position of the star are partially obscured by the symbol indicating the sample best-fit model, as there aren't many such models as in the Z = 0.02 case), so this results appears to be reasonably robust with respect to stellar chemical composition.

Overall, comparison between Z = 0.02 and Z = 0.004 favours the Z = 0.02 case, perhaps suggesting λ-Bootis characteristics for the star. The low-Z models predict slightly lower masses. However, the models do not contain rotation, and with a $v \sin i$ = 129 $\pm$ 11 km/s, rotation probably plays a large enough role to make the differences between the high- and low-metallicity fits insignificant, and it is probably inadvisable to draw many conclusions from the asteroseismic comparison. Regardless, once again, the result of pulsation at or near the acoustic cut-off limit appears to be robust with respect metallicity, and further reinforces this important finding.

In summary, V1366 Ori not only has the highest δ-Scuti frequencies reported, it has a distinct pulsation spectrum in two senses: the groupings of frequencies that are observed, and the abrupt cut-off in power above a certain frequency. If the groups are related to the large spacing of the star, then the groups and cut-off together very narrowly predict a set of solutions in the HRD where both the acoustic cut-off and the large spacing are in agreement with one another. These HRD positions are in agreeement with HRD positions as determined independently by spectroscopy, broad-band photometry, and parallax data. Finally, rotation may affect the pulsation spectrum of the star.

3.1.1.5 HD 37357

HD 37357 (PDS 191) is a V = 8.8 magnitude Herbig Ae star associated with the Orion A star-formation region (SFR), with spectral classifications ranging from B8/9 V (Sharpless 1952) through of A1 Va(e)r (Gray & Corbally 1998). The most recent spectral determinations have agreed upon spectral class to A0 or A1 Ve (*e.g.* Vieira

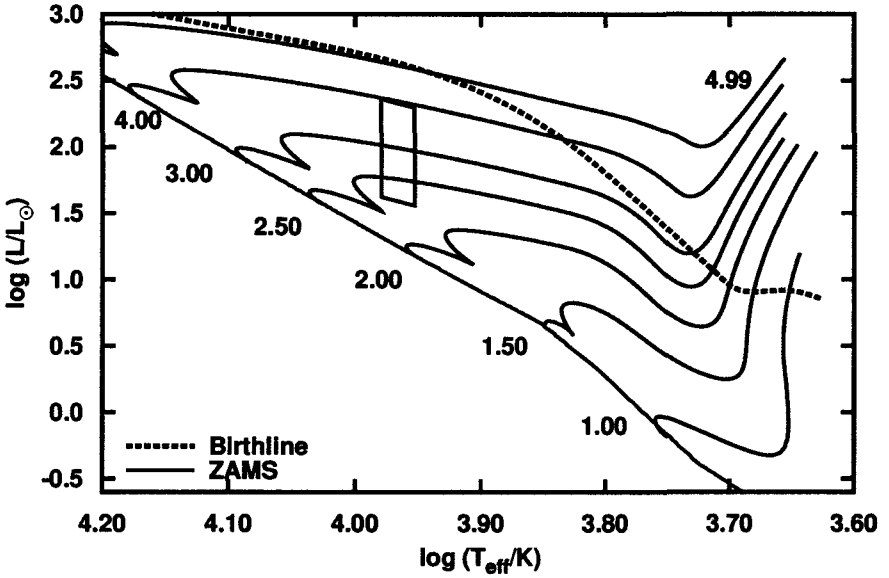

Figure 3.24: Position of HD 37357 in the HRD.

et al. 2003), so here I choose temperatures consistent with those two classes. The star has been included in a number of studies on HAeBe and similar stars (*e.g.* Malfait, Bogaert & Waelkens 1998; Vieira et al. 2003; Sartori et al. 2010). Unfortunately, the Tycho catalogue reports an unusable parallax of -0.2±10.1 mas (Perryman & ESA 1997). Therefore I use the distance range assigned by Vieira et al. (2003) of 300 to 700 pc from the star's association with the Orion A SFR. At present, there are no known $v \sin i$ determinations in the literature.

Observed by *MOST* as a guide star in November/December 2010 for approximately 14 days, during which BF Ori was the primary target, δ-Scuti pulsations were serendipitously discovered in the light curve of HD 37357 (K. Zwintz, private communication). Unfortunately, the complete analysis of the light curve is not yet available, and so only the above background information, and the star's position in the HRD are given (Figure 3.24). With a spectral class of A1, it is among the hotter stars in which PMS δ-Scuti pulsations have been detected. If the star's distance is correct, then it is also rather luminous; it will be interesting to discover if any of the

pulsation frequencies that are detected are low or high enough to put astroseismic constraints on the star's luminosity.

3.1.2 Multi-site ground-based observations

3.1.2.1 IP Per

IP Per is an UX Ori-type irregular variable that also exhibits δ-Scuti behaviour. The star most likely belongs to the Per OB2 association, with apparent magnitude usually around 10.4 in Johnson V, $B-V=0.33$ (Miroshnichenko et al. 2001). Note that the young open cluster, IC 348 (Section 3.3.2), is also thought to be part of Per OB2, and that IC 348 contains the PMS δ-Scuti star, V705 Per, hence V705 Per and IP Per could be closely related. Gray & Corbally (1998) report a spectral class of A7e kA3 mA3 III:e, indicating that the hydrogen lines have spectral class consistent with a A7 III star, with some uncertainty in the luminosity class, and with some emission apparent in the hydrogen lines. This classification also indicates that the star is metal-weak, exhibiting some λ-Bootis characteristics, with the metal lines resembling a hotter A3 star. Interestingly, the All-Sky Compiled Catalogue (ASCC; Kharchenko 2001) report a parallax for this star of $0.''042 \pm 0.''030$, corresponding

	2003 V dataset			2003 B dataset			2002 B dataset		
Label	Freq (c/d)	Amp (mmag)	Freq (μHz)	Freq (c/d)	Amp (mmag)	Freq (μHz)	Freq (c/d)	Amp (mmag)	Freq (μHz)
f_1	22.89	1 9	264 93	22 89	3 1	264 93	22.88	3 3	264 81
f_2	34 60	1 5	400 46	34.82	2 1	403 01	34 64	3 3	400 93
f_3	30 45	1 8	352 43	30 45	1 8	352 43	30 48	3 2	352 78
f_4	48 23	1 6	558 22	48 45	2	560 76	48.23	1 9	558 22
f_5	28 79	1 5	333.22				27 73	1 9	320 95
f_6	23 99	1 3	277 66						
f_7	9 30	1 3	107 64						
f_8	41 11	1 2	475 81	42 08	1 9	487 04	42 27	2 3	489 24
f_9	52 00	1 1	601 85						

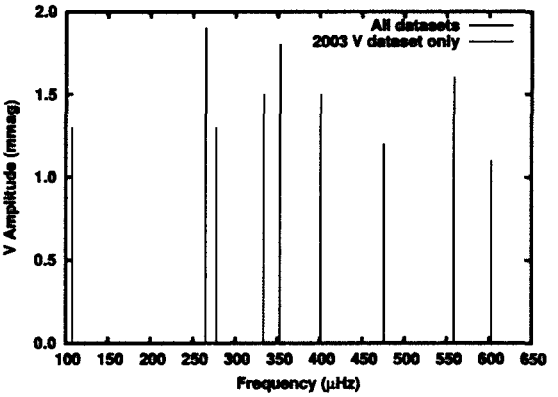

Figure 3.25: Pulsation frequency spectrum of IP Per as found by Ripepi et al. (2006). In the table, left to right respectively, uncertainties in the three datasets are $\pm$ 0.11, $\pm$ 0.15, $\pm$ 0.25 c/d, corresponding to ± 1.3, ± 1.7, and $\pm 2.9 \mu$Hz. In the graph, red lines indicate frequencies found in all datasets, whereas blue lines indicate additional frequencies found only in the 2003 V dataset.

to a distance of 14 to 79 pc. This distance contradicts all other evidence for the star, and places the star much too close to the sun for a star of its spectral class and apparent magnitude; for IP Per to be this dim at the distances reported in the ASCC would require massive amounts of reddening/extinction not otherwise supported by evidence such as the broad-band photometry and spectral classification. It suggests an error in the ASCC, and so this distance is not used in this analysis. The estimated distance to the Per OB2 association is used instead, ranging from 250 to 350 pc, as given by Černis & Straižys (2003) and de Zeeuw et al. (1999) respectively. Even these larger distances might be problematic: Figure 3.26 shows IP Per's position in the HR diagram after corrections for extinction and reddening have been performed, and shows the star's luminosity range straddles the ZAMS, inconsistent with the class III luminosity designation. It is quite possible that IP Per is a background star to Per OB2, and a larger distance might be indicated.

As part of a search for undiscovered pre-main-sequence δ-Scuti stars, variability in 5 to 9 frequencies ranging from 107 to 602 μHz was discovered, the result of a multi-site ground-based observing campaign performed by Ripepi et al. (2006). Not all frequencies were detected in all datasets, an indication of differing time baselines

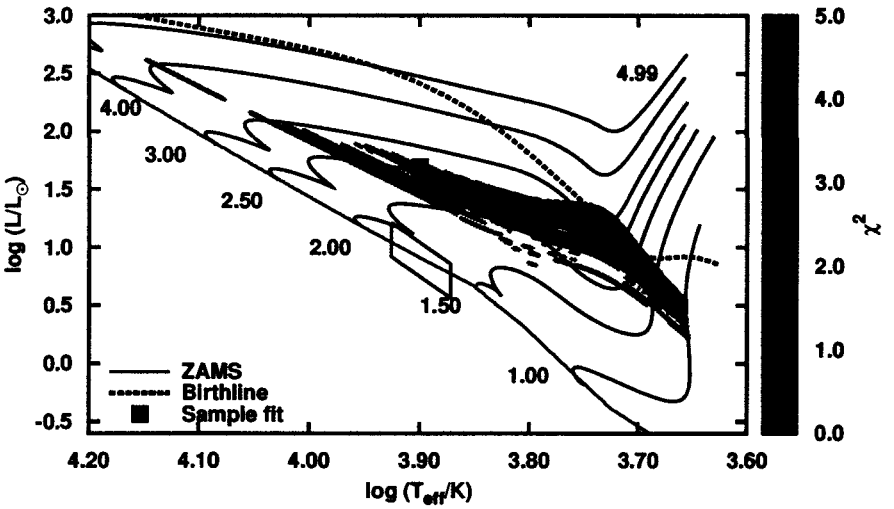

Figure 3.26: Simultaneous χ^2 fit $\ell = 0$ to 3 to all frequencies of the Ripepi et al. (2006) 2000 V dataset of IP Per, along with position of the star in the HRD.

for each dataset. The longest dataset (2003 V) yielded the most number of frequencies. The pulsation spectum is shown in Figure 3.25 in both tabular and graphical form. Unfortunately, depending upon the dataset, the uncertainty in frequencies of Figure 3.25 are large, ranging from ± 1.3 to ± 2.9 μHz, an indication of the short time base for each dataset, and so the likelihood of finding many possible asteroseismic solutions is large.

χ^2 fits to all nine frequencies of the 2003 V dataset (Figure 3.26) to PMS models reveal that all good fits to the data are much more luminous than the star's indicated position in the HR diagram, further suggesting that the distance to the star (and the assumption that it is part of the Per OB2 association) may be in error.

Figure 3.27 shows an echelle diagram for a good fit that is consistent with the temperature range of IP Per, and is therefore a potential solution if the star should prove to be a background star to Per OB2, and hence its luminosity underestimated. The diagram is revealing, in that it shows that the pulsation spectrum must span many radial orders of pulsation, regardless of the goodness of fit. With such a

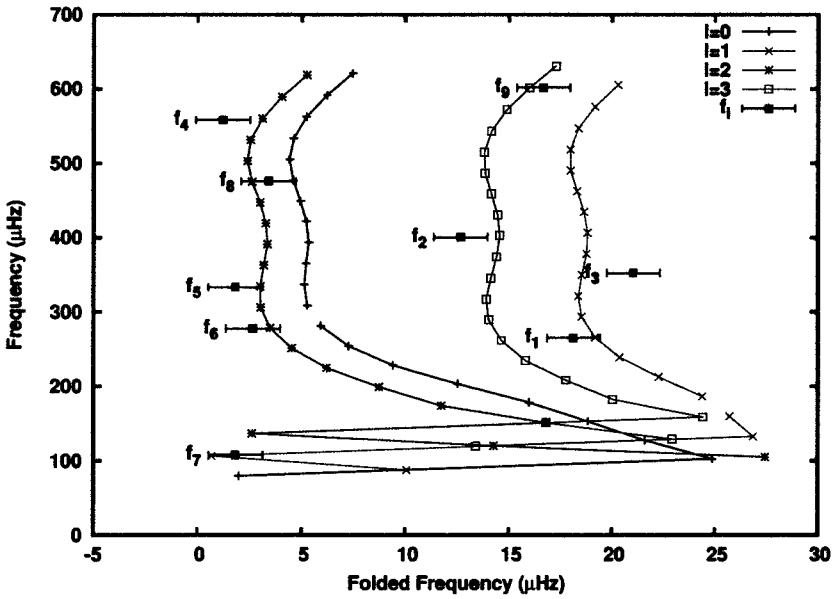

Figure 3.27: Sample echelle diagram for an over-luminous solution to the observed frequencies of IP Per. Model parameters: $\chi^2 = 1.2$, mass = 2.58 $M_\odot$, log (T_{eff}/K) = 3.99, log $(L/L_\odot)$ = 1.69, log g = 3.71.

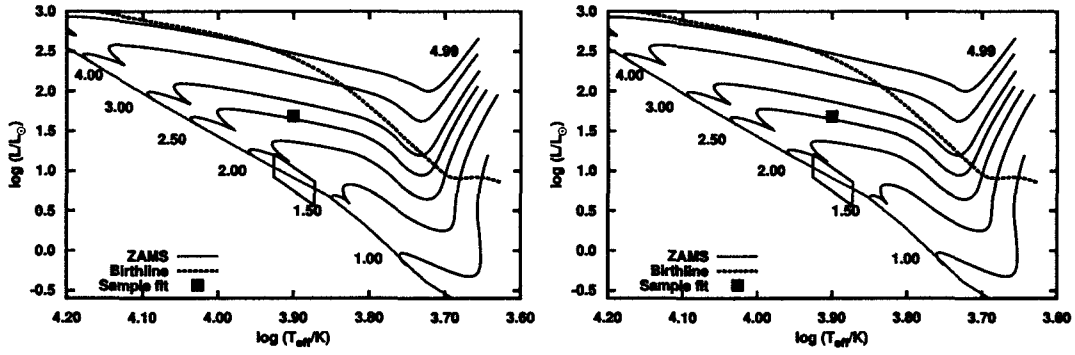

Figure 3.28: Left-hand side: models that can support the range of frequencies in the 2003 V dataset of IP Per, considering the fundamental and acoustic-cutoff frequencies of the models. Right-hand side: same as left-hand side, but minimum frequency considered is f_1 instead of f_7

wide range of frequencies, further insight can therefore be gained by considering the minimum ($f_7 = 107.64$ μHz) and maximum ($f_9 = 601.85$ μHz) frequencies observed, and using them to constrain the fundamental and acoustic cut-off frequencies of the models. Figure 3.28 reveals the models that can sustain all of the frequencies observed, along with the location of the sample fit from Figure 3.27. Significantly, none of the models consistent with IP Per's position in the HR diagram can support the minimum frequency, f_7 as a p-mode. This suggests that either f_7 is not a pressure mode, or IP Per is perhaps more distant than originally thought, and hence more

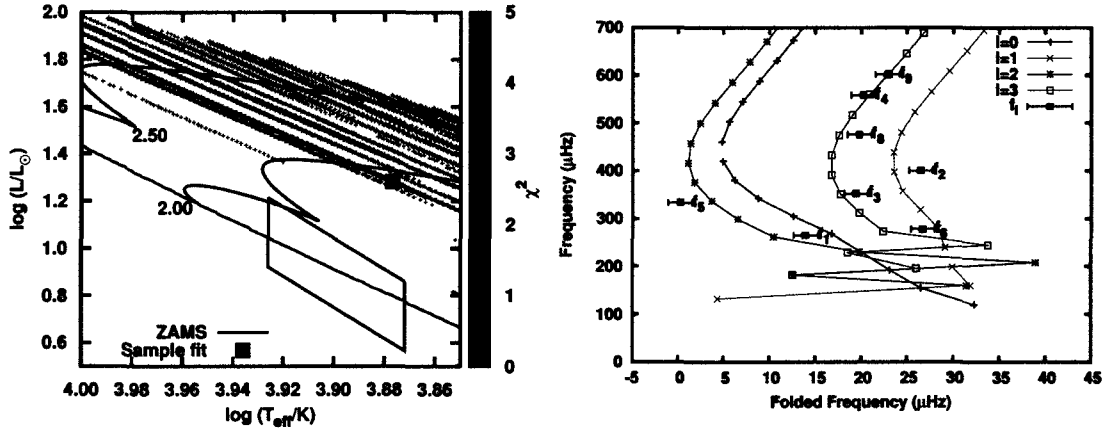

Figure 3.29: χ^2 fits to the frequencies of IP Per, excluding f_7, $\ell = 0$ to 3 modes only. Sample echelle is for $\chi^2 = 2.01$, M = 1.93 $M_\odot$, $\log(T_{eff}/\mathrm{K}) = 3.877$, $\log(L/L_\odot) = 1.282$.

luminous. However, it should be noted that f_7 is one of the frequencies detected only in the 2003 V dataset (and perhaps is therefore less reliable than those detected in all datasets), and if it should *not* be a p-mode frequency, then the analysis of the allowed models changes considerably when the next-lowest frequency, $f_1 = 264.93$ μHz, is used instead. The result is the right-hand side of Figure 3.28, and reveals that all models above the ZAMS, and otherwise consistent with the star's position in the HR diagram, *can* support IP Per's position in the HR diagram if f_7 is left out of the analysis. Does this help with further analysis? Figure 3.29 shows the results of χ^2 fits similar to the immediately preceeding case, except that f_7 is excluded from the analysis. Interestingly, although the frequency *range* is now compatible with IP Per's HRD position, χ^2 fits do not show any remarkable improvement over the previous case. There are many solutions compatible with higher luminosities, but none close to the star's position in the HRD. An echelle diagram with $\chi^2 = 2.01$ for a 1.93 $M_\odot$ star is typical. In this case, solutions in which f_8, f_4 and f_9 are indentified as modes of the same radial order are favoured, indicating large spacings of around 40 μHz. One again, the results support a higher-luminosity star despite excluding f_7 from the

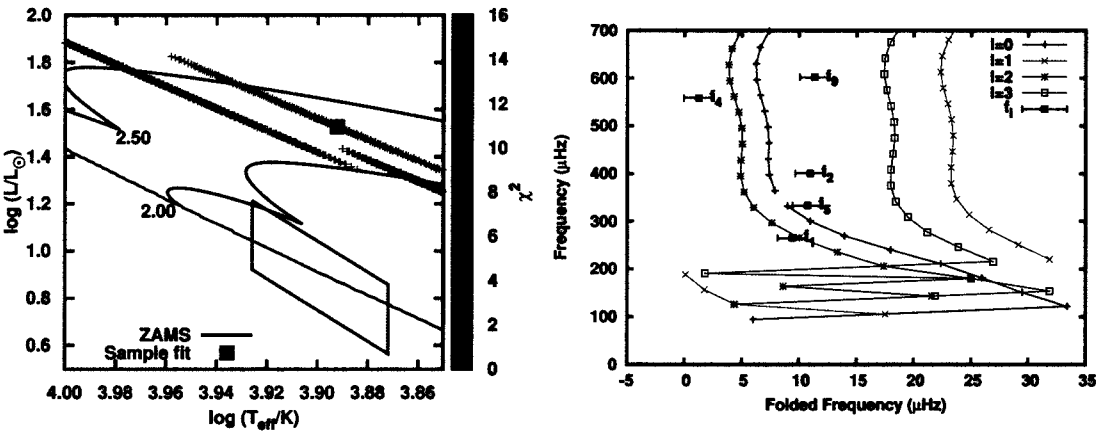

Figure 3.30: Simultaneous χ^2 fit to f_1, f_2, f_4, f_5, and f_9 of IP Per, radial modes only - best fits consistent with the star's temperature are an over-luminous family of solutions. Sample echelle is for $\chi^2 = 10.7$, M = 2.29 $M_\odot$, $\log(T_{eff}/\mathrm{K}) = 3.892$, $\log(L/L_\odot) = 1.528$. Note that even though non-radial modes appear in the echelle diagram, the frequencies were not permitted to be matched to these modes.

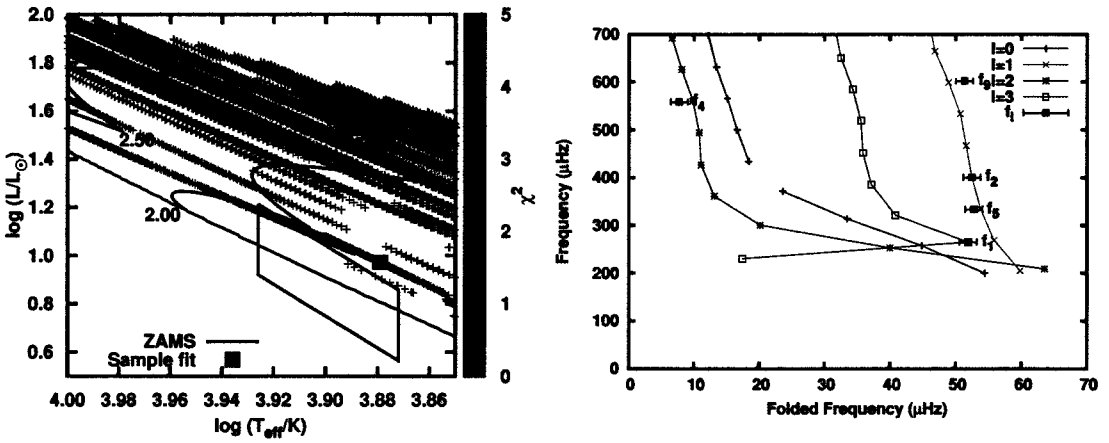

Figure 3.31: Simultaneous χ^2 fit $\ell = 0$ to 3 to the five frequencies (f_1, f_2, f_4, f_5, and f_9) of IP Per originally fit by Ripepi et al. (2006) to radial-only modes. Contrast to Figure 3.30. Sample echelle diagram is for $\chi^2 = 1.36$, M = 1.82 $M_\odot$, $\log(T_{eff}/\mathrm{K})$= 3.879, $\log(L/L_\odot)$= 0.973.

analysis, and therefore allowing for solutions of lower luminosity more compatible with IP Per position in the HRD.

Previously, Ripepi et al. (2006) reported, at best, to being able to simultaneously fit a model to radial modes for f_1, f_2, f_4, f_5, and f_9 only. I tried reproduce this result without success. Figure 3.30 shows χ^2 fits limited to these particular frequencies. There are no good fits in agreement with IP Per's position in the HR diagram. Indeed, once again, the best fit solutions (which aren't very good) are to over-luminous solutions, with a best-fit model of $\chi^2 = 10.7$ amongst those models that also happen to be consistent with the star's effective temperature. The right-hand side of Figure 3.30 shows the relevant echelle diagram, and illustrates the poorness of the fit between the models and the data.

χ^2 fits of the same set of frequencies to $\ell = 0$ to 3 modes provides more promising results (left-hand side of Figure 3.31), but illustrates the difficulty in narrowing down solutions with such large observational uncertainties in the frequencies - many solutions with low χ^2 exist. Nevertheless, the solution does indicate that non-radial modes are needed to explain the five frequencies. In this particular case, there are some solutions just above the star's position in the HRD with reasonably low χ^2 values, in this case an 1.82 $M_\odot$ solution with $\chi^2 = 1.36$ (echelle diagram on the right-hand

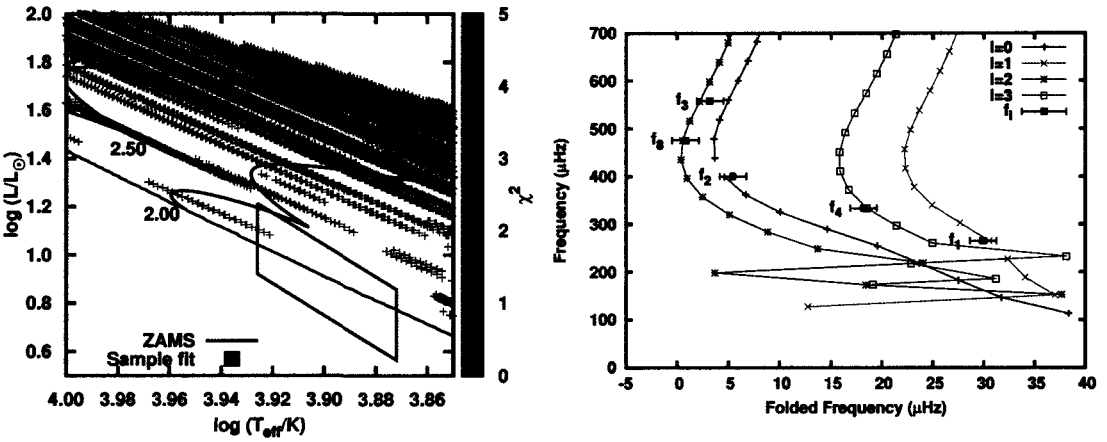

Figure 3.32: Simultaneous χ^2 fit to $\ell = 0$ to 3 modes of the five frequencies (f_1, f_2, f_3, f_4, and f_8) of IP Per present in all three datasets of Ripepi et al. (2006). Sample echelle diagram is for $\chi^2 = 0.28$, M = 1.96 $M_\odot$, $\log(T_{eff}/K)$= 3.872, $\log(L/L_\odot)$= 1.295.

side of Figure 3.31). However, there are many good solutions of higher luminosity, so many, in fact, that narrowing down the solution space in detail with just these observations is impossible.

Finally, Figure 3.32, shows χ^2 fits to the five frequencies (f_1, f_2, f_3, f_4, and f_8) that are present in all three datasets, as presumably these are the most reliable frequencies, and might perhaps yield a better solution. Fits are to $\ell = 0$ to 3 modes, and qualitatively yield a very similar set of solutions to the one immediately above. Good solutions, though, are more luminous than in the previous case, with no solutions comparable to the above as close to the star's position in the HRD. The corresponding sample echelle diagram is for a 1.95 $M_\odot$ star, with $\chi^2 = 0.28$.

In summary, collectively, the results for IP Per suggest that it is a star more luminous than that used in this analysis, and might indicate that is a background star to the Per OB2 association. Given its status as an UX Ori and HAe star, its PMS status is probably assured. Further observations of the light curve of the star could confirm/refute the wide range of pulsations detected by Ripepi et al. (2006); if the pulsation spectrum is confirmed by future observations, then relatively tight constraints on the intrinsic luminosity of the star could be placed on it, as indicated by the right-hand side of Figure 3.28.

Label	Frequency (c/d)	Err Freq. (c/d)	Freq (μHz)	err Freq (μHz)	V Amp. (mmag)	S/N
f1	15.687	0.03	181.56	0.35	22.9	6.8
f2	14.331	0.03	165.87	0.35	13.5	5.9
f3	12.754	0.03	147.62	0.35	8.4	5.7
f4	15.885	0.03	183.85	0.35	7.7	5.9
f5	12.817	0.03	148.34	0.35	4.8	4.6

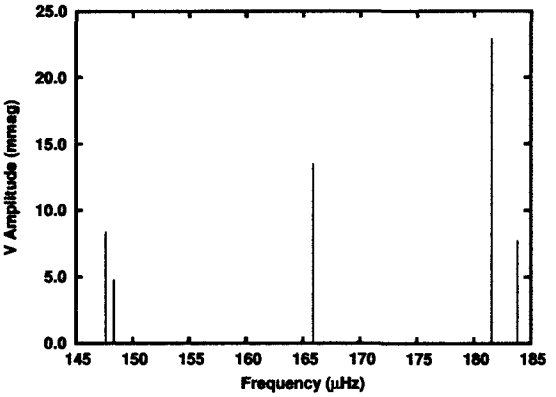

Figure 3.33: Frequencies of V351 Ori from multi-site ground-based observations from Ripepi et al. (2003).

3.1.2.2 V351 Ori

V351 Ori, nominally associated with the Orion B star-formation region, was first found to be variable by Hoffmeister (1934), however the light curve was mistakenly attributed to that of an Algol-type eclipsing binary. Later studies showed that the variability is irregular, like that shown by the RW Ari class of T-Tauri stars, and in this case subsequent observations discovered that the brightness varies by over 2.2 magnitudes in size, and that the colour changes with extinction level. This was ably demonstrated by van den Ancker, Thé & de Winter (1996) who performed an extensive multi-band photometric study of the light curve of the star, determining how the reddening changes as the level of extinction increases: at lower levels of extinction (less than about 1.75 magnitudes) the reddening follows the typical $R_{\rm v} = A_{\rm v}/E(B-V) = 3.1$ extinction law, whereas with larger amounts of extinction the star gets bluer, presumably as a result of reflected light in the CS material affecting the observations. It indicates that for a heavily obscured star, the typical reddening laws no longer apply, and one must be careful about how one applies these corrections. The latest Hipparcos reductions of van Leeuwen (2007) report a parallax of 5.96 ± 1.44 mas, indicating a distance range of 135 to 221 pc. In contrast, the associated distance to the Orion B star formation region, as used by Vieira et al.

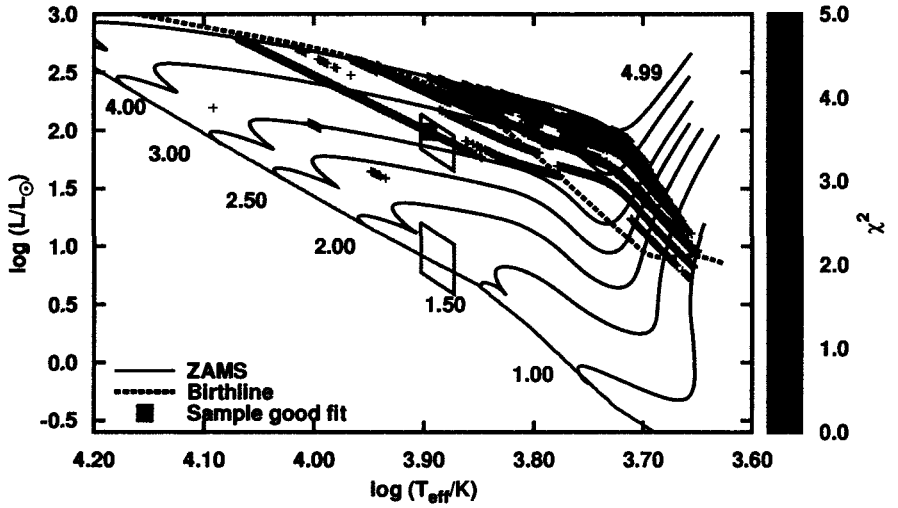

Figure 3.34: χ^2 fit to all five significant frequencies of V351 Ori detected by Ripepi et al. (2003), ℓ=0 to 3 modes. Lower box indicates luminosities computed using Hipparcos distances, and upper box indicates luminosities computed using distances to the Orion B star-formation region.

(2003) in their analysis of the star, is 460 to 650 pc, and is hard to reconcile with the Hipparcos distance.

Herbig (1960a) classified the star as A7 III, with Gray & Corbally (1998) reporting a more detailed classification of kA6 hA8 mA6 III (shell). For the analysis of this star we therefore use A7 III $\pm$ one spectral class, and the reddening curve in the CMD as found by van den Ancker, Thé & de Winter (1996) to calculate reddening and extinction, and ultimately, $\log L$. Using the Hipparcos distances, $\log(L/\mathrm{L}_\odot) = 0.628$ to 1.154 is found. In contrast, if the distances to the Orion B SFR are used, then $\log(L/\mathrm{L}_\odot) = 1.69$ to 2.09 is found.

Vieira et al. (2003) report $v \sin i$=119 km/s.

V351 Ori was one of the first PMS stars in which pulsation was detected, discovered by Marconi et al. (2000), in which a single frequency of 17.24 $\pm$ 0.44 c/d (199.4 $\pm$5.1 μHz) was observed. Later multi-site ground-based observations by Ripepi et al. (2003) detected five frequencies, displayed here in Figure 3.33, with amplitudes for the largest-amplitude frequencies larger than is typical for most PMS δ-Scuti stars. Here, the original frequency detected by Marconi et al. (2000) is most likely the 2 c/d

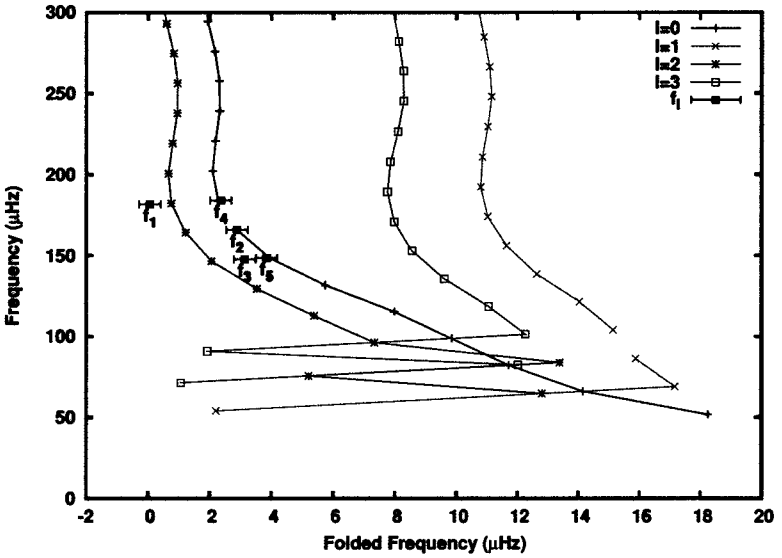

Figure 3.35: Echelle diagram, fit to all frequencies of V351 Ori, $\ell = 0$ to 3 modes. $\chi^2 = 2.67$, mass = 3.35 $M_\odot$, $\log(T_{eff}/K) = 3.896$, $\log(L/L_\odot) = 1.991$.

alias of f_1 from the multi-site observations. The Ripepi et al. (2003) frequencies are the ones I use in the asteroseismic analysis.

The analysis of V351 Ori is interesting, Figure 3.34 shows χ^2 fits to $\ell = 0$ to 3 modes for all five frequencies, showing the position in the HRD using Hipparcos distances (lower box) and Orion B distances (upper box). The former would normally be the preferred HRD position as it originates from a direct measurement of the star's parallax, whereas the latter is only inferred by assuming association with the Orion B star-formation region, an assumption that could very easily be wrong.

There is only one family of solutions that agrees with either position in the HRD, that of the upper error box, corresponding to the distance used for the Orion B cloud; there are no solutions in agreement with the error box associated with the Hipparcos distances. A sample echelle diagram (Figure 3.35) is shown for the one family of solutions in agreement. The particular model selected has a χ^2 value (2.67) for the family of solutions, and is representative of all solutions of that family. f_3 and f_5 form a close pair, causing difficulty with the fits, particularly at lower luminosities.

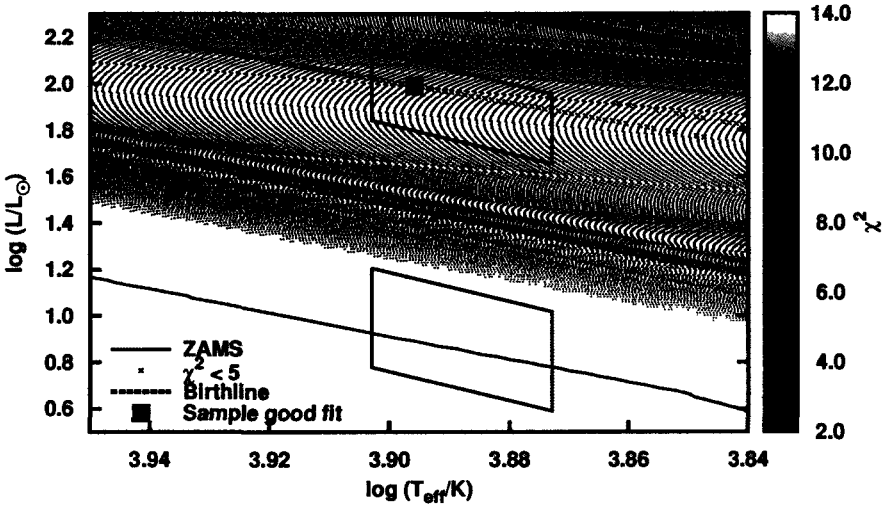

Figure 3.36: Models low enough to support $f_3 = 147.62$ μHz of V351 Ori, as well as estimates of the minimum rotational splitting caused by $v \sin i = 119$ km/s.

Figure 3.36 shows the models with a fundamental frequency low enough to support the lowest frequency, f_3. No model is in agreement with the star's lower position in the HRD, suggesting either the Hipparcos distance is not large enough, or that reddening and extinction have been underestimated. Regardless, if good fits did exist in the lower-luminosity range of allowed models, these models would have luminosities just outside the error box, but the good fits are *much* more luminous, and so they are hard to reconcile with the lower position in the HRD.

There are two close frequency pairs, f_1 and f_4, and f_3 and f_5 that might be a signature of rotational splitting. However, this is not likely, as Figure 3.36 also shows the minimum expected rotational multiplet splittings for this star, given $v \sin i$ =119 km/s. The upper position in the HRD has splittings of the order of 6 μHz, the lower position much higher than that, approaching 14 μHz, and higher, whereas the frequency differences in question are only one-to-two microHertz in value.

As an experiment, I limit the fits to the first three highest-amplitude frequencies (f_1, f_2, and f_3) as perhaps the most reliable frequencies, and also so as to use only one frequency from each of the two observed doublets. Better, but not conclusive, solutions are found, as shown in Figure 3.37, but only for the upper HRD position.

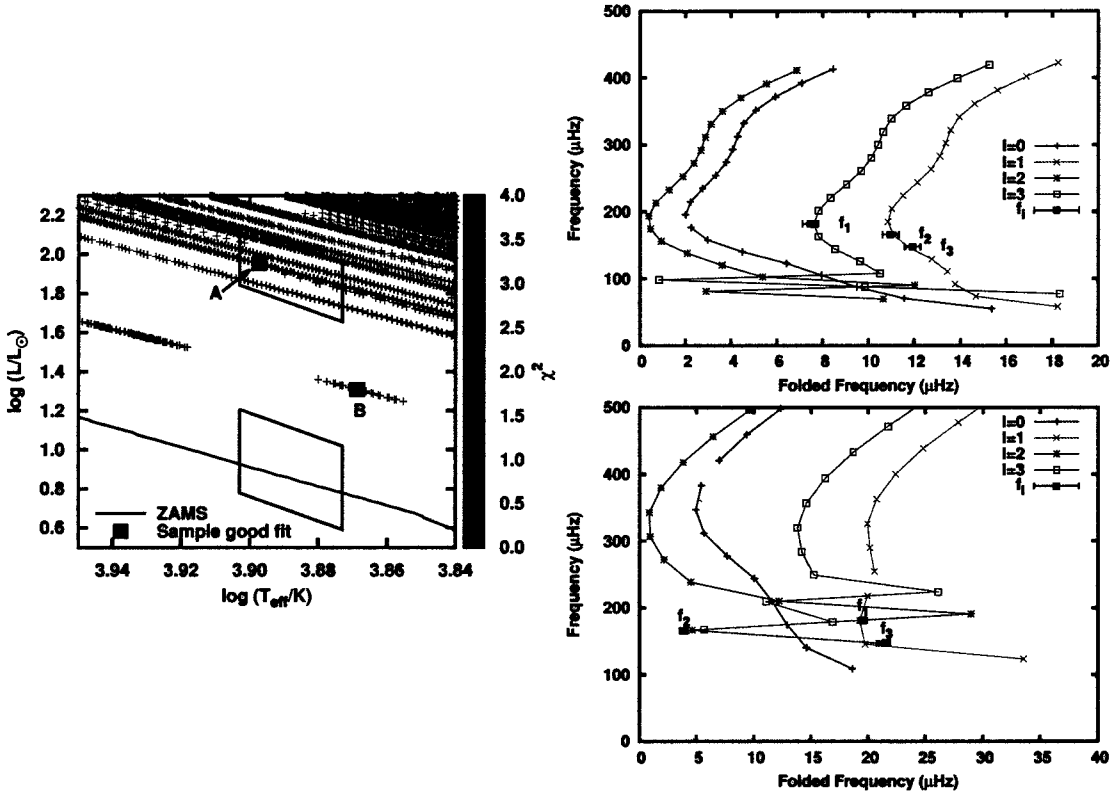

Figure 3.37: Left-hand side: χ^2 fit to f_1, f_2 and f_3 of V351 Ori detected by Ripepi et al. (2003), $\ell = 0$ to 3 modes. Top right-hand side: Solution A: $\chi^2 = 0.29$, mass = 3.23 $M_\odot$, $\log(T_{eff}/K) = 3.897$, $\log(L/L_\odot) = 1.950$. Bottom right-hand side: Solution B: $\chi^2 = 2.9$, mass = 1.99 $M_\odot$, $\log(T_{eff}/K) = 3.869$, $\log(L/L_\odot)$ =1.309.

The upper right-hand corner of Figure 3.37 shows the echelle diagram for Model "A", and identifies non-radial modes of mid-range radial order as the model frequencies that best fit the data, however many other solution also exist The lower right-hand panel of Figure 3.37 shows the best echelle for Model "B" for a family of solutions at mid range between the two HRD positions, the lowest-luminosity solutions available given the value of f_1, and the closest to the Hipparcos-determined HRD position. Model "B" identifies the three frequencies as lower-radial-order, non-radial modes, but the fits are still not good, and do not agree with either HRD position.

In summary, the best (but still not good) fits to the asteroseismic data were found for the upper position in the HRD, consistent with a distance to V351 Ori similar to that of the Orion B cloud. The astroseismology puts constraints on the

luminosity of V351 Ori which are not in agreement with a distance to V351 Ori as given by Hipparcos data. In the latter case, either the Hipparcos parallaxes are a bit off, or the amount of extinction associated with V351 Ori has been underestimated. Regardless, this star requires further investigation in order to reconcile the astroseismology with other observations. Rotation should also be playing a role in modifying the star's pulsation frequencies, perhaps the underlying reason for which lower-luminosity models could not be fit to the observed frequencies.

3.1.2.3 V346 Ori

V346 Ori (HD 287841, PDS 180) is a $V = 10.0$ magnitude Herbig Ae object thought to be part of the Orion SFR. Variability of approximately 1 magnitude was first detected by Morgenroth (1934), and mistakenly ascribed to an Algol-type eclipsing binary. The variations are due to UX-Ori type variations from obscuring circumstellar material, and V346 Ori was included within the list of HAeBe stars by Thé, de Winter & Perez (1994). It has been variously classified as A5 III by Herbig (1960a), kA6 hA7 mA7 III ((shell)) by Gray & Corbally (1998), and A8 V by Vieira et al. (2003). I therefore choose a temperature range consistent with A5 though A8 spectral classification. Vieira et al. (2003) associate V346 Ori with the Orion OB1a association, and as such assign a distance of 300 to 460 pc. The latest Hipparcos

	Weight Case				No-weight case			
Label	Freq. (c/d)	Freq. (μHz)	Ampl. (mmag)	S/N	Freq. (c/d)	Freq. (μHz)	Amp. (mmag)	S/N
f_1	35.107	406.33	2.23	12.1	35.107	406.33	2.20	8.8
f_2	32.227	373.00	1.64	9.1	32.227	373.00	1.46	5.9
f_3	31.611	365.86	1.18	6.6	31.611	365.86	1.11	4.6
f_4	29.652	343.19	1.22	6.9	29.651	343.19	1.33	5.5
f_5	29.159	337.49	0.86	4.9	29.159	337.49	1.08	4.5
f_6	30.828	356.81	1.01	5.7	29.823	345.17	1.01	4.2
f_7	24.833	287.42	0.82	4.6				
f_8	19.058	220.58	0.77	4.1				
f_9	12.936	149.72	0.77	4.1				
f_{10}	21.886	253.31	0.75	4.0				
f_{11}	27.446	317.66	0.78	4.5				
f_{12}	37.203	430.59	0.74	4.0				
f_{13}	8.045	93.11	0.69	4.0				

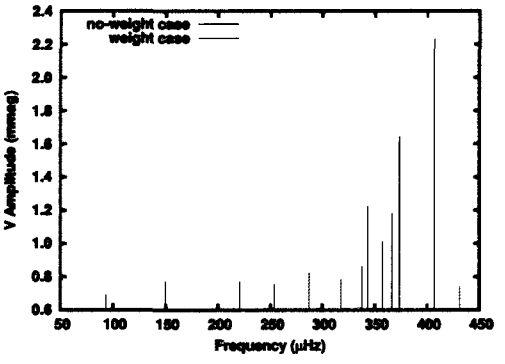

Figure 3.38: V346 Ori frequencies as found by Bernabei et al. (2009), in which they report estimated errors in frequency of ± 0.020 c/d or ± 0.23 μHz.

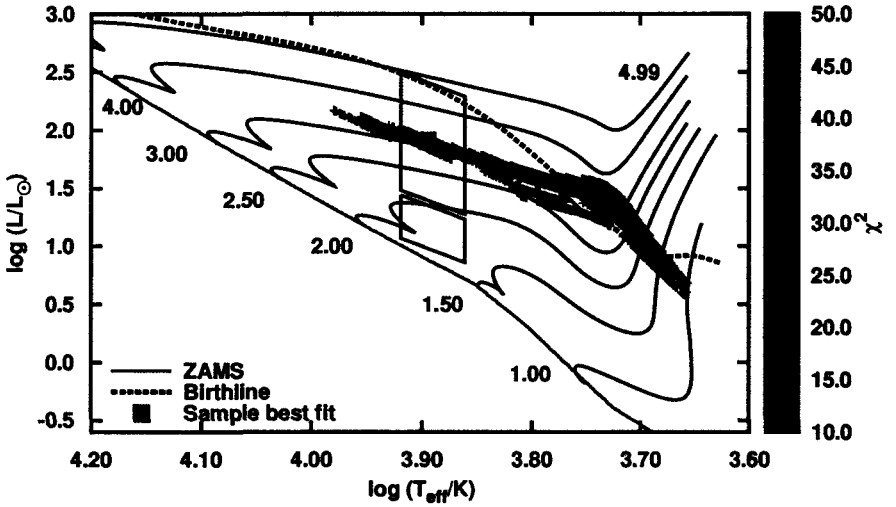

Figure 3.39: χ^2 fits to all frequencies of V346 Ori detected in the weighted case of Bernabei et al. (2009), along with positions of the star in the HRD.

reductions of van Leeuwen (2007) report a parallax of 2.07±2.01 mas, corresponding to a very wide distance range of 480 to 16700 pc. Obviously the Hipparcos data is not very precise, however it does establish a (maybe not-so-reliable) lower limit to the distance of 480 pc, not quite in line with the distance given to the Orion SFR, but close enough to not be mutually exclusive, given the uncertainty associated with each of those distance ranges. Here, I indicate both corresponding luminosity ranges in the HRD, as can be seen in Figure 3.39, except an upper limit to the luminosity for the Hipparcos range has been chosen at about $\log(L/\mathrm{L}_\odot) = 2.5$ to coincide with the birthline — we would not realistically expect a star of this class to have a higher luminosity. Note that $\log(L/\mathrm{L}_\odot) = 2.5$ for the bluest stars in the range corresponds to a star at a distance of about 1550 pc. It will be shown below that the asteroseismology supports a luminosity approximately in the middle of the Hipparcos range. Both Vieira et al. (2003) and Bernabei et al. (2009) found $v \sin i$ values in agreement with one another, with 125 km/s and 25±10 km/s reported respectively.

δ-Scuti variations were discovered by Pinheiro et al. (2003), who identified four pulsation frequencies ranging from 18.3 c/d to 45.7 c/d. Multi-site photometry by Bernabei et al. (2009) later identified six frequencies in their no-weight case, and

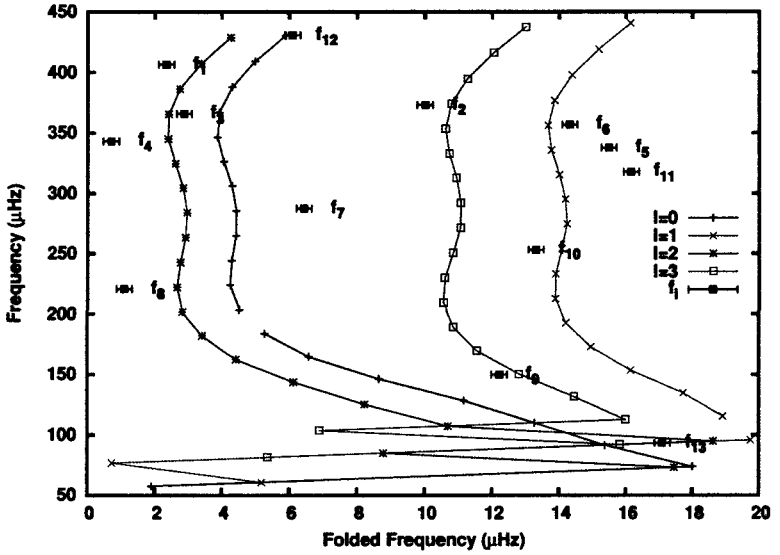

Figure 3.40: Best-fit model to all thirteen frequencies of V346 Ori detected in the weighted case of Bernabei et al. (2009). Model parameters: $\chi^2 = 31.8$, mass = 3.13 $M_\odot$, $\log(T_{eff}/K) = 3.895$, $\log(L/L_\odot) = 1.908$

thirteen with their weight case. The frequencies appear in Figure 3.38 in both tabular and graphical form. (In both cases they used the Period04 lightcurve-analysis software of Lenz & Breger 2005, to find the frequencies; the weighted case gave greater weight to portions of the lightcurve that were of higher photometric quality, thus allowing more frequencies to be identified, albeit marginally.)

Note that the first five frequencies in both cases are identical to one another. For f_6, however, the no-weight case has a value of 29.823 c/d, whereas the weight case has a value of 30.828 c/d, *i.e.* 1 c/d aliases of one another. In the forthcoming analysis I choose the weighted value for f_6 as perhaps more reliable. The remainder in the weighted case are marginal detections at best, however if they are real, then we are confronted with a wide range of frequencies, which will significantly limit the luminosities of the stellar models to which the frequencies can be matched.

Figure 3.39 shows both V346 Ori's position in the HRD, and χ^2 fits to all thirteen frequencies detected in the weighted case. The best-fit solution that falls within the error boxes is not good, with $\chi^2 = 31.8$, and Figure 3.40 reveals part

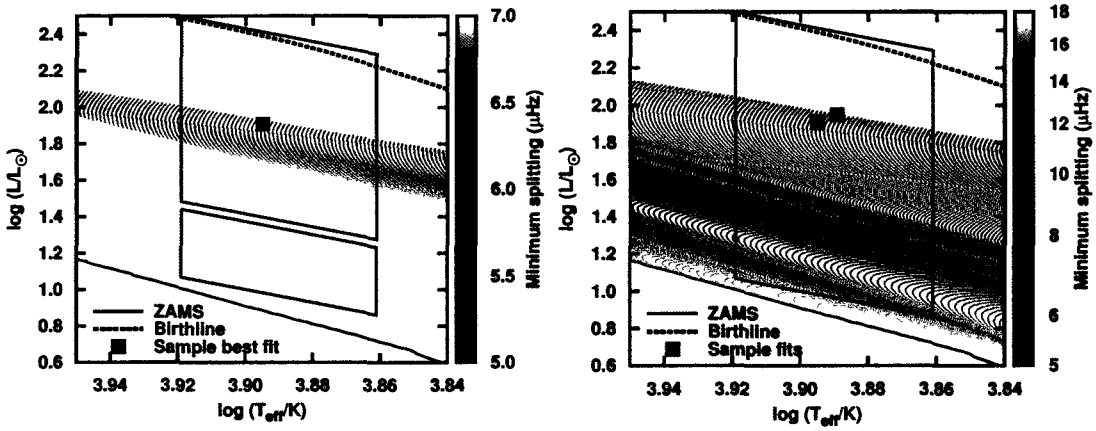

Figure 3.41: Stellar models that can support all the frequencies of V346 Ori that were observed by Bernabei et al. (2009) considering the fundamental and acoustic-cut-off frequencies of each model. Left-hand side: weighted case. Right-hand side: non-weighted case. Both diagrams also show the minimum expected rotational splitting assuming minimum rotational velocity of 110 km/s from Bernabei et al. (2009).

of the difficulty of achieving a good fit: the frequencies span many different radial orders, and only a relatively small range of models have acoustic cut-off frequencies and fundamental frequencies that allow all of the observed frequencies to be supported at the same time.

The right hand side of Figure 3.41 shows just how constraining the minimum (f_{13}) and maximum (f_{12}) frequencies are to the range of expected luminosities when compared against each model's fundamental and acoustic cut-off frequencies. If these frequencies are signals of pulsation, then the luminosities are now restricted to the mid-range of the upper error box, and would indicate a star in the background of the Orion SFR, significantly bounding the intrinsic luminosity of star, *and* the distance to the star.

If consideration is limited to the six frequencies of the no-weight case, then the luminosity range expands considerable. The maximum range does not change by much, as the maximum frequency, f_1 in this case, is not much lower than f_{12}, but the minimum luminosity now reaches down to the ZAMS, as f_6 is a much higher frequency than f_{13}, meaning a much higher fundamental mode is now allowed. Interestingly enough, χ^2 fits to *only* the six frequencies of the no-weight case (Figure 3.42) *still*

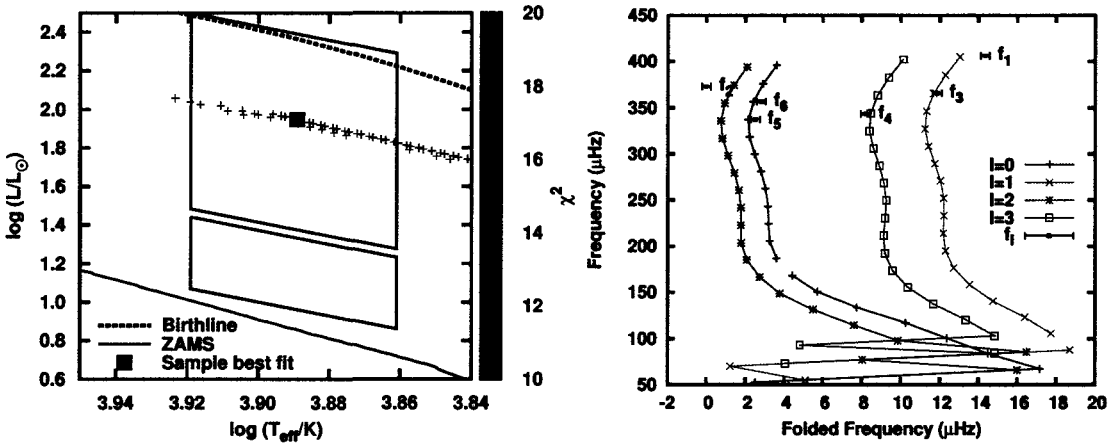

Figure 3.42: Left: χ^2 fits to the six frequencies of V346 Ori of the no-weight case of Bernabei et al. (2009). Right: Sample fit with model parameters $\chi^2 = 12.9$, mass = 3.27 $M_\odot$, $\log(T_{eff}/\mathrm{K}) = 3.889$, $\log(L/L_\odot) = 1.948$

choose high-luminosity solutions, despite a much wider range of models from which to choose. It is important to note that these solutions still don't yield χ^2 values better than 12.9. The sample echelle diagram on the right-hand side of Figure 3.42 shows the best solution, in which four of the frequencies are well-fit, but f_1 and f_2 are a bit off. This solution puts f_1 near the acoustic cut-off frequency for this particular model.

Figure 3.41 also shows the range of minimum expected rotational splittings between frequencies of a single multiplet within the allowed models. The splittings are around the same values as the differences between different ℓ orders, indicating that the effects of rotational will not be easy to spot, as multiplets and different non-radial orders will be mixed up with one another.

Looking at the pulsation spectrum, there does appear to be some periodicities in the data. The left-hand side of Figure 3.43 shows an echelle diagram with a folding frequency of 16.1 μHz that appears to line up a number of frequencies in a ladder-like manner. The right-hand side of the same figure shows the corresponding large spacing of the models allowed by all frequencies of the non-weighted case. 16 μHz would be in the upper luminosity range of the allowed models. Although not pictured here,

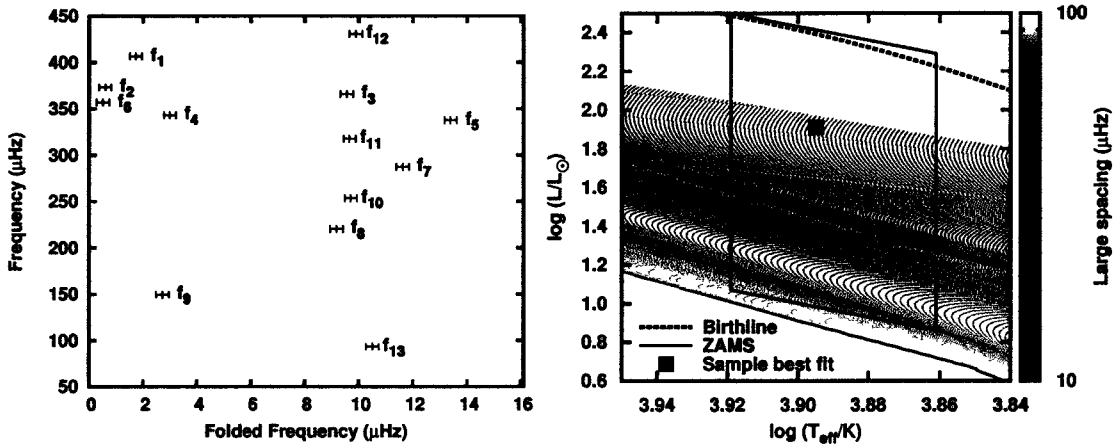

Figure 3.43: Left: Echelle diagram of V346 Ori with a folding frequency of 16.1 μHz, including all frequencies observed in the weighted case of Bernabei et al. (2009). Right: Large spacing of all models that can support all frequencies of the non-weighted case of Bernabei et al. (2009).

a folding frequency of about double that of 16 μHz did not produce as believable a result. As an experiment, Figure 3.44 shows χ^2 fits to six select frequencies on the right (f_{12}, f_3, f_{11}, f_{10}, f_8, and f_{13}) and three on the left (f_1, f_4, and f_9) of the echelle diagram of Figure 3.43. Also included in the fit is the second-most significant frequency, f_2. The best fits are to the right of the error boxes, with $\chi^2 = 10.2$, and don't align the observed frequencies as expected: the deviation of the modelled

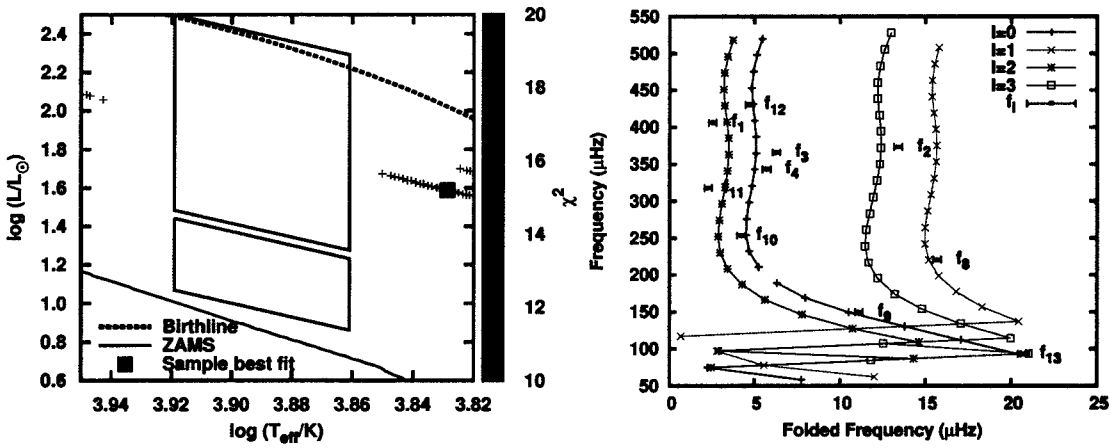

Figure 3.44: Left: χ^2 fits to the ten "aligned" frequencies of V346 Ori of the weighted case of Bernabei et al. (2009). Right: Sample fit with model parameters $\chi^2 = 10.2$, mass = 2.69 $M_\odot$, $\log(T_{eff}/\mathrm{K}) = 3.829$, $\log(L/L_\odot) = 1.588$.

frequencies from the asymptotic limit is significant enough in the lower radial orders to make the stacking from the echelle diagram of Figure 3.43 misleading, and perhaps a coincidence.

In summary, significantly, the asteroseismology supports the larger Hipparcos distance for V346 Ori, and that V346 Ori is at the very back, or indeed beyond, the Orion SFR. χ^2 fits seem to be universally bad, but the limits imposed by the largest and smallest frequencies are more robust, and support the higher-luminosity (and hence further away) solutions. Even when model fits are limited to the non-weighted case of Bernabei et al. (2009), the higher luminosities are still preferred, despite the unsatisfactory fits. With a minimum equatorial rotational velocity of 110 km/s, stellar rotation is expected to play a significant role in the problem.

3.1.3 Single-site ground-based observations

3.1.3.1 V375 Lac

V375 Lac (LkHα 233, HBC 313) is a HAe star, $V = 13.8$ magnitudes (with some UX Ori variability), with a collimated bipolar jet (Melnikov et al. 2008), embedded in the LkHα 233 dark cloud (LkHα 233 is another name for the star and region) at a distance of about 880 pc (Finkenzeller & Mundt 1984). Spectral classifications are usually given as A7, *e.g.* A7e by (Herbig 1960b) and A7 Ve (Calvet & Cohen 1978), although a few determinations have been of earlier types, such as A4e by Hernández et al. (2004) and A2e by Lee & Chen (2007). Here, I use a temperature range consistent with A5 through A8 spectral types. There are no known $v \sin i$ determinations in the literature.

Bernabei et al. (2004) report two frequencies of $f_1 = 5.2 \pm 0.5$ c/d and $f_2 = 9.9 \pm 0.5$ c/d (60 and 115 ± 6 μHz, respectively), in which f_2 may or may not be $2f_1$, hence only f_1 will be considered in this analysis. These frequencies are recovered from two separate datasets, one dataset from CCD data, the other from photometer

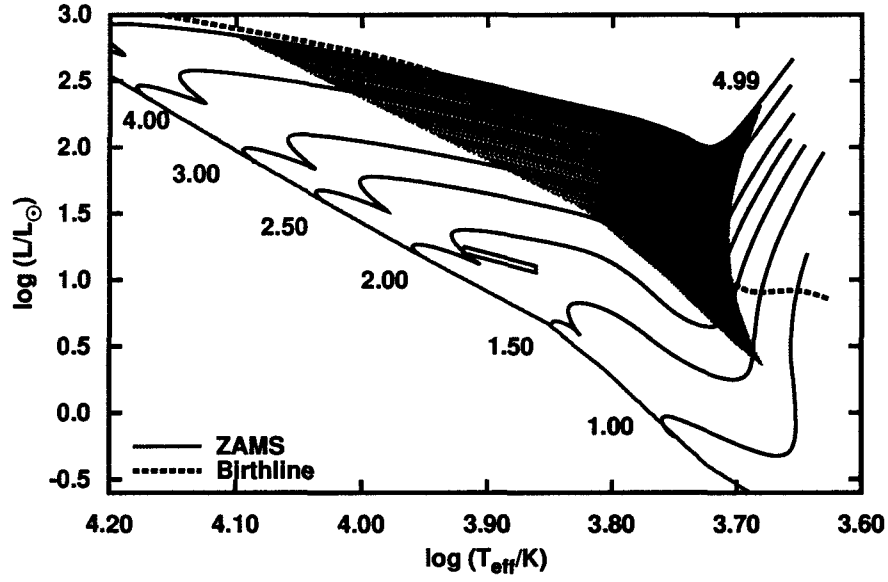

Figure 3.45: Models allowed by $f_1 = 60$ μHz of V375 Lac, observed by Bernabei et al. (2004), considering the fundamental mode of each model.

data. Given the uncertainties in the data, only a very broad asteroseismic analysis of f_1 is performed. $f_1 = 60$ μHz is quite low, assuming the frequency is a signal of pulsation, and therefore puts minimum luminosity constraints on the star, as shown in Figure 3.45. Note the observational luminosities reported in the figure, particularly the small range of values, are very artificial. The only distance for the star, established presumably through it's membership in the surrounding dark cloud, has been widely reported in the literature as 880 pc, however uncertainties in that distance are not quoted. In this figure I have artificially expanded the distance range to 850 to 900 pc, but the range should probably be much larger than that, hence the small range of calculated luminosities. Also, broad-band photometry of this star is significantly hampered by the surrounding emission and obscuration from the cloud. It is quite possible that this star is suffering from a bluing effect, and that the level of obscuration is much larger than calculated here. Certainly, if f_1 should should be confirmed by future observations, then larger luminosities than those indicated by the error box in Figure 3.45 are suggested for the star, and indicate that further observations of this star are needed to reconcile the photometric and astroseimic luminosities of the star.

Given the uncertainties in the frequencies, V375 Lac should be re-observed to confirm δ-Scuti pulsations, as a number of stars with similar quality data in the past in which δ-Scuti were thought to have been detected, have since been found to be false positives once greater-precision data had been collected. The false positives were presumably caused by circumstellar variability temporarily (for a night or two of observations) mimicking δ-Scuti pulsations. The observations for V375 Lac *are* on a more firm footing, though, as the pulsations were detected independently with two separate instruments, however it is unknown whether these observations were coeval, or not; if they are coeval, then both instruments might have been picking up the same misleading signal.

In summary, if the pulsation frequencies of V375 Lac are confirmed by future observations, the astroseismology indicates a star that is over-luminous compared to the photometric data, requiring reanalysis of the latter.

3.1.3.2 CQ Tau

CQ Tau is a redder-than-usual HAe star with a spectral class somewhere between F2 IVe (Herbig 1960a) and F5 IVe (Mora et al. 2001). It displays HAe phenomenology, but is very close to being a T Tauri star in the HRD, and is sometimes classified as such (*e.g.* Artemenko, Grankin & Petrov 2010). CQ Tau displays irregular variability of up to 2 magnitudes due obscuring CS material, and at its deepest minimum exhibits a bluing affect as reflected blue light from the CS material starts to contribute significantly to the flux (Bibo & The 1991). The star is one of the closer-known HAe stars, with a parallax of 8.85±1.80 mas, corresponding to a distance range of 94 to 142 pc (van Leeuwen 2007). Mora et al. (2001) report $v \sin i$ = 105±5 km/s, and Merín et al. (2004) 110±10 km/s. In this analysis, T_{eff} corresponding to spectral class F2 through F5 was used, and broad-band observations reported by de Winter

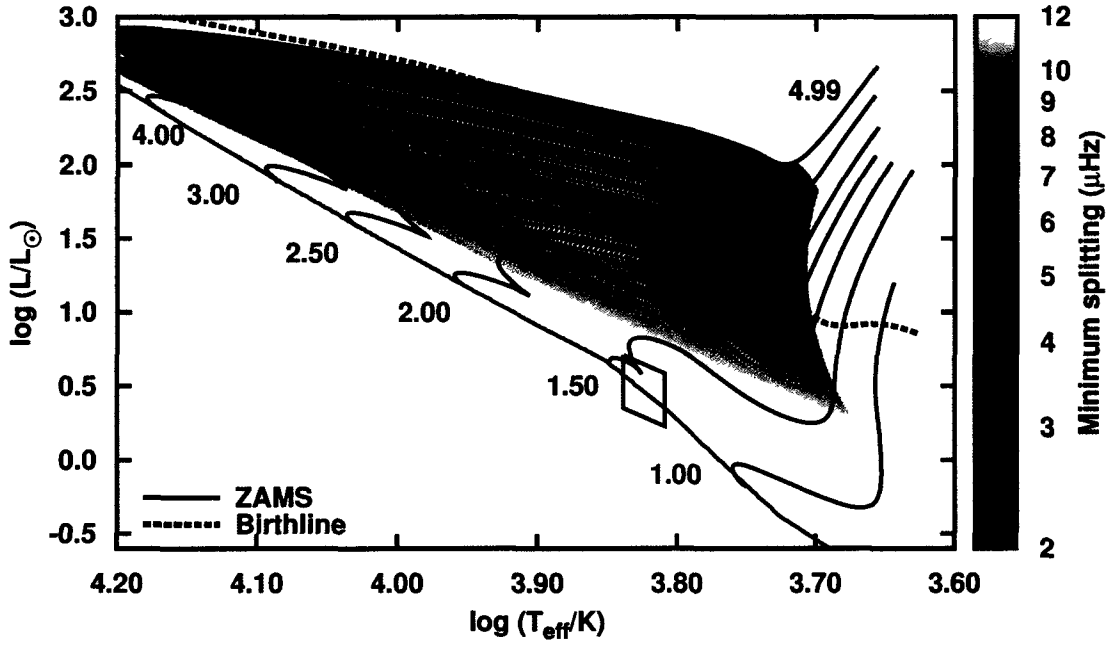

Figure 3.46: Allowed stellar models for CQ Tau given f_1 = 162 μHz, considering the fundamental mode of each model, and the minimum expected rotational splitting, given minimum equatorial rotational velocity of 100 km/s.

et al. (2001) for the star at its brightest were used for the de-reddening/extinction corrections ($V = 10.^{\rm m}22$, $B - V = 0.^{\rm m}78$).

Detection of pulsation is preliminary; Marconi and Ripepi reported to Zwintz (2008) via private communication a single frequency of 15.0 c/d, corresponding to 162 μHz. These results have not been otherwise published, and given the unknown quality of these observations, analysis can only be rudimentary. Follow-up observations are needed to confirm any pulsations, and CS variability may have been mistaken for pulsation. If the pulsation is confirmed by future observations, this star would be the coolest PMS δ-Scuti currently known.

Figure 3.46 shows the star's position in the HRD, and also shows the models that can support $f_1 = 163$ μHz, given the fundamental frequency of those models. The star straddles the ZAMS in the HRD, and falls just below the minimum luminosities indicated by the lone pulsation frequency that has been tentatively reported. The discrepancy between the indicated HRD position, and the minimum luminosity allowed by the asteroseismology might very well be due to the bluing effect, mentioned above, that is known to affect this star. Even at maximum brightness, it is possible that the normal $R_{\rm v} = 3.1$ extinction law does not apply to this star, in which case the luminosity would be underestimated just based upon the V and $B - V$ values.

If this frequency is confirmed by future observations, then the star is most likely pulsating in low radial order, otherwise the luminosity would be harder to reconcile with the broad-band observations of the star. Figure 3.46 also shows that any rotational splitting of a multiplet would be quite large, around 12 μHz for the lowest-luminosity models.

3.1.3.3 VV Ser

Pulsations were preliminarily reported in VV Ser by Bernabei et al. (2004) and confirmed by Ripepi et al. (2007), the latter a result of a three-season single-site observing campaign using the Loiano 1.5 m telescope in Italy. Ripepi et al. (2007) also provide an excellent review of the relevant data on the star collected to that

Label	Frequency (c/d)	Err Freq. (c/d)	Freq (μHz)	err Freq (μHz)	V Amp. (mmag)	S/N
f1	6.12	0.04	70.83	0.46	6.4	
f2	2.69	0.04	31.13	0.46	7.8	
f3	4.47	0.04	51.74	0.46	3.7	
f4	3.90	0.04	45.14	0.46	4.8	
f5	9.96	0.04	115.28	0.46	2.7	
f6	7.56	0.04	87.50	0.46	2.1	
f7	10.24	0.04	118.52	0.46	1.4	

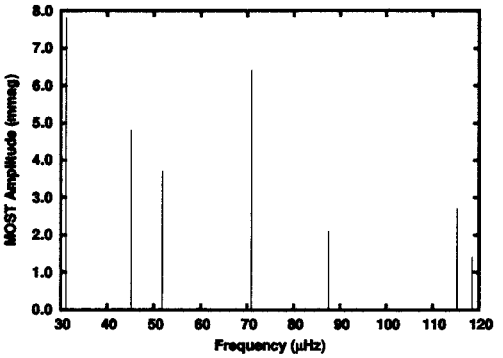

Figure 3.47: VV Ser frequencies as found by Ripepi et al. (2007). The lower frequencies may or may not be δ-Scuti pulsations.

time. VV Ser is a surprisingly ill-determined star, in that multiple studies by many observers often find contradictory values for the fundamental parameters of the star, much more so than with other stars. It is listed as a Herbig Ae star, but with spectral classifications ranging all the way from B1e-B3e by Finkenzeller & Mundt (1984) (since determined to be in error as it was based upon the He I 5876 Å line, which was later found to not be of photospheric origin, but originating from an accretion disk; Rostopchina, Grinin & Shakhovskoi 2001), to B5e (Fernandez et al. 1995) to A3eβ II

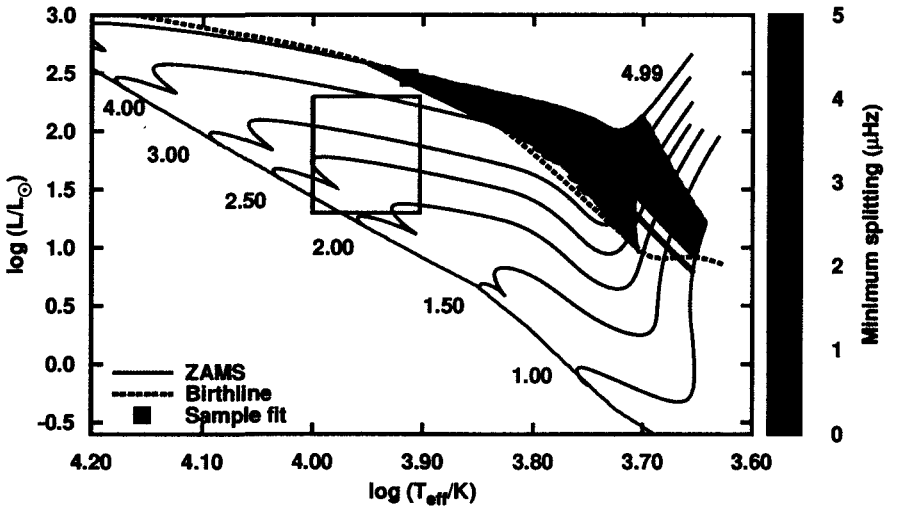

Figure 3.48: Models for which the fundamental frequency is $< f_2$ (underlying grey), and χ^2 fits to models of all frequencies, excluding f_7, of VV Ser (blue-black color palette.) Also indicated is the star's position in the HRD.

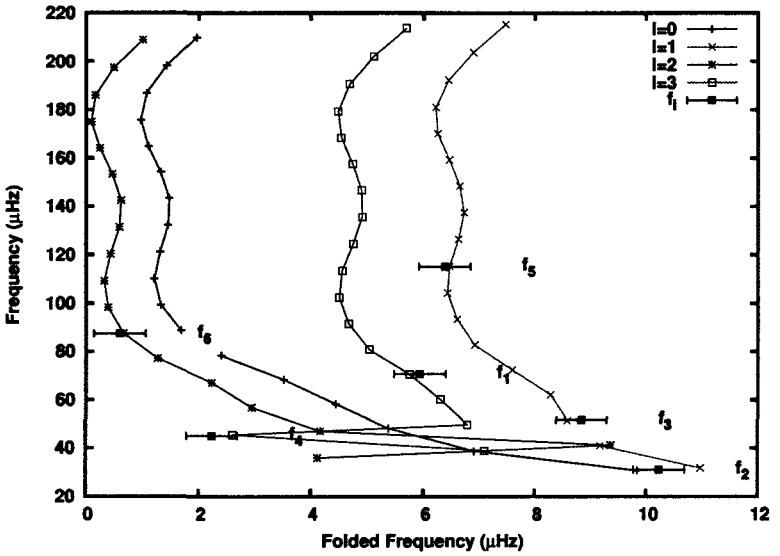

Figure 3.49: Best-fit model to all frequencies, except f_7, of VV Ser detected by Ripepi et al. (2007). Model parameters: $\chi^2 = 0.31$, mass = 4.81 $M_\odot$, $\log(T_{eff}/K) = 3.913$, $\log(L/L_\odot) = 2.458$.

(Gray & Corbally 1998). Luminosity classes have ranged from II to IV. $v \sin i$ values are similarly confused: 200 km/s (Hillenbrand et al. 1992), 85 km/s (Grady et al. 1996), 229±9 km/s (Mora et al. 2001), and 142 km/s (Vieira et al. 2003). VV Ser is associated with the Serpens Cloud, with a distance range of approximately 300 to 400 pc.

The frequencies observed by Ripepi et al. (2007) from their 2004 dataset (the one with the most frequencies, lowest uncertainties and longest time base for observations) appear in Figure 3.47 in both tabular and graphical format. The observations are Johnson V-band CCD photometry, taken with the Loiano 1.5 m telescope, with observations taken on 7 nights over a time base of about 26.3 days. Before performing the pulsation analysis, they subtracted a sinusoidal signal from the light curve with a period of 2.2 days, source unknown, but possibly some sort of signal of rotation, such as variability caused by sunspots. The frequency spectrum is not typical, with one frequency, f_2, below the typical cut-off of what are considered to be δ-Scuti pulsations. Also of note, $f_7 = 2f_1 - 1$ c/d, and so this may or may not

be an independent frequency, and so is not included in the following analysis. Like Ripepi et al. (2007), because of the large range of spectral classes and luminosities determined by various researchers over the years, I use a wide temperature range, T_{eff} = 9000±1000 K ($\log(T_{eff}/\mathrm{K})$ between 3.90 and 4.00), and wide luminosity range, $\log(L/\mathrm{L}_{\odot}) = 1.8 \pm 0.5$.

The nature of f_2 is not clear: it is probably too low to be a δ-Scuti pulsation, at least for a star in the PMS phase of evolution, as it implies minimum luminosities that happen to coincide approximately with the birthline, as show in Figure 3.48, with corresponding echelle diagram in Figure 3.49. It is not impossible that VV Ser is this luminous, but it is improbable, and would imply extreme youth, having just emerged from the cloud in which it formed.

The next three frequencies are also quite low, in sequence, they are f_4 = 45.14 μHz, f_3 = 51.74 μHz, and f_1 = 70.83 μHz. Figure 3.50 shows the consequences of successively eliminating f_2, then f_4, and finally f_3 from the χ^2 fits, essentially allowing a lower and lower luminosity range (gray dots) to each subsequent fit. Even using these higher frequencies to put constraints on the luminosity implies that VV Ser is a rather luminous, higher-mass star than most of its HAe counterparts. Sample echelle diagrams for each of these cases are also given in the same figure, and in all cases good fits exist to the observed frequencies.

Figure 3.51 provides one last set of limits on the models. Here, the *highest* frequency is the limiting frequency, and even in this case the minimum allowed luminosities are respectably high, although substantially lower than before. Also pictured are the expected minimum rotational splitting from the minimum $v \sin i$ = 85 km/s measurement of Grady et al. (1996). The values range from about 2 to 7 μHz, indicating that rotational-split multiplets are going to become confused with one another.

The astroseismic analysis of Ripepi et al. (2007) also included the calculation of gravity modes (g-modes), and came to the conclusion that the lower frequencies that were detected might be g-modes, and therefore allowed some lower-luminosity models to be fit to their data. Even so, their best-fit models were still fairly luminous,

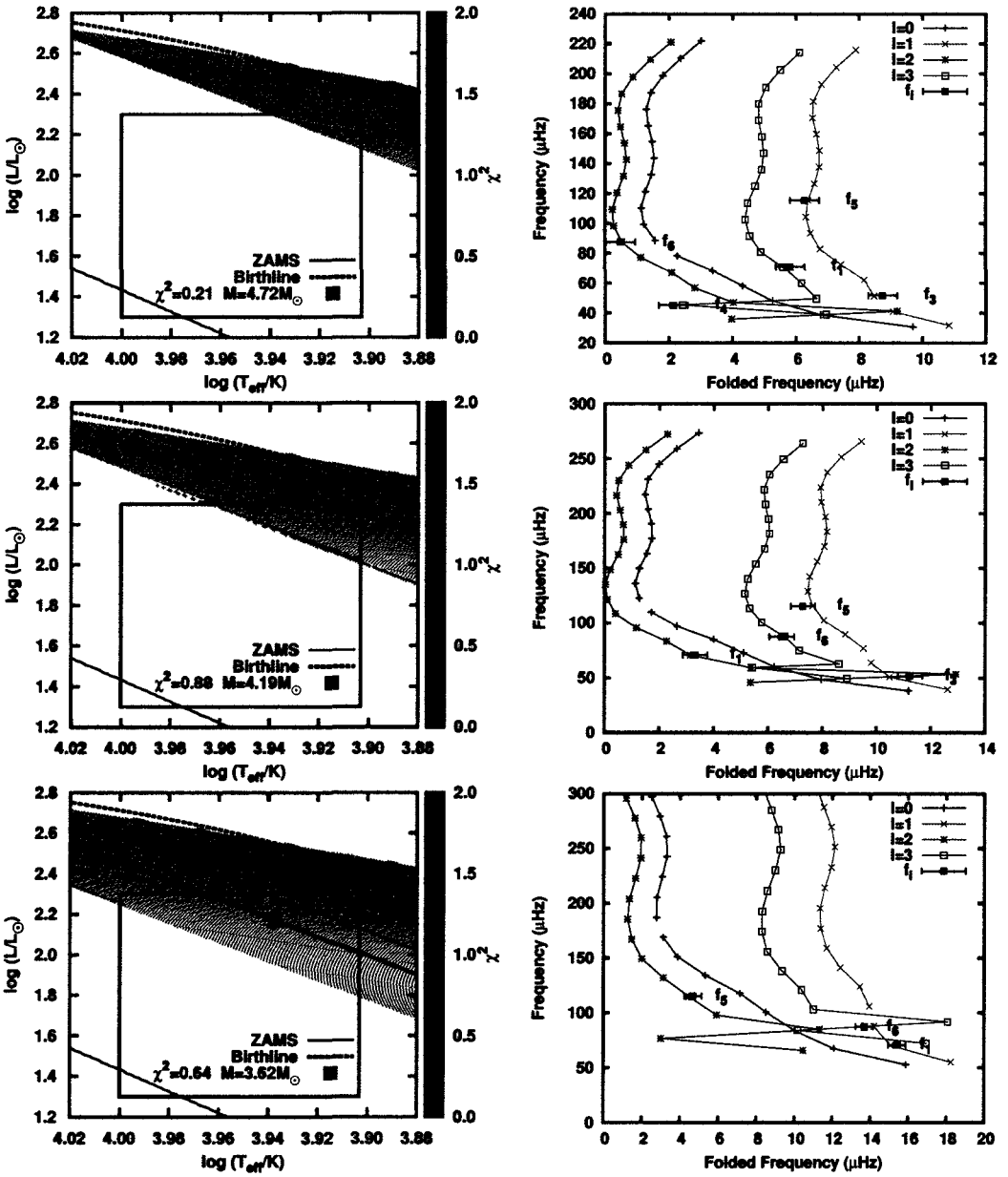

Figure 3.50: Analysis of VV Ser frequencies of Ripepi et al. (2007). Top row to bottom: allowed models and χ^2 fits to $\ell = 0$ to 3 modes with f_4, f_3, and f_1 subsequently serving as the minimum allowed frequencies in the fits, with all lower frequencies removed from consideration.

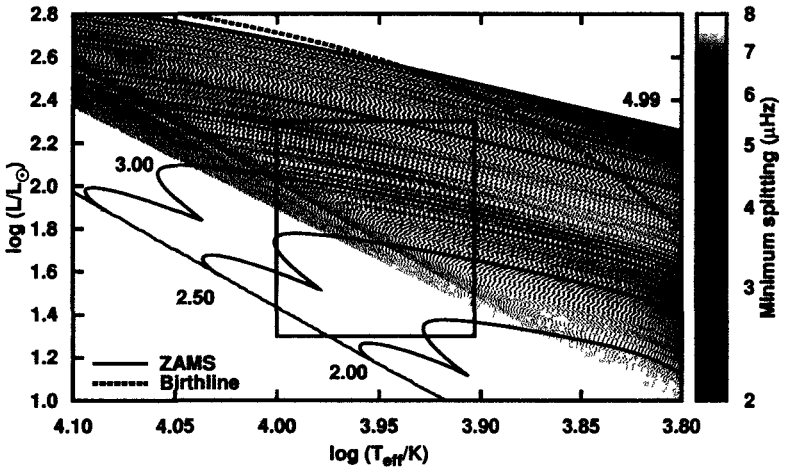

Figure 3.51: Models for VV Ser for which the fundamental frequency is $< f_5$, and also the approximate minimum rotational splitting that could be expected by the lowest measured $v \sin i = 85$ km/s by Grady et al. (1996).

in the upper range of the error box, $\log(L/\mathrm{L}_\odot) = 2.2$ and higher; the only fits to pure p-mode solutions were significantly cooler than what is indicated by the error box, at around $T_{eff} = 6000$ K. So, it is possible that gravity modes are being observed in this star, but g-modes were not calculated for this thesis, and so comparisons with g modes in this work is not possible at the current time. Even so, extreme caution must be taken before labelling any frequency (such as f_1) a g-mode, as stellar-surface peculiarities (*e.g.* sunspots), combined with rotation, might produce signals within this frequency range. Cycle/day integer aliases in the ground-based observations could also cause misidentification of the type of signal as well.

VV Ser might be a member of an interesting class of star as described in Aerts, Christensen-Dalsgaard & Kurtz (2010, page 64), a cool extension of the slowly-pulsating-B (SPB) stars into the late-B and early-A stars spectral range that can occur when stars are rapidly rotating, like VV Ser is. Four stars of this variety have been unambiguously identified to date in this spectral range, with periods ranging

from 2 hours (140 μHz) to 8 hours (38 μHz). These stars are γ UMi (A2 III, $v \sin i =$ 165 km/s), γ CrB (A0 V, $v \sin i = 112$ km/s), ET And (B9 IV, $v \sin i = 80$ km/s), and HD 121190 (B9 V, $v \sin i = 118$ km/s). The pulsations are thought to be rotationally-shifted κ-driven, non-radial, g-mode frequencies. It is the rotational shifting of modes that make the pulsations viable in stars which are otherwise cooler than most SPB stars (Aerts & Kolenberg 2005, and references therein). If these frequencies hold up to future observations, then VV Ser would be the first PMS star of this sub-class of SPB stars to have been observed, if not identified as such at the time, and indeed, could be a hybrid star, given the higher δ-Scuti-frequencies also observed.

In summary, VV Ser is a very intriguing object, in which space-based observations will probably be needed to further study the pulsation spectrum of the star, and unambiguously determine the pulsation frequencies of the star. It may be a rapidly-rotating SPB with δ-Scuti characteristics, or a very luminous pure δ-Scuti star that has recently emerged from its birth cloud.

3.1.3.4 PDS 2

PDS 2 (GSC 08474-00024) is a PMS star in Phoenix, first identified as such in the Pico dos Dias Survey (PDS) of Gregorio-Hetem et al. (1992). It is one of the cooler stars appearing in this thesis, with spectral classifications F3 Ve by Vieira et al.

Label	Freq (c/d)	Err Freq (c/d)	Freq (μHz)	err Freq (μHz)
f_1	17.1	0.1	197	2
f_2	13.8	0.1	159	2
f_3	24.2	0.1	281	2

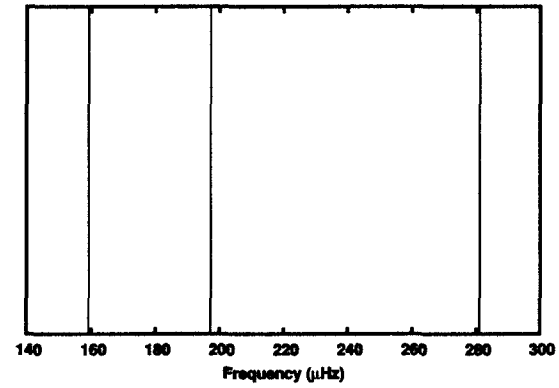

Figure 3.52: PDS 2 frequencies as found by Bernabei et al. (2007). Amplitudes were not indicated in the source paper, hence the lack of such a label for the y-axis of the graph.

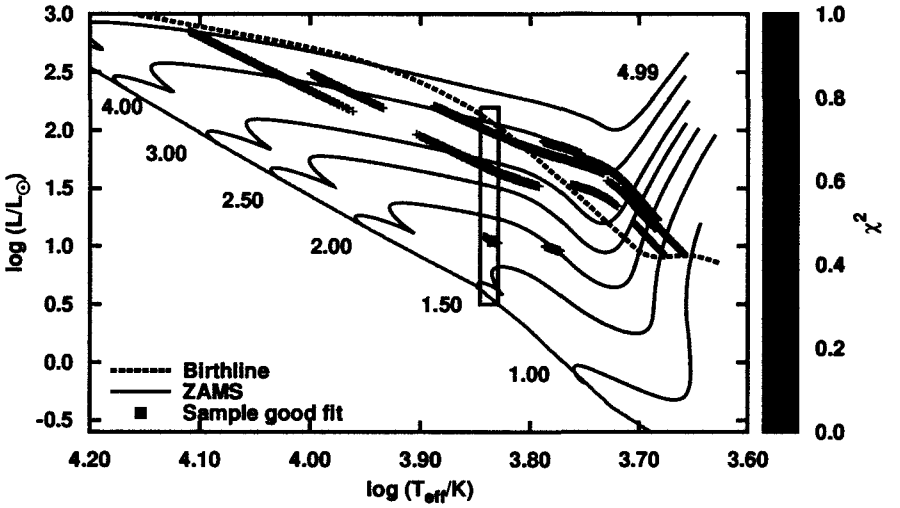

Figure 3.53: χ^2 fits to radial modes only to the three frequencies of PDS 2, as observed by Bernabei et al. (2007). There are no distance estimates available for the star, so the minimum and maximum luminosities merely indicate the possible range of values available to a PMS δ-Scuti star at the indicated temperatures.

(2003) and of F6e by Suárez et al. (2006). The F3 Ve classification does not appear to have been determined by Vieira et al. (2003), but they are reporting a result from the PDS survey, however I have not been able to track down the original determination. Confusingly, in their Table 3, Vieira et al. (2003) also report a spectral class of B0 V, far too hot a designation for a δ-Scuti star; they also report $v \sin i = 175$ km/s, which is a typical value for this class of star. The Cape Photographic Catalog reports a spectral type of F2 (Jackson & Stoy 1996). The broad-band photometry does not support the F6e class - such a star would be redder intrinsically than the $B-V = 0.36$ magnitudes that have been observed. An F3 spectral class would essentially imply zero reddening, with F2 or F1 indicating very minimal reddening. Given the broad-band photometry, I use in this analysis temperatures consistent with an F1 through F3 class star. Unfortunately, the distance to PDS 2 is unknown. Tycho measurements report an unusable parallax of 9.7±23.1 mas (Perryman & ESA 1997). Vieira et al. (2003) were unable to associate it clearly with any particular star-formation region,

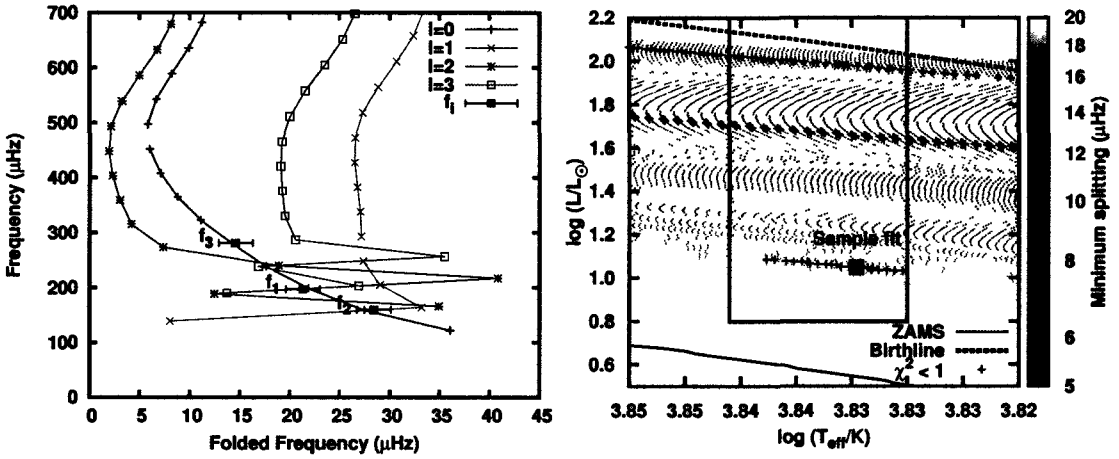

Figure 3.54: Echelle diagram for PDS 2 for the sample fit of Figure 3.53. Model parameters: $\chi^2 = 0.16$, mass = 1.71 $M_\odot$, $\log(T_{eff}/K) = 3.835$, $\log(L/L_\odot) = 1.049$. Left: minimum rotational splitting given a $v \sin i = 175$ kms/, as well as the models that can support all of the frequencies observed by Bernabei et al. (2007).

labelling it as "isolated?", and thus not even able to use the distance to an associated SFR as a distance estimate for PDS 2.

Bernabei et al. (2007) reported the detection of three frequencies in PDS 2, however analysis was left to a future paper[3], with the amplitudes of the frequencies not reported in the notice. The frequencies are listed in Figure 3.52 in both tabular and graphical form. Observations were performed using the 0.6 m REM telescope at La Silla, Chile, over a time base of 7 nights.

Figure 3.53 shows the result of fitting the three frequencies to radial modes only. Unsurprisingly, given the large uncertainties associated with each frequency, there are solutions available, and if one of these frequencies happens to be a non-radial mode, then many more solutions would also be possible. Note that due to the inability to assign a distance to the star that the error bars in luminosity for the star's HRD position are merely place holders to guide the eye, and indicate all possible luminosities available to this class of star. Figure 3.54 on the left shows a sample echelle diagram from the low-luminosity family of solutions at around $\log(L/L_\odot) = 1$,

[3]See Marconi et al. (2010), a reference which was discovered too late for the results to be included within this analysis.

indicating that for that particular family of solutions, the observed frequencies would be low-order radial modes. The high-luminosity solutions would indicate much higher radial orders for those particular solutions. The right-hand side of Figure 3.54 shows the minimum expected rotational splittings of a multiplet, given $v \sin i = 175$ km/s, as listed above. The expected splittings range from about 4 to 22 μHz. Also shown are the stellar models that can support the reported frequencies, given the minimum frequency of $f_2 = 159$ μHz, and maximum frequency of $f_3 = 281$ μHz. In order to support f_2, the star must be more luminous than the ZAMS, indicating youth, if this is, indeed, a PMS star.

Without a distance estimate, the luminosity ranges available to the star from astroseismology, the spectral class, and the broad-band photometry of Vieira et al. (2003) ($V = 10.87$, $B-V = 0.38$ magnitudes) can be used to work backwards to make a distance estimate for the star: from these values, a minimum distance of 400 pc and maximum distance of about 1600 pc are implied. Note that if the luminosity class from the spectral classifications are correct, then the lowest luminosity solutions, and therefore the closest distances would be the preferred solution. Similarly, Vieira et al. (2003) inferred a photometric distance to PDS 2 of 340 pc, which would not have included the extra constraints imposed upon the star by asteroseismology, and so are not in great disagreement with the estimate of 400 pc.

In summary, the unknown distance to PDS 2, coupled with the large error bars associated with the frequency determinations mean that there are many possible solutions to an astroseismic analysis of the star, including ones that identify radial modes for all of the observed frequencies. The lowest frequency observed does imply a minimum possible distance for the star of around 400 pc.

3.1.3.5 DX Cha, RS Cha (A and B)

DX Cha and RS Cha are HAe systems that also happen to be members of very sparse open clusters in the Chamaeleontis star-formation regions. As such they are treated together in the Open Clusters section of this chapter, along with EE Cha

and EF Cha under the cluster heading "η and ϵ Chamaeleontis Clusters". Please see Section 3.3.1 for details.

3.1.4 Stars to be observed by *MOST*

3.1.4.1 PX Vul

PX Vul (LHα 483-41) is a PMS star thought to be part of the Vul R2 association, distance 420 pc (Herbst et al. 1982). Spectral classifications put it on the region of the HRD where HAe and T Tauri stars (TTS) meet, and so in the literature it has been labelled as either, depending upon the project. Examples are F0 Ve (Herbst et al. 1982), F3 Ve TTS (Mora et al. 2001), and F3±1.5 HAe star (Hernández et al. 2004). (Note that in the latter, Herbig Fe star, instead of Herbig Ae star, might be a more appropriate label.) Given PX Vul's spectral class, it is one of the coolest stars considered in this thesis. Eisner et al. (2005) found $v \sin i$ = 78±11 km/s, and active accretion at 1.3×10^{-6}M$_\odot$/yr. For this analysis, I use V = 11.54, $B-V$ = 0.83 magnitudes (Manoj et al. 2006).

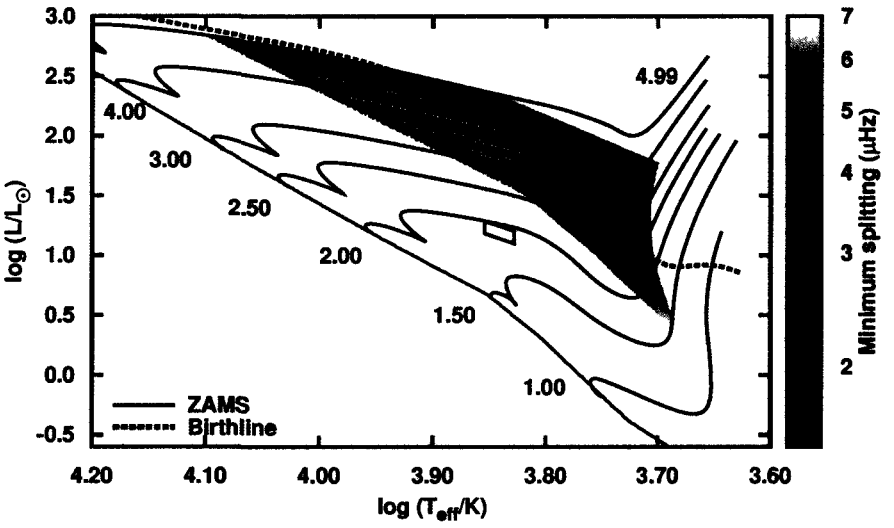

Figure 3.55: Models allowed by f_1 = 60 μHz of PX Vul, observed by Bernabei et al. (2004), considering the fundamental mode of each model. Also shown are the minimum expected rotational splitting expected from $v \sin i$= 67 km/s of Eisner et al. (2005).

Non-periodic variability was first detected by Herbst et al. (1982) of $\Delta V \sim 0.3$ magnitudes. Suspected δ-Scuti variability was reported by Bernabei et al. (2004), with two very preliminary frequencies of $f_1 = 5 \pm 3$ c/d and $f_2 = 13 \pm 3$ c/d observed. To confirm/refute the pulsations in PX Vul, it (along with WW Vul) is scheduled for observation by *MOST* July 16-29, 2011, targets suggested by K. Zwintz and myself for observation for this very purpose. Analysis is not available at the time of this work. Given the uncertainties associated with the preliminary frequency determinations of Bernabei et al. (2004), only a very speculative analysis of f_1 can be given. Figure 3.55 shows the models that can support $f_1 = 60$ μHz, and also shows the minimum rotational splitting that could be expected from $v \sin i$= 67 km/s. The star's position in the HRD is quite under-luminous given that the frequency of f_1. Several reasons for this discrepancy could exist, either the extinction has been underestimated, the distance to the star is greater than what has been assumed, or the frequency detected by Bernabei et al. (2004) is not a signal of p-mode pulsation. The *MOST* observations should be able to address the latter.

3.1.4.2 WW Vul

WW Vul is a HAe object displaying UX Ori variability in V in the range 10.4 to 12.6 magnitudes. Observations of this behaviour date back as far as 1929 (*e.g.* Friedemann et al. 1993a,b), with most of the time spent at or near light maximum (10.4 V magnitudes), except for when it is eclipsed by a circumstellar cloud. Spectral classifications range mostly from A0 Ve to A3 Ve (*e.g.* Jacchia 1941; Mora et al. 2001; Hernández et al. 2004), or even A4IV-V(e)b shell (Gray & Corbally 1998). $v \sin i$ = 125 km/s (Corporon & Lagrange 1999), 220±22 km/s (Mora et al. 2001), and 150 km/s (Grinin et al. 2001) have been measured. WW Vul is not associated with any particular star-formation cloud, but with a general area of nebulosity and young stars in Vulpecula. As such, there are not any distance estimates to WW Vul based upon colour-magnitude diagrams of a nearby star cluster. Friedemann et al. (1993b) estimate a distance of 534 pc based upon a reddening-verses-distance diagram

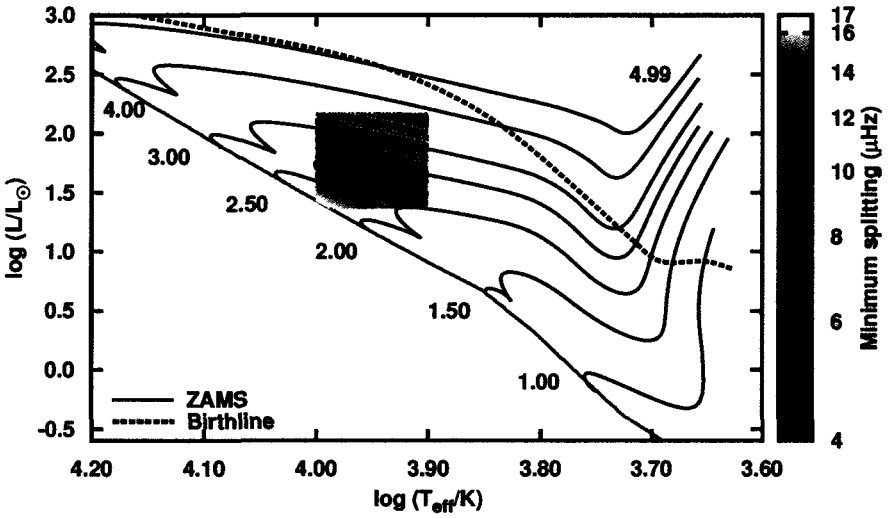

Figure 3.56: Position of WW Vul in the HRD, along with the minimum expected rotational splitting expected from $v \sin i$= 125 km/s of Corporon & Lagrange (1999).

for stars within 0.5 degrees of the star in the sky. They do not assign an uncertainty to this calculation. Estimating by eye from their Figure 1, I assign a crude error estimate of about 75 pc, corresponding to a distance range of 509 to 659 pc.

Bernabei et al. (2004) found very preliminary evidence for pulsation at about 5 c/d, and so WW Vul has been selected as a *MOST* target for observation from July 16-29, 2011 at the suggestion of K. Zwintz, and myself for confirmation/refutation of those pulsations. The analysis of the light curve will not be available prior to the completion of this thesis. Due to the extremely tenuous pulsation detection, no asteroseismic analysis is attempted here, except for an estimate of the star's minimum expected rotational splitting, given the minimum $v \sin i$ = 125 km/s value initially quoted above. The results of this analysis appear in Figure 3.56. The star is above the ZAMS, with minimum expected splitting of the order of 10 μHz.

3.1.5 Stars removed from PMS δ-Scuti list through *MOST* observations.

The following three stars were previously suspected, but not confirmed, to harbour δ-Scuti pulsations. *MOST* observations of these stars have shown that they are *not* pulsating, and the previous detections were probably of some other sort of

variability briefly mimicking a pulsation. In all cases, original observations were over short time bases (a night or two at most), and so the detections were considered tentative, requiring further observations. These star are mentioned only briefly. They all appeared in the most recent list of PMS δ-Scuti stars (confirmed or suspected) compiled by Zwintz (2008).

3.1.5.1 UX Ori

UX Ori is the HAe prototype star for those stars exhibiting deep, Algol-like eclipses, not from a companion star blocking the light from another member of a binary system, but from circumstellar clouds occasionally blocking part of the light from the star. Many of the HAe stars in this study exhibit UX Ori-type variability. UX Ori has a spectral type around A4 IVe (Mora et al. 2001, and references therein), with the parallax of 3.57±2.28 mas from the latest reductions of van Leeuwen (2007), indicating a distance range of 170 to 780 pc. Suspected δ-Scuti behaviour was communicated to Zwintz (2008) by P. Amado via private communication. *MOST* observed this star from November 15 to December 7, 2006, and δ-Scuti pulsations were not found in the light curve (K. Zwintz, private communication). These results have yet to be published.

3.1.5.2 HD 35929

HD 35929 is a HAe F0 IIIe foreground star to the Orion OB1 association, parallax 2.78±0.72 mas, corresponding to a distance range of 290 to 490 pc (van Leeuwen 2007).

In a targeted search for PMS δ-Scutis, Marconi et al. (2000) observed the star for two nights in December 1998 using Strömgren CCD photometry and the 0.9 m DUTCH telescope. They observed a frequency of about 5.1 c/d, attributed to pulsation, although the true frequency could have been one of the integer cycle/day aliases seen in the power spectrum. This frequency was observed in all the filters in which the star was observed. In order to confirm/refute this pulsation, at the

suggestion of K. Zwintz and myself, *MOST* observed HD 35929 from November 22-30, 2010, and was found *not* to be pulsating. The results have yet to be published. This is a most interesting result, as HD 35929 was considered to be one of the earliest detections of PMS δ-Scuti pulsation, and further analysis of the *MOST* light curve is warranted. In particular, it needs to be investigated whether there are other signals within the light curve, or not, that can mimic δ-Scuti pulsations when observed on such a short time scale from a single ground site.

3.1.5.3 BF Ori

BF Ori is a HAe star thought to be a member of the Orion Ob1c association, with spectral classifications ranging from A0 (Parenago 1954; Bernacca 1967) to A6 IV shell Nab7 (Gray & Corbally 1998) in the literature. Unfortunately, the Hipparcos parallax is unphysical (-0.55±1.58 mas; van Leeuwen 2007).

Bernabei et al. (2004) reported a frequency of 4.7±1.0 c/d. Upon *MOST* not detecting δ-Scuti pulsations in HD 35929 (see Section 3.1.5.2), targeting was switched to BF Ori in order to see if pulsations could be detected in that star. The observations ran from November 30 to December 12, 2010, and preliminary analysis of the light curve showed that the star was *not* pulsating. Serendipitously, another star within the field of observations, the HAe star HD 37357, *was* discovered to be pulsating (Section 3.1.1.5), and so the combined observing run of candidate PMS pulsators of November/December 2010 turned out to be quite productive: two null results, and one serendipitous detection of a previously-unsuspected member of the class.

3.2 Open cluster stars – *MOST* observations

3.2.1 NGC 2264 in Monoceros

Six stars exhibiting δ-Scuti pulsations have been previously identified in the field of NGC 2264, a young open cluster that is part of the larger Monoceros OB1 association. It was in NGC 2264 that the first two PMS δ-Scuti stars, V588 Mon and V589 Mon, were identified by Breger (1972). The other four stars were identified

by *MOST* observations by Zwintz et al. (2009a), three of which are probably PMS δ-Scuti stars (NGC 2264 104, HD 261771, and HD 261387) and the fourth perhaps a field star (HD 261230). Asteroseismic analysis of these six stars was performed by this research group in Guenther et al. (2009) using the *MOST* observations, with mixed results. Further analysis of V588 Mon and V589 Mon was performed in Zwintz et al. (2011) using both the *MOST* data and information collected with the *CoRoT* satellite. In the *CoRoT* data, signatures of granulation are thought to have been found, the result of a very-near-surface convection layer in the stars, interfering with the interpretation of the pulsation spectra from the *CoRoT* light curves of these two stars.

Importantly, the *MOST* frequencies reported in Zwintz et al. (2009a) were confirmed in the *CoRoT* data, and thus these frequencies are most likely due to pulsation, not granulation; granulation would produce random, non-repeatable (except by coincidence) frequencies from one observing session to the next, and so in this case one would not expect the precise frequencies observed by *MOST* to then be confirmed by *CoRoT*. *CoRoT* was able to pick up the more subtle signatures of granulation due to increased photometric precision. With this in mind, I perform a reanalysis of the *MOST* frequencies of the six stars analysed in Guenther et al. (2009), using the techniques developed since publication to add further insight, and to make the analysis consistent with the other stars appearing in this study. In this analysis the minimum distance to NGC 2264 is taken from Sung, Bessell & Lee (1997), where they found a distance modulus of 9.4 ± 0.25 for a minimum distance of 676 pc. The maximum distance is from Baxter et al. (2009), who find 913 ± 110 pc, corresponding to a maximum distance of 1023 pc and a maximum distance modulus of 10.05.

3.2.1.1 V588 Mon

V588 Mon (NGC 2264 2, HD 261331) is a $V = 9.7$ apparent-magnitude star with a spectral class, at least with respect to temperature, remarkably in agreement

ID	freq. (c/d)	err freq. (c/d)	freq (μHz)	err freq. (μHz)	Amp (mmag)
f_1	5.141	0.026	59.5	0.3	8.7
f_2	10.938	0.026	126.6	0.3	5.9
f_3	5.262	0.026	60.9	0.3	5.3
f_4	7.033	0.026	81.4	0.3	3.3
f_5	5.547	0.026	64.2	0.3	2.2
f_6	8.294	0.026	96.0	0.3	2.0
f_7	7.664	0.026	88.7	0.3	1.9
f_8	10.981	0.026	127.1	0.3	0.6

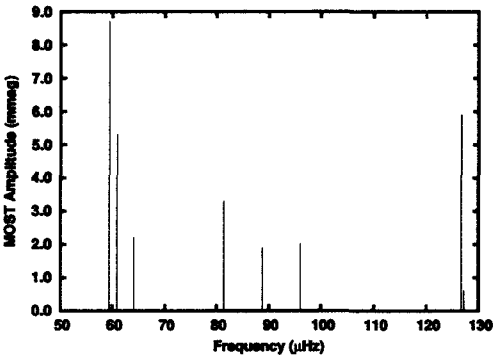

Figure 3.57: Frequencies of V588 Mon in NGC 2264 as observed by *MOST*.

over many observers, A7 III or IV (Walker 1956) or A7 V (Voroshilov et al. 1985; Kuznetsov et al. 2000).

As mentioned before, Breger (1972) discovered δ-Scuti pulsations in this star, and along with V589 Mon in the same study, these two stars were the first PMS δ-Scuti stars to be discovered. The star's proper motion is consistent with that of the cluster (Høg et al. 2000). This, along with a consistent place in the colour-magnitude diagram for the cluster as a whole, mean that cluster membership is likely, and that

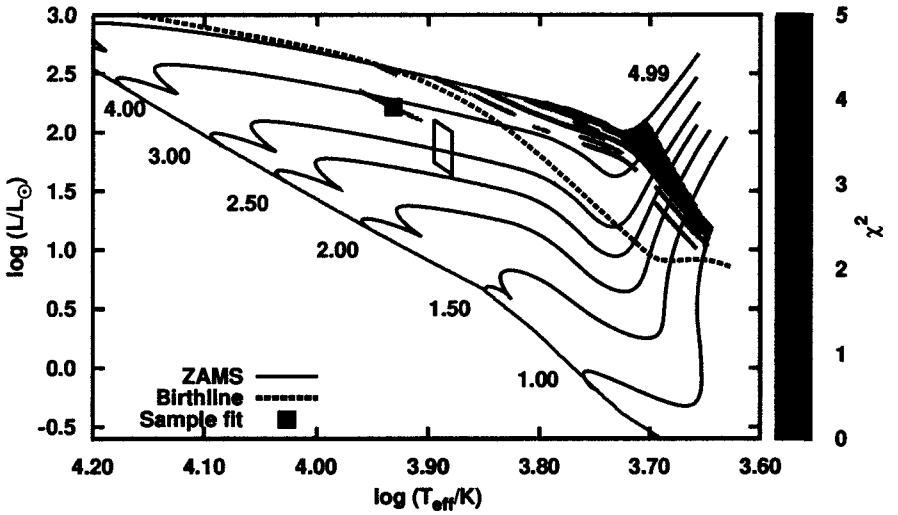

Figure 3.58: χ^2 fit to all frequencies of V588 Mon in NGC 2264 observed by *MOST*, $\ell = 0$ to 3 modes, along with the star's position in the HRD.

the star is in the PMS phase of evolution. Kallinger, Zwintz & Weiss (2008) measured a typical $v \sin i = 130 \pm 20$ km/s for the star.

Eight frequencies attributed to pulsation were observed by *MOST* by Kallinger, Zwintz & Weiss (2008), and later analysed asteroseismicly by Guenther et al. (2009). Those observations, combined with observations from *CoRoT* were analysed by Zwintz et al. (2011), in which a signature from granulation appears to have been observed (see the introduction for the NGC 2264 subsection for more details). It is the *MOST* observations upon which I will perform an analysis. The frequencies range from 59.5 to 127.1 μHz, and appear in tabular and graphical form in Figure 3.57.

Figure 3.58 shows V588 Mon's position in the HR diagram, well above the ZAMS, consistent with PMS star status. Also shown is the result of χ^2 fitting to $\ell = 0$ to 3 modes to all pulsation frequencies as observed by *MOST*. Within the star's position in the HRD, there are no fits with $\chi^2 < 5$, although there are a few such solutions that are slightly hotter and more luminous than the HRD position. An echelle diagram is given for one of these fits in Figure 3.59. In this case, the

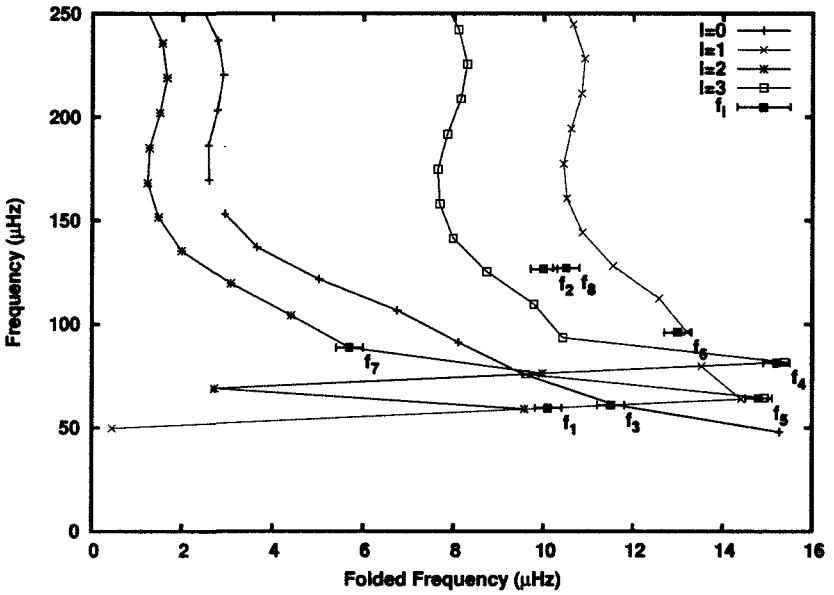

Figure 3.59: Sample echelle diagram for all frequencies of V588 Mon as observed by *MOST*. Model parameters: $\chi^2 = 4.3$, mass = 3.80 $M_\odot$, $\log(T_{eff}/K) = 3.93$, $\log(L/L_\odot) = 2.21$.

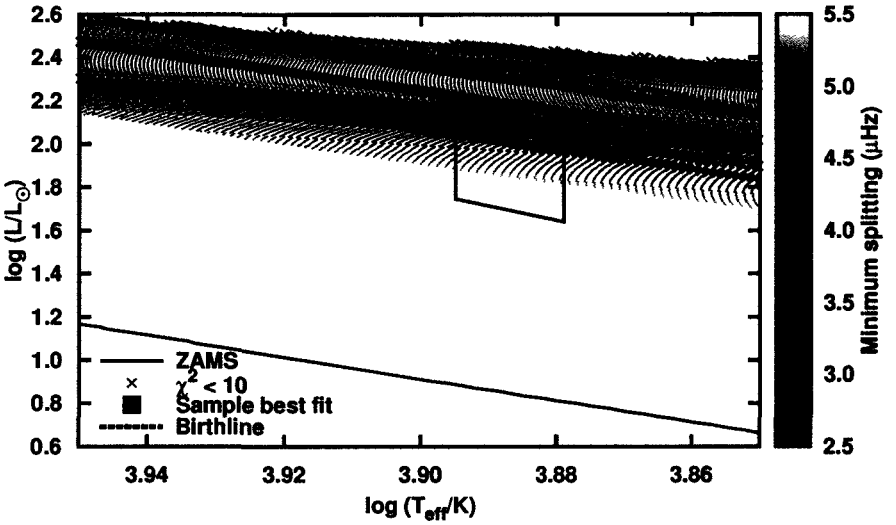

Figure 3.60: Stellar models that can support all the frequencies of V588 Mon of NGC 2264 that were observed by *MOST* considering the fundamental frequency of each model. Blue "×" indicate models with $\chi^2 < 10$. Also given are the minimum expected rotational splittiing, given $v \sin i = 130 \pm 20$ km/s.

echelle diagram reveals fits to both radial and non-radial modes of low radial order. The lowest pulsation frequency, $f_1 = 59.5$ μHz, is quite low, and therefore suggests looking for the minimum luminosities that the star could have. Figure 3.60 show the models with a fundamental frequency less than f_1, and so therefore can support p-mode pulsations of that frequency or less, along with all models with $\chi^2 < 10$. The minimum luminosities form a line cutting through the middle of the star's position in the HRD, thus explaining why only high-luminosity models were found for the χ^2 fitting to models, and further supports the star pulsating in low radial orders.

Figure 3.60 also shows the approximate minimum expected rotational splittings, between two adjacent frequencies in a multiplet, assuming minimum rotational velocity of 110 km/s (from $v \sin i = 130 \pm 20$ km/s of Kallinger, Zwintz & Weiss 2008). For the star's position in the HR diagram, minimum splittings are in the range of 3.5 to 5.5 μHz, a bit too large for the frequency differences between f_1 and f_3 and also f_2 and f_8 which are on the order of 1.5 and 0.5 μHz respectively, making this possibility less likely. It is possible that distortion from rotation could bring two

members of a multiplet closer together into this range of frequency differences, but this effect would be hard to untangle from the spacings between pulsations of different ℓ orders without further calculations.

In summary, just by considering the values of f_1, constraints upon the luminosity of V588 Mon have been imposed, consistent with the star's HRD position, and therefore confirming the star's PMS nature, if it is indeed a cluster star. Stellar rotation appears to be modifying the observed frequencies, however not in such a way that suggests the observed frequency pairs are members of single, rotationally-split multiplet.

3.2.1.2 V589 Mon

V589 Mon (NGC 2264 20, HD 261446) is the other of the two original δ-Scuti stars discovered by Breger (1972) in NGC 2264. It is one of the coolest stars in this study, with spectral classifications running from F0 V (Young 1978) to F3 V (Kuznetsov et al. 2000) and F2 III (Walker 1956), with apparent V magnitude = 10.3. With $v \sin i$ = 60±10 km/s it has one of the lower known projected rotational velocities amongst PMS δ-Scuti stars (Kallinger, Zwintz & Weiss 2008). Like V588 Mon, V589 Mon has been observed by *MOST*, and *CoRoT* with 12 frequencies attributed to pulsation detected in the light curve by *MOST* (Kallinger, Zwintz & Weiss 2008; Guenther et al. 2009), and with signals of granulation thought to have

ID	freq. (c/d)	err freq. (c/d)	freq (μHz)	err freq. (μHz)	Amp (mmag)
f_1	6.489	0.026	75.1	0.3	14.0
f_2	6.990	0.026	80.9	0.3	8.7
f_3	8.303	0.026	96.1	0.3	3.3
f_4	5.763	0.026	66.7	0.3	3.3
f_5	8.700	0.026	100.7	0.3	2.4
f_6	10.195	0.026	118.0	0.3	2.3
f_7	9.469	0.026	109.6	0.3	1.5
f_8	6.281	0.026	72.7	0.3	1.6
f_9	9.314	0.026	107.8	0.3	1.5
f_{10}	10.264	0.026	118.8	0.3	1.5
f_{11}	10.990	0.026	127.2	0.3	1.4
f_{12}	6.696	0.026	77.5	0.3	0.8

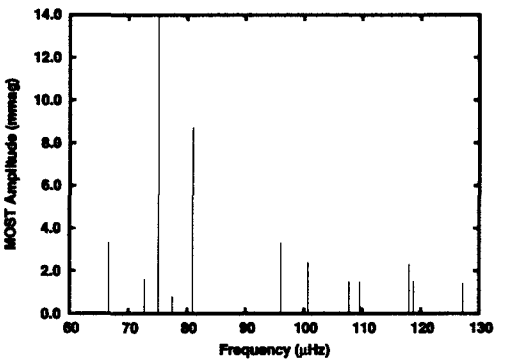

Figure 3.61: Frequencies of V589 Mon in NGC 2264 as observed by *MOST*.

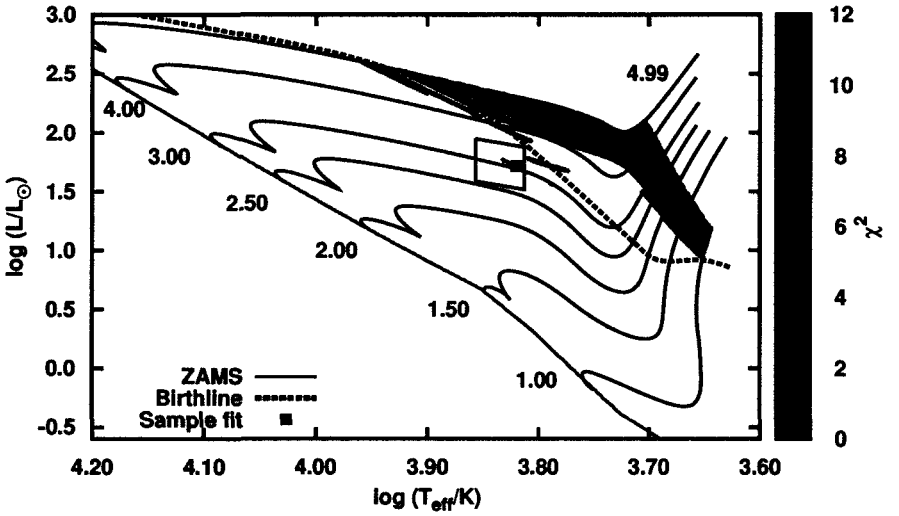

Figure 3.62: χ^2 fit to all highly-significant frequencies of V589 Mon in NGC 2264, $\ell = 0$ to 3 modes, along with the star's position in the HRD.

been detected by *CoRoT* (Zwintz et al. 2011). The pulsation frequencies detected by *MOST* were confirmed by *CoRoT*. The asteroseismic analysis of V589 proved difficult, with no good solutions found within the PMS models of Guenther et al. (2009).

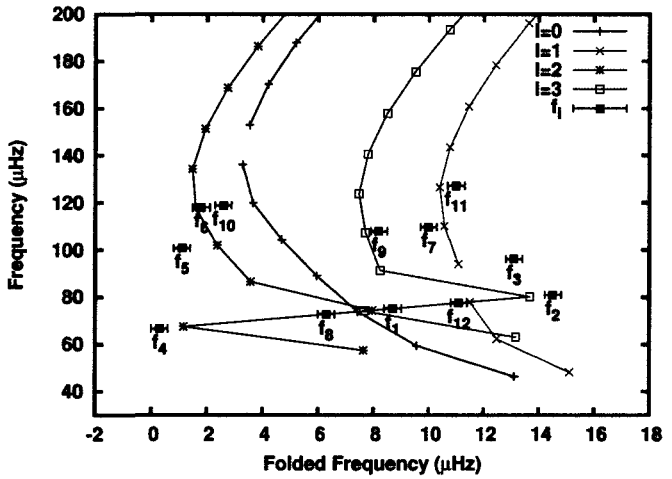

Figure 3.63: Sample echelle diagram for all frequencies of V589 Mon as observed *MOST*. Model parameters: $\chi^2 = 10.3$, mass = 3.06 $M_\odot$, $\log(T_{eff}/K) = 3.82$, $\log(L/L_\odot) = 1.71$.

Figure 3.61 displays the frequencies observed by *MOST* in both tabular and graphical form. Coincidentally, V589 Mon has a similar pulsation spectrum to V588 Mon in that it covers a similar frequency range.

Figure 3.62 shows χ^2 fits to $\ell = 0$ to 3 modes of all 12 frequencies detected by *MOST*. There are no good fits near the star's region of the HRD, with a best-fit value within the error box of $\chi^2 = 10.3$

Figure 3.63 shows the sample echelle diagram for that model, and demonstrates that the star is probably pulsating in frequencies of low radial order, and requires non-radial modes to explain the pulsations. The similarity between V589 Mon's pulsation spectrum to that of V588 Mon suggest a similar analysis is in order. Figure 3.64 shows an HRD of the PMS models that have a fundamental frequency low enough to support $f_4 = 66.7$ μHz, the lowest frequency amongst those detected. It shows the minimum-luminosity models are in agreement with the star's position in the HRD, and would *not* support a dimmer (and hence foreground) star, adding a piece of evidence in favour of V589 Mon being a member of NGC 2264. I further note that

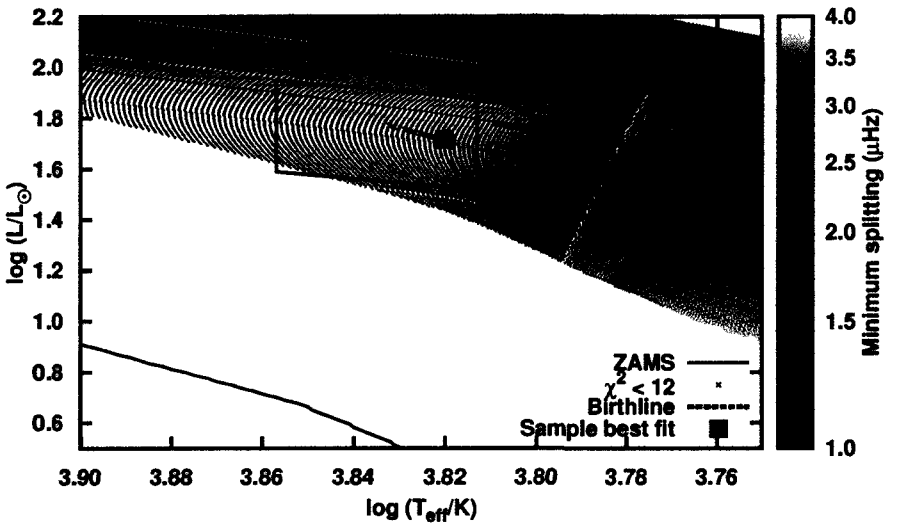

Figure 3.64: Stellar models that can support all the frequencies of V589 Mon of NGC 2264 that were observed by *MOST* considering the fundamental frequency of each model. Blue "×" indicate models with $\chi^2 < 12$.

this star is very close to the birthline, further suggesting extreme youth if the star should be a cluster member.

Given a $v \sin i = 60 \pm 10$ km/s, Figure 3.64 also shows the minimum rotational splittings expected for a $v \sin i$ of 50 km/s. In the region of the star's position in the HRD, splittings of at least 2 to 3 μHz can be expected. This is on the order of the splittings seen between f_8, f_1 and f_{12}, between f_9 and f_4, and larger than that between f_6 and f_{10} (Figure 3.63). The first two of these sets could be adjacent members of a rotationally-split multiplet, however, once again, the difference between frequencies of different ℓ orders is of the same order, and so telling the difference between the two cases is not possible here, and requires further investigation.

In summary, once again, by considering the minimum frequency, constraints have been put on V589 Mon's luminosity, and significantly, in such a way as to support its membership in NGC 2264, and hence its status as a PMS star.

3.2.1.3 HD 261711

HD 2617711 (NGC 2264 39; GSC 00746-01783) is a rather dim star compared to the other stars in this study from NGC 2264, at V = 11.4 magnitudes. δ-Scuti pulsations were detected by *MOST* (Zwintz et al. 2009a). There is only one known spectral classification in the literature, A2 V from Voroshilov et al. (1985). Assuming an uncertainty in classification of one subclass, this yields a temperature range of $\log(T_{eff}/\mathrm{K}) = 3.941$ to 3.965, recognizing that a more modern determination of the spectral classification would be useful. As noted in Zwintz et al. (2009a), proper motion studies are consistent with cluster membership (Høg et al. 2000). The star's position in a dereddened V versus $B-V$ colour-magnitude diagram is consistent with cluster membership; it is located around the position where the pre-main-sequence stars are starting to intersect the main sequence, suggesting a star at or near the ZAMS if it is a cluster member. (*e.g.* Walker 1956).

MOST observed two rather high frequencies attributed to pulsation (Zwintz et al. 2009a), but with only two frequencies, the astroseismic analysis resulted in

ID	freq. (c/d)	err freq. (c/d)	freq (μHz)	err freq. (μHz)	Amp (mmag)
f_1	61.475	0.004	711.52	0.05	5.0
f_2	58.010	0.005	671.41	0.06	1.0

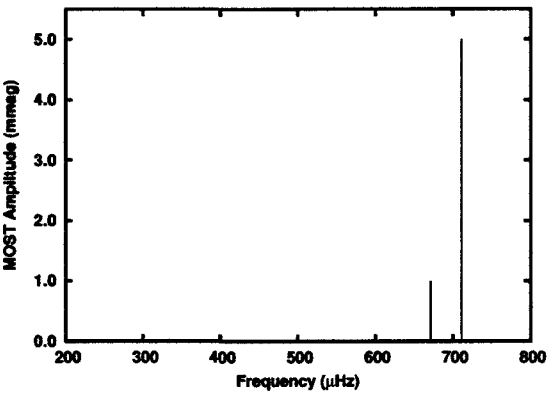

Figure 3.65: Frequencies of HD 261711 in NGC 2264 as observed by *MOST*.

ambiguity (Guenther et al. 2009). Nevertheless, over what was previously published, even with only two frequencies, some useful information can be extracted from the frequencies. Figure 3.65 shows these two frequencies in both tabular and graphical form.

Figure 3.66 shows χ^2 fits to $\ell = 0$ and 1 modes only. (Including $\ell = 2$ and 3 modes in the fits admits many more potential solutions without substantially changing the forthcoming qualitative analysis.) Even with just the $\ell = 0$ and 1 solutions, there

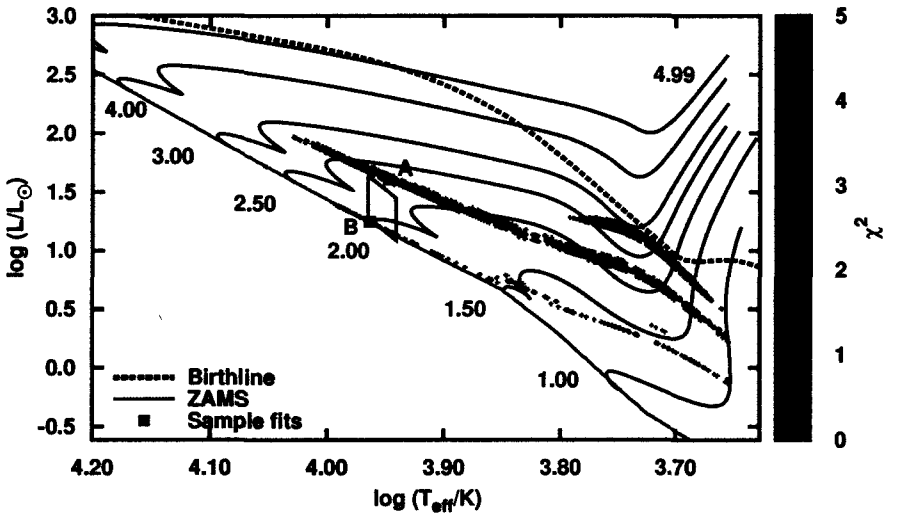

Figure 3.66: χ^2 fit to all highly-significant frequencies of HD 261711 in NGC 2264, $\ell = 0$ and 1 modes only.

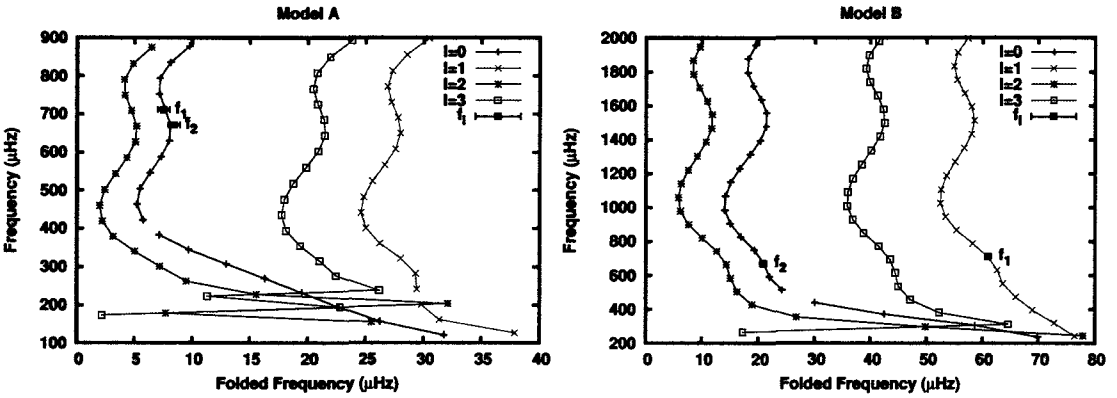

Figure 3.67: Echelle diagrams for χ^2 fits to frequencies of HD 261711. The left and right plots are for models A and B respectively in Figure 3.65. Model A specs: χ^2 = 0.23, M = 2.28 $M_\odot$, $\log(T_{eff}/\mathrm{K})$= 3.947, $\log(L/L_\odot)$= 1.605, $\log(L/L_\odot)$= 1.247. Model B specs: χ^2 = 0.10, M = 2.04 $M_\odot$, $\log(T_{eff}/\mathrm{K})$= 3.964.

are two bands of solutions that are evident, one just above HD 261711's position in the HRD, and a second group on or just above the ZAMS. There are two representative models indicated in Figure 3.66, Model A for the luminous group, which is a fit to two consecutive high-order radial modes, and model B, in which one frequency is fit to an $\ell = 0$ mode, and the other to an $\ell = 1$ mode. Echelle diagrams for both models appear in Figure 3.67. Note that the upper group is not a homogeneous family of solutions, with mode identifications the same from model to model for each frequency, but is rather a mix of solutions that do have one important commonality: in each model either f_1 and f_2 are identified as two radially-consecutive $\ell = 0$ modes, or two radially-consecutive $\ell = 1$ modes. All of these models would therefore have similar large spacings, as given by the difference in frequency between f_1 and f_2 (approximately 40 μHz). The lower group, as previously mentioned, identifies the star as very close to, or on the ZAMS.

However, the most insight can be gained by considering f_1 =711.52 μHz, which is a rather high frequency for a δ-Scuti pulsation; only models with an acoustic cut-off frequency larger than f_1 can support this pulsation frequency, and with this high a frequency, luminosity constraints can therefore be potentially placed upon the star. Figure 3.68 shows the result of this analysis. Importantly, these models are in

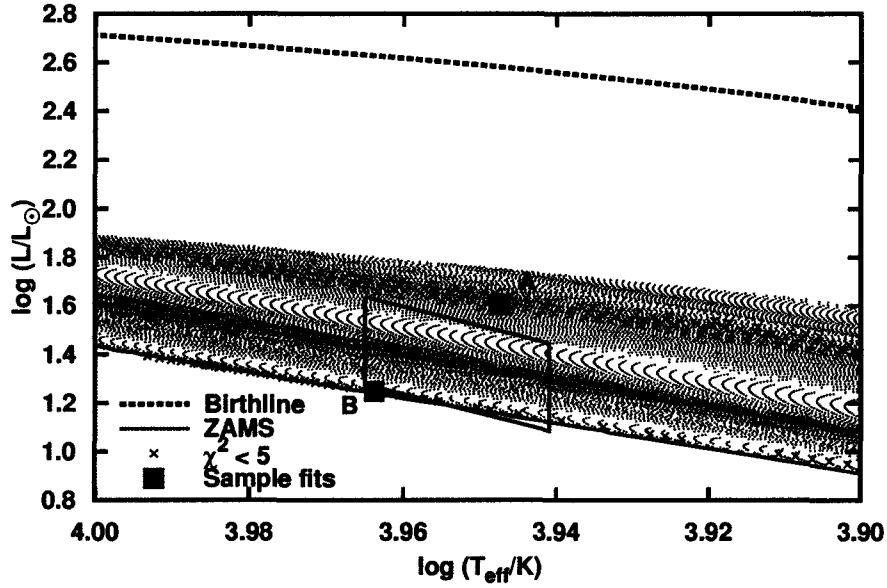

Figure 3.68: Stellar models that can support all the frequencies of HD 261711 of NGC 2264 that were observed by *MOST* considering the fundamental and acoustic-cut-off frequencies of each model. Blue "×" indicate models with $\chi^2 < 5$.

agreement with HD 261711's position in the HRD, and do not support it either being a background star of higher luminosity, or even a cluster member of higher luminosity and higher mass that is closer to the birthline. Of course, it is always possible that it is a field star that just happens to be spatially coincident with NGC 2264, but as previously mentioned, the proper motion of the star is consistent with cluster membership.

So, in summary, although two frequencies are not enough to significantly narrow the number of potential solutions, particularly considering that $\ell = 2$ and 3 modes were excluded from the χ^2 fits and would therefore admit many more solutions than what is presented here, based upon the value of f_1, important constraints have been placed upon the luminosity of the star. Those constraints are in agreement with the star's position in the HRD, and are consistent with the star being a member of NGC 2264.

3.2.1.4 HD 261387

HD 261387 (NGC 2264 49, GSC 00750-01597) is another relatively dim star in NGC 2264, V = 11.3 apparent magnitude, with spectral classifications in the literature of A1 (Pribulla et al. 2009), A2 (Voroshilov et al. 1985), and A3 V (Zwintz et al. 2009a), indicating a temperature range, $\log(T_{eff}/\mathrm{K}) = 3.941$ to 3.965. Proper motions are consistent with cluster memberships (Høg et al. 2000). $v \sin i = 140 \pm 10$ km/s is given by Zwintz et al. (2009a) and 127 km/s by Pribulla et al. (2009). Four frequencies attributed to pulsation were observed by *MOST* in Zwintz et al. (2009a) and analysed astroseismically by this research group in Guenther et al. (2009). The analysis showed that there were a few models in agreement with the star's position in the HRD. The analysis used $V = 10.6$ for luminosity determinations, however collectively the literature suggests $V = 11.3$ is more appropriate (Walker 1956; Mendoza V. & Gomez 1980; Mayne et al. 2007); the star is otherwise non-variable, except for the δ-Scuti pulsations, which are otherwise too small to account for this discrepancy. Regardless, the star's position in the HRD diagram will therefore be less luminous than in Guenther et al. (2009).

The four frequencies observed by *MOST* appear in tabular and graphical form in Figure 3.69. f_4, in particular is rather high, and will have implications on the maximum luminosity allowable for any stellar models. Figure 3.70 shows best-fit

ID	freq. (c/d)	err freq. (c/d)	freq (μHz)	err freq. (μHz)	Amp (mmag)
f_1	34.6939	0.0043	401.55	0.05	3.7
f_2	21.583	0.017	249.8	0.2	1.0
f_3	34.361	0.017	397.7	0.2	0.9
f_4	68.316	0.017	790.7	0.2	0.8

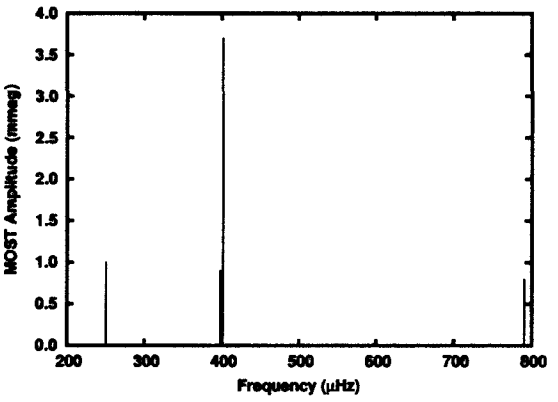

Figure 3.69: Frequencies of HD 261387 in NGC 2264 as observed by *MOST*.

models with $\chi^2 < 5$, $\ell = 0$ to 3 modes to all pulsation frequencies observed by *MOST*. Two models of note are selected for further examination, indicated by models A and B in Figure 3.70.

Model A is the best-fit solution that falls within the error box of HD 261387 in the HRD. The echelle diagram on the left-hand side of Figure 3.71 for the model indicates that each frequency maps to a different ℓ order, with $\chi^2 = 3.61$. Model B is the best fit ($\chi^2 = 0.36$) of the models that are consistent with the star's temperature, but are otherwise over-luminous compared to the star's position in the HRD. In this case three frequencies map to $\ell = 2$ mode, with f_1 mapping to a mid-range radial mode. In both models, a wide range of radial orders are required to fit the frequencies, and given the high value of $f_4 = 790.7$ μHz, a check of models with a high enough acoustic cut-off frequency to support this pulsation is in order.

Figure 3.72 shows the result of this analysis, and shows that only models of fairly low luminosity can be supported, and like the previous star considered (HD 261711), gives models consistent with the star's position in the HRD. Using $v \sin i$ =127 kms/s from Pribulla et al. (2009) as a minimum estimate of the projected rotational velocity, and therefore of the expected rotational splitting, Figure 3.72 also

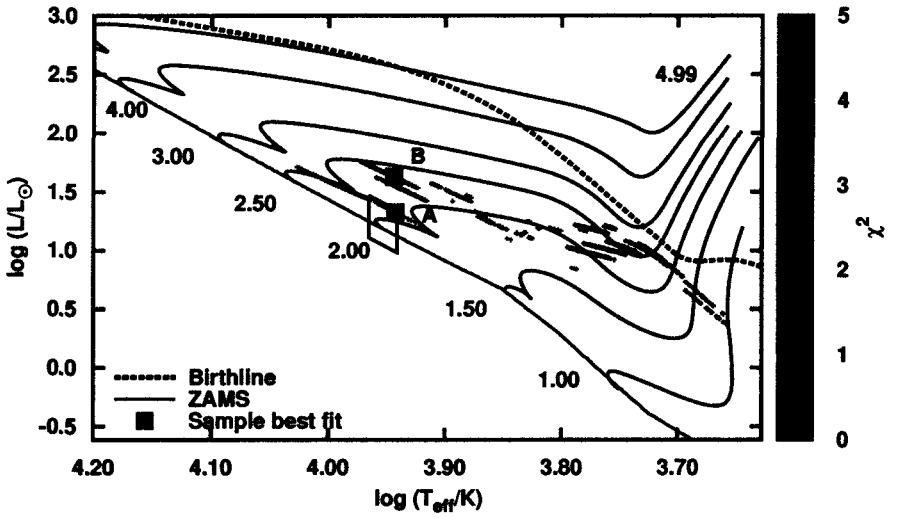

Figure 3.70: χ^2 fit to all highly-significant frequencies of HD 261387 in NGC 2264, $\ell = 0$ to 3 modes, along with the star's position in the HRD.

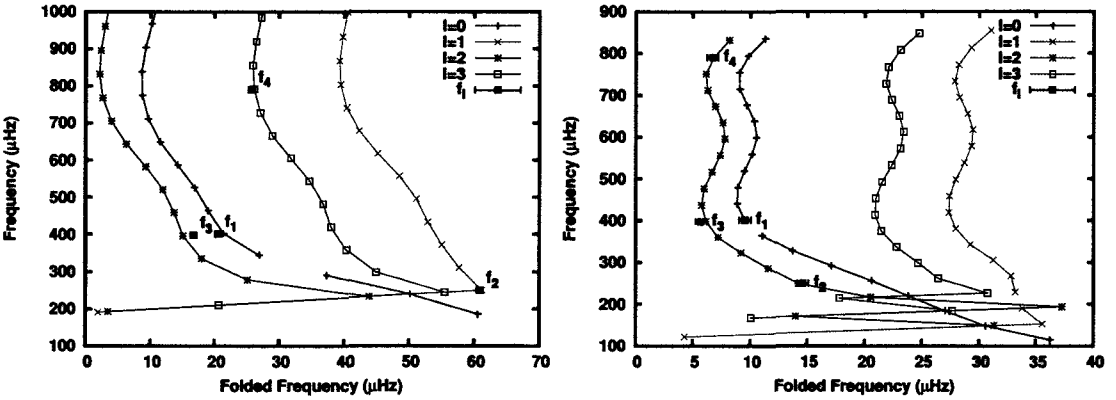

Figure 3.71: Echelle diagrams for χ^2 fits to frequencies of HD 261387. The left and right plots are for models A and B respectively in Figure 3.72. Model A specs: χ^2 = 3.61, M = 2.20 $M_\odot$, $\log(T_{eff}/\mathrm{K})$= 3.942, $\log(L/L_\odot)$= 1.324. Model B specs: χ^2 = 0.36, M = 2.32 $M_\odot$, $\log(T_{eff}/\mathrm{K})$= 3.944, $\log(L/L_\odot)$= 1.626.

shows the result of this calculation. The minimum splittings are large, 14 μHz and higher for the models that fall within the star's HRD position. For the higher luminosity models, such as Model B, the minimum splittings drop to around 10 μHz. Comparing these values to the echelle diagrams of Figure 3.71, the splittings are

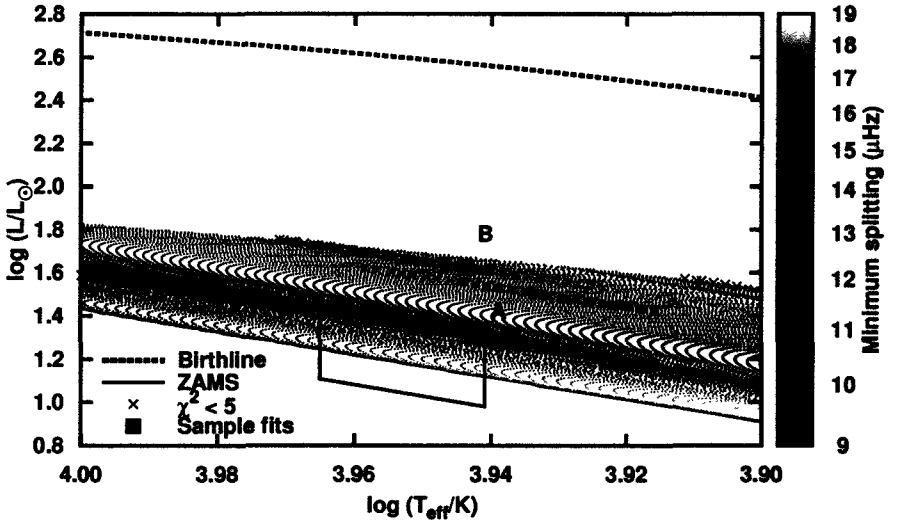

Figure 3.72: Stellar models that can support all the frequencies of HD 261387 of NGC 2264 that were observed by *MOST* considering the fundamental and acoustic-cut-off frequencies of each model. Blue "×" indicate models with $\chi^2 < 5$. Also indicated are the minimum splittings expected from $v \sin i$ = 127 km/s.

larger than the spacings between different non-radial orders, rendering mode identification difficult. On the other hand, the difference between f_1 and f_3 is around 4 μHz, much smaller than the numbers expected for the a typical splitting, and so the likelihood that these two frequencies are members of the same rotationally-split multiplet becomes less likely.

In summary, the asteroseismic analysis of HD 261387 supports cluster membership for the star, but otherwise suggests that rotation makes model identification rather difficult. The highest frequency observed suggests a star closer to the ZAMS than the birthline.

3.2.1.5 NGC 2264 104

NGC 2264 104 (GSC 00750-01183) is a $V = 11.4$ magnitude star in which δ-Scuti pulsations were detected by *MOST* (Zwintz et al. 2009a). Two spectral classifications were found in the literature, A5 IV (Walker 1956) and A6 V (Neri, Chavarria-K. & de Lara 1993). No known measurements of $v \sin i$ where found in the literature.

Three frequencies attributed to pulsation were found in the *MOST* light curve, and these appear in tabular and graphical format in Figure 3.73. Analysis by Guenther et al. (2009) failed to find stellar models with pulsations that agreed with the

ID	freq. (c/d)	err freq. (c/d)	freq (μHz)	err freq. (μHz)	Amp (mmag)
f_1	35.2037	0.0043	407.45	0.05	9.4
f_2	32.9011	0.0086	380.8	0.1	4.6
f_3	32.5987	0.0086	377.3	0.1	4.5

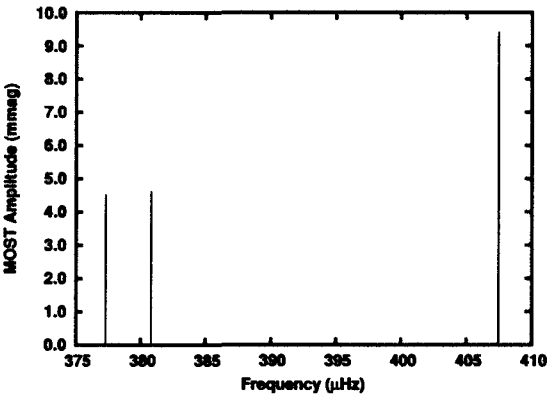

Figure 3.73: Frequencies of NGC 2264 104 in NGC 2264 as observed by *MOST*.

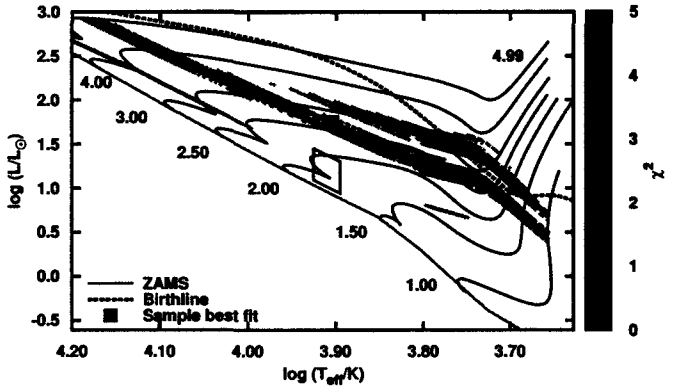

Figure 3.74: χ^2 fit to all highly-significant frequencies of NGC 2264 104 in NGC 2264, $\ell = 0$ to 3 modes, along with the star's position in the HRD.

star's position in the HRD, all the models that fit the pulsations were significantly over-luminous. The current analysis will largely reaffirm that result.

Figures 3.74 shows χ^2 fits to all three frequencies observed by *MOST*. Good solutions are significantly over-luminous compared to the star's HRD position. Figure 3.75 shows a sample echelle diagram of such a model. Without invoking rotation in some manner, the diagram reveals that f_2 and f_3 are typically probing the small spacing between the $\ell = 1$ and 3 modes, or the $\ell = 0$ and 2 modes, while the difference between f_1 and f_3 or f_1 and f_2 would be simultaneously sampling the large spacing of a model. With this particular combination of frequency differences between the three different observed frequencies, lower-luminosity solutions in agreement with the star's position in the HR diagram don't seem to occur.

Note that if the star's position in the HRD is correct, with a frequency difference, $\delta f = f_1 - f_3 = 3.5$ μHz, typical rotational splittings for stars with typical $v \sin i$ values would be much larger than δf, suggesting that f_1 and f_3 are not likely to be two members of the same rotationally-split multiplet.

Although $f_1 = 407.45$ μHz is not very high, it is high enough to provide an upper limit to the luminosity of NGC 2264 104, as shown in Figure 3.76, and does not contradict the star's position in the HRD. However, all of the good fits from the analysis are in the high end of the allowable luminosity range. A best guess is that

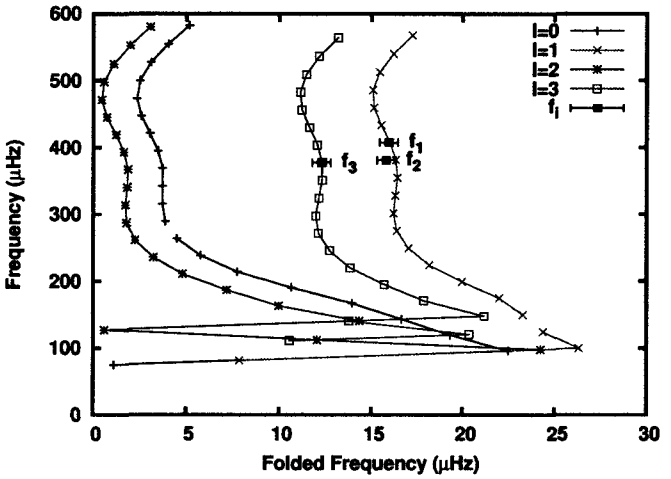

Figure 3.75: Echelle diagram a sample χ^2 fit to frequencies of NGC 2264 104. This particular model matches the temperature of the star, but it otherwise over-luminous compared to observation. $\chi^2 = 0.38$, M = 2.71 $M_\odot$, $\log(T_{eff}/K) = 3.904$, $\log(L/L_\odot) = 1.755$.

either the star's distance determination, and hence position in the HRD diagram is in error, and/or rotation is affecting the values of the observed frequencies. These possibilities are best explored by future observations.

In summary, the frequencies of NGC 2264 104 do not put overly strong limitations on the luminosity of the star, nor do they contradict the star's position in the HRD, it is only collectively that the frequencies cast doubt upon the HRD position.

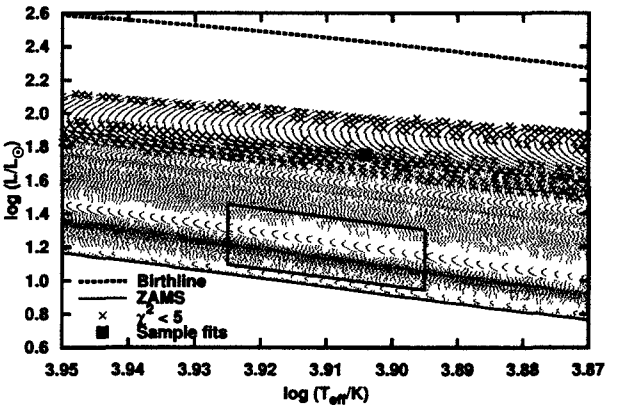

Figure 3.76: Stellar models that can support all the frequencies of NGC 2264 104 that were observed by *MOST* considering the fundamental and acoustic-cut-off frequencies of each model. Blue "×" indicate models with $\chi^2 < 5$.

However, it is likely that the inability to find a good fit has been adversely affected by rotation, and/or by a bad distance determination. Future observations of the $v \sin i$ of the star would be particularly useful.

3.2.1.6 HD 261230

HD 261230 (GSC 00750-00863) is a $V = 9.4$ magnitude star, with spectral classifications ranging from A7 V (Voroshilov et al. 1985) to F0 (Cannon & Pickering 1993) to F2 V (Pribulla et al. 2009). Interestingly, with $B - V = 0.25$, this does not support the cooler spectral classifications, and would limit the spectral classifications to around A8 V at the coolest. For this analysis, I therefore choose a temperature range consistent with a spectral class of A7 V through A8 V. Zwintz et al. (2009a) report $v \sin i = 95 \pm 5$ km/s. Kharchenko (2001) report an unusable parallax, -18±20 mas. No formal membership calculations have been performed on this star, however Zwintz et al. (2009a) report that the proper motions of the star from TYCHO (Høg et al. 2000) do not compare favourably with that of NGC 2264 as a whole, meaning that cluster membership is unlikely.

The *MOST* observations reported in Zwintz et al. (2009a) discovered 7 frequencies attributed to pulsation. These frequencies appear in tabular and graphical form in Figure 3.77. The frequencies are somewhat evenly spread out between 113 μHz and

ID	freq. (c/d)	err freq. (c/d)	freq (μHz)	err freq. (μHz)	Amp (mmag)
f_1	19.596	0.009	226.8	0.1	2.8
f_2	10.930	0.009	126.5	0.1	2.8
f_3	12.027	0.009	139.2	0.1	2.7
f_4	9.789	0.017	113.3	0.2	1.8
f_5	21.021	0.017	243.3	0.2	1.8
f_6	16.788	0.017	194.3	0.2	1.7
f_7	13.556	0.017	156.9	0.2	1.7

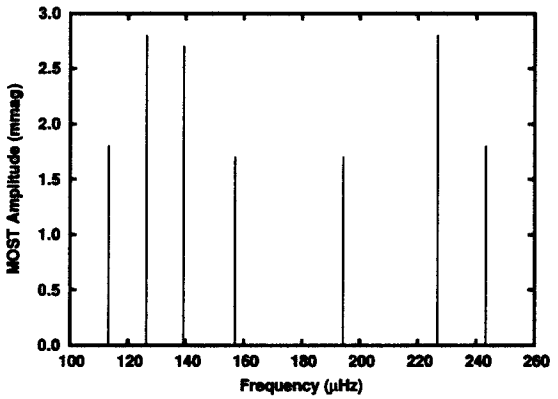

Figure 3.77: Frequencies of HD 261230 in NGC 2264 as observed by *MOST*.

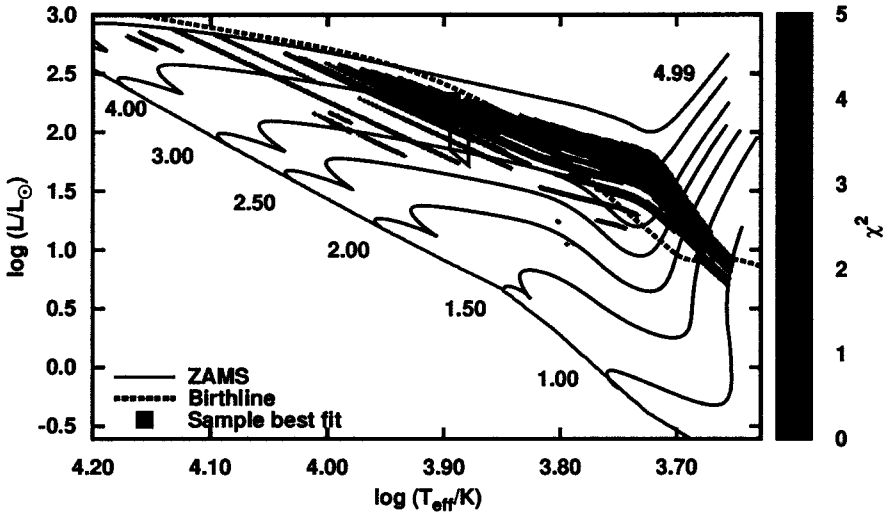

Figure 3.78: χ^2 fit to all frequencies of HD 261230 in NGC 2264 observed by *MOST*, $\ell = 0$ to 3 modes.

243 μHz. In the asteroseismic analysis of Guenther et al. (2009), no viable fits to all seven frequencies were found. Here, because of the larger uncertainties used, some fits are found just above the star's position in the HRD (Figure 3.78). Indeed, there are a number of viable fits, and by looking at the sample echelle diagram in Figure 3.79, the reason is easy to see: the differences between model frequencies are often of the order of the error bars on the individual observed frequencies, a common problem

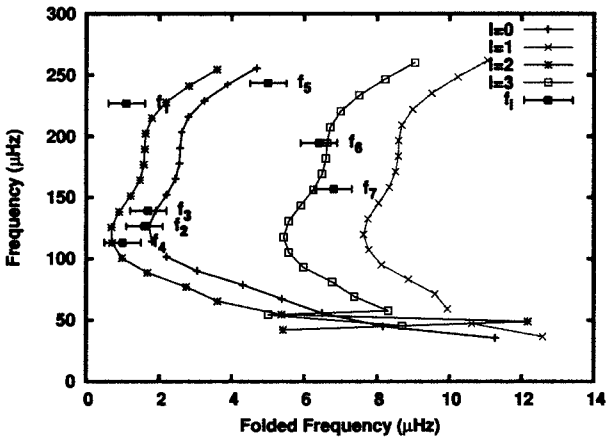

Figure 3.79: Echelle diagram a sample χ^2 fit to frequencies of HD 261230 of NGC 2264. Model specs: $\chi^2 = 1.68$, M = 4.24 $M_\odot$, $\log(T_{eff}/\mathrm{K}) = 3.894$, $\log(L/L_\odot) = 2.265$.

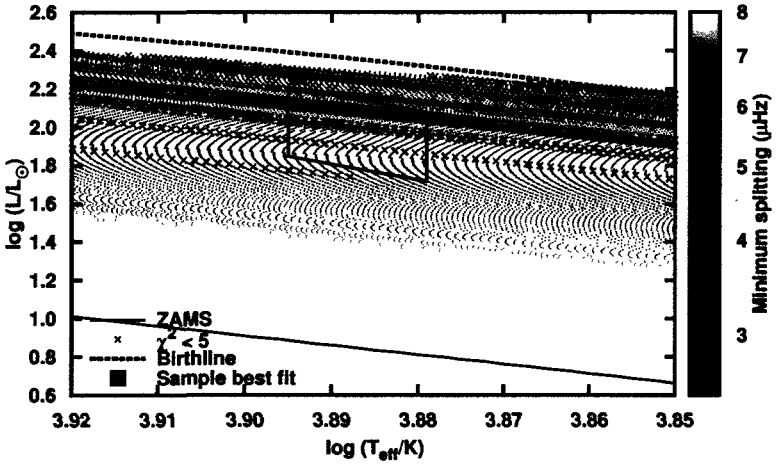

Figure 3.80: Stellar models that can support all the frequencies of HD 261230 of NGC 2264 that were observed by *MOST* considering the fundamental frequency of each model. Blue "×" indicate models with $\chi^2 < 5$.

in higher-luminosity models, where the theoretical frequencies are much more tightly packed in frequency space than they are at lower luminosities, and so it is easier to find a good fit to any observed frequencies.

With the range of frequencies observed, minimum and maximum luminosity constraints can be put upon the star. Figure 3.80 shows the selection of models within the PMS grid that can support the range of frequencies indicated by the lowest frequency ($f_4 = 113.3$ μHz) and the highest frequency ($f_5 = 243.3$ μHz). These models are consistent with the star's position in the HRD, and do not support a star with much greater luminosity than the error box indicated in the HRD. Importantly, they also do not support a star close to the ZAMS, indicating either a younger PMS star, or an evolved post-MS star. Regardless, the star would need to be at a similar distance to NGC 2264, whether a member or not, to support these frequencies, and to fall within the correct intrinsic luminosity range.

Figure 3.80 also shows the minimum expected rotational splitting using $v \sin i =$ 90 km/s. They range from 8 μHz at the low range of the luminosities to 2 μHz at the high end, once again highlighting the problems that rotation will cause given that

these are similar to the differences between difference ℓ orders, making any signature of rotation hard to spot.

In summary, HD 261230 may or may not be a member of NGC 2264, however the asteroseismology indicate that the star *is* probably at a similar distance to NGC 2264, whether it is a formal member, or not. I note that the luminosity classifications for this star (class V) are not consistent with the asteroseimology, nor the inferred luminosity of the star from broad-band observations.

3.2.2 NGC 2244 in Monoceros

NGC 2244 is a young open cluster, part of the complex star-formation region in Northern Monoceros. The area is dominated by the Rosette nebula, and also contains NGC 2264, the cluster in which the first PMS δ-Scuti stars were discovered (V588 Mon and V589 Mon by Breger 1972). Unfortunately, NGC 2244 is far enough away that reliable Hipparcos parallaxes are not available. Distances have thus been previously determined by main-sequence fitting and from photometry/spectroscopy of the bright stars. The results of various authors, as reviewed in Kaltcheva, Kuchera & Hathaway (2010) have varied dramatically, from 800 to 2200 pc, a cause for concern when determining the intrinsic luminosity for dimmer stars, such as at the luminosities expected for δ-Scuti stars. In a detailed study of stars earlier than A0, Kaltcheva, Kuchera & Hathaway (2010) nicely demonstrated the probable reason for the wide variety of distance determinations for NGC 2244: it would appear that NGC 2244 is not a single cluster of stars, but a stream of stars strung out along the line of sight, perhaps a chance alignment of subgroups of stars, or maybe a "sheet" of stars viewed edge on. In any case, assigning a single distance to NGC 2244 with small error bars does not appear appropriate, so for the purposes of this study, I choose 1100 to 2100 pc, as demonstrated by Figure 4 of Kaltcheva, Kuchera & Hathaway (2010).

NGC 2244 is young enough to contain PMS δ-Scutis. It was observed for 25.559 days in 2008 (frequency resolution of 0.039 c/d or .453 μHz) by *MOST* for the main purpose of observing the O and B stars in the field for A. Moffat. In the

Star	Alternate name	Spectral class	Ref	V	E(B-V)		A_v		$\log(L/L_\odot)$		$\log(T_{eff}/K)$	
					Min	Max	Min	Max	Min	Max	Min	max
45	HD 258859	A0	(1)	10.6	0.1	0.5	0.3	1.7	2.02	3.12	3.95	4.00
		A1 V	(2)									
		A1 IV	(3)									
271	GSC 00154-00076	A7 V	(3)	10.8	0.1	0.2	0.3	0.7	1.79	2.56	3.87	3.89
399	GSC 00154-00307	A0 V	(2)	11.4	0.14	0.19	0	0.42	0.60	2.71	3.97	3.99
		A7 V	(3)		0.0	0.0	0.0	0.0	1.30	2.28	3.89	3.91
183	GSC 00154-01629	A2 V	(2)	11.4	0.2	0.6	0.5	2.0	1.92	3.17	3.94	3.97
		A8 III	(3)		0	0.4	0	1.4	1.69	2.89	3.86	3.89

Table 3.1: PMS δ-Scuti stars detected by *MOST*. References for spectral classes: (1) Cannon & Pickering (1993); (2) Voroshilov et al. (1985); (3) Verschueren (1991).

process, four A-class stars were found to exhibit δ-Scuti variability. Previous to these observations there were no known PMS δ-Scutis associated with the cluster. The photometry was reduced by M. Hareter, the light curve analysed by K. Zwintz for pulsations, and the results passed on to me for asteroseismic analysis. The results appear here in written form for the first time. Tabulated properties appear in Table 3.1, with individual pulsation frequencies further tabulated as appropriate in the subsection for each star below.

Collectively, these stars have not been well studied in the past, as it is only with the detection of δ-Scuti pulsation in these stars that they have appeared unusual in any way. For example, none of these stars have had $v \sin i$ measured. Fortuitously, at least one spectral classification has been performed for each star. Unfortunately, where multiple classifications exist, there is not necessarily agreement. The Ph.D. thesis of Verschueren (1991) provides spectral classes for all four stars, the catalogue of Voroshilov et al. (1985) for three of them, and the Henry Draper Catalogue, one star (Cannon & Pickering 1993). Only for HD 258859 are the classes in approximate agreement, at least in terms of temperature, and more observations are needed. Given the strung-out nature of the cluster along the line of sight, and the complex nature of the interstellar clouds in this region, individual dereddening/extinction solutions to each star are necessary, as using an average E(B-V) for the whole cluster would produce inaccurate results — two stars of almost identical position on the sky could have quite different distances, and thus have considerably different amounts of dust

and gas between the star and the observer. Aside from the δ-Scuti variability, none of these stars appear to exhibit variability, particularly of the UX-Ori type exhibited by many HAe stars.

Here I use the numbering system for NGC 2244 established by Ogura & Ishida (1981), also used by WEBDA. I will now present the asteroseismic analysis for each of the four stars.

3.2.2.1 NGC 2244 45 (HD 258859)

NGC 2244 45 (HD 258859) has been classified as A1 V by Voroshilov et al. (1985) and A1 IV by Verschueren (1991). Dias et al. (2006) and Chen, de Grijs & Zhao (2007) find 0.62 and 0.84 probability of cluster membership, respectively. The uncertainties in the Tycho parallax render it unusable for a distance determination (-5.70 $\pm$ 49.30 mas), and so the distance to the cluster must be used as a distance estimate for the star instead.

In the *MOST* observations only one pulsation frequency was found, $f_1 = 8.448$ $\pm$ 0.001 c/d (97.77 $\pm$ 0.01 μHz), with an amplitude of 11.5 mmag.

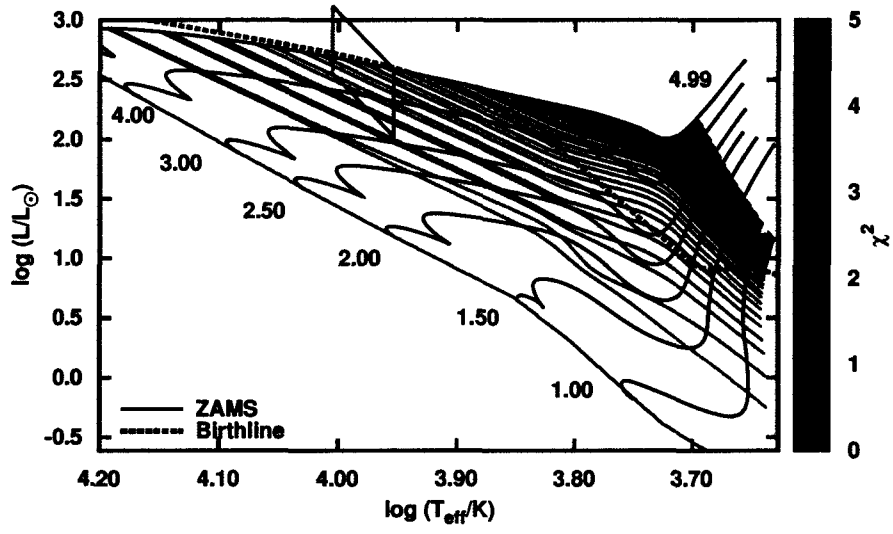

Figure 3.81: Positions of models in the HRD with $f_1 = 8.448$ c/d (97.77 μHz) of NGC 2244 45, $\ell = 0$ to 1 modes, as well as the star's observed position in the HRD.

With such little data on the star, only minimal constraints can be put on the star. However, if this is a p mode, then the minimum luminosity the star can have is given as in Figure 3.81, which shows models with $\ell = 0$ and 1 modes that match $f_1 = 97.77$ μHz. The lowest family of solutions in the figure indicates the fundamental-mode solution, the dimmest possible set of solutions for the star at any given temperature (the second line from the bottom is the $n = 1$, $\ell = 1$ modes solutions, the third the $n = 1$, $\ell = 0$, etc.) This set of solutions is below the observational error box, indicating that the star must be pulsating in low, but not the lowest, radial orders.

Regardless, even the fundamental-mode solution above requires luminosities more consistent with a class III star, different than the luminosity classes determined by various observers (IV and V). At the moment it is hard to reconcile the distance, luminosity class, and asteroseismology of the star.

3.2.2.2 NGC 2244 271 (GSC 00154-00076)

NGC 22444 271 (GSC 00154-00076) is a $V = 10.38$ magnitude, $B - V = 0.37$ magnitude with only one prior spectral classification, A7 V, by Verschueren (1991). Membership probability is given between 0.59 (Dias et al. 2006) and 0.98 (Chen, de Grijs & Zhao 2007). Given the discrepancies between the various spectral classifications for two other A7-range stars by these authors, and those given by others, this classification could be in error.

Eight significant frequencies were detected by *MOST*, plus four frequencies of lesser significance, all of which can be seen in tabular and figure form in Figure 3.82. The position in the HRD appears to be over luminous considering the class V luminosity. Once again, it is more consistent with a class III luminosity, which could be due to a classification error, or this star is (much) more in the foreground, perhaps a evolved field star.

ID	Freq (c/d)	Err. Freq. (c/d)	Freq. (μHz)	Err. Freq. (μHz)	Amp. (mmag)
f_1	20.963	0.005	242.63	0.06	2.3
f_2	14.467	0.006	167.44	0.07	1.9
f_3	21.878	0.008	253.21	0.09	1.5
f_4	23.96	0.01	277.30	0.11	1.1
f_5	23.19	0.01	268.36	0.13	1.0
f_6	16.42	0.01	190.04	0.13	1.0
f_7	12.32	0.01	142.63	0.14	0.9
f_8	14.76	0.01	170.78	0.14	0.8
(f_9)	11.29	0.01	130.64	0.15	0.8
(f_{10})	13.10	0.01	151.62	0.16	0.8
(f_{11})	20.02	0.02	231.75	0.18	0.7
(f_{12})	9.91	0.02	114.74	0.18	0.7

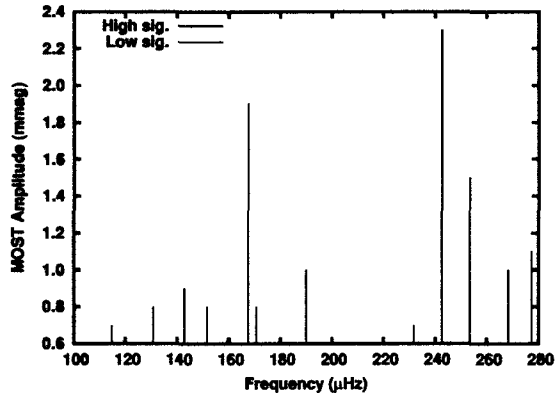

Figure 3.82: Frequencies of NGC 2244 271 as observed by *MOST*.

One interesting note: $f_6 = \frac{4}{3}f_3$ and $f_7 = \frac{4}{3}f_6$. This may be a mathematical coincidence, and are certainly not of the nature of the linear-combination non-independent pulsation frequencies one finds in many high-amplitude δ-Scuti stars (of which this star is *not* an example). If these combinations are *not* a coincidence, *i.e.* f_6 and f_7 are *not* modes independent of f_3, then the mechanism for these particular combinations are not known, and further research is needed beyond this analysis.

Regardless, with all frequencies used in the fit, there is one family of solutions with realistic fits within the error box, with a $\chi^2 = 2.75$, as demonstrated in Figure 3.83, with the corresponding echelle diagram shown in the left-hand side of Figure 3.84. With this family of solutions the star is at the acoustic cut-off frequency with respect to f_4, *i.e.* a star more luminous would not be able to support this particular frequency. This is further demonstrated in Figure 3.85 which shows the models that can support all of the high-significance frequencies, as observed by *MOST*. Note that the frequencies collectively impose both minor maximum-luminosity constraints, and some minimum-luminosity constraints: the star cannot be either at the birthline, nor on the ZAMS. Also note that in determining these constraints, the low-significance frequencies were not used. One of these latter frequencies is quite low,

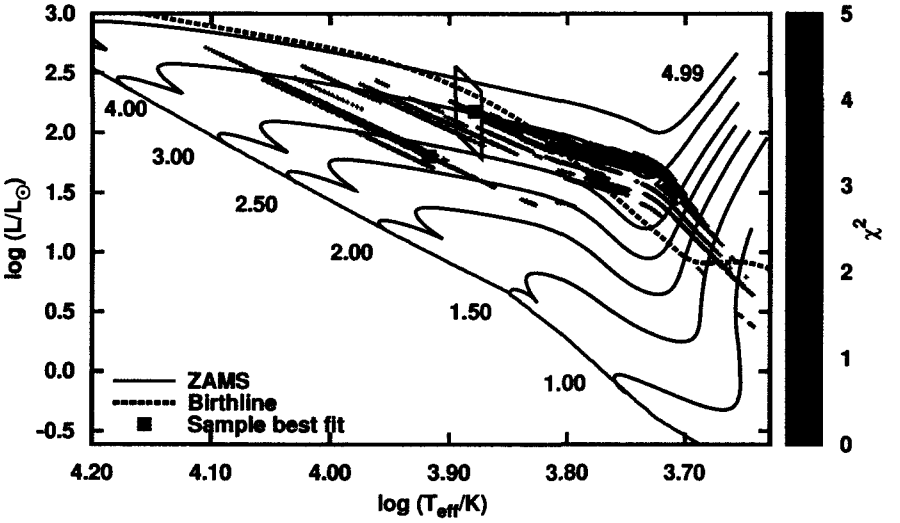

Figure 3.83: χ^2 fit to all highly-significant frequencies of NGC 2244 271, $\ell = 0$ to 3 modes, along with the star's position in the HRD.

$f_{12} = 114.74$ μHz, which would require higher minimum luminosities to support this frequency if the signal should turn out to be a p-mode pulsation signal.

Given potential errors in spectral class, and overestimates of distance for the star, there is one family of solutions at hotter temperatures and lower luminosities

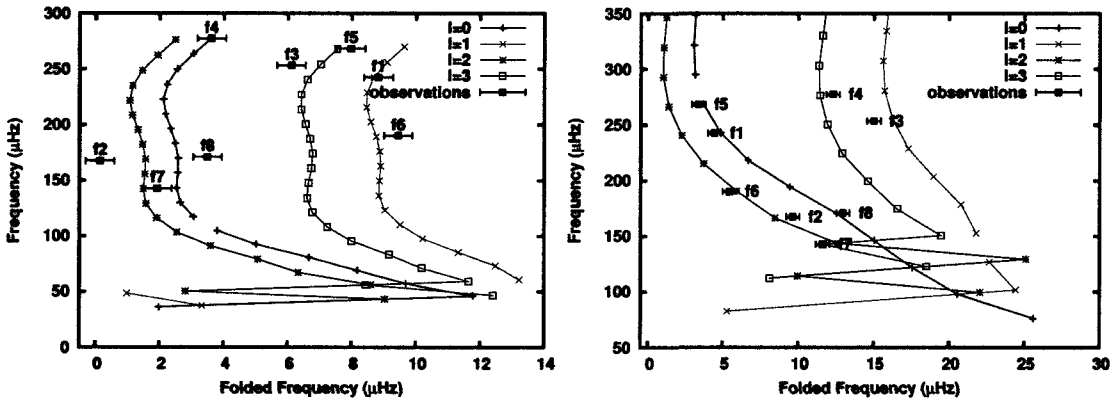

Figure 3.84: Echelle diagrams for sample models of NGC 2244 271 in Figure 3.83. Left hand side: model inside error box, just below ACF, model specs $\chi^2 = 2.77$, mass = 4.05 $M_\odot$, $\log(T_{eff}/\mathrm{K}) = 3.88$, $\log(L/L_\odot) = 2.81$. Right-hand side: model outside error box, mode specs $\chi^2 = 2.75$, mass = 2.76 $M_\odot$, $\log(T_{eff}/\mathrm{K}) = 3.92$, $\log(L/L_\odot) = 1.80$ (this final solution is hotter and less luminous than the star's position in the HRD, but is where one might expect the star to be if errors in spectral classification and overestimates of distance have been made).

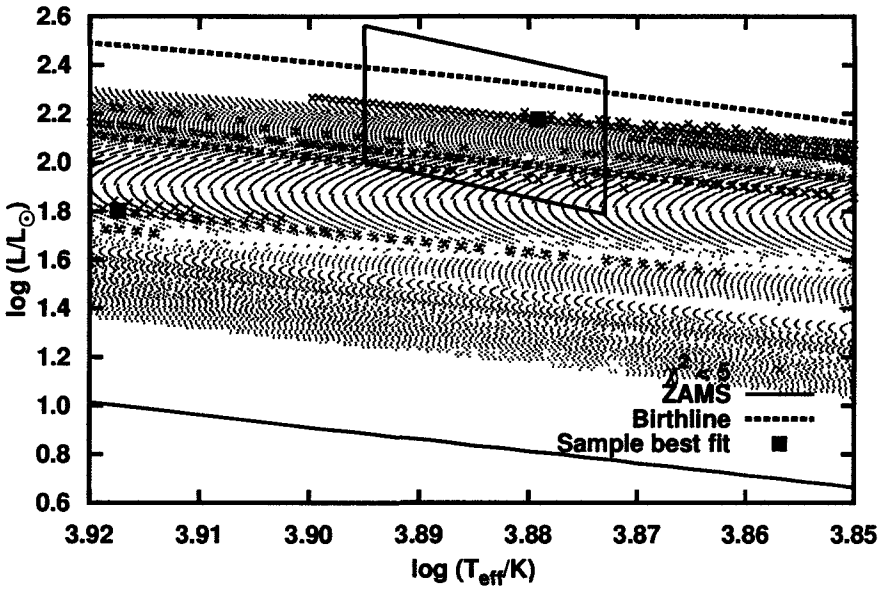

Figure 3.85: Models that can support the frequencies of NGC 2244 271 as observed by *MOST*.

to the given star's position in the HRD, indicated by the sample fit outside the error box in Figures 3.83. A sample echelle diagram for this family of solutions is shown on the right-hand side of Figure 3.84. This second echelle diagram is perhaps more convincing than the the first echelle, as the fit is of similar quality, but the error bars on the observed frequencies are smaller relative to the frequency differences between different modes of oscillation for that particular star; a good fit is less likely, so when it does happen it is more convincing.

As an experiment, fits without f_6 and f_7 were tried in the assumption that they are somehow tied to f_3; they were discarded as they are the frequencies of the three with the smaller amplitudes. Unsurprisingly, within the error box, more families of solutions with $\chi^2 < 5.0$ appear, as shown in Figure 3.86, along with an echelle diagram for the best solution. The solutions are not much better than the original case that used all frequencies in the fit. Interestingly, the family of solutions outside the error box from the all-frequency case is *not* improved by removing f_6 and f_7 from the fits, as these two frequencies were otherwise well fit to the model frequencies for these solutions, and thus helped improve the χ^2 values for these fits. The results of

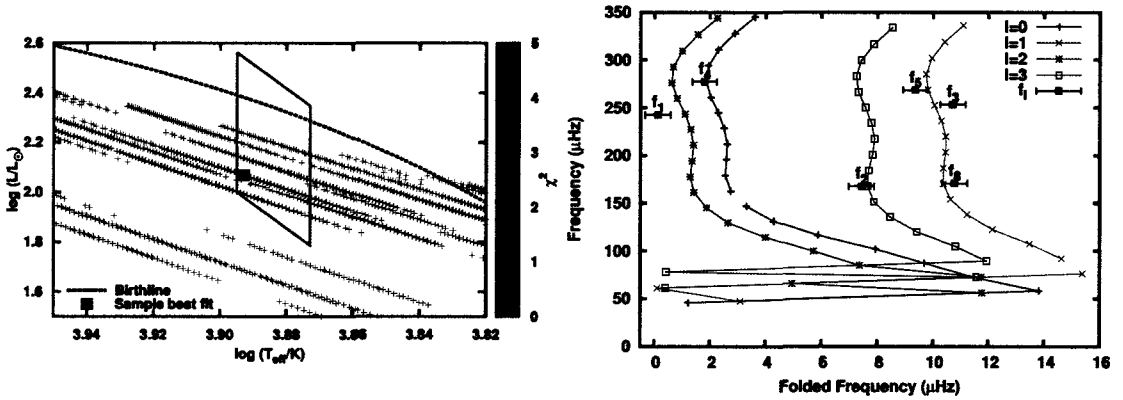

Figure 3.86: Left: χ^2 fit to all highly-significant frequencies of NGC 2244 271 except f_6 and f_7, $\ell = 0$ to 3 modes. Right: echelle diagram for sample solution, model parameters $\chi^2 = 1.45$, mass = 3.60 $M_\odot$, $\log(T_{eff}/K)$= 3.89, $\log(L/L_\odot)$= 2.07.

this test are therefore ambiguous.

In summary, the asteroseismology for NGC 2244 271 provides solutions, but they are not unique, and less uncertainty is needed in the fundamental parameters of this star for this situation to improve. The observed frequencies *do* support the star's position in the HRD, with some luminosity constraints imposed both at the high and low end of the possible luminosity range.

3.2.2.3 NGC 2244 399 (GSC 00154-00307)

NGC 2244 399 (GSC 00154-00307) is a $V = 11.4$, $B - V = 0.17$, star with two very different spectral classifications at different ends of the A-class range: A0 V by Voroshilov et al. (1985), and A7 V by Verschueren (1991). Further observations are needed to resolve this discrepancy. The hotter spectral classification is perhaps the more credible in this case, as an A7 V star is expected to be redder than $B - V = 0.17$, and otherwise implies that the light from this star does not suffer from any extinction/reddening, an unlikely scenario. Asteroseismic solutions for both spectral classifications will be given.

ID	Freq. (c/d)	Err. freq. (c/d)	Freq. (μHz)	Err. freq. (μHz)	Amp. (mmag)
f_1	7.228	0.002	83.66	0.02	6.6
f_2	1.826	0.007	21.14	0.08	1.4
f_3	3.841	0.007	44.46	0.08	1.3
f_4	6.286	0.008	72.76	0.09	1.2
f_5	0.302	0.008	3.49	0.09	1.1
f_6	1.283	0.009	14.86	0.10	1.0
f_7	0.16	0.01	1.87	0.13	0.7
f_8	5.12	0.01	59.22	0.13	0.7

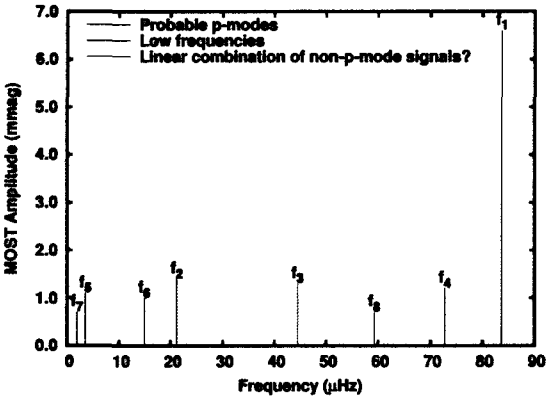

Figure 3.87: Frequencies of NGC 2244 399 as observed by *MOST*.

MOST observations of this star are unique. Eight frequencies were detected, the spectrum can be seen in Figure 3.87. The frequencies are quite low, and f_2, f_5, f_6 and f_7 are too low to be δ-Scuti pulsations. Of these, $f_5 = 2f_7$. Furthermore, both f_3 and f_8 are high enough to be δ-Scuti pulsations, but $f_3 = 3f_6$ and $f_8 = 4f_6$, integer linear combinations of a frequency (f_6) that is too low to be δ-Scuti pulsation; this makes these two frequencies suspect. This leaves only f_1 and f_4 as reliable pulsation frequencies.

With such low frequencies under consideration, the *minimum* luminosity of the star must be considered. Figure 3.88 shows both the result of considering the models with a fundamental frequency that can support f_3, which may or may not be an independent pulsation frequency (gray shading). The models that support this frequency are over luminous compared to the star's positions in the HRD, although given the uncertainties associated with the star's distance, the discrepency isn't that large. Figure 3.88 also shows the result of considering the *additional* models that can support the lowest reliable p-mode, that of $f_4 = 72.76$ μHz, indicated by the rose-coloured shading. In this case, there are now models that are consistent with the star's position in the HRD, albeit with only the upper portion of the position, indicating that this is a high-luminosity δ-Scuti star.

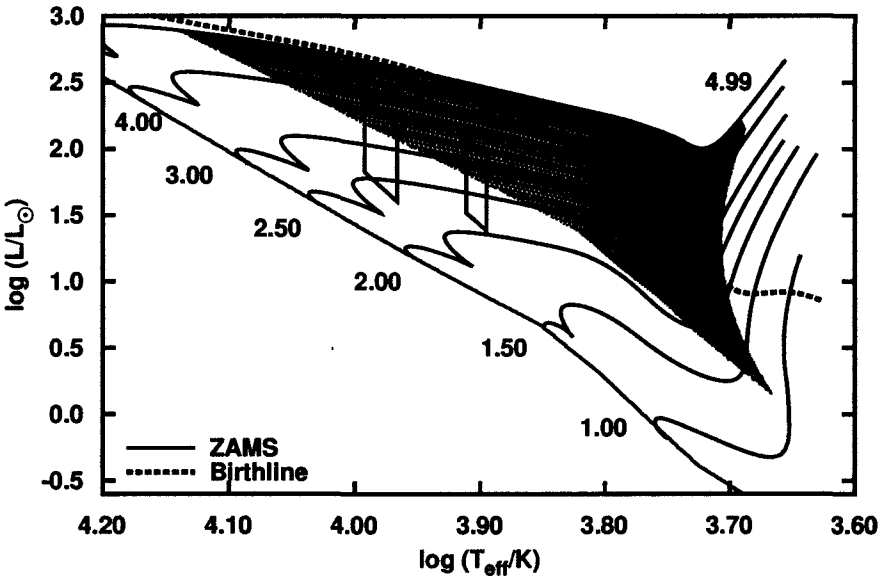

Figure 3.88: Models with a fundamental frequency that can only support $f_3 = 44.45$ μHz (grey shading), and models that can suport $f_4 = 72.76$ μHz (extra rose-coloured shading). Note that f_3 may or may not be an independent pulsation frequency. The two error boxes indicate the positions in the HRD for the hot A0 V (left) and cool A7 V (right) spectral classifications for the star.

Simultaneous χ^2 fits to both f_1 and f_4 were performed (the two "reliable" pulsation frequencies), and $\ell = 0$ and 3 modes were required to find good fits consistent with the star's position in the HRD (right-hand side of Figure 3.89). One family of solutions clips the upper part of the HRD position for the hot (A0) star and runs through the cool (A7) position as well; a slightly-more-luminous alternate solution also exists for the cool HRD position. The left-hand side of Figure 3.89 shows a sample echelle diagram for the best-fit solution for the hot HRD position. Mode identification is the two lowest-radial-order $\ell = 2$ modes.

For completeness, fits that also included the two ambiguous frequencies, f_3 and f_8, were also performed against $\ell = 0$ to 3 modes. An interesting result is found, in that almost the same family of solutions from the previous case is found, as can be seen in the left-hand side of Figure 3.90. The right-hand side of Figure 3.90 shows the best-fit solution to the hot HRD position, with $\chi^2 = 2.01$. The model is slightly different from the model depicted in the echelle diagram of Figure 3.89, but to three

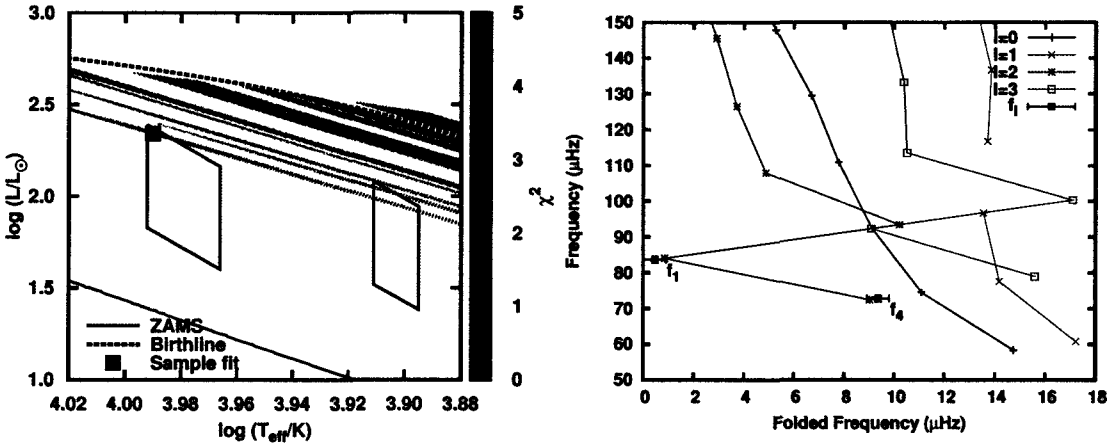

Figure 3.89: Left: χ^2 fit to f_1 and f_4 of NGC 2244 399, $\ell = 0$ to 3 modes. Right: echelle diagram for sample solution, model parameters $\chi^2 = 0.67$, mass = 3.85 $M_\odot$, $\log(T_{eff}/K)$= 3.99, $\log(L/L_\odot)$= 2.34.

significant digits in the indicated temperatures and luminosities, the two models occupy the same spot in the HRD. The main difference between this model and the previous one is the mode identification of f_4: it has shifted from the (0,2) mode to the (1,0) mode, although the former is still close enough in frequency space to be potentially identified as the mode associated with f_4. Better fits exist for the cool

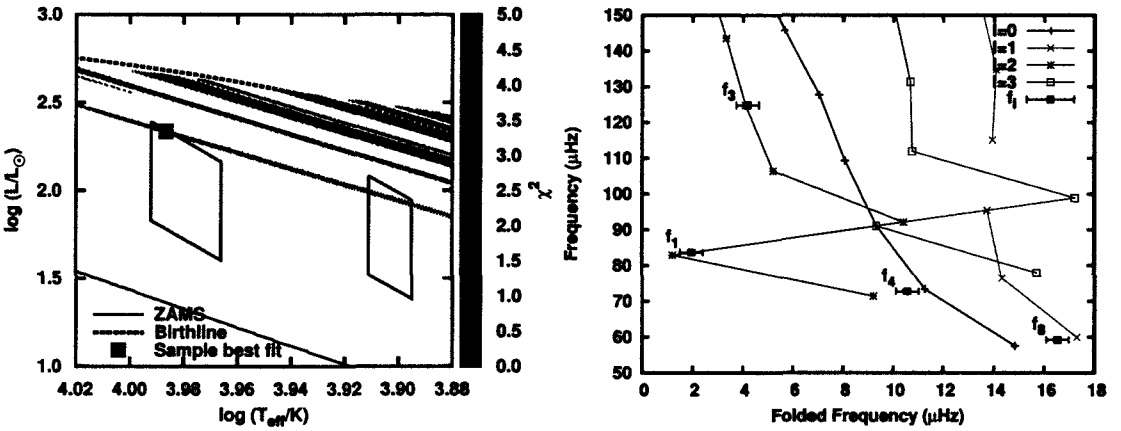

Figure 3.90: Left: χ^2 fit to p-mode frequencies of NGC 2244 399, $\ell = 0$ to 3 modes. Right: echelle diagram for sample solution, model parameters $\chi^2 = 2.01$, mass = 3.85 $M_\odot$, $\log(T_{eff}/K)$= 3.99, $\log(L/L_\odot)$= 2.34. The stellar parameters only slightly different from the sample model of Figure 3.89.

HRD position, but qualitatively the echelle diagram is similar, and is therefore not given here. Slightly better fits exist than that depicted in Figure 3.90, just outside the hot position, but once again, qualitatively the echelle diagram is similar, and so it is not given here. It is interesting to note that including the ambiguous frequencies in the fit does not change the solution much, and is therefore unable to address the question of whether f_3 and f_8 are associated (or not) with the non-p-mode frequency, f_6.

In summary, NGC 2244 399 has a frequency spectrum with unique peculiarities, including possible linear combinations of non-pulsation frequencies that happen to fall into the δ-Scuti range of frequencies. All the detected frequencies are fairly low, suggesting high luminosity for the star, supported by the star's position in the HRD otherwise determined by spectral classifications and broad-band photometry. The star would appear to be pulsating on low radial-order modes. Once again, the luminosity class found from spectral classification does not agree with the star's luminosity found by asteroseismology.

3.2.2.4 NGC 2244 183 (GSC 00154-01629)

MOST detected three frequencies in NGC 2244 183 ranging from 110 to 125 μHz, as show in Figure 3.91 in graphical and tabular form. As a group, the frequencies place constraints on the minimum luminosity that the star can have, with $f_1 = 110.07$ μHz implying a minimum luminosity that is approximately 0.5 dex above the main sequence at any given temperature, as can be seen in Figure 3.92.

NGC 2244 183 suffers from the same problems as the previous star: two disparate spectral classifications, A2 V by Voroshilov et al. (1985), and A7 III by Verschueren (1991). Otherwise, it is a $V = 11.4$, $B - V = 0.44$ star, and appears to be somewhat over-luminous in the HRD compared to what would be expected for a class V object, as can be seen in Figure 3.92. Membership probabilities from different researchers vary widely, from identification as a field star (Kuznetsov et al. 2000) to

ID	Freq. (c/d)	Err. freq. (c/d)	Freq. (μHz)	Err. freq. (μHz)	Amp. (mmag)
f1	9.51	0.009	110.07	0.10	1.8
f2	11.42	0.01	132.19	0.12	1.4
f3	10.79	0.01	124.88	0.12	1.4

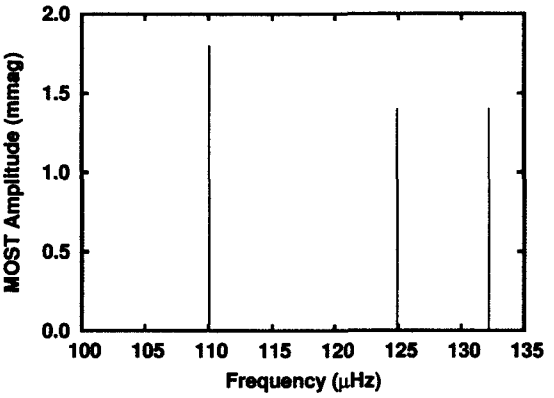

Figure 3.91: Frequencies of NGC 2244 183 as observed by *MOST*.

probability of membership of 0.98 (Chen, de Grijs & Zhao 2007). There are no known $v \sin i$ determinations in the literature.

Simultaneous χ^2 fits to all three frequencies to purely radial modes do not yield any solutions. In Figure 3.93, χ^2 fits limited to $\ell = 0$ and 1 modes yields several families of solutions consistent with *both* hot (A2) and cold (A7) positions in the HRD. More families of solutions would be added if fits to $\ell = 2$ and 3 modes are also

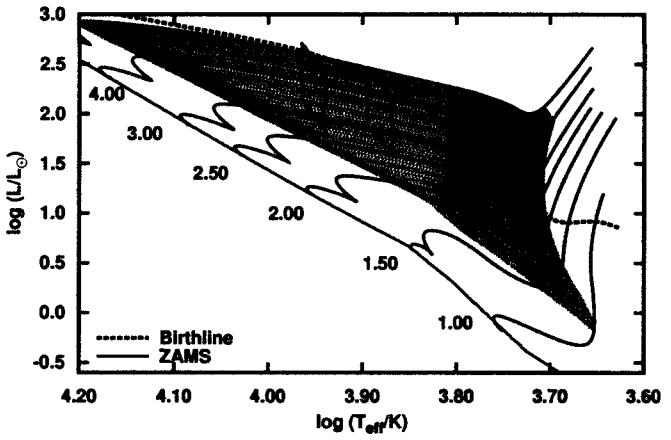

Figure 3.92: Models that can support $f_1 = 110.07$ μHz of NGC 2244 183 as observed by *MOST*. Also shown are the two disparate positions indicated by differing spectral classes available in the literature, A2 V (left-hand error box), and A7 V (right-hand error box). Neither derived position is consistent with a class V star, however the luminosities do agree with the asteroseismology.

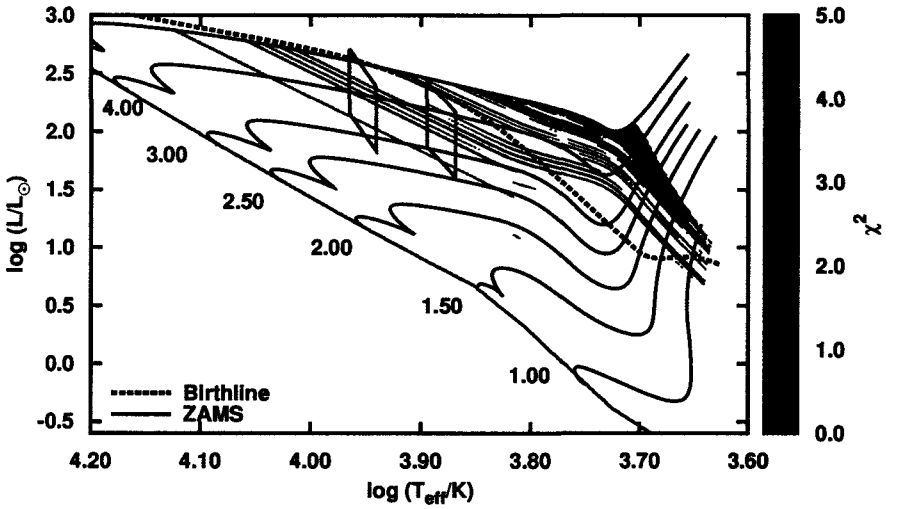

Figure 3.93: χ^2 fits to all three frequencies observed by *MOST* of NGC 2244 183, $\ell = 0$ to 1 modes. Multiple families of solutions are indicated.

allowed, however including these does not improve clarity, so they are not depicted here.

As can be seen more clearly in Figure 3.94, there are two highly-significant families of solutions (better χ^2 fits), and a few less-significant families. I chose two models as representative of the type of fits obtained for this star. The first model is for

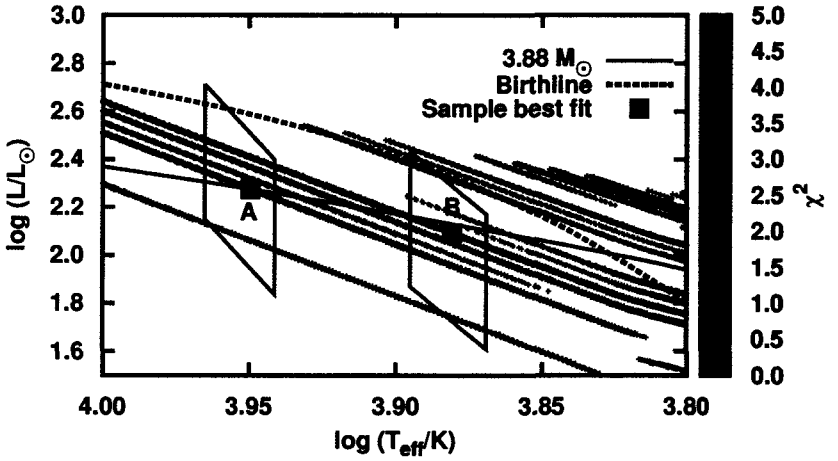

Figure 3.94: χ^2 fits to all three frequencies observed by *MOST* of NGC 2244 183, $\ell = 0$ to 1 modes. Also indicated are the two models "A" and "B" chosen as representative in the text, and for which echelle diagrams are shown in Figure 3.95.

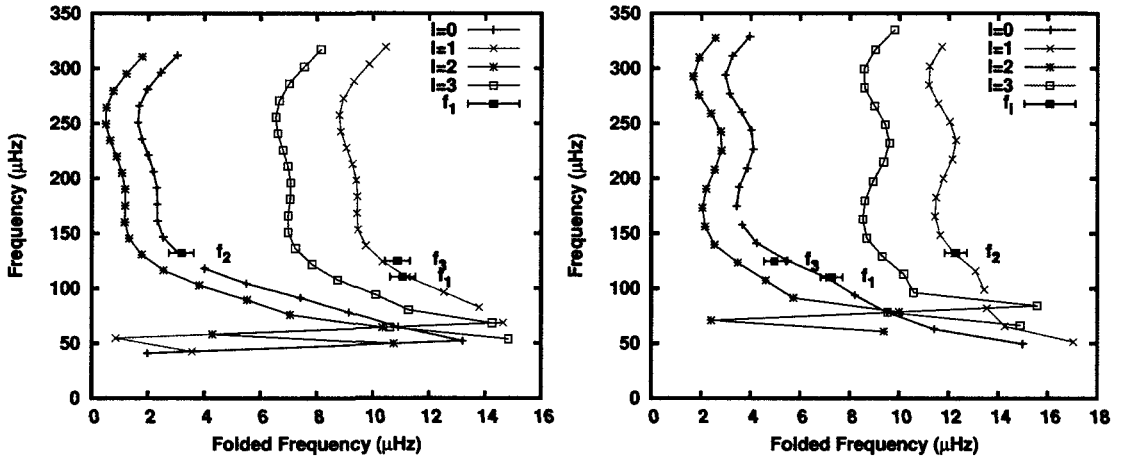

Figure 3.95: Echelle diagrams demonstrating the two different families of solutions of Figure 3.94 to the observations frequencies of NGC 2244 183. Left: Model A (Spectral class A2 solution) with specs $\chi^2 = 0.52$, mass = 3.88 $M_\odot$, $\log(T_{eff}/K)$= 3.95, $\log(L/L_\odot)$= 2.28. Right: Model B (spectral class A7 solution) with specs $\chi^2 = 0.51$, mass = 3.76 $M_\odot$, $\log(T_{eff}/K)$= 3.88, $\log(L/L_\odot)$= 2.09.

the less-luminous family of highly-significant solutions, a model consistent with the hot (A2 spectral class) HRD position, indicated by "A" in Figure 3.94. The echelle diagram for this case is shown on the left-hand side of Figure 3.95 and demonstrates that f_1 and f_3 correspond to consecutive $\ell = 0$ modes ($n = 4$ and 5 respectively), while f_2 is an $\ell = 1$ mode ($n = 6$).

The second model (indicated by "B" in Figure 3.95) is for the cold (A7 spectral class) HRD position for the more-luminous family of solutions. The echelle diagram for this model is shown in the right-hand side of Figure 3.95. The diagram is very similar to that of model "A", expect in this case we find the ℓ orders swapped, *i.e.* f_1 and f_3 corresponding to two consecutive $\ell = 1$ modes ($n = 6$ and 7 respectively), with f_2 identified as a purely-radial mode (n=8). This identification applies to all fits within the family of solutions, a family that also continues to the hot HRD position as well. Aside from the two cases being of slightly different radial order, without some sort of future independent mode identification, there is very little to chose between one set of solutions and another. Including $\ell = 2$ or 3 modes would cloud the problem

even more.

In summary, NGC 2244 183 appears to be over-luminous compared to what one would expect for a class V star, however, the asteroseismic analysis supports a luminosity of at least 0.5 dex in $\log L$ above the ZAMS, in agreement with the broad-band spectroscopy used to determine the star's position in the HRD.

3.3 Open cluster stars – confirmed stars from ground-based observations

3.3.1 η and ϵ Chamaeleontis Clusters

The ϵ Chamaeleontis stellar group, and the η Chamaeleontis sparse open cluster are very nearby groups of stars (approximately 100 pc) with young associated ages of < 10 Myr that appear to be in the process of dispersing into the field (*e.g.* Mamajek, Lawson & Feigelson 2000; Murphy, Lawson & Bessell 2010). η Chamaeleontis has the distinction of being the first open cluster initially detected through X-Ray observations (Mamajek, Lawson & Feigelson 1999).

Five PMS δ-Scutis are associated with this region, two of which are the constituent parts of the double-lined eclipsing binary, RS Cha (Böhm et al. 2009). DX Cha, a well-studied HAe star, has proper motions and parallax consistent with membership, or at least an origin, in the ϵ Cha cluster, but requires radial-velocity measurements to further support/refute this membership (Mamajek, Lawson & Feigelson 2000).

δ-Scuti pulsations were discovered in EE Cha and EF Cha in Kurtz & Müller (1999), the same work that confirmed the δ-Scuti photometric pulsations in DX Cha, however, in this work EE Cha and EF Cha were not recognized as PMS stars, as they do not otherwise exhibit such things as HAe characteristics indicative of youth. It was the study of Mamajek, Lawson & Feigelson (2000) that identified EE Cha and EF Cha as ROSAT X-Ray sources, with spatial motions consistent with cluster

membership, that identified these stars as PMS candidates. Unfortunately, prior to this thesis, the connections between these two stars being both PMS stars and δ-Scutis were not made, and hence have been left out of the list of PMS δ-Scutis until now.

Collectively, these five stars are perhaps the most useful stars of the PMS δ-Scuti class to study, for the simple reason that they are the closest members of the class to the Sun, and hence the easiest to study: they can serve as calibrators for stellar models. RS Cha A and B are members of a double-lined eclipsing binary system with a measured parallax, hence both members have independently had their fundamental parameters determined to extremely high precision, and hence are the perfect calibrators of any stellar models (see Böhm et al. 2009, and references therein). Unfortunately, this region of the sky is very far south, with declinations ranging from approximately -75° to -80°, and so are out of the reach of the current space observatories (*MOST*, *CoRoT*, *Kepler*) that would otherwise provide excellent pulsation data on these stars. Multi-site photometry from southern observatories might be able close this observational gap in the future.

In an effort to improve the light curve on EE Cha and EF Cha, and perhaps detect more pulsation frequencies, K. Zwintz and I had an observing proposal accepted to do photoelectric Stroemgren photometry at the 50 cm telescope of the South African Astronomical Observatory (SAAO). The observing run was for two weeks, from March 3 to 16, 2010, but unfortunately the weather did not cooperate: data could only be taken on seven of the assigned nights, and on only three of these nights was any data of sufficient quality to be worth analysis. However, even upon analysis, these three nights of data were subject to unacceptable levels of noise due to high humidity and thin clouds in the area, and so the observing run rendered no usable data (Zwintz 2011, private communication).

Here I present the data on these five stars in greater detail.

3.3.1.1 RS Cha A and B

RS Cha was first discovered to be an eclipsing binary by Strohmeier (1964). It was found to be a double-lined spectroscopic binary, with both components of almost equal luminosity, spectral class about A5, by Popper (1966). This was further refined to A8 IV + A8 IV by (Jones 1969). Andersen (1975) was the first to recognize that small perturbations in the line profiles of certain spectral lines used in the radial-velocity determinations for orbital parameters of the system might be due to δ-Scuti pulsations. McInally & Austin (1977) confirmed the pulsations photometrically, although the data was of insufficient quality to determine any frequencies of pulsation, or whether one or both stars were pulsating. Over time, researchers have determined the fundamental parameters of the two stars in the system to a very high precision (see Alecian et al. 2007, and references therein); there is a hint that a third star might be part of the system. RS Cha was thought to be an evolved system, until X-Ray emission was detected, and spatial motion and parallax measurements established its PMS nature by membership in the newly-discovered young open cluster, η Cha (Mamajek, Lawson & Feigelson 1999). Using spectroscopic measurements,

	RS Cha A	RS Cha B	Reference
Spectral Type	A8 IV	A8 IV	[1]
Mass ($M_\odot$)	1 89 ± 0 01	1 87 ± 0 01	[2]
Radius ($R_\odot$)	2 15 ± 0 06	1 87 ± 0 01	[2]
$\log(T_{eff}/\mathrm{K})$	3 883 ± 0 004	3 859 ± 0 004	[3]
$\log(L/L_\odot)$	1 15 ± 0 09	1 13 ± 0 09	[4]
$\log(g/\mathrm{cm\ s^{-1}})$	4 05 ± 0 06	3 96 ± 0 06	[4]
$v \sin i$(km/s)	64 ± 6	70 ± 6	[2]
System			
Period (days)	1 67		[2]
i (°)	83 4 ± 0 3		[5]
[Fe/H]	0 17 ± 0 01		[2]
parallax (mas)	10 77 ± 0 24		[6]
min distance (pc)	90 8		calculated
max distance (pc)	95 0		calculated

Table 3.2: Parameters of the RS Cha system. References: [1] Jones (1969); [2] Alecian et al (2005); [3] Ribas et al (2000); [4] Bohm et al (2009); [5] Clausen & Nordstrom (1980); [6] van Leeuwen (2007)

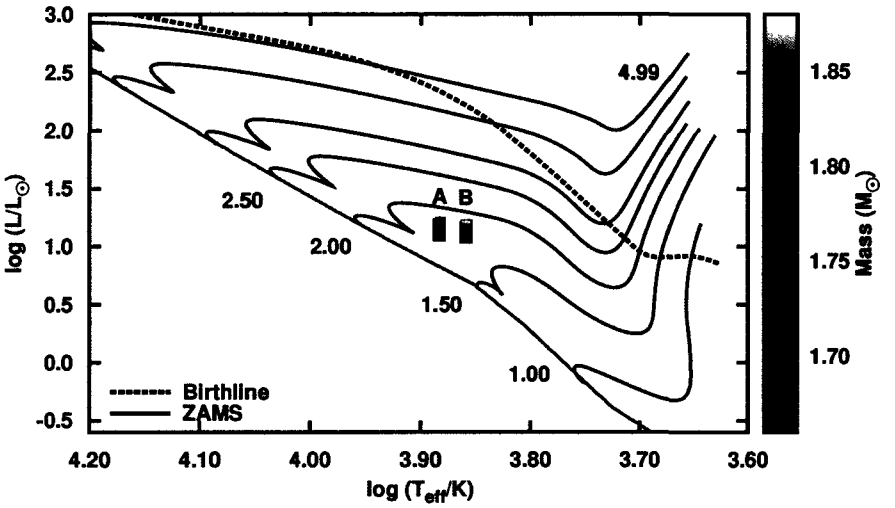

Figure 3.96: Position of the components of RS Cha in the HRD.

Böhm et al. (2009) discovered that *both* components of the system are pulsating in multiple frequencies, some frequencies identified as high ℓ and m modes.

Of all the PMS δ-Scutis in this study, RS Cha A and B have (by far) the most well-determined fundamental parameters, and as such, should be the ultimate calibrators for PMS stars. Unfortunately, spectroscopic radial-velocity measurements of pulsations can be sensitive to higher non-radial orders than photometric measurements are, and since this project has concentrated on photometric light-curve measurements, $\ell > 3$ modes have not been calculated. As such, an asteroseismic analysis of the frequencies observed by Böhm et al. (2009) will not be given, however for completeness, the fundamental parameters of the stars are listed in Table 3.2 below to demonstrate their high precision. Both star's position in the HRD are shown in Figure 3.96. Of particular note in the fundamental parameters: these are the only PMS δ-Scutis for which equatorial rotational velocities (as opposed to just $v \sin i$) are known, as the system's orbit has been circularized, and the orbital inclination, determined by the geometry of the eclipses, is perpendicular to the rotation axis of both stars. Therefore an orbital inclination of $i = 83.4 \pm 0.3$ degrees corresponds to $v \sin i \approx 0.989$ km/s, and so, within error bars, $v \approx v \sin i$. Figure 3.97 therefore

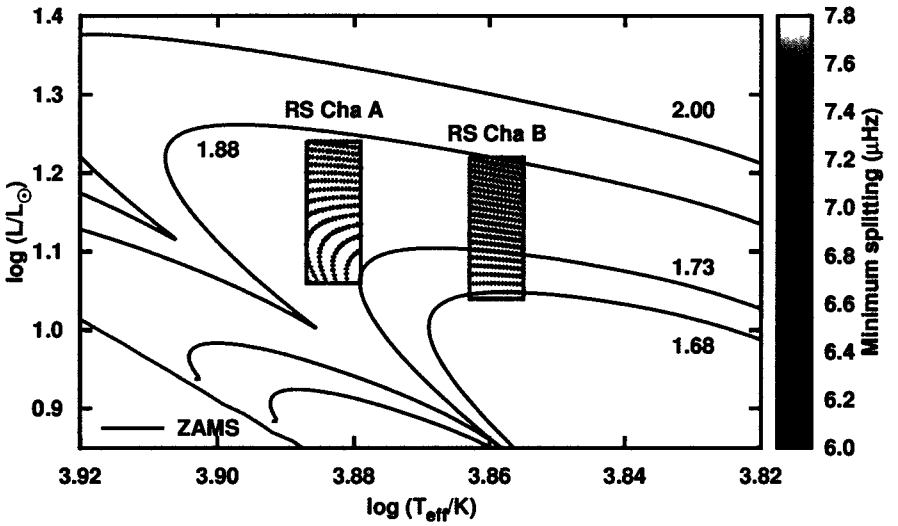

Figure 3.97: Minimum rotational splitting expected for RS Cha A and B. Maximum splitting would not be too much greater.

shows the minimum rotational splitting that could be expected for these two stars, ranging from 6.0 to 7.8 μHz.

3.3.1.2 DX Cha

DX Cha (HD 104237) is a stellar system in which the primary component is an HAe star, part of the ϵ Chamaeleontis moving of stars, with apparent magnitude $V = 6.6$. It has a well-determined parallax of 8.72±0.36 mas, corresponding to a

ID	freq. (c/d)	err freq. (c/d)	freq (μHz)	err freq. (μHz)	Amp (km/s)
f1	33.289	0.04	385.29	0.46	1.302
f2	35.606	0.04	412.11	0.46	0.474
f3	28.503	0.04	329.90	0.46	0.195
f4	30.954	0.04	358.26	0.46	0.139
f5	33.862	0.04	391.92	0.46	0.099
f6	32.616	0.04	377.50	0.46	0.105
f7	34.88	0.04	403.70	0.46	0.10
f8	25.28	0.04	292.59	0.46	0.05

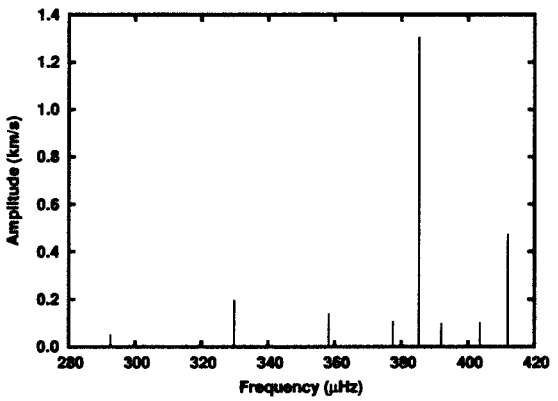

Figure 3.98: Frequencies of DX Cha.

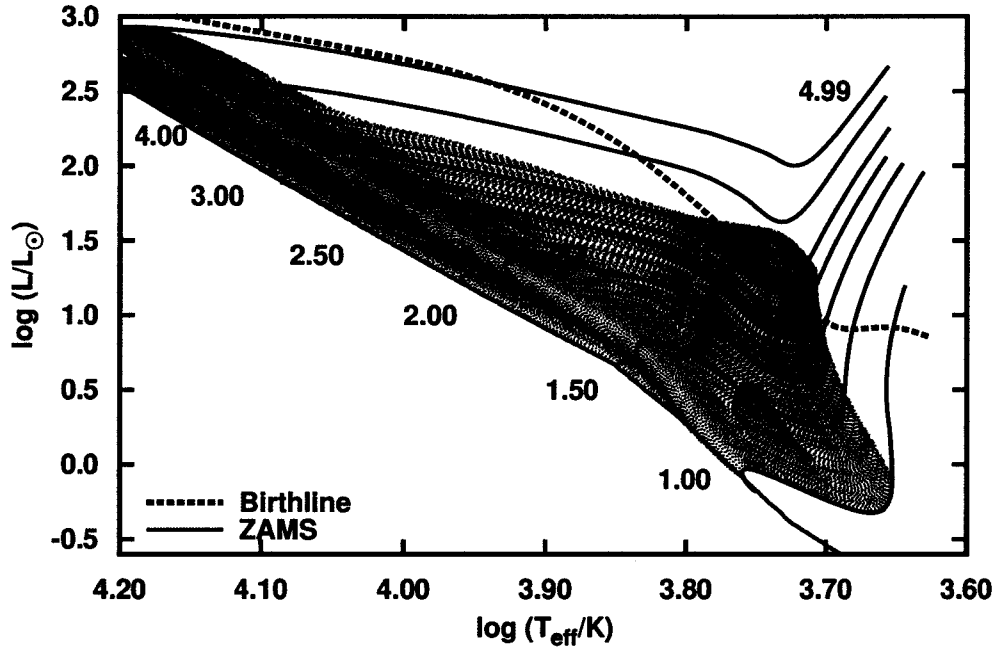

Figure 3.99: Position of the primary component of DX Cha in the HRD, along with the models of the grid that can support all observed frequencies of DX Cha. The error bars encompass masses ranging from 2.00 to 2.25 $M_{\odot}$.

distance range of 110.1 to 119.6 pc. First identified as an emission-line star by Henize (1976), DX Cha was further identified as a candidate HAe star by Hu, The & de Winter (1989). Spectral classifications of the primary include A7 IV (Brown et al. 1997) and and A7.5 to A8 Ve (Grady et al. 2004). Feigelson, Lawson & Garmire (2003) found that that DX Cha is a multiple system, with at least five members, including a couple of classical T-Tauri stars, and DX Cha b, a K or M-class star, orbiting close enough to the primary to form a spectroscopic binary with the primary (see also Böhm et al. 2004). δ-Scuti variations were first detected in the spectral-line profiles taken by Donati et al. (1997), and were the serendipitous discovery of an observing campaign studying the spectropolarimetric characteristics of active stars and otherwise searching for magnetic fields. As a result, DX Cha A was among the first handful of PMS δ-Scutis to be discovered. Donati et al. (1997) also reported $v \sin i = 12 \pm 2$ km/s, suggesting that DX Cha A is rotating almost pole-on with respect to the line of sight, or it is an intrinsically slow rotator. The former is the

most likely, but if the latter, then it could be the slowest-rotating PMS δ-Scuti known. Pulsations were later confirmed by the photometric observations of Kurtz & Müller (1999), in which two frequencies were detected, 33.29 and 36.61 c/d ($\pm$ 0.24 c/d).

Time-series spectroscopic observations of DX Cha A and b by (Grady et al. 2004; Dupret et al. 2006) further extracted the orbital radial-velocity curve for those two stars of the DX Cha system, and at the same time, detected up to eight pulsation frequencies in the radial-velocity curve, depending upon the observing season. These frequencies appear in Figure 3.98 in tabular and graphical form. Note that the amplitudes are in km/s, not magnitudes, and so are not directly comparable to other similar graphs in this thesis. Note also that radial-velocity measurements are sensitive to different non-radial orders than photometry.

Due to the binary nature of DX Cha A and b, extracting the luminosity of DX Cha A from BV broad-band photometry is difficult without knowing more about DX Cha b (the other components of the system are far enough that they should not be contaminating the broad-band photometry), and so here I use $\log(L/\mathrm{L}_{\odot})=1.42^{+0.04}_{-0.07}$ and spectral class A7.5 to A8 Ve from Grady et al. (2004), who took these factors into consideration in their luminosity calculations. Figure 3.96 shows the primary's position in the HRD, along with the the models in the grid that can support the reported frequencies. The highest frequency puts maximum luminosity constraints on the star that are in agreement with the star's position in the HRD.

3.3.1.3 EE Cha

The discovery of δ-Scuti pulsations in EE Cha (HD 105234) was the serendipitous result of the observing campaign that confirmed the PMS δ-Scuti pulsations in DX Cha (Kurtz & Müller 1999). Both EE and EF Cha were chosen as comparison stars in the study, but both were found to be δ-Scuti variables. Fortunately, a third comparison star, ϵ Cha, the star for which a moving group of PMS stars is named, is not variable, and was able to be used for the needed steady comparisons. For DX Cha the observations were taken over several nights, but EE Cha was only observed for

ID	freq. (c/d)	err freq. (c/d)	freq (μHz)	err freq. (μHz)	Amp (mmag)
f1	33.88	0.86	392.1	9.9	10.5
f2	29.31	0.86	339.2	9.9	5.4

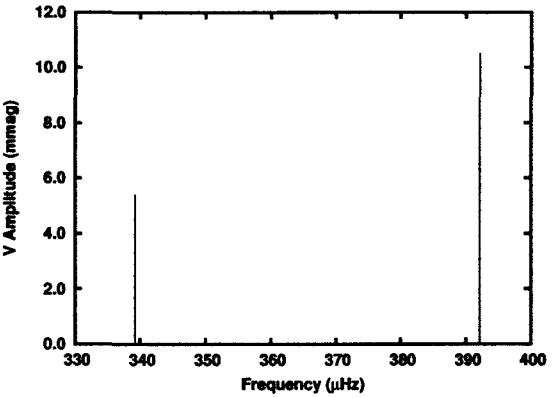

Figure 3.100: Frequencies of EE Cha as observed by Kurtz & Müller (1999).

two consecutive nights, for a total base line of 1.17 days, or a frequency resolution of 0.86 c/d, or 9.9 μHz. The observations were photoelectric Johnson B-band photometry taken at the South African Astronomical Observatory 0.5-m telescope, and despite the short time base, two pulsation frequencies were discovered. The frequencies appear in tabular and graphical format in Figure 3.100. The short time base line of the observations, and spectral window of the single-site observations mean that

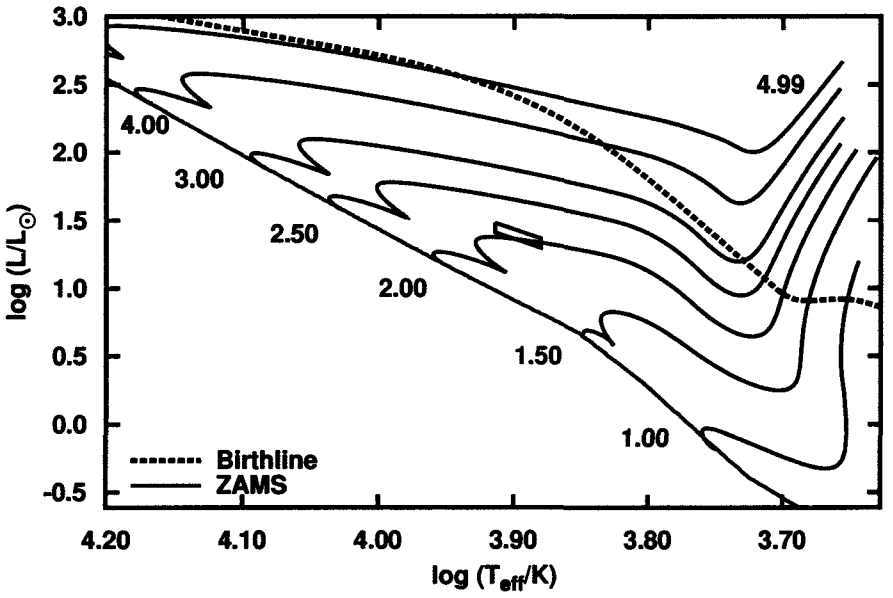

Figure 3.101: Position of EE Cha in the HRD.

the frequency resolution is very low and that integer-cycle/day aliases of the true frequencies may have been identified instead of the true frequencies. At the time, EE Cha was not recognized as a PMS star, but shortly thereafter Mamajek, Lawson & Feigelson (2000) identified EE Cha as a ROSAT X-Ray source, with spatial motions consistent with the newly-named-and-discovered η Cha sparse open cluster, with ages consistent with PMS evolutionary status. It has only been with the literature searches associated with this thesis, though, that this star has been added to the list of PMS δ-Scutis, as its combined status as both types of stars had previously not been appreciated. EE Cha with $V = 6.7$ magnitudes has only one spectral classification in the literature, A7 V (Houk & Cowley 1975). There is an earlier, incomplete, classification of A2 in the Cape Observatory Photographic Catalogue (Stoy 1966), however such a classification seems unlikely, given the proximity of the star to the Sun, and the larger amount of extinction and reddening that a class A2 star would imply. Here I choose an effective-temperature range consistent with class A5 V through A8 V as a compromise. EE Cha has two estimates of $v \sin i$ in agreement with one another, 100 km/s by Grenier et al. (1999), and 93±7 km/s by (Royer et al. 2002a). EE Cha has a well-determined parallax of 9.23±0.37 mas (van Leeuwen 2007), corresponding

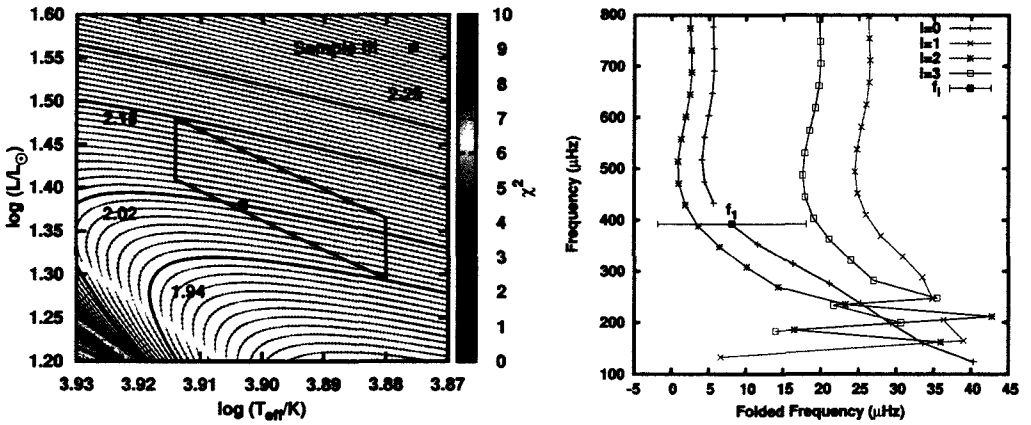

Figure 3.102: Sample echelle for EE Cha demonstrating the approximate radial order of pulsation. Mass = 2.02 $M_\odot$, $\log(T_{eff}/\mathrm{K}) = 3.903$, $\log(L/L_\odot) = 1.380$.

to a distance range of 104 to 113 pc. Figure 3.101 shows the star's position in the HRD.

Despite the large uncertainties associated with the observed frequencies, the narrow range of well-determined luminosities for the star means that the approximate radial order of pulsation can still be estimated. Figure 3.102 shows χ^2 fits of f_1 to $\ell = 0$ modes only as a way of estimating the approximate radial order. The centre of each purple band in the plot indicates a radial mode corresponding to $f_1 = 339.24$ μHz. The corresponding echelle diagram of the indicated model shows that f_1 would correspond to approximately a radial order of $n = 7$, indicating that EF Cha is pulsating in a mid-range radial order, not near the fundamental frequency, nor near the acoustic cut-off frequency.

3.3.1.4 EF Cha

Like with EE Cha, the discovery of δ-Scuti pulsations in EF Cha (HD 105234) was the serendipitous result of the observing campaign that confirmed the PMS δ-Scuti pulsations in DX Cha (Kurtz & Müller 1999). Both EE and EF Cha were chosen as a comparison stars in the study, but both were found to be δ-Scuti variables. Fortunately, a third comparison star, ϵ Cha, the star for which a moving group of PMS stars is named, is not variable, and was able to be used for the needed steady comparisons. The observations were from photoelectric Johnson B-band photometry

ID	freq. (c/d)	err freq. (c/d)	freq (μHz)	err freq. (μHz)	Amp (mmag)
f_1	18.91	0.24	218.9	2.7	3.9
f_2	29.11	0.24	336.9	2.7	2.7

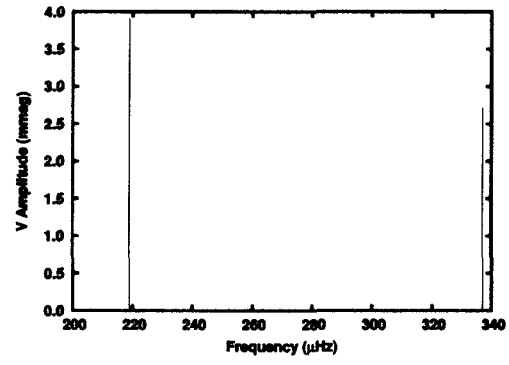

Figure 3.103: Frequencies of EF Cha as observed by Kurtz & Müller (1999).

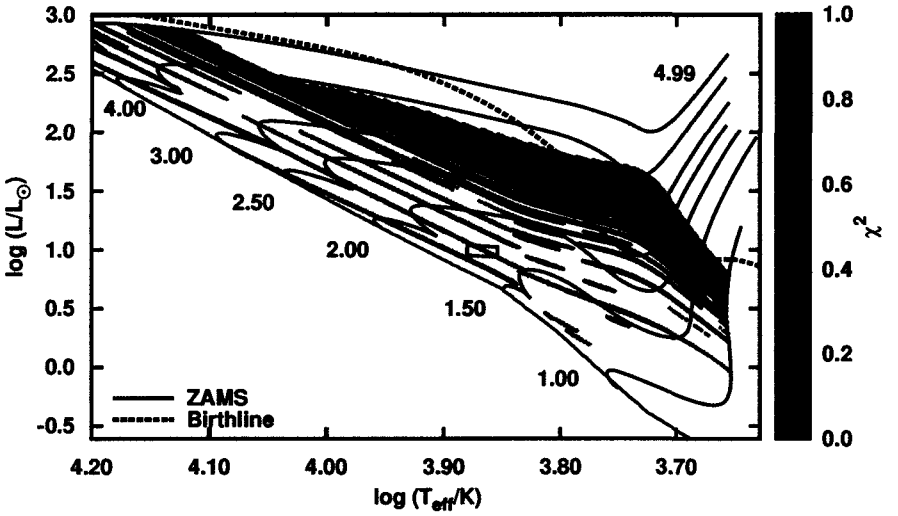

Figure 3.104: χ^2 fit to all highly-significant frequencies of EF Cha, $\ell = 0$ and 1 modes only, as well as the star's observed position in the HRD.

taken at the South African Astronomical Observatory 0.5-m telescope over several nights, total time baseline of 4.25 days, for a frequency resolution of 0.24 c/d, or 2.7 μHz. Two frequencies were discovered, and appear in tabular and graphical format in Figure 3.103. The short base line of the observations, and spectral window of the single-site observations mean that the frequency resolution is very low and that integer-cycle/day aliases of the true frequencies might have been identified instead of the true frequencies. At the time, EF Cha was not recognized as a PMS star, but shortly thereafter Mamajek, Lawson & Feigelson (2000) identified EF Cha as a ROSAT X-Ray source, with spatial motions consistent with the newly-named-and-discovered η Cha sparse open cluster, with ages consistent with PMS evolutionary status. It has only been with the literature searches associated with this thesis, though, that this star has been added to the list of PMS δ-Scutis, as its combined status as both types of stars had previously not been appreciated. Besides the X-Ray observations, PMS status is further corroborated by observations of a warm-dust shell around EF Cha (Rhee, Song & Zuckerman 2007).

EF Cha only has one spectral classification, A9 III/IV by Houk & Cowley (1975), and so a temperature between an A8 and F0 star has been assumed. EF Cha

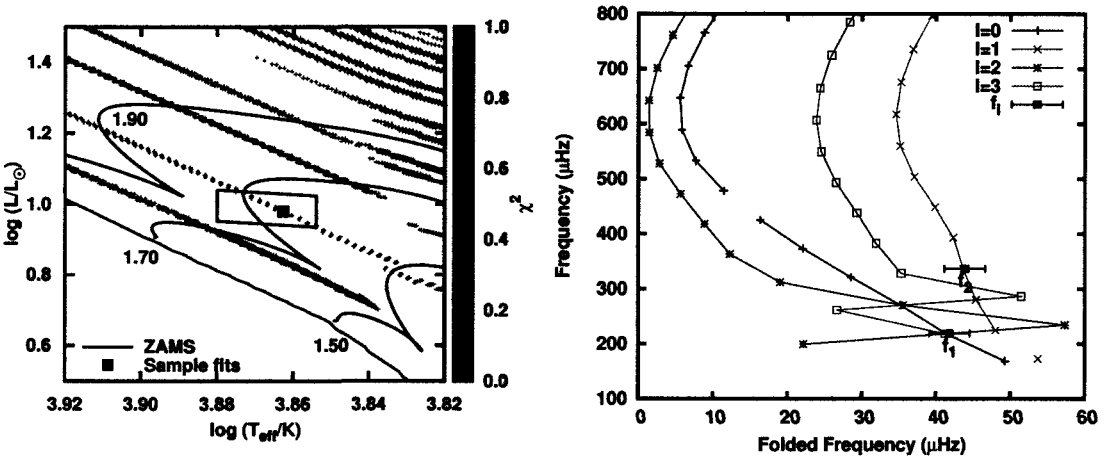

Figure 3.105: χ^2 fits to weighted frequencies for EF Cha, $\ell = 1$ models only. Sample echelle is for $\chi^2 = 0.02$, M = 1.65 $M_\odot$, $\log(T_{eff}/\mathrm{K})$= 3.862, $\log(L/L_\odot)$= 0.979.

is very close by, with a well-determined parallax of 9.71±0.49 mas, corresponding to a distance range of 98 to 109 pc. With apparent $V = 7.5$, and $(B - V) = 0.26$ magnitudes, it has little or no extinction. There are no known $v \sin i$ measurements in the literature.

With such high uncertainties associated with the two discovered frequencies, ambiguous results might be expected from any asteroseismic analysis for the star. However, the good distance determination of the star, and the lack of substantial extinction means that the star's intrinsic luminosity is much more well known than for most stars in this study, hence the results are far less ambiguous than expected. Figure 3.104 shows the result of the analysis, fit to $\ell = 0$ and 1 modes only. More solutions would presumably exist, if higher non-radial orders were also allowed. Note that the colour scheme of Figure 3.104 is slightly different, limited to fits of $\chi^2 < 1$ instead of $\chi^2 < 5$. The rather precise position of EF Cha in the larger HRD of Figure 3.104 is hard to see, but there is clearly only one family of solutions consistent with the star's position in the HRD. This family of solution is depicted in Figure 3.105, and corresponds to f_1 identified as a radial mode (first overtone), and f_2 as an $\ell = 1$ mode, mass in the 1.50-to-1.95-$M_\odot$ range. Note that if such fits had been considered,

a brief examination of the echelle diagram shows that for this particular model f_1 could also have fit an $\ell = 3$ mode.

So, in summary, despite poor frequency resolution, the precise position of EF Cha in the HRD demonstrates the usefulness of such stars in narrowing down the solution space for any asteroseimic analysis. Future time-series observations of this star would be extremely useful towards finding more pulsation frequencies, and therefore helping to calibrate PMS evolutionary models. Observations of $v \sin i$ would also be crucial for such calibrations.

3.3.2 IC 348 - V705 Per (IC 348 H254)

IC 348 is a young open cluster in Perseus, part of the Perseus OB2 association. Using Hipparcos data, Scholz et al. (1999) estimated the distance range to IC 348 as 238 to 288 pc, and using main-sequence fitting, Herbig (1998) found 316 pc. I will use a distance to IC 348 that therefore spans 238 to 316 pc. Note that the Herbig Ae PMS δ-Scuti star, IP Per (see Section 3.1.2.1), is also thought to be a member of Per OB2, and so may be closely related to the stars in IC 348.

In a targeted search for PMS δ-Scuti stars in IC 348, Ripepi et al. (2002) discovered pulsations in one star in their field, that of V705 Per (IC 348 H254 in their study). The initial discovery was from observations during Sept 2001 using the 1.54 m Loiano Observatory in Italy, with a follow-up study with multi-site observations in December 2001/January 2002 over 7 nights, using the Italian telescope, and the 1.5 m telescope in San Pedro Martir in Mexico. The frequencies that I use, are from the multi-site observing run, and were obtained in Johnson BV filters at one site, and Strömgren *ubvy* filters at the other, and then combined for the total light curve. Four frequencies were detected, however only one of them, $f_4 = 7.406$ c/d, is a δ-Scuti-range signal (Figure 3.106). The nature of the other three frequencies are unknown at this time, but it is possible that they are g-modes, or perhaps a signal of rotation from sunspots upon the surface of the star.

Label	Freq (c/d)	Err Freq (c/d)	Freq (μHz)	err Freq (μHz)	V Amp. (mmag)	Period days
f_1	0.157	0.008	1.82	0.09	12.5	6.37
f_2	0.283	0.008	3.28	0.09	9.0	3.53
f_3	0.931	0.008	10.78	0.09	6.5	1.07
f_4	7.406	0.008	85.72	0.09	5.4	0.14

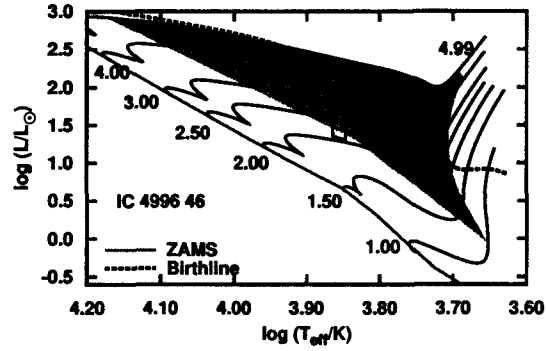

Figure 3.106: Left: frequencies of V705 Per in IC 348, including non-δ-Scuti frequencies. Right: models allowed by $f_4 = 85.72$ μHz, considering the fundamental mode of each model.

V705 Per is a $V = 10.56$, $B - V = 0.99$ magnitude star (Herbig 1998), with a spectral type of F0 or perhaps F0 m: (Herbig 1998; Harris, Morgan & Roman 1954). Here, I will use a temperature range consistent with spectral classes F0 $\pm$ one spectral class. There does not appear to be any $v \sin i$ measurements in the literature. The left-hand side of Figure 3.106 shows the frequencies of V705 Per, along with the periods of the signals to indicate the multi-day nature of f_1 through f_3, whatever the nature of these first three frequencies might happen to be. Note that any of these frequencies might be cycle/day aliases of any true signal. The right-hand side of the figure shows the constraints on luminosity of V705 Per, given $f_4 = 85.72$ μHz. The star must be significantly above the ZAMS to support f_4 as a p-mode, in agreement with the star's HRD position, as determined from non-astroseismic measurements.

3.3.3 NGC 6383 in Scorpius

NGC 6383 is a young open cluster that is part of the Sgr OB1 association, along with NGC 6530, another cluster that is part of this study. Fitzgerald et al. (1978) found a distance to the cluster of 1500$\pm$200 pc.

Zwintz et al. (2005) observed the cluster in Johnson B and V filters using CCD photometry at the Cerro Tololo Interamerican Observatory (CTIO) 0.9 m Telescope in Chile over approximately 12 nights in August 2001. Two stars were found to be δ-Scuti pulsators in both filters, with a third star displaying a marginal detection in

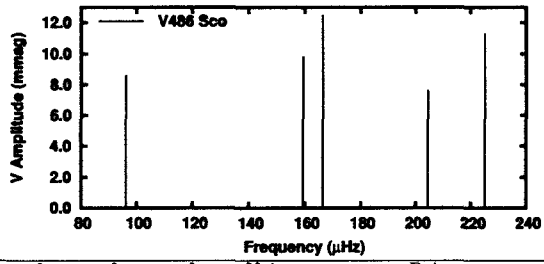

star	ID	freq. (c/d)	err freq. (c/d)	freq (μHz)	err freq. (μHz)	V Amp (mmag)	err (mmag)	B Amp (mmag)	err (mmag)	Spec. class	ref.	V (mag)	B-V (mag)
GSC 07380-00975	f_1	19.024	0.082	220.19	0.95	20.8	0.9	26.4	0.6			12.820	0.572
V486 Sco	f_1	14.376	0.082	166.39	0.95	12.5	0.8	16	0.6	A5 IIIe	(1)	12.761	0.659
	f_2	19.436	0.082	224.95	0.95	11.3	0.3	14.9	0.5				
	f_3	13.766	0.082	159.33	0.95	9.8	0.4	12.3	0.7				
	f_4	8.295	0.082	96.01	0.95	8.6	0.7	11.1	0.7				
	f_5	17.653	0.082	204.32	0.95	7.6	0.9	9.8	0.5				
GSC 07380-00173	f_1	2.550	0.082	29.51	0.95			30	1	F1 F0 Ve	(1) (2)	12.305	0.578

Figure 3.107: Upper panel: pulsation spectrum of V486 Sco. References for spectral classes: (1) van den Ancker, Thé & de Winter (2000); (2) The et al. (1985). Lower panel: frequencies of stars of NGC 6383 as found by Zwintz et al. (2005) with relevant spectral classifications and Johnson BV phometry. Broad-band spectroscopy is from Rauw, Manfroid & De Becker (2010).

one filter only, with a frequency somewhat low for δ-Scuti pulsation. The frequencies are displayed in tabular form in Figure 3.107, along with the pulsation spectrum in graphical form of V486 Sco, the only star for which more than one frequency was found. Also shown in the table are the relevant spectral classifications and broad-band photometry (references are listed in the figure caption).

There are no $v \sin i$ determinations for any of the stars, and there does not appear to be any spectral classification available for GSC 07380-00975. Also note that V486 Sco is listed as an eclipsing binary system with a period of about 60 days in Malkov et al. (2006), an eclipsing-binary catalogue, although the quality of that detection is hard to ascertain from the literature, and should probably be more fully investigated in the future. The light curve of Zwintz et al. (2005) presumably did not capture an eclipse of the star.

An astroseismic analysis of V486 Sco (NGC 6383 170) performed in Zwintz, Guenther & Weiss (2007) was able to successfully explain the observed frequencies using non-radial modes; Zwintz et al. (2005) had been unable to fit all of the modes

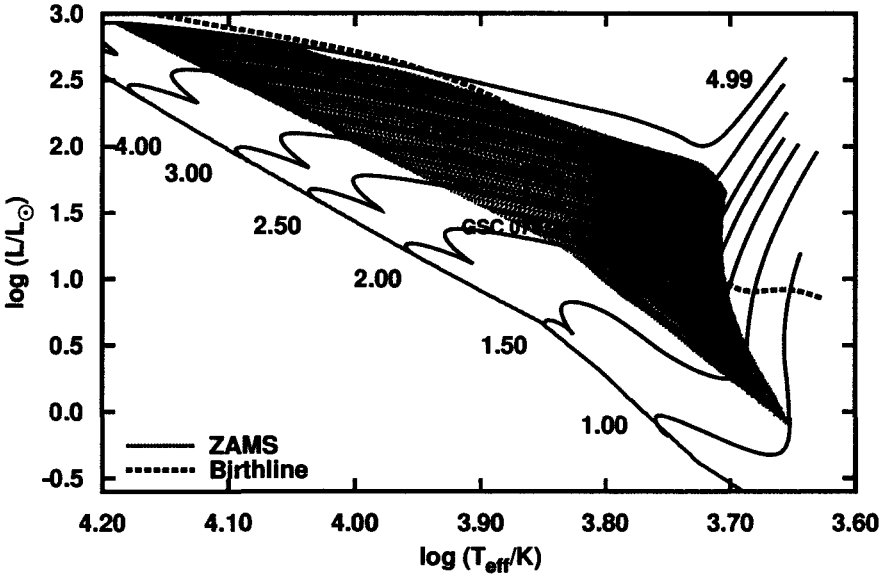

Figure 3.108: Position of V486 Sco and GSC 07380-00173 of NGC 6383 in the HRD, along with the stellar models that can support all of the observed frequencies of V486 Sco of Zwintz et al. (2005).

identified in V486 Sco using purely radial modes. A reanalysis of these stars will not be performed here, except to place V486 Sco in the HRD (Figure 3.108), and use the minimum and maximum frequencies in the pulsation spectrum to limit the star's position in the HRD. The astroseismic HRD position, and the position determined from broad-band photometry and spectroscopy are in agreement.

Figure 3.108 also shows the HRD position of GSC 07380-00173. The detection of $f_1 = 2.550$ μHz was marginal, with the signal only appearing in the B band, and so this star is considered a candidate PMS δ-Scuti star only. The frequency is very low for a δ-Scuti star, and therefore imposes luminosity constraints on the star that would place it just below the birthline. This minimum luminosity constraint does not agree with the star's HRD position, and so the detection of this signal might be spurious, a g-mode, or of some other phenomenon as yet to be identified, or the star's position in the HRD might be in error.

And finally, the lack of a spectral class for GSC 07380-00975 means that a position for that star in the HRD has not been determined. However, similarities

between the broad-band photometry of this last star, and that of the other two stars suggests the former would fall within the HRD without difficulty should a spectral class for the star be determined.

3.3.4 NGC 6530 in Sagittarius

NGC 6530 is a young open cluster in Sagittarius, part of the Lagoon Nebula, also known as M8, at a distance of 1860±70 pc (*e.g.* McCall, Richer & Visvanathan 1990, with good agreement between various studies). In a targeted search for such stars, and using the Cerro Tololo Interamerican Observatory (CTIO) 0.9 m telescope in Chile, Zwintz & Weiss (2006) discovered six δ-Scuti pulsating stars in the field, with a seventh possible detection. The first six stars were found to be pulsating in both Johnson B- and V-filter CCD images, and with the seventh, a single frequency was detected with significance in V-band only. Guenther et al. (2007) performed a reanalysis of the light curves, in one case finding more frequencies than had been detected previously; those frequencies are shown in Table 3.3. They then performed an asteroseismic analysis of the stars with some success. Here, except for the marginal detection, NGC 6530 ZW 288, I show each star's pulsation spectrum in Figures 3.109 and 3.110, and the constraints the minimum and maximum pulsation frequencies of each star put on the luminosity in the HRD, and otherwise a reanalysis of each star is not performed. Unfortunately, there are no positions plotted in the HRD from spectroscopy and photometry. Although two of these stars have spectral classifications inferred from broad-band photometry (ZW 85 and ZW 278, A1 III/A0 and A0/A4, respectively from Chini & Neckel 1981; van den Ancker et al. 1997), none of these stars has been found to have a proper MKK spectral classification available in the literature, and so I refrain from pursuing an HRD solution without those available. There are also no $v \sin i$ measurements available in the literature. Table 3.3 also lists the V and $B-V$ parameters of each star, as determined by Sung, Chun & Bessell (2000).

A few brief summary notes on each star will now be given.

ZW	Walker/ WEBDA	ID	Freq (c/d)	err Freq (c/d)	Frequency (μHz)	err Freq (μHz)	V amp (mmag)	err V amp (mmag)	B amp (mmag)	err B amp (mmag)	V (mag)	B-V (mag)
5	159	f_1	46 596	0 009	539 31	0 10	1 4	0 3	1 8	0 3	13 592	0 435
		f_2	53 417	0 009	618 25	0 10	1 0	0 3	1 1	0 3		
82	78	f_1	38 531	0 006	445 96	0 07	2 4	0 3	2 8	0 3	13 969	0 610
		f_2	34 671	0 007	401 28	0 08	2 2	0 3	2 4	0 3		
		f_3	24 829	0 009	287 37	0 10	1 8	0 3	1 7	0 3		
85	53	f_1	15 579	0 001	180 31	0 01	30 2	0 3	39 1	0 3	13 072	0 648
		f_2	12 700	0 001	146 99	0 01	17 1	0 3	23 0	0 3		
		f_3	15 531	0 002	179 76	0 02	8 2	0 3	11 4	0 3		
		f_4	10 585	0 004	122 51	0 05	3 5	0 3	4 7	0 3		
		f_5	31 148	0 008	360 51	0 09	1 8	0 3	2 0	0 3		
		P_2	11 524		133 38							
		P_4	14 469		167 47							
		P_7	15 634		180 95							
		P_8	28 280		327 31							
263	57	f_1	19 223	0 002	222 49	0 02	7 1	0 2	8 3	0 3	13 671	0 632
278	38	f_1	7 200	0 002	83 33	0 02	6 6	0 2	9 4	0 3	12 169	0 531
		f_2	12 121	0 002	140 29	0 02	9 4	0 2	12 4	0 3		
		f_3	13 218	0 002	152 99	0 02	9 9	0 2	13 8	0 3		
		f_4	4 178	0 002	48 36	0 02	6 2	0 2	8 0	0 3		
		f_5	9 488	0 003	109 81	0 03	5 0	0 2	6 6	0 3		
		f_6	6 013	0 004	69 59	0 05	3 6	0 2	5 0	0 3		
		f_7	11 984	0 003	138 70	0 03	4 9	0 2	6 7	0 3		
		f_8	15 684	0 005	181 53	0 06	2 9	0 2	3 7	0 3		
		f_9	13 896	0 006	160 83	0 07	2 6	0 2	3 5	0 3		
281	13	f_1	43 418	0 004	502 52	0 05	4 2	0 2	4 7	0 2	13 349	0 452
		f_2	40 017	0 004	463 16	0 05	3 9	0 2	5 1	0 2		
		f_3	37 457	0 006	433 53	0 07	2 4	0 2	2 7	0 2		
		f_4	41 702	0 009	482 66	0 10	1 7	0 2	1 5	0 2		
		f_5	40 367	0 008	467 21	0 09	1 9	0 2	2 2	0 2		
		f_6	30 691	0 009	355 22	0 10	1 4	0 2	1 5	0 2		
		f_7	38 245	0 007	442 65	0 08	2 1	0 2	2 1	0 2		
288	28	f_1	17 996		208 29		0 8				13 233	0 415

Table 3.3: Frequencies of stars, f_i of NGC 6530 as listed in Zwintz & Weiss (2006), with additional frequencies , P_i, reported in Guenther et al (2007) In column one "ZW" indicates the star designations as used in both papers, and the second column gives the numbering system originally used by Walker (1957), and since extended and used by WEBDA Photometric data in the last two columns are from Sung, Chun & Bessell (2000).

NGC 6530 ZW 5

Two frequencies detected, with both frequencies rather high. $f_2 = 618.25\ \mu$Hz puts some limits on the maximum luminosity of the star.

NGC 6530 ZW 82

Three frequencies detected, the highest frequency, $f_1 = 445.96\ \mu$Hz, puts minor constraints on the maximum luminosity of the star, implying that the star could be no more massive than approximately 3 $M_\odot$.

NGC 6530 ZW 85

Five frequencies were detected by Zwintz & Weiss (2006), ranging from $f_4 = 122.51$ μHz to $f_5 = 360.51$ μHz, with four more added with the reanalysis of Guenther et al. (2007). This is the only δ-Scuti star in NGC 6530 in which the frequency spectrum simultaneously puts limits on both the minimum and maximum luminosity for the star. There is a very close frequency triplet, f_1, f_3 and P_7, with a difference of approximately 0.6 μHz that in Guenther et al. (2007) was thought to be perhaps a rotationally-split multiplet, requiring a very slow equatorial rotational velocity of about less than 10 km/s. Observations of other PMS δ-Scuti stars have shown that such a slow rotator would be unprecedented by a large margin, indicating its unlikelihood. However, unlike other stars with a similar number of frequencies detected, the frequencies in this star *were* able to be fit to models with some ease by Guenther et al. (2007). Perhaps the reason is that it *is* a slow rotator, and thus the pulsation spectrum of the star hasn't been significantly altered by rotation, rendering a detailed solution possible. Observations of the $v \sin i$ of the star are required to test this supposition. If true, though, this star might then turn out to be an important calibration star for PMS models.

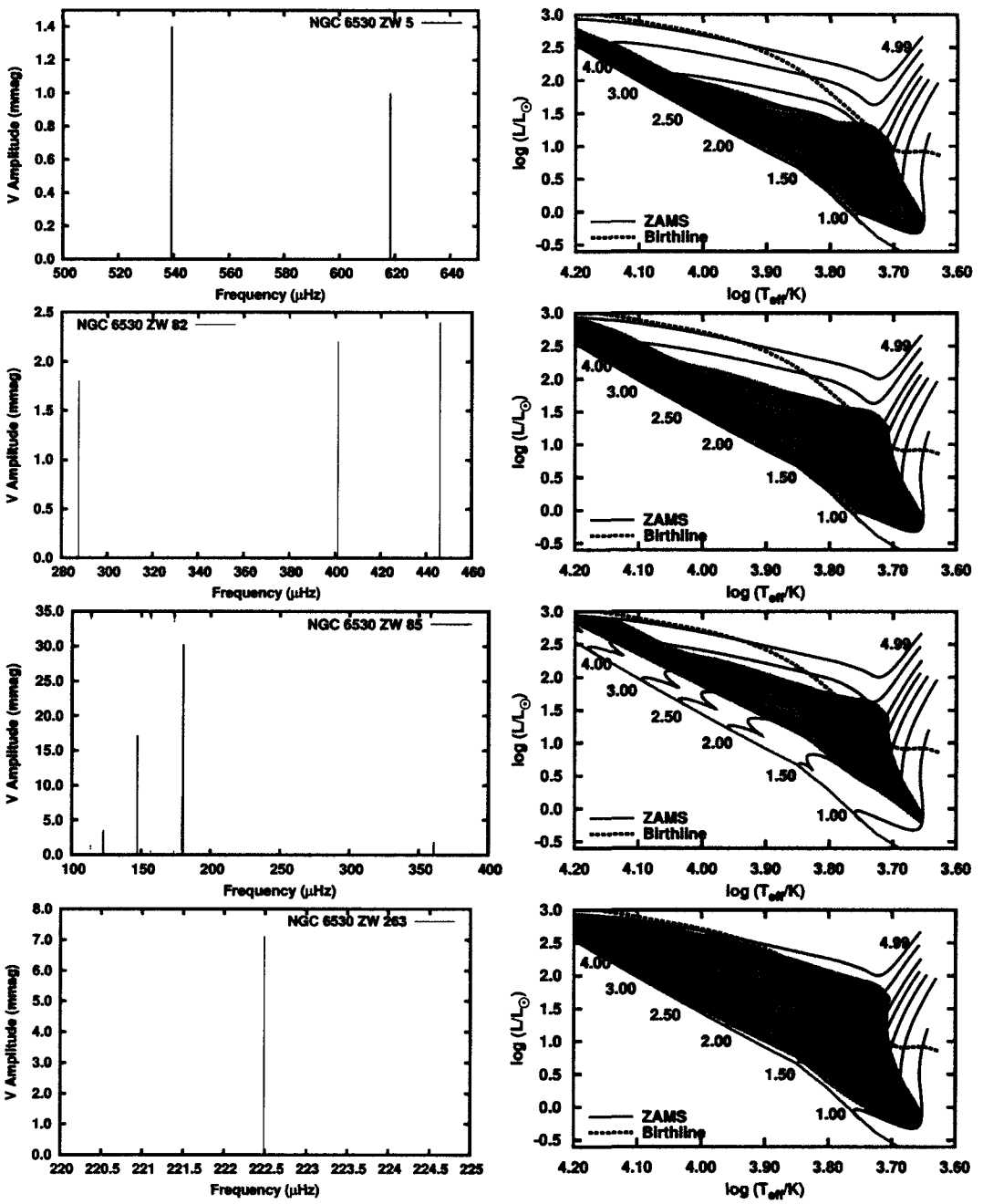

Figure 3.109: Observed frequencies (left) and the constraints those frequencies put on the HRD (right) for NGC 6530 ZW 5, 82, and 85, 263, respectively, top to bottom rows. In the case of ZW 85 the extra doted lines indicate the new frequencies detected upon reanalysis of the light curve by Guenther et al. (2007) for which amplitudes were not reported.

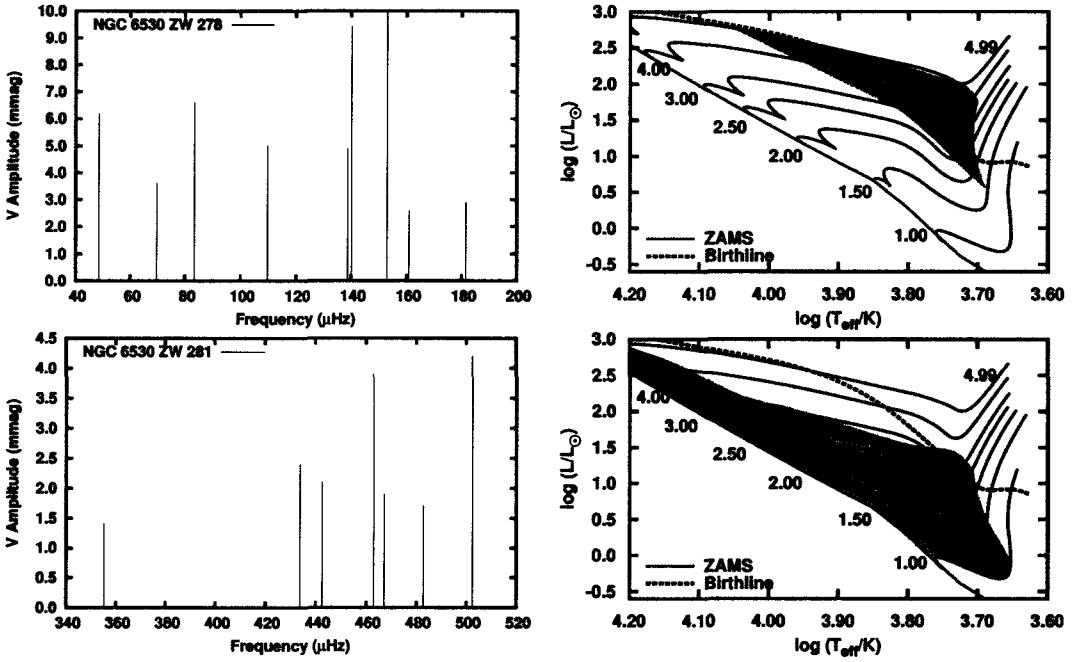

Figure 3.110: Observed frequencies (left) and the constraints those frequencies put on the HRD (right) for NGC 6530 ZW 278, and 281, respectively, top to bottom rows.

NGC 6530 ZW 263

One frequency detected, $f_1 = 222.49$ μHz. This frequency is mid-range for δ-Scuti pulsations, and therefore puts no constraints on either the maximum or minimum luminosity of the star.

NGC 6530 ZW 278

Nine frequencies detected, all in the lower range of frequencies expected for a δ-Scuti star. This puts significant constraints on the minimum luminosity of the star, putting it among the more-luminous possible. If the lowest frequency, $f_4 = 48.36$ μHz, is a not a p-mode, then this would ease the luminosity constraints on the star somewhat, but would then raise the question as to what the nature of f_4 actually is.

NGC 6530 ZW 281

Five frequencies detected, with the highest frequency, $f_1 = 502.52\ \mu$Hz, putting some constraints on the maximum allowed luminosity of the star.

NGC 6530 ZW 288

One marginal frequency detection. If real, the lone frequency, $f_1 = 208.29\ \mu$Hz, is midrange, and would not put any significant luminosity constraints on the star.

3.3.5 NGC 6823 in Vulpecula

NGC 6823 is a young open cluster in Vulpecula, thought to be the core of the Vul OB1 association, with distance estimates between 2000 and 2500 pc (*e.g.* Turner 1979; Guetter 1992; Massey, Johnson & Degioia-Eastwood 1995). There appears to be large amounts of differential reddening across the cluster (*e.g.* Turner 1979).

As part of a systematic search for B-type variable stars in this and other young clusters, Pigulski, Kolaczkowski & Kopacki (2000) discovered two PMS δ-Scuti stars in the cluster, NGC 6823 HOAG 157 and NGC 6823 BL50, among the first handful of the class to be discovered. In both stars, two relatively-low pulsation frequencies of fairly-high amplitudes in Cousins I_c band were detected. The observations were from two observing seasons in 1998 and 1999 using the Białków Observatory of the Wrocław University, Poland, in which the frequencies were extracted from both seasons simultaneously, hence the frequencies are known to very high precision. Table 3.4 lists the frequencies, along with the designation used in the WEBDA database, and

NGC 6823 ID	WEBDA ID	Freq ID	Freq (c/d)	err Freq (c/d)	Freq (μHz)	err Freq (μHz)	I_c amp (mmag)	V (mag)	B-V (mag)
HOAG 157	230	f_1	12 72557	0 00002	147 2867	0 0002	27	14 48	0 93
		f_2	15 52437	0 00003	179 6802	0 0003	20		
BL50	279	f_1	13 9175	0 0005	161 08	0 01	18	12 86	0 55
		f_2	9 8878	0 0009	114 44	0 01	6		

Table 3.4: Specifications and frequencies of PMS δ-Scuti stars in NGC 6823. Frequencies are as observed by Pigulski, Kolaczkowski & Kopacki (2000).

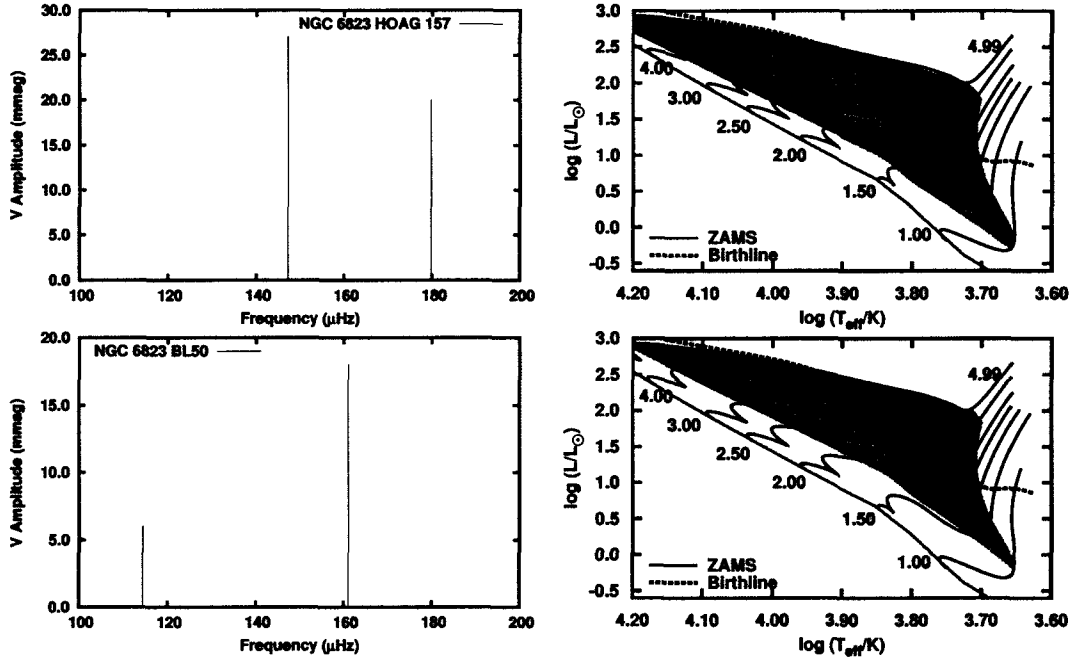

Figure 3.111: Observed frequencies (left) and the constraints those frequencies put on the HRD (right) for NGC 6823 HOAG 157 and NGC 6823 BL50, respectively, top to bottom rows.

V and $B - V$ values from the literature. In the case of HOAG 157, the photometry is from Hoag et al. (1961), and in the case of BL50, from Stone (1988). Unfortunately, there do not appear to be any spectral classification nor $v \sin i$ determinations available in the literature.

Figure 3.111 shows the pulsation spectrum for each star, along with the constraints those frequencies put on each star in terms of luminosity. Note that because of the lack of MKK-type spectral classifications, the stars have otherwise not been placed in the HRD. In both cases the story is similar: both stars must be above the ZAMS, BL50 slightly more so than HOAG 157, and neither star has upper limits to the luminosity within the range of models considered.

3.3.6 IC 4996 in Cygnus

IC 4996 is a young open cluster in Cygnus, part of a much larger, extended region of active star formation, containing a number of other clusters such as Be 86,

IC 4996 # ZW	WEBDA	Freq ID	Freq (c/d)	err Freq (c/d)	Frequency (microHz)	err Freq (microHz)	V amp (mmag)	B amp (mmag)	Sp Class	V (mag)	(B-V) (mag)
37	201	f_1	33.569	0.007	388.53	0.08	7.6	8.5	A5	15.30	0.80
40	171	f_1	31.875	0.009	368.92	0.10	4.6	5.1	A4	15.03	0.75
46	1085	f_1	4.0		69		5.4			15.30	0.72
		f_2	3.7		75		3.8				
		f_3	5.0		56			4.2			
		f_4	6.5		43			4.2			

Table 3.5: Frequencies, B, and $B-V$ of stars in IC 4996 observed to be pulsating by Zwintz & Weiss (2006). Also given are spectral classes for two of the stars, as given by Delgado, Miranda & Alfaro (1999). The star IDs are as used in Zwintz & Weiss (2006), with alternates as used by WEBDA.

NGC 6913 and the Cyg OB 1 association (see Delgado, Miranda & Alfaro 1999, and references therein). Photometric studies by various authors (*e.g.* Alfaro et al. 1985) agree on a distance between 1500 and 2000 pc.

In a search for PMS δ-Scuti stars, Zwintz & Weiss (2006) observed IC 4996 over a total time base of 14 nights in September 2002. Johnson B and V-filter CCD images were taken using the 1.5 m telescope at the Sierra Nevada Observatory in Spain. Two stars, IC 4996 37 and IC 4996 40 (using their numbering system), each had one frequency detected with significance in both filters. A third star, IC 4996 46, had four frequencies detected, but each frequency was only detected in one filter, two in B band and two in V band, so this star is labelled a suspected PMS pulsator, with more observations required for confirmation.

Figure 3.112 shows a brief analysis of the pulsations of each of the stars, commented upon below.

IC 4996 37

The top left corner of Figure 3.112 indicates the position in the HRD of IC 4996 37, given a spectral class of A5 as determined by Delgado, Miranda & Alfaro (1999). The position is just above the ZAMS, in agreement with luminosity limitations that $f_1 = 388.53$ μHz, the single pulsation frequency imposes, which are relatively minor on the high end of the luminosity range otherwise available to the star.

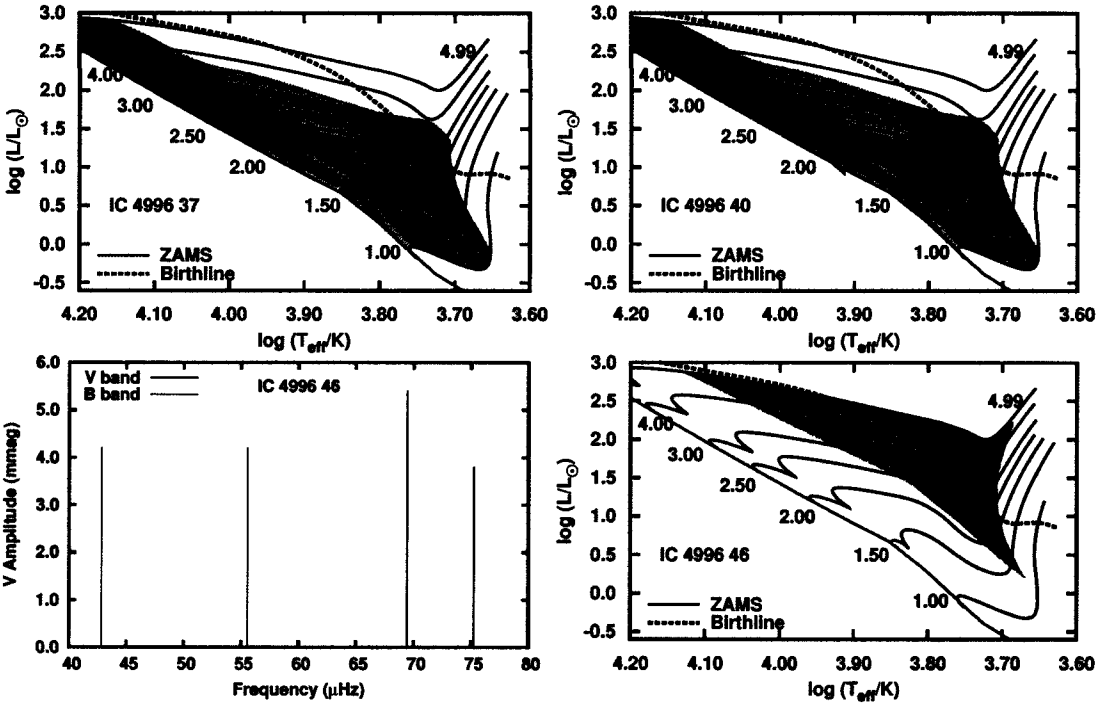

Figure 3.112: Top left: HRD position, plus luminosity constraints of IC 4996 37; top right: same, but for IC 4996 40. Bottom left: pulsation frequencies of IC 4996 46, sorted by filter; bottom right: constraints on luminosity for IC 4996 46, grey shading indicates B-band limits, rose shading indicates V-band limits.

IC 4996 40

The analysis for IC 4996 40 in the upper right-hand corner of Figure 3.112 is almost identical to that of IC 4996 37, with a very similar single frequency determined, $f_1 = 368.92$ μHz, and a slightly different spectral class, A5, also determined by Delgado, Miranda & Alfaro (1999). This star falls just above the ZAMS, with minor maximum luminosity constraints imposed upon the star by f_1.

IC 4996 46

The bottom right hand corner of Figure 3.112 shows the unconfirmed pulsation spectrum of IC 4996 46, sorted by the filter in which each of the frequencies were detected. If these frequencies are p-mode frequencies, then the lowest B-band frequency, $f_4 = 43$ μHz, puts significant minimum constraints on the luminosity of

the star (lower right-hand corner of Figure 3.112), putting the star at the high end of its available luminosity range (gray shading). If the minimum V-band frequency, f_2 = 69 μHz, is used instead, then the minimum allowed luminosities are significantly lower (rose-coloured shading), but still significantly above the ZAMS, and quite a bit brighter than the previous two stars. Note the star lacks any spectral-class determinations, and so a HRD position is not given. However, from the broad-band photometry in Table 3.5, it is interesting to note that the star has the same V-band apparent magnitude as IC 4996 37, and is slightly bluer, which means that to reach the required luminosities, the star must be either further away, and/or suffering a significantly-higher amount of extinction than the other two stars.

3.4 Clusters containing PMS δ-Scuti stars, but previously not identified as such

In searching WEBDA for young open clusters for which future observations might lead to the discovery of more PMS δ-Scuti stars, a number of sufficiently-young clusters were identified in which δ-Scuti stars had *already* been discovered. Unfortunately, neither the authors of the relevant studies that discovered the stars, nor the community at large recognized these stars for their special status as PMS δ-Scutis, and therefore they have been left off the corresponding lists. Here, I rectify this situation. For the most part, these stars are further away than the majority of the stars presented in this thesis, hence observations are more difficult, including any determinations of cluster membership for any individual star, so some of these stars may be post-ZAMS δ-Scuti field stars, instead of PMS δ-Scuti stars. Asteroseismic analysis of these stars will not be performed. This list is meant to notify the astronomical community at large of the existence of these stars, so future observations can be made to determine each relevant star's true status. In some cases, the detections are marginal.

3.4.1 Scorpius OB1 Association

The Scorpius OB1 association is a rather extended and confused OB association with distance determinations for different parts of the association ranging from 1600 pc (Seggewiss 1968) to 2400 pc (Schild, Neugebauer & Westphal 1971). The association contains at least two open clusters, Trumpler 24, and NGC 6231, in which variability studies have been performed, and δ-Scuti stars appear to have been discovered.

3.4.1.1 Trumpler 24 in Scorpius OB1

Trumpler 24 is a young open cluster, age < 10 Myr, with a distance and membership that has proved difficult to define, with distances ranging from 1600 to 2300 pc (*e.g.* see discussion in Heske & Wendker 1985), with PMS stars scattered throughout the cluster, merging into the overall Scorpius OB1 association field. A

Table 3.6: Variables displaying δ-Scuti-range signals in Trumpler 24 in the observations of Fu et al. (2003) and Fu, Bouzid & Sterken (2005). First column is their ID, followed by alternate Simbad designations and WEBDA number. Spectral type and B magnitudes are also from their work. Final column is a preliminary attempt identify the pulsation class.

FSD number	Simbad	WEBDA	B (mag)	Spec Type	Freq ID	Freq (c/d)	Freq (μHz)	B amp (mmag)	Pulse Type
V5	GSC 7872 1974	524	11 4	A1	f_1	3 27	37 8	13 3	δ Scu/SPB?
					f_2	1 64	19 0	2 6	
V6	NSV 20856	502	12 3	B9	f_1	14 81	171 4	4 9	δ Scu?
					f_2	12 63	146 2	3 1	
V7	GSC 07872-00700	501	12 1	B2	f_1	3 30	38 2	5 5	β Cep?
					f_2	2 31	26 7	4 4	
V8	HD 322449	505	10 8	K5	f_1	2 01	23 3	22 4	background
					f_2	0 35	4 1	5 0	red giant?
					f_3	5 02	58 1	5 1	
V10	GSC 07872-00415	507	11 7		f_1	2 76	31 9	3 8	unknown
					f_2	0 37	4 3	2 8	
					f_3	2 50	28 9	2 7	
V11	V1217 Sco	553	13 3	A7	f_1	8 90	103 0	16 7	δ Scu
					f_2	10 54	122 0	14 0	
V16	V1221 Sco	565	12 6	F5	f_1	8 89	102 9	28 1	δ Scu
					f_2	9 13	105 7	16 0	
					f_3	12 72	147 2	7 1	
V17	V1222 Sco	566	14 2	F3	f_1	7 57	87 6	28 6	δ Scu
					f_2	9 00	104 2	5 5	
V18	GSC 07872-00632	570	10 4	B2	f_1	12 78	147 9	12 5	β Cep?
					f_2	12 54	145 1	3 4	
					f_3	3 02	35 0	4 3	
					f_4	2 01	23 3	4 5	
V36	GSC2 S230011212406		16 2		f_1	1 54	17 8	33 8	unknown
					f_2	4 73	54 7	20 8	background?
					f_3	5 42	62 7	16 9	

search for variability in stars in Trumpler 24 was performed by Fu et al. (2003), and continued in Fu, Bouzid & Sterken (2005).

At least ten stars where discovered in their fields of observations in which pulsation was either detected or suspected. The pulsation class of the star might be ambiguous in certain cases, and so for completeness, all pulsating stars with frequencies of about 1 cycle/day and above are reported here, as regardless of pulsation type, all of these stars would benefit from future observations. The results are summarized in Table 3.6. The FSD number indicates the numbering system used in both Fu et al. (2003) and Fu, Bouzid & Sterken (2005). Alternate Simbad and WEBDA designations are also given. The spectral types are as determined by those authors, as are the Johnson B magnitudes. There are no known $v \sin i$ determinations for any of the stars in the literature.

V11, V16, and V17 all appear to be δ-Scuti stars. V5 has δ-Scuti-range pulsations, but has a slightly hot spectral type of B9, and so is only listed as a possible δ-Scuti. V6 and V18 are possible β Cep stars. V8 is probably a background red giant. V10 and V36 both have δ-Scuti-range pulsation frequencies, but without spectral classifications, their nature remains unknown. V36, however, is rather dim to be a cluster member, and so is potentially a background star.

3.4.1.2 NGC 6231 in Scorpius OB1

NGC 6231 is a young open cluster, age about 3-5 Myr, (*e.g.* see Balona & Laney 1995, and references therein), in which previous studies have detected six β Cep stars (Balona & Shobbrook 1983; Balona & Engelbrecht 1985), and a (maybe) foreground candidate δ-Scuti star, now known as V1205 Sco (Balona & Laney 1995). The study of Arentoft et al. (2001), however, detected a number of δ-Scuti stars, for which if they are cluster members, would make them members of the PMS δ-Scuti subclass. Several other variables were also detected, as summarized below, and in Table 3.7. The GCVS designations were assigned after the study of Arentoft et al. (2001) appeared. The numbering system is as established by Sung, Bessell & Lee

Table 3.7: Confirmed and candidate variable stars of δ-Scuti and γ Doradus-class pulsators in NGC 6231 from Arentoft et al. (2001). The GCVS designation was given to these stars after the original study appeared. The WEBDA designation is also the numbering system used in the paper. All other information is from Arentoft et al. (2001). The amplitude refers to semi-amplitude of the highest-amplitude pulsation detected in an individual star. γ Dor candidate designations, in particular, must be viewed as very uncertain.

GCVS	WEBDA	V (mag)	B-V (mag)	Freq ID	Freq (c/d)	Freq (μHz)	Amp (mmag)	Pulse type
V1199 Sco	306	13 987	0 668	f_1	15 6	181	6 5	δ Scu
				f_2	113	9 8		
				f_3	275	23 8		
V1200 Sco	332	15 713	1 217	f_1	1 9	22	18 7	unknown
				f_2	1 1	13		γ dor?
				f_3	5 3	61		
				f_4	4 4	51		
V1203 Sco	432	14 692	0 696	f_1	30 8	356	2 6	δ Scu
				f_2	31 0	359		
				f_3	38 4	444		
				f_4	4 5	52		
				f_5	0 3	3		
V1205 Sco	455	13 455	0 611	f_1	23 8	275	10 7	δ Scu
				f_2	21 8	252		
				f_3	18 9	219		
–	508	14 12	1 082	f_1	0 3	3	12 3	γ Dor?
				f_2	3 1	36		
				f_3	4 7	54		
V1209 Sco	595	14 334	0 585	f_1	41 4	479	1 6	δ Scu
				f_2	36 2	419		
				f_3	41 1	476		
V1210 Sco	598	13 791	0 448	f_1	3 6	42	2 7	unknown
				f_2	1 05	12		
V1213 Sco	628	15 033	1 258	f_1	1 2	14	36 1	γ Dor?
				f_2	3 4	39		
V1214 Sco	636	15 118	0 886	f_1	1 9	22	1 6	γ Dor/δ Scu?
				f_2	4 5	52		
				f_3	8 9	103		
V1215 Sco	646	15 671	0 828	f_1	2 1	24	4 8	γ Dor?
				f_2	3 7	43		
				f_3	4 8	56		

(1998), and is also the system used by the WEBDA database. The amplitude refers to the semi-amplitude of the highest-amplitude frequency of the frequencies in an individual star.

δ-Scuti pulsations were confirmed in V1205 Sco, for which such variability had previously been tentatively detected by Balona & Laney (1995). Concidentally, V1205 Sco is also the only star for which a stellar classification has been obtained, A5 III (or perhaps IV as the classifiers state) by Garrison & Schild (1979), and it may or may not be a foreground star. Three other stars (V1199, V1203, and V1209 Sco) exhibit fairly conclusive δ-Scuti variability, and if they are cluster members, then they should be PMS stars. The rest of the variables in Table 3.7 are potential γ Doradus stars, but given the ambiguities in detecting γ Dor pulsations from the ground, these

labels are by no means conclusive, as for example, the observed frequencies could be some sort of signal of rotation, instead of pulsation. Note that V1214 Sco, besides having potential γ Dor signals, also has one frequency ($f_3 = 8.9$ c/d) that also mark it as a potential δ-Scuti star.

Although not listed here, it should be mentioned that Arentoft et al. (2001) also confirmed the pulsations in the six previously-discovered β Cep stars in NGC 6231. They also detected one new and one candidate β Cep star, and detected three other variables that might be slowly-pulsating B stars.

In summary, NGC 6231 should be regarded as a cluster harbouring PMS δ-Scuti stars, for which further investigation is needed. In particular, spectral classifications and $v \sin i$ measurements would be quite useful.

3.4.2 NGC 581 (M103) in Cassiopeia

NGC 581 (M103) in Cassiopeia is a very marginal case for harbouring PMS δ-Scuti stars. According to Phelps & Janes (1994), the cluster is fit well with 22 Myr isochrones, however there are a number of brighter stars that for which if this age were the case, the stars would have evolved off the main sequence by now, and for which a maximum main-sequence age of 10 Myr would be expected. This fact would indicate that stars must be younger than the other stars, or the product of stellar mergers. Assuming these stars are not the product of a merger, this suggests the cluster might have undergone multiple episodes of star formation, or this is a chance superposition of two close, but separate clusters along the line of sight.

Unfortunately, at a distance of 2700 pc (Maeder & Meynet 1991; Phelps & Janes 1994), any PMS stars in the cluster colour-magnitude diagram are difficult to observe, with potentially significant contamination from field stars. This cluster is mentioned here because, nevertheless, it is a relatively young cluster, and any δ-Scuti stars, if among the youngest stars in the cluster, may still be in the very last phases of PMS evolution, or otherwise would be fairly recently-arrived main-sequence stars. One would not expect any evolved δ-Scuti stars, nor any PMS δ-Scuti

Lee ID	GCVS	V (mag)	Period (days)	Freq (c/d)	Freq (μHz)
V8	V1119 Cas	14 03	0 0725	13 79	159 6
V9	V1113 Cas	15 16	0 1239	8 07	93 4
V10	V1117 Cas	15 76	0 0282	35 46	410 4
V11	V1118 Cas	15 84	0 0736	13 59	157 3
V12	V1124 Cas	15 96	0 1463	6 84	79 1
V14	V1126 Cas	16 74	0 3551	2 82	32 6
V15	V1111 Cas	16 98	0 1100	9 09	105 2

Table 3.8: δ-Scuti stars, as observed by Lee et al (2005) in NGC 581. Multiple frequencies, if found, were not reported. Note that V14, with a frequency of 36.2 μHz, although reported as a δ-Scuti star, would either have to be a background star, or *not* a δ-Scuti star, perhaps a γ Doradus star instead.

stars significantly above the main sequence. As such, studying the δ-Scuti stars in such a cluster *would* allow the oldest PMS and the youngest MS models to be more thoroughly tested than with some of the younger clusters studied in this thesis.

Lee et al. (2005) reported the discovery of seven δ-Scuti stars in the field of NGC 581. Given the possible age ranges for stars in the cluster, these stars should not automatically be considered PMS δ-Scuti stars, and should only be labelled as such if future observations should support such a designation. Contamination from field stars is also a very real possibility. The stars are potential targets of interest (Table 3.8), recognizing the difficulty in observing these targets, given the distance to the cluster. Table 3.8 lists the stars using the numbering system in Lee et al. (2005), and the recent GCVS designations (Kazarovets et al. 2011). Only the dominant frequency for each star was reported by the authors. Note that some of the low frequencies, such as those for V12 and V14, put constraints on the minimum luminosity of the star if these are p-mode frequencies — these stars would be fairly high off the main sequence, arguing against cluster membership, and for identification as background stars. In the case of V14, γ Doradus-type variability is also a possibility, otherwise the star must be a very luminous background δ-Scuti star, or the signal is not indicative of pulsation at all, but perhaps of something like the rotational period of the star.

On a final note, no spectral classifications, nor $v \sin i$ measurements, were found in the literature for any of the stars in Table 3.8.

Chapter 4

Collective results

I now look at some of the collective results for PMS δ-Scuti star, collecting and displaying the various data, with the goal of showing some of the generalities that have been discovered within the data.

4.1 List of stars

Tables 4.1 and 4.2 provide a list of the various candidate and confirmed PMS δ-Scuti stars that have been examined in this thesis. Table 4.1 lists the stars in which spectral classifications from spectra (as opposed to estimates from photometry) are known, and sorts them in order of increasing minimum estimated distance to the Earth as a way of approximately ranking the stars for ease of observations, as stars that are closer to the Earth are generally easier to observe. Table 4.2 does the same thing, except for the stars in which spectral classifications are *not* known. Both of these tables list the star-formation region or open cluster with which the star is associated, and the minimum and maximum estimated distances to each star. B and $B-V$ photometry is also listed, recognizing that for the HAe stars that display UX Ori-type variability, this will represent only one point within the star's variability range — see the individual section on each star in Chapter 3 for more details. In Table 4.1, $v \sin i$ is listed for each star, if known (17 stars); none are known for any of the stars in Table 4.2. For each star, the number of observed frequencies are listed, along with the lowest, and highest pulsation frequencies observed in each star's pulsation spectrum. Finally, the frequency of maximum amplitude is listed, as well as the amplitude for that frequency. The instruments that took the information are also listed. The amplitudes might be in one of a number of units, in that all stars

Star	Alternate Name	SFR/cluster	HAe	Min D (pc)	Max D (pc)	Spectral Class	$v \sin i$ (km/s)	V (mag)	$B-V$ (mag)	N f	low f (μHz)	high f (μHz)	Max A f (μHz)	Max A	Instrument
(1)	(2)	(3)	(4)	(5)	(6)	(7)	(8)	(9)	(10)	(11)	(12)	(13)	(14)	(15)	(16)
1) RS Cha a	HD 75747 a	η Cha OC	no?	90 8	95	A8 IV	64±6	**6.07**	**0.21**	2	244 3	351 6	244 3	—	1m Mt John, NZ, (spec)
2) RS Cha b	HD 75747 b	η Cha OC	no?	90 8	95	A8 IV	70±6	**6.07**	**0.21**	3	148 3	284 3	148 3	—	1m Mt John NZ, (spec)
3) CQ Tau	HD 36910	Taurus MC	yes	94	142	F2 to F5	105±5	10 22	0 78	1	162 0	162 0	162 0	40 0	
4) EF Cha	HD 105234	ϵ Cha MG	no	98	109	A9 III/IV	—	7 48	0 26	2	218 9	336 9	218 9	3 9	SAAO 0 5m,South Africa
5) V1026 Sco	HD 142666	Sco R1	yes	100	160	A8 Ve	70±2, 72±2	8 67	0 34	12	66 8	324 4	254 6	2 6	MOST
6) EE Cha	HD 104036	ϵ Cha MG	no	104	113	A2, A7V	—	6 7	0 2	2	339 2	392 1	392 1	10 5	SAAO 0 5m,SA
7) DX Cha A	HD 104237 A	ϵ Cha MG	yes	110 1	119 6	A7 IV, A7 5 to A8 Ve	12±2	**6.59**	**0 22**	8	292 6	412 1	385 3	1 3	(spec)
8) V351 Ori	HD 38238	Orion B	yes	**135**	**221**	A6 III to A7 III	119	9 7	0 5	5	147 6	183 9	181 6	22 9	Multi-site
9) V1366 Ori	HD 34282	Orion	yes	145	280	A0 to A3	129±11	7 84	0 17	22	618 4	919 2	919 2	6 3	MOST
10) V856 Sco	HR 5999	Lupus 3 DC	yes	149	180	A7e III/IV, A8/A9	180±50 204	7 08	0 31	5(4)	32 9	76 5	32 9	3 1	MOST
11) V705 Per	IC 348 H254	IC 348 (Per OB2)	no	238	316	F0	—	10 56	0 99	4(1)	85 7	85 7	85 7	5 4	Two-site
12) IP Per	HD 278937	Per OB2	yes	250	350	A7 III	—	10 40	0 33	9	107 6	558 2	264 9	1 9	Multi-site
13) V1247 Ori	HD 290764	Orion OB1b	yes	270	640	A5 III, F0 V	—	9 81	0 35	8	119 4	237 0	119 4	11 2	MOST
14) VV Ser	HBC 282	Serpens Cloud	yes	300	400	B5 to A3	85, 142, 200, 229	11 92	0 93	1	31 1	118 5	31 1	7 8	Loiano 1 5m,Italy
15) V346 Ori	HD 287841	Orion OB1a	yes	**300**	**460**	A5 to A8	125±10	10 16	0 20	13	93 1	430 6	406 3	2 2	Multi-site
16) HD 37357	PDS 191	Orion A	yes	300	700	B8/9 to A1 Ve	—	8 85	0 13	—	—	—	—	—	MOST
17) PX Vul	HBC 293	Vul R2	yes	**400**	**450**	F0 to F3	78±11	11 54	0 83	2	57 9	150 5	—	—	Single-site
18) WW Vul	HD 344361	In Vulpecula	yes	509	659	A0 to A4	125, 150, 220±22	10 70	0 44	1	57 9	57 9	—	—	Single-site
19) HD 261711	NGC 2264 39	NGC 2264	no	676	1023	A2 V	—	11 32	0 13	2	671 4	711 5	711 5	5 0	MOST
20) NGC 2264 104	GSC 00750-01183	NGC 2264	no	676	1023	A5 IV, A6 V	—	11 36	0 26	3	377 3	407 5	407 5	9 4	MOST
21) HD 261387	GSC 00750-01597	NGC 2264	no	676	1023	A1 to A3 V	127, 140±10	11 34	0 12	4	249 8	790 7	401 6	3 7	MOST
22) V588 Mon	NGC 2264 2	NGC 2264	no	676	1023	A7 III to IV	130±20	9 68	0 27	8	59 5	127 1	59 5	8 7	MOST
23) V589 Mon	NGC 2264 20	NGC 2264	no	676	1023	F0 V to F3 V	60±10	10 27	0 43	12	66 7	127 2	75 1	14 0	MOST
24) HD 261230	GSC 00750-00863	NGC 2264	no	676	1023	A7 to A8, F2 V	95±5	9 48	0 23	7	113 3	243 3	226 8	2 8	MOST
25) V375 Lac	LkHα 233	LkHα 233 DC	yes	850	900	A5 to A8	—	13 82	0 88	2(1)	60 2	**114.6**	—	—	Single-site
26) NGC 2244 45	HD 258859	NGC 2244	no	1100	2100	A0, A1 V, A1 IV	—	10 42	0 34	1	97 8	97 8	97 8	11 5	MOST
27) NGC 2244 271	GSC 00154-00076	NGC 2244	no	1100	2100	A7 V	—	10 76	0 41	12(8)	114 7	253 2	242 6	2 3	MOST
28) NGC 2244 399	GSC 00154-00307	NGC 2244	no	1100	2100	A0 V, A7V	—	11 44	0 17	8(4)	44 5	83 7	83 7	6 6	MOST
29) NGC 2244 183	GSC 00154-01629	NGC 2244	no	1100	2100	A2 V, A8 III	—	11 41	0 44	3	110 1	132 2	110 1	1 8	MOST
30) V486 Sco	GSC 07380-00691	NGC 6383	no	1300	1700	A5 IIIe	—	12 76	0 66	5	96 0	225 0	166 4	12 5	CTIO 0 9m, Chile
31) GSC 07380-01173	NGC 6383 ZMR 152	NGC 6383	no	1300	1700	F1, F0Ve	—	12 31	0 58	1	29 5	29 5	29 5	30 0	CTIO 0 9m, Chile (B)
32) IC 4996 37		IC 4996	no	1500	2000	A5	—	15 3	0 8	1	388 5	388 5	388 5	7 6	Ser Nev Obs ,1 5m, US
33) IC 4996 40		IC 4996	no	1500	2000	A4	—	15 03	0 75	1	368 9	368 9	368 9	4 6	Ser Nev Obs 1 5m, US
34) PDS 2	TYC 8474-24-1	isolated in Phe	yes	unknown	unknown	F3 Ve to F6e	175	10 87	0 38	7(6)	159 4	280 6	—	—	0 6m REM, Chile

Table 4.1: Specifications of candidate or known PMS δ-Scutis with known spectral classes, sorted in order of increasing minimum distance to the star. Columns: (1) star name; (2) alternate name; (3) star-formation region or cluster associated with the star (OC = open cluster, MC = molecular cloud, MG = moving group); (4) Herbig Ae/Fe star or not; (5) and (6) minimum and maximum distances for stars (**Bold face** indicates a pecularity with the distance for the star, and that the section on that star should be consulted); (7) Spectral classes; (8) $v \sin i$ (km/s); (9) and (10) V, $B-V$ photometry (**Bold face** indicates a known binary system in which these numbers are the values for the unresolved components of the system); (11) Number of frequencies detected (Number used/reliable in analysis); (12) lowest frequency detected (μHz); (13) highest frequency detected (μHz); (14) frequency of maximum amplitude (μHz); (15) Amplitude for (14). Amplitudes are V-band or *MOST* amplitudes unless indicated in (16); (16) Instrument used (Spec. indicates a spectrograph was used and that the units for (15) are therefore km/s).

Star	Alternate Name	SFR/cluster	Min D (pc)	Max D (pc)	V (mag)	$B-V$ (mag)	N f	low f (μHz)	high f (μHz)	Max A f (μHz)	Max A	Instrument
(1)	(2)	(3)	(4)	(5)	(6)	(7)	(8)	(9)	(10)	(11)	(12)	(13)
1) GSC 07380-00975	NGC 6383 ZMR 198	NGC 6383	1300	1700	12 82	0 672	1	220 2	220 2	220 2	20 8	CTIO 0 9m, Chile
2) IC 4996 46		IC 4996	1500	2000	15 3	0 72	4(2)	42 8	75 2	69 4	5 4	Ser Nev Obs 1 5m, US (B/V)
3) NGC 6530 ZW 5		NGC 6530	1790	1930	13 592	0 435	2	539 3	618 3	539 3	1 4	CTIO 0 9m, Chile
4) NGC 6530 ZW 82		NGC 6530	1790	1930	13 969	0 61	3	287 4	446 0	446 0	2 4	CTIO 0 9m, Chile
5) NGC 6530 ZW 85		NGC 6530	1790	1930	13 072	0 648	8(4)	122 5	360 5	180 3	30 2	CTIO 0 9m, Chile
6) NGC 6530 ZW 263		NGC 6530	1790	1930	13 671	0 632	1	222 5	222 5	222 5	7 1	CTIO 0 9m, Chile
7) NGC 6530 ZW 278		NGC 6530	1790	1930	12 169	0 531	9	48 4	181 5	153 0	9 9	CTIO 0 9m, Chile
8) NGC 6530 ZW 281		NGC 6530	1790	1930	13 349	0 452	7	355 2	502 5	355 2	1 4	CTIO 0 9m, Chile
9) NGC 6530 ZW 288		NGC 6530	1790	1930	13 233	0 415	1?	208 3	208 3	208 3	0 8	CTIO 0 9m, Chile
10) NGC 6823 HOAG 157		NGC 6823	2000	2500	12 86	0 55	2	147 3	179 7	147 3	27 0	60cm Białkow Telescope, Poland (I_c)
11) NGC 6823 BL50		NGC 6823	2000	2500	14 48	0 93	2	114 4	161 1	161 1	18 0	60cm Białkow Telescope, Poland (I_c)

Table 4.2: Specifications of candidate or known PMS δ-Scutis without known spectral classes, sorted in order of increasing minimum distance to the star. Columns: (1) star name; (2) alternate name; (3) star-formation region or cluster associated with the star (OC = open cluster, MC = molecular cloud, MG = moving group); (4) and (5) minimum and maximum distances for stars, (6) V, $B-V$ photometry; (6) Number of frequencies detected (Number used/reliable in analysis); (8) lowest frequency detected (μHz); (9) highest frequency detected (μHz); (10) frequency of maximum amplitude (μHz); (11) Amplitude for (10). Amplitudes are V-band unless indicated in (13); (13) Instrument used (alternate filter).

have Johnson V magnitudes unless: 1) the star has been observed by *MOST*, in which case the units are millimagnitudes of the unique *MOST* broad-band optical filter; 2) the "Instruments" column lists in parenthesis the filter or spectrograph that was used (spectrograph units would be km/s, other filters would be in millimagnitudes of the corresponding filter). In Table 4.1 there are a total of 34 stars for which spectral classes are known, and in Table 4.2, for which only photometry is given, 11 stars are listed. This gives a total over the two tables of 45 stars.

These lists do *not* include the 27 stars listed in Section 3.4, the stars for which pulsation might have been identified in the past, but prior to this study, were not recognized as potential PMS δ-Scuti stars. Further observations are recommended before transferring any of these stars to the final list, although the candidacy for inclusion for some of these stars is much better than for others.

Due to lack of time, not included in this study are the unpublished results of four stars in NGC 6611 in which δ-Scuti pulsation has been identified by K. Zwintz. Her observations add 4 stars to the list of PMS δ-Scuti stars, for a grand total of $45 + 27 + 4 = 76$ candidate or confirmed stars on the list.

For the stars for which spectral classifications are available, Table 4.3 lists the derived T_{eff} and $\log(L/\mathrm{L}_\odot)$ for each star, with the numbering scheme as used in Table 4.1. Stars #28 (NGC 2244 399; Section 3.2.2.3) and #29 (NGC 2244 183; Section 3.2.2.4) have two entries, a) and b), one each for the two disparate spectral classifications available for each star (the relevant classifications appears below the name of the star). The rows labelled "c" and "h" for each star indicate the coolest and hottest T_{eff} respectively used in the analysis for an individual star, along with the minimum and maximum luminosities corresponding to those coolest and hottest temperatures. The various T_{eff} and $\log(L/\mathrm{L}_\odot)$ pairs then define the four vertices used to construct the error box in the HRD for an individual star. "yes" or "no" in the "min L" column indicate whether or not a minimum luminosity constraint was placed upon the star via the fundamental frequency test, and similar labelling is used in the "max L" column to indicate if maximum luminosity constraints were placed

upon the star by the acoustic-cut-off frequency test. "Min/Max agree" then indicates if the star's position in the HRD diagram from the T_{eff} and $\log(L/L_{\odot})$ columns are then in agreement with limitations on the luminosities from astroseismic analysis. If χ^2 analysis was performed on the frequency spectrum of a particular star, then the minimum χ^2 that was obtained is listed, and the "χ^2 agree" column indicates if that solution fell within the error box of the star, or not. A "—" indicates that the relevant value was not calculated for a particular star. "(1)" in the "χ^2 " column indicates that only one frequency was detected for that star, and so χ^2 analysis is not relevant in this case, however the "χ^2 agree" column still indicates whether that frequency still fell within the HRD error box, or not. Star #9 (V1366 Ori) has two χ^2 values quoted, the first for the "raw" frequency spectrum, the second for the averaged frequency spectrum (see Section 3.1.1.4). Star #21 (HD 261387) also has two entries, indicating case (A) and (B) as outlined in Section 3.2.1.4. Stars #8 (V351 Ori; Section 3.1.2.2) and #15 (V346 Ori; Section 3.1.2.3) both had conflicting distance determinations associated with the star, implying different luminosity ranges for the star, thus for these stars, "y/n" in both the "Min/max agree" and "χ^2 agree" columns indicate that for one of the HRD positions the asteroseismology position agreed with it, but for the other HRD position it did not. The data from Table 4.3 will be used to construct HRDs in Section 4.3.

	Star		T_{eff}	$\log(L_{min})$	$\log(L_{max})$	min L	max L	Min/max Agree	χ^2	χ^2 agree
1)	RS Cha a	c	3 879	1 06	1 24	no	yes	yes	—	—
		h	3 887	1 06	1 24					
2)	RS Cha b	c	3 855	1 04	1 22	yes	yes	yes	—	—
		h	3 863	1 04	1 22					
3)	CQ Tau	c	3 809	0 23	0 59	yes	no	no	—	—
		h	3 838	0 35	0 71					
4)	EF Cha	c	3 854	0 93	1 02	no	yes	yes	< 1	yes
		h	3 880	0 95	1 04					
5)	V1026 Sco	c	3 880	0 75	1 33	yes	yes	no	16	no
		h	3 895	0 75	1 33					
6)	EE Cha	c	3 880	1 30	1 37	no	yes	yes	0 02	yes
		h	3 914	1 41	1 48					
7)	DX Cha A	c	3 875	1 35	1 46	no	yes	yes	—	—
		h	3 895	1 35	1 46					
8)	V351 Ori	c	3 872	0 59	1 02	yes	no	y/n	2 67	y/n
		h	3 903	0 78	1 21					
9)	V1366 Ori	c	3 926	1 15	1 72	no	yes	yes	915	yes
		h	3 979	1 45	2 03				1 79	yes
10)	V856 Sco	c	3 860	1 47	1 63	yes	no	no	1 15	no
		h	3 895	1 64	1 80					
11)	V705 Per	c	3 846	1 30	1 55	yes	no	yes	—	—
		h	3 863	1 36	1 61					
12)	IP Per	c	3 872	0 57	0 97	yes	yes	no	1 2	no
		h	3 926	0 92	1 33					
13)	V1247 Ori	c	3 845	0 87	1 62	yes	no	yes	3 6	no
		h	3 919	1 15	1 90					
14)	VV Ser	c	3 903	1 30	2 30	yes	no	no	0 31	no
		h	4 000	1 30	2 30					
15)	V346 Ori	c	3 860	1 27	2 29	yes	yes	y/n	31 8	y/n
		h	3 919	1 48	2 50					
16)	HD 37357	c	3 953	1 56	2 29	—	—	—	—	—
		h	3 979	1 62	2 36					
17)	PX Vul	c	3 828	1 10	1 20	yes	no	no	—	—
		h	3 854	1 19	1 29					
18)	WW Vul	c	3 941	1 57	1 79	yes	no	no	—	—
		h	3 979	1 75	1 97					
19)	HD 261711	c	3 941	1 09	1 45	no	yes	yes	0 1	yes
		h	3 965	1 28	1 64					
20)	NGC 2264 104	c	3 895	0 94	1 30	no	yes	yes	0 38	no
		h	3 924	1 10	1 46					
21)	HD 261387	c	3 904	0 97	1 22	no	yes	yes	(A) 3 61	yes
		h	3 927	1 05	1 30				(B) 0 36	no
22)	V588 Mon	c	3 880	1 64	2 00	yes	no	yes	4 3	no
		h	3 895	1 75	2 11					
23)	V589 Mon	c	3 813	1 45	1 81	yes	no	yes	10 3	yes
		h	3 857	1 59	1 95					
24)	HD 261230	c	3 880	1 72	2 08	yes	no	yes	1 68	no
		h	3 895	1 85	2 21					
25)	V375 Lac	c	3 860	1 06	1 11	yes	no	no	(1)	no
		h	3 919	1 20	1 25					
26)	NGC 2244 45	c	3 953	2 02	2 58	yes	no	yes	(1)	yes
		h	4 004	2 56	3 12					
27)	NGC 2244 271	c	3 872	1 79	2 35	yes	yes	yes	2 77	yes
		h	3 895	2 00	2 56					
28a)	NGC 2244 399	c	3 966	1 60	2 16	yes	no	yes	0 67	yes
	(A0 V)	h	3 992	1 83	2 39					
28b)	NGC 2244 399	c	3 895	1 38	1 94	yes	no	yes	< 1	yes
	(A7 V)	h	3 911	1 52	2 08					
29a)	NGC 2244 183	c	3 941	1 84	2 40	yes	no	yes	0 52	yes
	(A2 V)	h	3 965	2 15	2 71					
29b)	NGC 2244 183	c	3 869	1 61	2 17	yes	no	yes	0 51	yes
	(A8 III)	h	3 895	1 87	2 43					
30)	V486 Sco	c	3 904	1 68	1 91	yes	no	yes	—	—
		h	3 927	1 77	2 00					
31)	GSC 07380-01173	c	3 837	1 57	1 80	yes	no	no	—	—
		h	3 863	1 63	1 86					
32)	IC 4996 37	c	3 904	0 97	1 22	no	yes	yes	—	—
		h	3 927	1 05	1 30					
33)	IC 4996 40	c	3 914	0 93	1 18	no	yes	yes	—	—
		h	3 927	1 04	1 29					
34)	PDS 2	c	3 831	0 80	2 01	yes	yes	yes	0 16	yes
		h	3 846	0 87	2 08					

Table 4.3: T_{eff} and $\log(L/L_{\odot})$ ranges for stars with spectral classifications, plus indications of whether asteroseimology imposes luminations upon each star. See text for further explanations.

4.2 Summary of pulsation spectra

The following series of figures shows the pulsation spectra of each of the stars for each of the confirmed or candidate PMS δ-Scuti stars in this study, except for several stars for which only one frequency was detected. Each spectrum is displayed to the same horizontal scale for comparison between stars. The vertical axis and associated amplitude units (mmag in a specific filter, or km/s in the case of spectroscopic observations) are specific to each star, and so comparison of the absolute values of the amplitudes between any two given stars may or may not be appropriate. The dotted line on the left part of the graph around 50 μHz in an approximate lower limit for p-mode frequencies in PMS δ-Scuti stars, although it is not a firm limit. Frequencies to the left of this line need to be treated with particular caution given that these frequencies may or may not be p-mode frequencies. Figures 4.1 through 4.4 display the stars for which spectral classifications have been determined, sorted by earliest plausible spectral classification for a given star (if there are multiple determinations). Figures 4.5 and 4.6 show the same information for stars in which spectral classifications are *not* known. These stars are listed in terms of increasing apparent $B-V$ value, recognizing that due to different levels of reddening associated with each star, that this is not a rigorous measure of the effective temperature of the star.

The most striking aspect of the collective set of spectra is the wide range of behaviour that has been observed. There are often no obvious generalities from one star to the next, even with stars of similar spectral class. One generality that does seem important is seen among the few stars for which very low frequencies have been reported (10 to 40 μHz, or 1 to 4 c/d): these frequencies always seem to be accompanied by frequencies within the low δ-Scuti range, but not with any frequencies in the higher ranges, say above 110 μHz (which is quite low compared to the total range available). These lowest frequencies are not normally associated with δ-Scuti pulsations, and their presence could be because of one of many phenomena, such as some signal of rotation (sunspots), or perhaps as a g-mode, or even the result of integer cycle/day aliasing misidentifications as a result of the spectral window of

the ground-based observations. However, if low-frequency signals were attributed to rotation or misidentifications instead of pulsation, one might expect them to appear in stars with *higher* frequencies as well, but they do not. In the few cases here these signals only appear in stars that are pulsating at the low end of the frequency spectrum (VV Ser, NGC 2244 399, V856 Sco), suggesting this is a low-end extension of the pulsation spectrum, and may be genuine detections of pulsation. Regardless, given the low numbers of stars involved, observations of more stars are needed before any conclusions can be made.

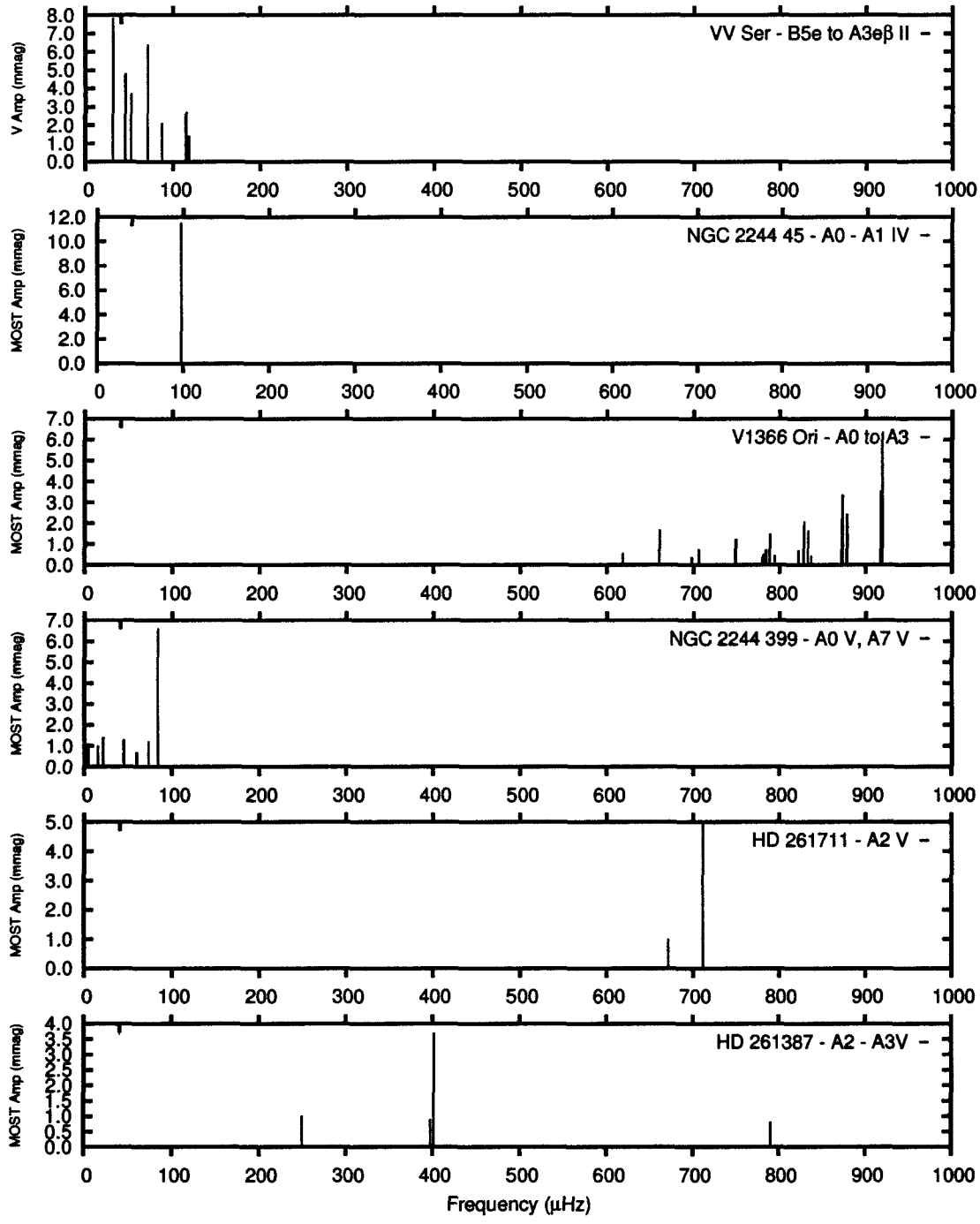

Figure 4.1: Part 1 of 4: Pulsation spectra of stars with spectral classifications, sorted by earliest plausible spectral class.

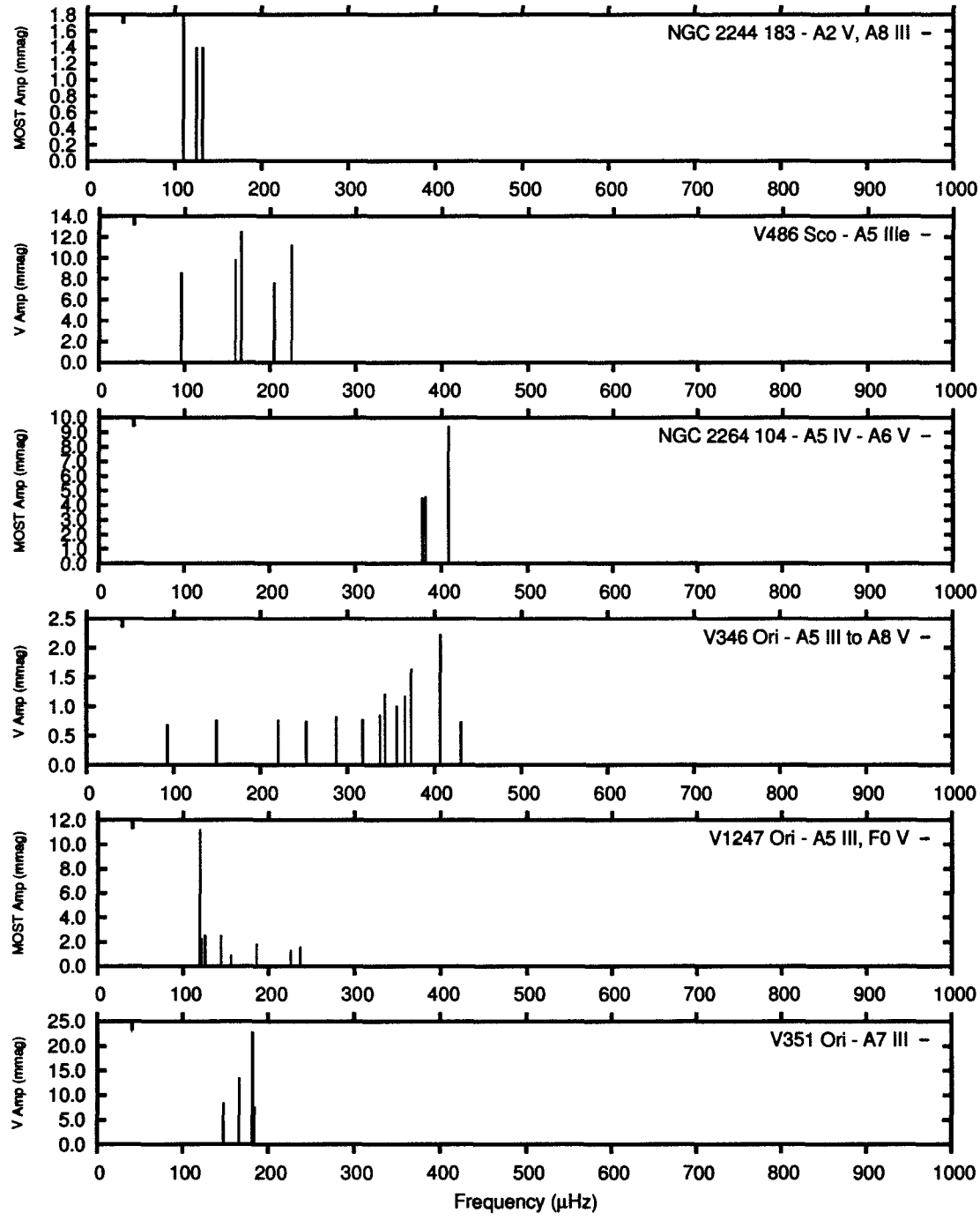

Figure 4.2: Part 2 of 4: Pulsation spectra of stars with spectral classifications, sorted by earliest plausible spectral class.

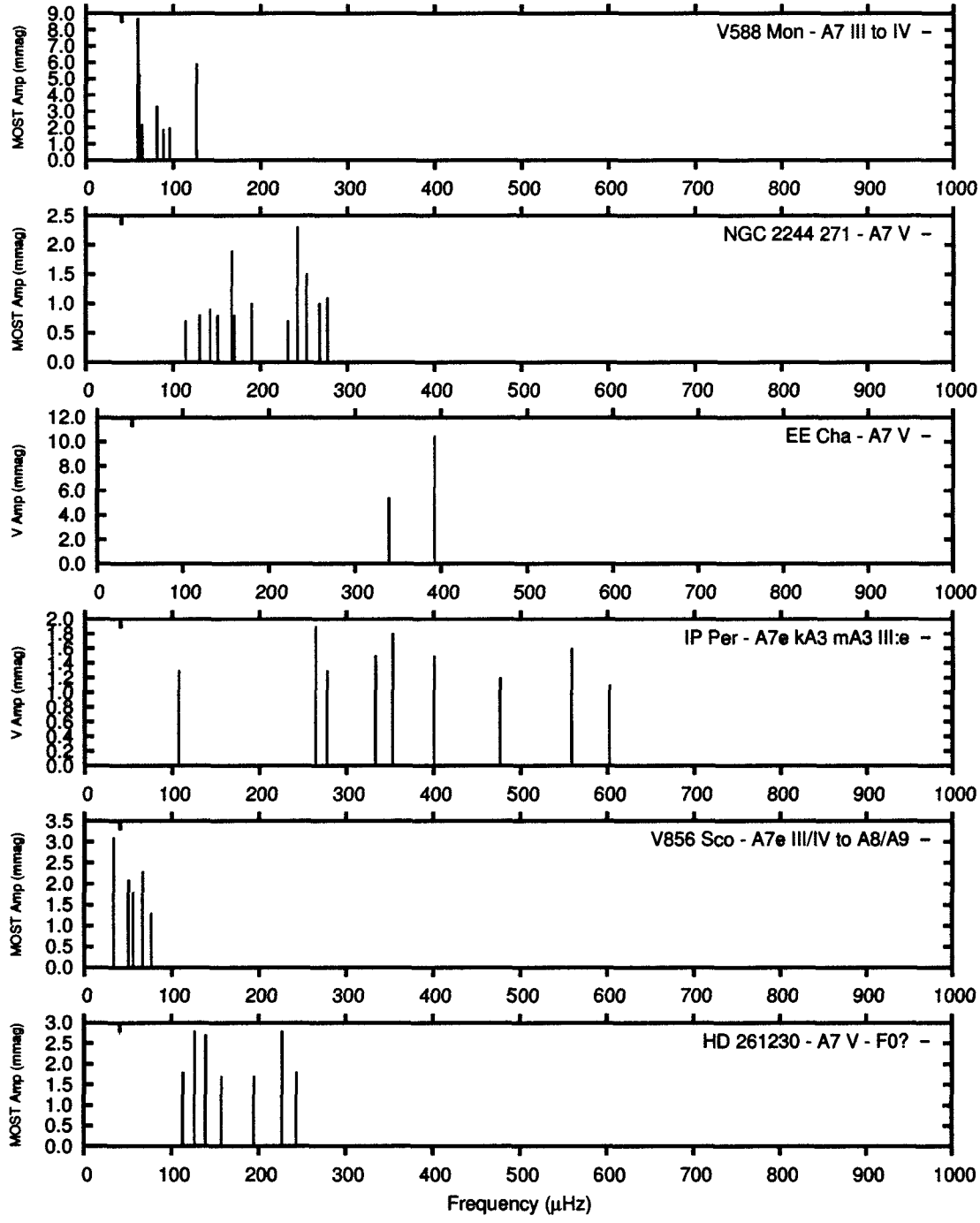

Figure 4.3: Part 3 of 4: Pulsation spectra of stars with spectral classifications, sorted by earliest plausible spectral class.

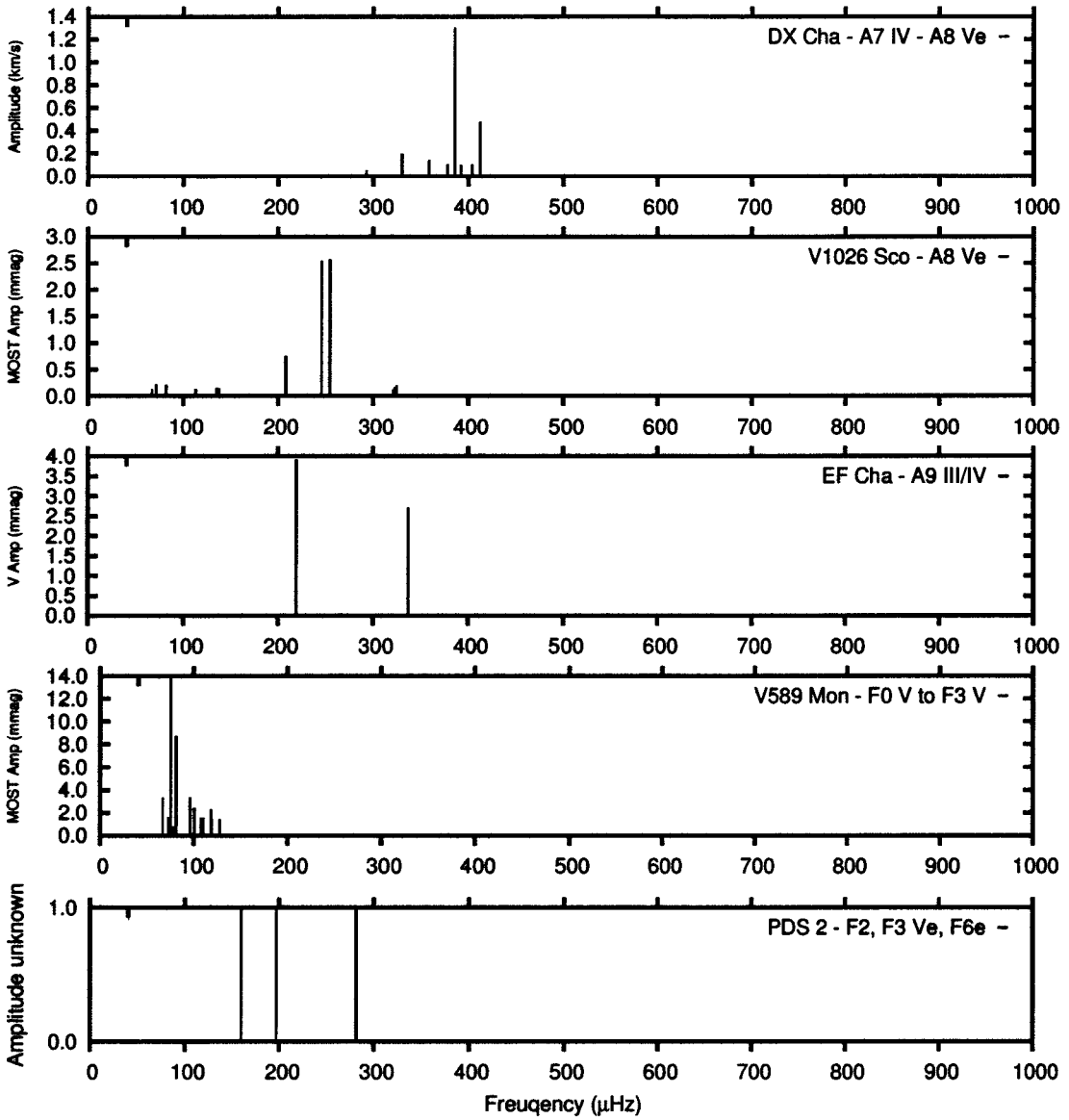

Figure 4.4: Part 4 of 4: Pulsation spectra of stars with spectral classifications, sorted by earliest plausible spectral class.

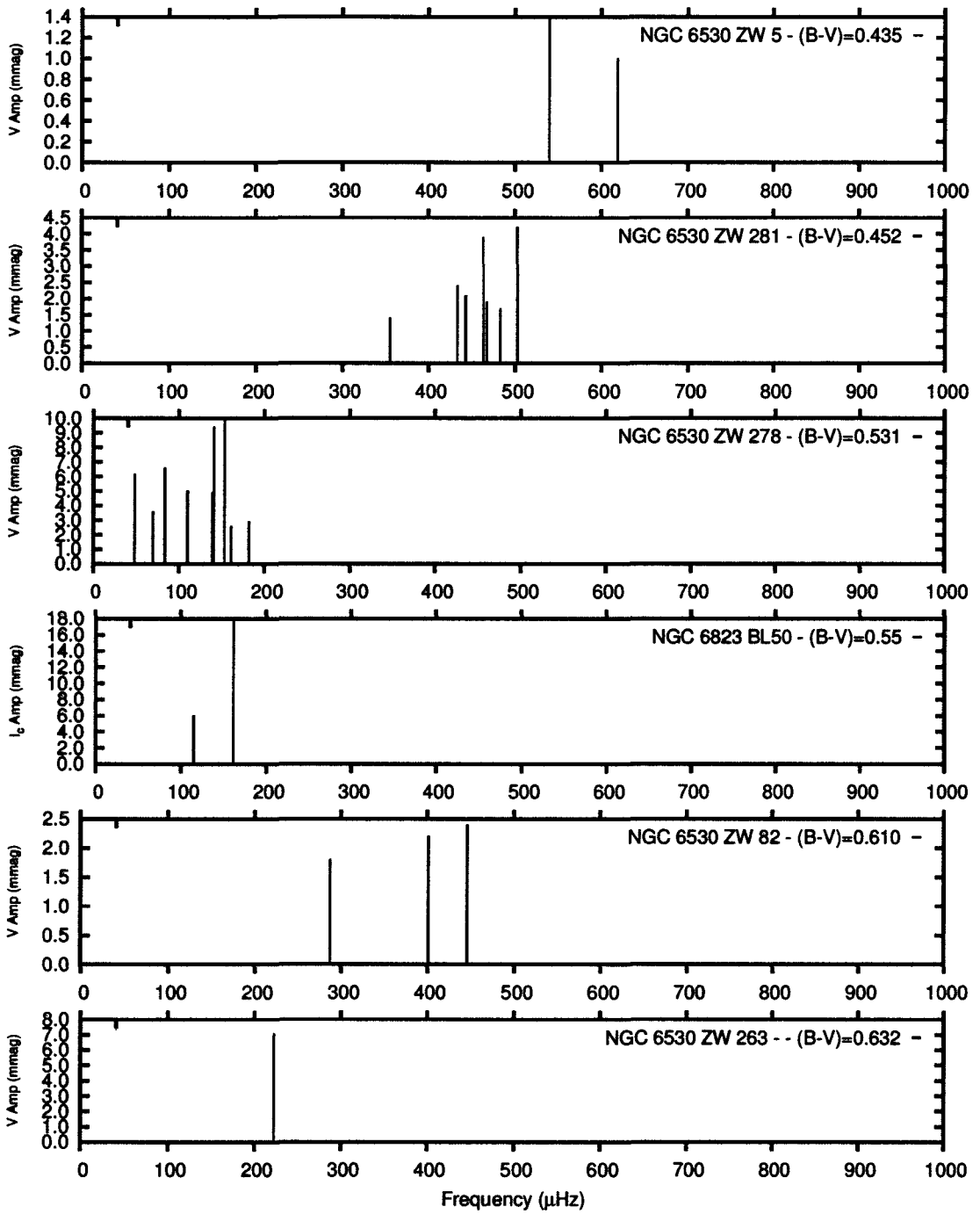

Figure 4.5: Part 1 of 2: Pulsation spectra of stars without spectral classifications, sorted by increasing $B - V$ colour.

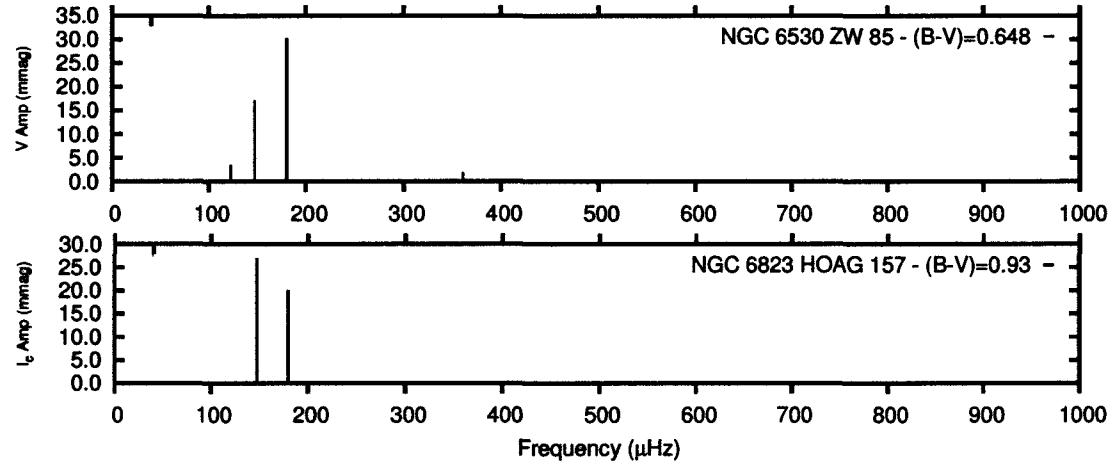

Figure 4.6: Part 2 of 2: Pulsation spectra of stars without spectral classifications, by sorted increasing $B - V$ colour.

4.2.1 Stars for which the lowest frequency observed imposes luminosity limitations on the star.

The approximate fundamental frequency of a star on the ZAMS in the region of the instability strip is approximately 225 μHz (Figure 2.8), with lines of constant fundamental frequency approximately (and conveniently) running parallel to the ZAMS. Therefore, any star with a lowest-detected frequency *below* about 225 μHz suggests that the star's luminosity must be above the ZAMS at some minimum locus of points approximately paralleling the ZAMS. This assumes that the signals are p-modes, not g-modes, nor some signal of some other phenomenon such as rotation or variability caused by circumstellar material. The stars for which the lowest-observed frequency imposes such limitations are shown in Table 4.4, listed in order of increasing lowest frequency, *i.e.* from the stars with the greatest to smallest limitations. To indicate just how significant the limitations are for a particular star, also listed are the luminosities of a stellar model with a fundamental frequency equivalent to the lowest observed pulsation frequency of a given star at both the cool and hot limits of the uncertainties assigned the stars in Table 4.3. "BL" indicates that the BL is the limiting luminosity, not one imposed by asteroseismology. The final two columns then

Star	SFR/cluster	Spectral Class	lowest f (μHz)	amp (mmag)	$\log(L_{fund}/L_\odot)$ cool	hot	$\Delta \log L$ cool	hot
1) GSC 07380-01173	NGC 6383	F1 F0Ve	29 5	30	2 13	2 26	1 55	1 51
2) VV Ser	Serpens Cloud	B5 to A3	31 1	7 8	2 40	BL	1 47	—
3) V856 Sco	Lupus 3 DC	A7e III/IV A8/A9	32 9	3 1	2 16	2 32	1 43	1 43
4) IC 4996 46	IC 4996		42 8	4 2	1 83	2 52	1 30	1 20
5) NGC 6530 ZW 278	NGC 6530		48 4	6 2	1 73	2 43	1 20	1 11
6) PX Vul	Vul R2	F0 to F3	57 9	—	1 59	1 71	1 07	1 01
7) WW Vul	In Vulpecula	A0 to A4	57 9	—	2 12	2 30	0 99	0 98
8) V588 Mon	NGC 2264	A7 III to IV	59 5	8 7	1 81	1 88	0 99	0 98
9) V375 Lac	LkHα 233 DC	A5 to A8	60 2	—	1 71	1 99	0 98	0 97
10) V589 Mon	NGC 2264	F0 V to F3 V	66 7	3 3	1 38	1 62	1 00	0 90
11) V1026 Sco	Sco R1	A8 Ve	66 8	0 1	1 72	1 79	0 90	0 90
12) NGC 2244 399 (hot)	NGC 2244	A0 V	72 8	1 2	2 07	2 19	0 81	0 80
(cool)		A7 V			1 73	1 81	0 83	0 83
13) V705 Per	IC 348 (Per OB2)	F0	85 7	5 4	1 38	1 46	0 73	0 71
14) V346 Ori	Orion OB1a	A5 to A8	93 1	0 7	1 38	1 66	0 65	0 65
15) V486 Sco	NGC 6383	A5 IIIe	96 0	7 6	1 57	1 68	0 63	0 62
16) NGC 2244 45	NGC 2244	A0 A1 V A1 IV	97 8	11 5	1 78	2 03	0 60	0 58
17) IP Per	Per OB2	A7 III	107 6	1 3	1 33	1 58	0 54	0 54
18) NGC 2244 183 (cool)	NGC 2244	A8 III	110 1	1 8	1 30	1 42	0 53	0 53
(hot)		A2 V			1 64	1 76	0 52	0 51
19) HD 261230	NGC 2264	A7 to A8 F2 V	113 3	1 8	1 33	1 40	0 51	0 50
20) NGC 6823 BL50	NGC 6823		114 4	6	1 07	1 80	0 54	0 47
21) NGC 2244 271	NGC 2244	A7 V	114 7	0 7	1 29	1 39	0 50	0 50
22) V1247 Ori	Orion OB1b	A5 III F0 V	119 4	11 2	1 13	1 48	0 48	0 46
23) NGC 6530 ZW 85	NGC 6530		122 5	3 5	1 01	1 75	0 48	0 43
24) NGC 6823 HOAG 157	NGC 6823		147 3	27	0 87	1 63	0 34	0 30
25) V351 Ori	Orion B	A6 III to A7 III	147 6	8 4	1 11	1 26	0 32	0 32
26) RS Cha b	η Cha open cluster	A8 IV	148 3	—	1 02	1 06	0 32	0 32
27) PDS 2	isolated in Phoenix	F3 Ve to F6e	159 4	—	0 82	0 93	0 28	0 28
28) CQ Tau	Taurus molecular cloud	F2 to F5	162 0	40	0 63	0 86	0 29	0 27
29) NGC 6530 ZW 288	NGC 6530		208 3	0 8	0 65	1 40	0 12	0 08
30) EF Cha	ϵ Cha Moving Group	A9 III/IV	218 9	3 9	0 77	0 90	0 07	0 07
31) GSC 07380-00975	NGC 6383		220 2	20 8	0 60	1 37	0 08	0 04
32) NGC 6530 ZW 263	NGC 6530		222 5	7 1	0 60	1 36	0 07	0 04

Table 4.4: PMS δ-Scuti stars for which the lowest observed pulsation frequency imposes limitations on the minimum luminosity the star can have $\log(L_{fund}/L_\odot)$ indicates the luminosity of the model that has a fundamental frequency corresponding to the lowest f observed for the star at both the cool and hot edges of the temperature range for a given star $\Delta \log L$ indicates the difference in $\log L$ between the ZAMS at the cool and hot edges of the HRD position and the model's luminosity

give $\log(L_{fund}/L_\odot) - \log(L_{ZAMS}/L_\odot) = \log(L_{fund}/L_{ZAMS}) = \Delta \log L$, indicating in $\log L$ space how far above the ZAMS the star must be in order to support the lowest pulsation frequency. For stars in which no spectral classification is known the "cool" and "hot" limits were given by the temperature range for which PMS pulsators seem to be observed as a whole, T_{eff} from 3.83 to 3.98 In total there are 32 such stars for which limitations are found, some with only minor limitations, falling just above the ZAMS, to a few stars in which the stars must be close to the birthline, if the

limiting frequencies are p-modes. Regardless, assuming these stars are PMS δ-Scuti stars, these are limitations that support the youth of the stars.

4.2.2 Stars for which the highest observed frequency imposes luminosity limitations on the star.

The acoustic cut-off frequency for stars on the birthline is approximately 250 μHz. Stars of greater luminosity would have lower acoustic cut-off frequencies, but would be above the birthline, and if PMS stars, not likely to be seen, as they are likely to be still enshrouded within their protostellar clouds. Therefore, stars with frequencies greater than approximately 250 μHz (assuming the frequency is a p-mode) must have luminosities placing them below the birthline, imposing maximum luminosities upon the star. Table 4.5 lists the stars in this study for which this is the case, in order of decreasing maximum frequency detected, *i.e.* approximately in the order from the stars with the greatest to smallest limitations. Like the previous table, also listed are the severity of the constraints in $\log L$ space, this time calculated by

Star	SFR/cluster	Spectral Class	highest f (μHz)	amp (mmag)	$\log(L_{ACF}/L_\odot)$ cool	hot	$\Delta \log L$ cool	hot
1) V1366 Ori	Orion	A0 to A3	919 2	6 3	1 78	1 93	0 73	0 73
2) HD 261387	NGC 2264	A1 to A3 V	790 7	3 7	1 66	1 74	0 90	0 89
3) HD 261711	NGC 2264	A2 V	711 5	5 0	1 73	1 80	0 83	0 82
4) NGC 6530 ZW 5	NGC 6530		618 3	1 0	1 48	1 93	0 55	0 73
5) IP Per	Per OB2	A7 III	558 2	1 9	1 68	1 85	0 61	0 66
6) NGC 6530 ZW 281	NGC 6530		502 5	4 2	1 62	2 07	0 40	0 60
7) NGC 6530 ZW 82	NGC 6530		446 0	2 4	1 71	2 15	0 32	0 52
8) V346 Ori	Orion OB1a	A5 to A8	430 6	2 2	1 82	2 01	0 40	0 48
9) DX Cha A	ϵ Cha moving group	A7 IV, A7 5 to A8 Ve	412 1	1 3	1 90	1 96	0 40	0 43
10) NGC 2264 104	NGC 2264	A5 IV, A6 V	407 5	9 4	1 97	2 06	0 43	0 45
11) EE Cha	ϵ Cha moving group	A2, A7V	392 1	10 5	1 95	2 05	0 38	0 42
12) IC 4996 37	IC 4996	A5	388 5	7 6	2 03	2 10	0 40	0 42
13) IC 4996 40	IC 4996	A4	368 9	4 6	2 10	2 14	0 38	0 38
14) NGC 6530 ZW 85	NGC 6530		360 5	1 8	1 85	2 29	0 17	0 38
15) RS Cha a	η Cha open cluster	A8 IV	351 6	—	2 02	2 04	0 30	0 32
16) EF Cha	ϵ Cha moving group	A9 III/IV	336 9	3 9	1 97	2 05	0 21	0 27
17) V1026 Sco	Sco R1	A8 Ve	324 4	2 6	2 08	2 12	0 25	0 27
18) RS Cha b	η Cha open cluster	A8 IV	284 3	—	2 09	2 12	0 09	0 12
19) PDS 2	isolated in Phoenix	F3 Ve to F6e	280 6	—	2 03	2 08	0 00	0 06
20) NGC 2244 271	NGC 2244	A7 V	253 2	2 3	2 22	2 29	0 06	0 10

Table 4.5: PMS δ-Scuti stars for which the highest observed pulsation frequency imposes limitations on the maximum luminosity the star can have.

determining the luminosity of the birthline at a particular temperature, and comparing that to the luminosity of a stellar model with an acoustic cut-off frequency of the highest observed pulsation frequency of a given star, both at the maximum (hot) and minimum (cool) deduced temperatures for the star. The luminosities of the models with the given acoustic cut-off frequencies are also listed. There are 20 such stars in the list.

4.2.3 Stars for which frequencies impose both minimum *and* maximum luminosity limitations on the star.

Examining the previous two tables yields a total of 7 stars in which the frequency spectra impose limitations on both the minimum and maximum luminosity of the stars; these stars are listed in Table 4.6 in order of increasing lowest frequency detected. Interestingly, none of these stars appear hotter than A5 spectral class, and it will be interesting to find out whether future discoveries also follow this trend. Regardless, should all of the frequencies within these stars prove to be p-mode frequencies, then all of these stars have useful limitations put upon them with respect to their position in the HRD independent of other observations, and so therefore they will provide useful calibrations for stellar evolution models.

Note that there is only a narrow band of frequencies between about 225 and 250 μHz for which *no* limitations at all are placed upon stars. If even a single frequency outside this narrow range should appear in the pulsation spectrum of a star, then a

Star	Spectral Class	lowest freq (μHz)	$\Delta \log L$ cool	$\Delta \log L$ hot	highest f (μHz)	$\Delta \log L$ cool	$\Delta \log L$ hot
1) V1026 Sco	A8 Ve	66.8	0.90	0.90	324.4	0.25	0.27
2) V346 Ori	A5 to A8	93.1	0.65	0.65	430.6	0.40	0.48
3) IP Per	A7 III	107.6	0.54	0.54	558.2	0.61	0.66
4) NGC 2244 271	A7 V	114.7	0.50	0.50	253.2	0.06	0.10
5) NGC 6530 ZW 85	—	122.5	0.48	0.43	360.5	0.17	0.38
6) RS Cha b	A8 IV	148.3	0.32	0.32	284.3	0.09	0.12
7) PDS 2	F3 Ve to F6e	159.4	0.28	0.28	280.6	0.00	0.06

Table 4.6: PMS δ-Scuti stars for which the highest *and* lowest observed pulsation frequency both impose limitations on the luminosity the star can have.

limitation, however minor, can be placed upon the star. This implies that for the seven stars in Table 4.6 that their pulsation spectra must straddle this region, and that for stars upon which no limitations were placed, pulsation spectra must be contained within this narrow frequency range.

4.2.4 Stars out of position in the HRD according to asteroseismology.

Table 4.7 lists the stars for which comparisons of the star's HRD position from spectroscopy and broad-band photometry do not match the luminosity constraints put on the stars, as outlined above. There are 10 such stars. Note that for some of these stars if one of the limiting pulsation frequencies were eliminated, then perhaps the positions would agree, however such considerations are best left to the analysis on a particular star in Chapter 3.

All of the stars that are out of position in the HRD are *under-luminous*, perhaps suggesting systematic underestimates in the reddening and extinction corrections for these stars. Except for GSC 07390-01173, all of the stars are Herbig Ae stars and are particularly prone to this sort of underestimate because of the circumstellar material associated with this class of star, so this is perhaps not surprising, but does emphasize the need to get a better handle on the intrinsic parameters HAe stars. It should be emphasized, though that a number of these stars (WW Vul, V375 Lac, PX Vul) only have tentative detections of pulsation, and these detections could be in error, in which case it might be the asteroseismology that is in error. The same may be said for VV Ser with the possibility that g-modes have been identified in the pulsation spectrum of the star, which would then cause the fundamental frequency test to be in error, with the luminosity constraints therefore not as severe as in Table 4.7.

The stars of Table 4.7 are listed in order of decreasing disagreement between the stars' asteroseismic and spectroscopic HRD positions. The column $\Delta \log L$ lists how under-luminous the star is at the hot and cool boundary of the HRD error box of the star, calculated by comparing the maximum luminosity of the star to the minimum luminosities expected from the fundamental frequency tests on the individual stars

at the relevant temperatures. Some of the discrepancies are fairly minor, while others are off by more than $\Delta \log L > 0.5$. Note the the luminosity of VV Ser is limited at the hot end of it's range by the birthline (BL), and not the asteroseismology. Also, the discrepancy for V351 Ori is for the Hipparcos distance only, not for the distance derived from the distance to the Orion B SFR. This list of stars turns out to be quite useful in the following section in which the collective HRDs for PMS δ-Scuti stars are constructed.

Star	SFR/cluster	$\Delta \log L$	
		cool	hot
1) V375 Lac	LkHα 233 DC	0.60	0.74
2) V856 Sco	Lupus 3 DC	0.53	0.52
3) V1026 Sco	Sco R1	0.39	0.46
4) PX Vul	Vul R2	0.38	0.42
5) IP Per	Per OB2	0.36	0.25
6) GSC 07380-01173	NGC 6383	0.33	0.40
7) WW Vul	In Vulpecula	0.33	0.32
8) VV Ser	Serpens Cloud	0.10	0.42 (BL)
9) V351 Ori (Hip)	Orion B	0.09	0.05
10) CQ Tau	Taurus molecular cloud	0.04	0.16

Table 4.7: Stars determined to be out of position in the HRD according to asteroseismology. All stars are dimmer than asteroseismology would suggest.

4.3 HR diagrams

I will now present a series of HRDs for the stars for which spectral classes are known (*i.e.* from Table 4.1). The top panel of Figure 4.7 shows an HRD, colour coded according to the largest pulsation frequencies detected for each star. A couple of general characteristics can be seen:

1. The stars with the highest maximum frequencies all reside in the lower part of the HRD on the left-hand (hot) side, suggesting that hot temperatures are needed to drive these frequencies. This is consistent with the following scenario: As stars get hotter within the δ-Scuti temperature range, the ionization region

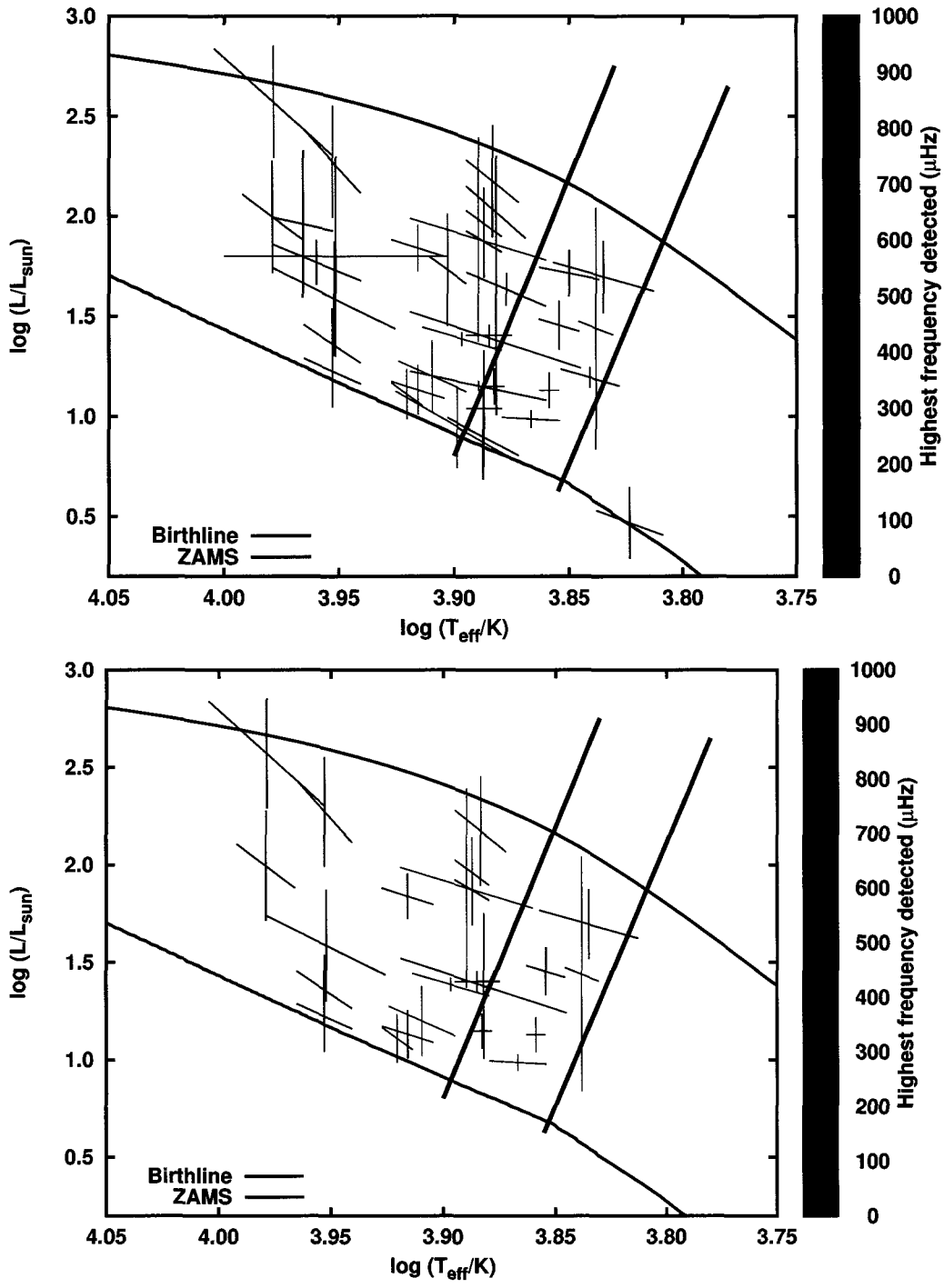

Figure 4.7: HRD of PMS pulsators for which spectral classes are available. The colour bar gives the maximum frequency detected for each stars. Black indicates HD 37357 for which pulsations have been reported, but the pulsation frequencies are not yet available. Top: All stars. Bottom: Does not include stars for which the asteroseismic and spectral class/broad-band positions in the HRD disagree.

that is thought to drive the pulsations moves to positions higher in the star's envelope into regions in which higher frequencies tend to propagate. These high frequencies get triggered, but due to the luminosity constraints imposed by the acoustic cut-off frequencies of these stars, they can only be driven in the lower part of the HRD. In other words, this is the only part of the HRD in which these frequencies can be driven at a high enough amplitude for detection with current instrumentation.

2. Mid-range maximum frequencies (green in the colour palette) all seem to fall in the middle of the collective temperature range reported for these stars.

3. Low frequencies (blue range) are generally in the upper half of the allowable luminosity range, an unsurprising result, as even though these are maximum frequencies, these frequencies must still be above the fundamental frequency of the star, implying higher luminosities. The stars with low frequencies that fall near the ZAMS are probably stars with ill-determined positions in the HRD from spectroscopy and broad-band photometry.

4. Overall, the red edge of the theoretical instability strip in Figure 4.8 matches the observations quite well, whereas a large number of stars are hotter than the instability strip. It is important to note that the instability strip is from Marconi & Palla (1998), which calculated the first three radial pulsation modes only, and that most of the stars that are hotter than the instability strip appear to be pulsating in higher-order modes than the range for which the strip is applicable. For the reasons outlined in item 1, higher-order modes are associated with higher temperatures, and so finding a number of hotter stars pulsating in higher-order modes is not unexpected.

Removing the stars from the HRD diagram for which the asteroseismic and spectral class/broad-band photometry HRD positions do *not* agree (Table 4.7) might improve clarity. Such a diagram is shown in the bottom panel of Figure 4.7, and the trends are clearer, with all remaining stars in agreement with the trends within

the error bars of the observations. It suggests a topology to the frequencies within the instability strip. Interestingly, the three stars in the upper left-hand side of the graph, with low frequencies, but high luminosity and temperature, that also seem to be somewhat separate from other stars within the HRD are from the *same cluster*, NGC 2244. If these HRD positions hold up to further scrutiny, then the common origins for these three stars may be responsible for all three stars inhabiting a similar spot in the HRD, and having similar pulsation frequencies. These stars need to be more closely studied, with particular care taken to determining the fundamental properties of the stars so that placement within the HRD is more certain.

It is important to note the lack of stars above $\log(T_{eff}/\mathrm{K})= 4.00$, and below $\log(T_{eff}/\mathrm{K})= 3.80$. This may be the range of the instability strip, although there may be a partial selection bias here, in that some targeted searches for PMS δ-Scuti stars only looked at A-range spectral types, perhaps missing variable stars at the boundaries, and just beyond. There is growing evidence that on the hot side of the instability strip that δ-Scutis might overlap with slowly-pulsating B stars (see Section 3.1.3.3 on VV Ser, which could be one of these stars), and they definitely overlap on the cool side with γ-Doradus pulsators, with numerous hybrids between the two now being detected (*e.g.* BD+18 4914, detected via *MOST* observations by Rowe et al. 2006a).

The top panel of Figure 4.8 shows an HRD in which stars are colour coded according to each star's minimum pulsation frequency detected. Once again, the stars with higher frequencies are confined to the low-luminosity and hot part of the HRD. Stars with lower frequencies are mainly found in the upper part of the diagram, in keeping with the need for the star to have a fundamental frequency lower than the lowest frequency detected, provided the frequency is a p-mode. Stars with low frequencies and low luminosities quite likely have ill-determined positioned in the HRD. The bottom of Figure 4.8 shows the same plot but without the stars for with

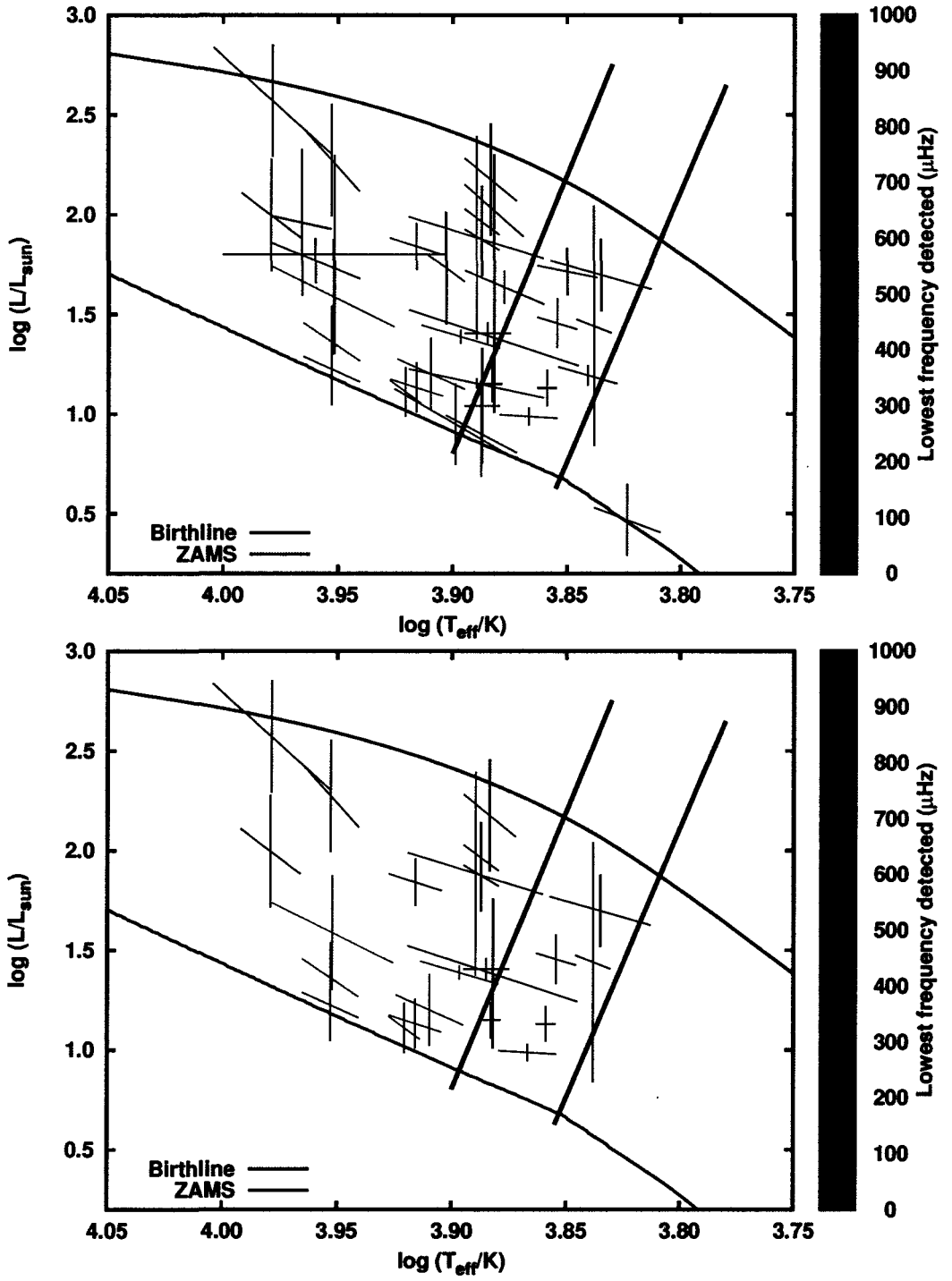

Figure 4.8: HRD of PMS pulsators for which spectral classes are available. Colour bar gives minimum frequency detected for each star. Top: all stars. Bottom: does not include stars for which the asterseismic and spectral class/broad-band positions in the HRD disagree.

the asteroseismology and HRD position do not agree. With this modification, the overall trends become much clearer.

The top panel of Figure 4.9 shows a final HRD, in which stars are colour coded in term of frequency of maximum amplitude, *i.e.* the part of the pulsation spectrum in which the most power seems to be residing. This is perhaps a result less dependant upon the sensitivity of observations than for the previous two figures, as generally observations of lower sensitivity or time resolution will still pick out the region of the spectrum with the most power in it, as these would be the frequencies that are most easily detected; the exact values might not be as precise, but a high-frequency pulsator is unlikely to be labelled a low-frequency pulsator. The results are fairly similar to Figure 4.7, in that the high frequencies (for the most part) are in the lower-left of the HRD, with the mid-range values clustered around $\log(T_{eff}/\mathrm{K}) = 3.90$. Except for a few points, low frequencies are at high luminosity. Once again, the bottom of Figure 4.9 eliminates the stars for which asteroseismic and spectroscopic/broad-band phometry HRD positions are not in agreement. Once again the aforementioned trends are more obvious.

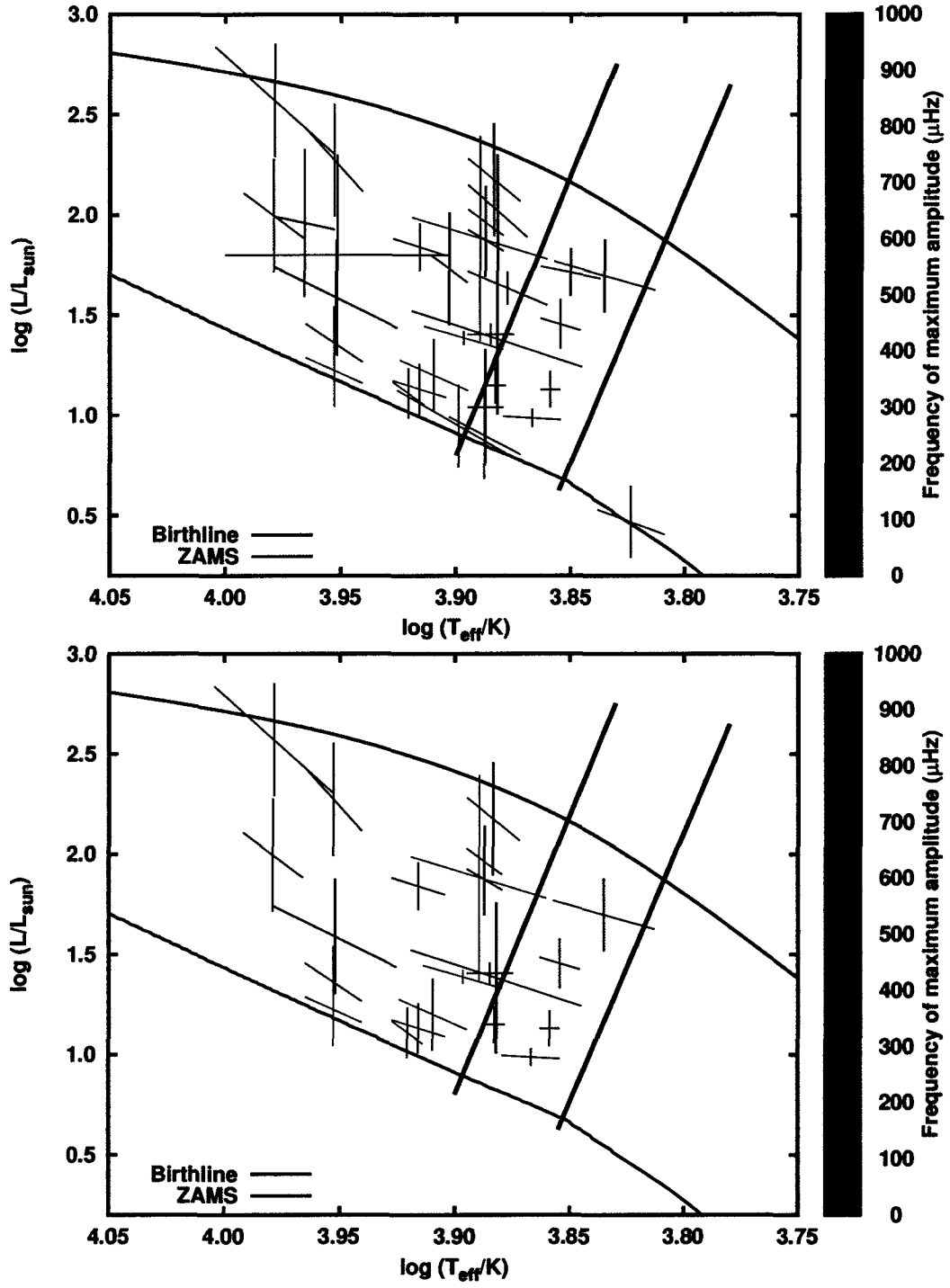

Figure 4.9: HRD of PMS pulsators for which spectral classes are available, with colour coding according to the frequency of maximum amplitude detected withing the pulsation spectrum of an individual star. Top panel: all stars. Bottom panel: does not include stars for which the asteroseismic and spectral class/broad-band positions in the HRD disagree.

4.4 Various relationships

4.4.1 Highest pulsation amplitude versus corresponding pulsation frequency.

Figure 4.10 plots the highest amplitude of pulsation among the frequencies of a given star versus the corresponding pulsation frequency itself. Although far from conclusive, there is a suggestion that the highest frequencies do not have the larger amplitudes that some of the stars pulsating at lower frequencies have. There does not seem to be a difference in behaviour between cluster (+) and field (x) stars. The amplitudes are measured in a mix of photometric systems, so detailed comparisons between individual stars should not be made, instead it is the overall trends that should be noted.

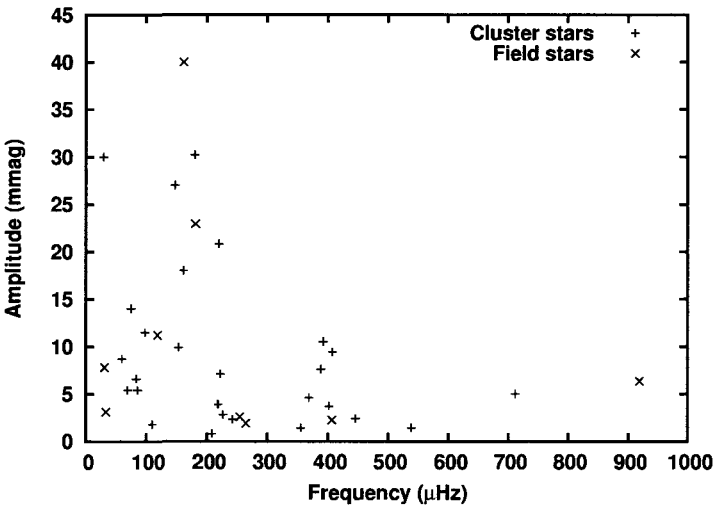

Figure 4.10: Highest amplitude of pulsation versus frequency for individual stars for both field (+) and cluster (x) stars

4.4.2 $v \sin i$ versus pulsation amplitude

As previously mentioned in Section 1.1, in evolved δ-Scutis, pulsation amplitude appears to be tied to rotational velocity. High-amplitude δ-Scutis (HADS, pulsation amplitudes greater than about 100 mmags, and up to 800 mmags) have been observed to only occur on stars with $v \sin i < 25$ km/s (*e.g.* Breger 2007). There are stars with low amplitudes and low $v \sin i$ values, however without further information on the inclination angle, i, of the star, it is impossible to determine whether these low-amplitude, low $v \sin i$ stars are truly rotating slowly or if they are just being viewed pole on. Statistically the latter would be expected for at least some of the stars. Regardless, PMS stars generally have $v \sin i$ values much larger those of the HADS, and so perhaps HADS should not be expected among PMS δ-Scuti stars. So far there have been no observations to contradict this picture. Unfortunately, there only twelve stars in the study for which both $v \sin i$ values and amplitude data for the maximum-amplitude frequency are also available. Figure 4.11 show the result of such a plot. There are no HADS among the stars, including the stars for which $v \sin i$ has

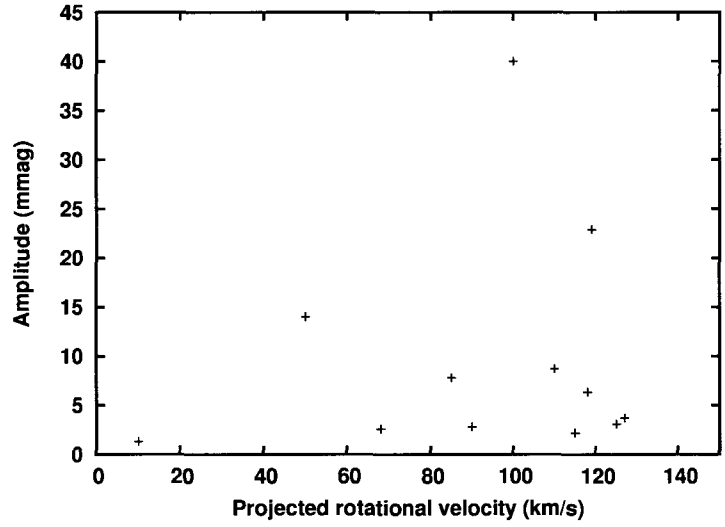

Figure 4.11: Highest amplitude of pulsation versus $v \sin i$ for individual stars. If multiple $v \sin i$ determinations exist for an individual star, the the lowest value was chosen for the figure. The photometric systems are mixed.

yet to be measured. Like the last graph (Figure 4.10), the amplitudes are of mixed photometric system, so caution is recommended when comparing two different stars.

4.4.3 Frequency versus effective temperature.

Figure 4.12 reinvisions some of the results shown in the HRDs of Section 4.3, specifically the relationship of frequency of highest-amplitude of pulsation versus temperature. Except for three of the stars of NGC 2244 that appear in the lower left-hand corner of Figure 4.12, all of the stars with known spectral class follow a trend of high temperature and high pulsation frequency to low temperature and low pulsation frequency. As better physical parameters for stars are obtained, and more stars are discovered, it will be interesting to see if this trend will be reinforced or weakened.

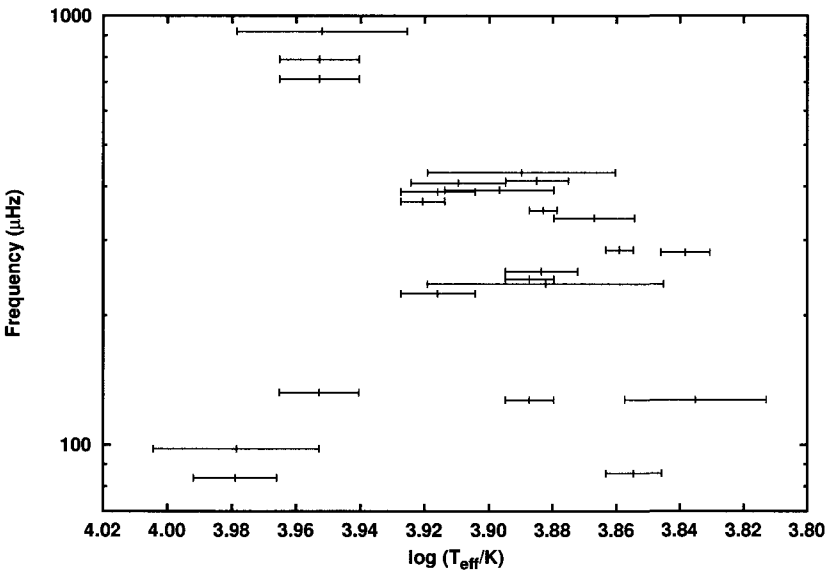

Figure 4.12: Frequency of highest pulsation amplitude versus T_{eff} for stars with spectral classifications, and for which the asteroseimic and spectroscopic positions in the HRD agree with one another.

4.4.4 Frequency vs luminosity above ZAMS

Since lines of constant pulsation frequency run approximately parallel to the ZAMS, calculating a star's position above the ZAMS, and comparing that to pulsation frequency might be useful. Figure 4.13 shows maximum-amplitude pulsation frequency verses $\log(L/\mathrm{L}_\odot) - \log(L_{ZAMS}/\mathrm{L}_\odot) = \log(L/L_{ZAMS})$. The range of values are determined by the minimum and maximum values at the cool and hot edges of the HRD error box respectively for a particular star, and comparing those values to the luminosity of the ZAMS at a correct temperature. Once again, high frequencies seemed to be restricted to low luminosities relative to the ZAMS, with a slight trend towards lower frequencies with increasing luminosity, but given the large uncertainties associated with some stars, and the limited number of stars, it is difficult to see any firm trends in this data.

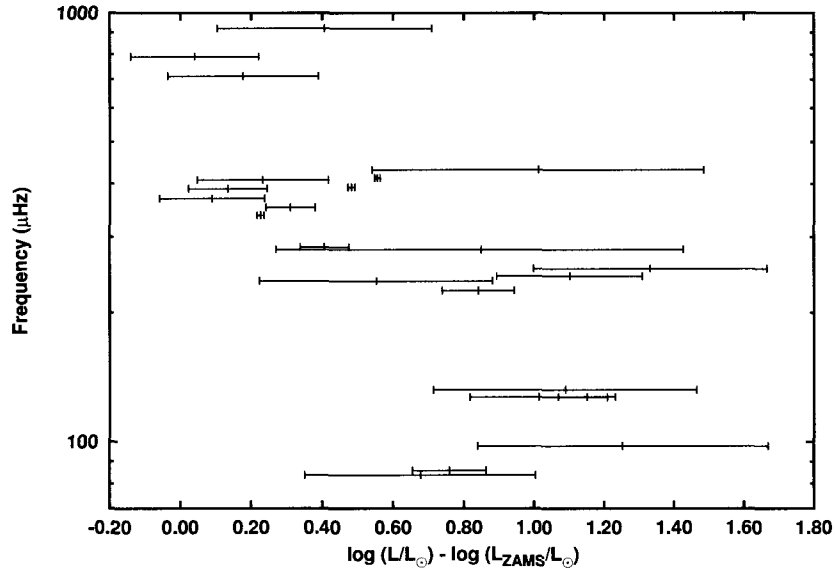

Figure 4.13: Highest-amplitude pulsation frequency versus luminosity above ZAMS for stars with spectral classifications, and for which the asteroseimic and spectroscopic positions in the HRD agree with one another.

4.4.5 Modified HRD

Figure 4.14 is a modified HRD with luminosity above the ZAMS on the y-axis (as opposed to luminosity of the star, itself), with each star colour coded according to its highest-amplitude pulsation frequency. On any individual stellar PMS evolutionary track, proximity to the ZAMS implies an older star compared to a more luminous star, but also implies a more slowly-evolving star, as the final approach to the ZAMS progresses at a slower rate that the more-luminous stages of PMS evolution. The fastest-evolving stars will be the most-luminous stars of Figure 4.14, with the implication that pulsation frequencies may change on time scales short enough to be readily observable, perhaps on the scale of a decade, or two. Future observations should target the highest-luminosity stars in Figure 4.14 for period changes so that insight may be gained on the accuracy of stellar evolution rates predicted by stellar models.

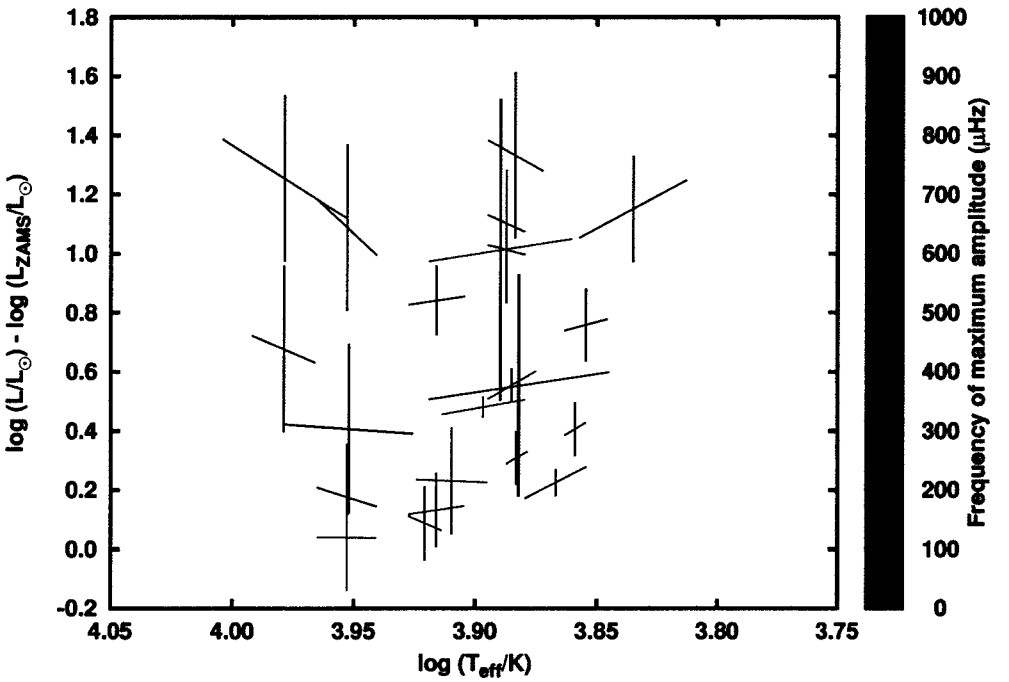

Figure 4.14: Highest-amplitude pulsation frequency versus luminosity above ZAMS for stars with spectral classifications, and for which the asteroseimic and spectroscopic positions in the HRD agree with one another.

Chapter 5

Discussion and conclusions

In this thesis asteroseismic analyses of as many PMS δ-Scuti stars as possible (several tens of stars) were performed, to varying degrees of sophistication, depending upon the circumstances surrounding any particular star. The initial analysis of each star involved matching observed stellar-pulsation spectra to modelled pulsation spectra from PMS evolutionary-model grids. Some of these analyses met with success, some not. In the process, several tests were used and/or developed that allowed information to be extracted from pulsation spectra when χ^2 tests were otherwise failing to find good matches between models and observation. One of these tests, the test for approximate minimum average splitting of a multiplet, has most likely pointed to the reason why asteroseismic analyses of richer pulsation spectra (*i.e.* stars in which more than a few pulsation frequencies have been detected), using χ^2 tests with our current model grids, don't work very well: the models are inadequate as they do not include the effects of stellar rotation on the pulsation spectrum of a star. Generally, the observational echelle diagrams of PMS δ-Scuti stars with rich pulsation spectra do not reveal any obvious patterns, such as the large or small spacings of the star, that should otherwise become obvious when a slowly-rotating star is pulsating at frequencies in the asymptotic regime. If such patterns *were* detected, but fits to models still failed, then this might indicate that certain types of physics that were left out in these model calculations for simplicity (*e.g.* non-adiabatic effects, convective overshooting, different composition or accretion history) probably need to be added to the models to obtain good fits, or even that the star should be compared to evolved δ-Scuti models instead. These effects would generally change the spacings in the pulsation spectrum of a star, but not the echelle-like nature of the frequencies, particularly in the asymptotic regime.

As has been demonstrated with even the most-basic first-order approximations of the rotational splitting of multiplets that can be expected for PMS δ-Scuti stars, rotation should destroy the echelle-like nature of the observed frequencies. Observed doublet or triplet frequencies, upon further investigation, appear to have differences between them that are too small to be of the same multiplet, and are most likely the chance overlap of frequencies from different multiplets, the result of large rotational splittings of individual multiplets that are so large that the various non-radial orders, normally well separated, begin to overlap. Identification of different members of the same multiplet is now extremely difficult, if not impossible, with the χ^2 techniques used in this thesis: the individual frequencies of a multiplet are not expected to be split symmetrically about the $m = 0$ member of the multiplet, and so simple χ^2 testing with the current models can no longer do the job. Furthermore, calculation of the pulsation spectrum of a star that properly accounts for rotation requires computationally expensive 2D models of a star, beyond the scope of this thesis.

However, in the absence of the χ^2 techniques, two powerful, basic tests have been used in this thesis to significantly limit the range of luminosities available to a δ-Scuti star. The fundamental frequency and the acoustic cut-off frequency are quantities that (under normal circumstances) are less sensitive to such things as rotation than the pulsation spectrum of the star as a whole is, and so in the case of PMS δ-Scutis, can be used as diagnostics where the χ^2 tests appear to be failing. Testing is required to see how sensitive these tools are to the input physics, but under the assumption that we are encountering p-modes in our observations that are not modified by such things as magnetic fields (in the case of the acoustic cut-off frequency for roAp stars), they can be used to help calibrate models, *i.e.* find the stellar-model parameters that allow those models to be better matched to observations. If model calibration fails on these points, we know there is a problem, and other solutions must be sought. Indeed, it is the failure of the χ^2 techniques for fitting and calibrating PMS stars which has led to the realization that more research is needed into the effects of rotation on PMS pulsation frequencies. The fundamental-frequency test compares

the lowest pulsation frequency observed in a star to the fundamental frequencies of all model stars within the grid of models. Even if this lowest frequency is not the fundamental frequency, it stills needs to be greater than the fundamental frequency of the star to be a p-mode frequency, generally imposing minimum luminosity constraints upon the star that are fairly robust against changes in input physics. Similarly, the acoustic-cut-off frequency (ACF) of a star imposes an upper limit to the pulsation frequencies of a star, and an upper limit on the star's luminosity; all observed pulsation frequencies under normal circumstances must be below the ACF, and so by comparing the highest observed frequency in a pulsation spectrum to model ACFs, maximum luminosity constraints are put on the star.

The above simple tests have led to upper limits on luminosity for 20 stars, and lower limits for 32 stars, with 7 stars in common to both lists such that both upper and lower luminosity limits are imposed upon the common stars. Ten stars (with varying degrees of disagreement) were pulsating at frequencies not consistent with the star's position in the HRD determined via spectroscopy, broad-band photometry and distance estimates, showing that further work is needed with these stars to bring these various measurements into agreement.

There are a number of stars in this study for which reasonable fits were obtained without too much difficulty, *e.g.* V1247 Ori (Section 3.1.1.2). Two possible reasons for which these fits to data worked, while others failed: 1) the models *do* reflect reality for that particular star, and good models have been found; 2) they are the result of "false positives", *i.e.* chance matching of model frequencies with observed frequencies. Given the modifications of a pulsation spectrum made by rotation, unless a star is rotating slowly, the former isn't likely. The "false positives" option is the more likely, but requires future testing to see if this could be the case, *e.g.* one could take a number of random frequencies, or selected modes from a rotating model, such as those of Deupree & Beslin (2010), but in the correct mass/T_{eff}/luminosity range for a PMS δ-Scuti star, and match them against our PMS model grids. If the rate of false positives (we *know* these models aren't correct for the comparisons that

are being performed, so they *would* be false positives) is similar to the rate of good fits among the sample in the study, then this would suggest the cause for our false positives.

One other potential problem is the misidentification of an observed frequency that *isn't* a p-mode *as* a p-mode. Although g-modes were not calculated for these models, in a number of cases (such as VV Ser), g-modes have potentially been observed. If these are interpreted as p-modes, this implies very high luminosities for a star that otherwise does not need to be that luminous if the frequency is a g-mode, and perhaps a mismatch between the asteroseismic HRD position and the HRD position determined via other means would not exist in that case. Misidentification of a signal caused by rotation or instrumentation as a p-mode is another possibility of which one must be always aware.

The collective properties of PMS δ-Scuti stars show some general trends for stars in which the star's position in the HRD determined through other means (broad-band photometry, spectroscopy, *etc.*) agree with the asteroseismic limits imposed upon the luminosity of the stars. Stars in the low luminosity and hot sector pulsate in high frequencies (> 600 μHz, spectral types approximately A0 to A3, between about 0 and 0.5 dex in $\log(L/\mathrm{L}_\odot)$ above the ZAMS). Stars in the lower-temperature ranges (later than A4), but also with low luminosities, tend to pulsate in mid-range frequencies (300 to 600 μHz). Star in the upper half of the $\log(L/\mathrm{L}_\odot)$ range between the ZAMS and the birthline pulsate in lower frequencies (< 200 μHz). There are no high-amplitude δ-Scuti stars in the sample, a phenomenon associated with slowly rotating stars ($v \sin i < 25$ km/s).

One star in particular, V1366 Ori, shows rather strange behaviour, with frequencies bunched in groups, and an abrupt cut-off in power above the highest frequency recorded. At the time of this writing this star has the highest-known δ-Scuti-type pulsation frequencies any type of δ-Scutis, PMS or not. The spacings between the groups of frequencies, and the abrupt cut-off simultaneously fit the large spacings

and the ACF of the models in a part of the HRD in agreement with the star's position determined via other means. It was this star's strange behaviour that prompted the use of the acoustic cut-off frequency as a diagnostic tool, and as far as can be determined, it is the first δ-Scutifor which pulsation at or near the ACF has been identified. The dense model grids used in this study, plus the *MOST* observations for this star were instrumental in these determinations.

Similarly, there are a couple of stars with a rather wide range of pulsation frequencies (V1026 Sco, IP Per in particular, with a range of several hundred microHertz), generally much larger than most stars of the class, that prompted the combined use of the fundamental and acoustic-cut-off frequency tests, once it was realized that the pulsation spectra as a whole must impose restrictions on the possible luminosities of the stars. It was a rather surprising result that so many stars had these restrictions place upon them, particularly on the upper end of the pulsation spectrum, not something that had been appreciated before this work had begun. Another prime implication of this work is that even if the exact radial and non-radial orders of pulsation cannot be identified, collectively PMS δ-Scuti stars can pulsate in any radial order from the fundamental mode up to the last highest orders below the ACF. In turn, this implies that to explain the pulsation spectrum of any individual star requires the calculation of pulsation frequencies throughout the indicated range, both radial and non-radial modes. Furthermore, if detection of only a frequency or two is made from a particular observation, to assume that is a low-order radial mode (as was often done in the past when non-radial orders were not necessarily even suspected) is most likely to be wrong without looking at the rest of the characteristics of the star in greater detail.

The overall message from this work is that it was only through looking at all of the stars collectively were these useful tests and conclusions able to be developed; different stars presented different parts of the puzzle, the big picture hard to see when only looked at one star at a time. Future work in the field needs to both build up the collection of high-quality space-based pulsation spectra so that a better sample size

is obtained, and also needs to probe the effects of rotation on the pulsation spectrum of a star, both theoretically and observationally. A potential way of investigating the latter is to study evolved slowly-rotating δ-Scutis. High-amplitude δ-Scuti stars are slow rotators, all of them evolved stars that seem to pulsate in one or two radial-order high-amplitude frequencies, but their pulsation spectra are probably not rich enough to provide the details needed to probe the interiors of the stars in greater detail. However, there are some intermediate stars between high- and low-amplitude δ-Scutis that exhibit the behaviour of both classes (44 Tau and 1 Mon for example) — one or two higher-amplitude pulsation frequencies with linear combinations of these frequencies appearing in the pulsation spectra, plus low-amplitude frequencies that appear to be independent of all other frequencies. These stars are also fairly slowly rotating. It is possible that these stars might be rotating slowly enough, with a rich enough pulsation spectrum to allow disentanglement between the effects of rotation and the other physics that might be needed to explain the pulsation spectrum of the stars. Once this is better understood, then perhaps applying that knowledge to PMS δ-Scuti stars might result in further illumination.

Bibliography

Aerts C., Christensen-Dalsgaard J., Kurtz D. W., 2010, Asteroseismology, Astrononmy and Astrophysics Library. Springer

Aerts C., Kolenberg K., 2005, A&A, 431, 615

Alecian E., Catala C., van't Veer-Menneret C., Goupil M.-J., Balona L., 2005, A&A, 442, 993

Alecian E., Lebreton Y., Goupil M.-J., Dupret M.-A., Catala C., 2007, A&A, 473, 181

Alexander D. R., Ferguson J. W., 1994, ApJ, 437, 879

Alfaro E. J., Delgado A. J., Garcia-Pelayo J. M., Garrido R., Saez M., 1985, A&AS, 59, 441

Amado P. J., Moya A., Suárez J. C., Martín-Ruiz S., Garrido R., Rodríguez E., Catala C., Goupil M. J., 2004, MNRAS, 352, L11

Amado P. J., Rodríguez E., Choo K., Kim S., Garrido R., Suárez J. C., Moya A., Martín-Ruíz S., 2006, Mem. Soc. Astron. Italiana, 77, 97

Andersen J., 1975, A&A, 44, 445

Arentoft T., Sterken C., Knudsen M. R., Freyhammer L. M., Duerbeck H. W., Pompei E., Delahodde C. E., Clasen J. W., 2001, A&A, 380, 599

Artemenko S. A., Grankin K. N., Petrov P. P., 2010, Astronomy Reports, 54, 163

Audard N., Kupka F., Morel P., Provost J., Weiss W. W., 1998, A&A, 335, 954

Bahcall J. N., Pinsonneault M. H., Basu S., 2001, ApJ, 555, 990

Balona L. A., Engelbrecht C. A., 1985, MNRAS, 212, 889

Balona L. A., Laney C. D., 1995, MNRAS, 276, 627

Balona L. A., Shobbrook R. R., 1983, MNRAS, 205, 309

Baxter E. J., Covey K. R., Muench A. A., Fűrész G., Rebull L., Szentgyorgyi A. H., 2009, AJ, 138, 963

Bernabei S. et al., 2007, Communications in Asteroseismology, 150, 57

Bernabei S., Ripepi V., Marconi M., Terranegra L., Ferrara P., Marinoni S., Schisano E., Palla F., 2004, in IAU Symposium, Vol. 224, The A-Star Puzzle, J. Zverko, J. Ziznovsky, S. J. Adelman, & W. W. Weiss, ed., pp. 812–817

Bernabei S. et al., 2009, A&A, 501, 279

Bernacca L. P., 1967, Mem. Soc. Astron. Italiana, 38, 169

Bessell M. S., Eggen O. J., 1972, ApJ, 177, 209

Bibo E. A., The P. S., 1991, A&AS, 89, 319

Boehm T., Catala C., 1995, A&A, 301, 155

Böhm T., Catala C., Balona L., Carter B., 2004, A&A, 427, 907

Böhm T., Zima W., Catala C., Alecian E., Pollard K., Wright D., 2009, A&A, 497, 183

Böhm-Vitense E., 1958, ZAp, 46, 108

Breger M., 1972, ApJ, 171, 539

—, 2007, Communications in Asteroseismology, 150, 25

Brown A., Djie H. R. E. T. A., Blondel P. F. C., Harper G. M., Bennett P. D., Skinner S. L., 1997, in Astronomical Society of the Pacific Conference Series, Vol. 121, IAU Colloq. 163: Accretion Phenomena and Related Outflows, D. T. Wickramasinghe, G. V. Bicknell, & L. Ferrario, ed., pp. 448–+

Calvet N., Cohen M., 1978, MNRAS, 182, 687

Cannon A. J., Pickering E. C., 1993, VizieR Online Data Catalog, 3135, 0

Casey M. P. et al., 2011, MNRAS, in preparation

Chen L., de Grijs R., Zhao J. L., 2007, AJ, 134, 1368

Chini R., Neckel T., 1981, A&A, 102, 171

Clausen J. V., Nordstrom B., 1980, A&A, 83, 339

Corporon P., Lagrange A.-M., 1999, A&AS, 136, 429

Cunha M. S., 2002, MNRAS, 333, 47

de Winter D., van den Ancker M. E., Maira A., Thé P. S., Djie H. R. E. T. A., Redondo I., Eiroa C., Molster F. J., 2001, A&A, 380, 609

de Zeeuw P. T., Hoogerwerf R., de Bruijne J. H. J., Brown A. G. A., Blaauw A., 1999, AJ, 117, 354

Delgado A. J., Miranda L. F., Alfaro E. J., 1999, AJ, 118, 1759

Demarque P., Guenther D. B., Li L. H., Mazumdar A., Straka C. W., 2008, Ap&SS, 316, 31

Deupree R. G., 2011. private communication

Deupree R. G., Beslin W., 2010, ApJ, 721, 1900

Dias W. S., Assafin M., Flório V., Alessi B. S., Líbero V., 2006, A&A, 446, 949

Donati J.-F., Semel M., Carter B. D., Rees D. E., Collier Cameron A., 1997, MNRAS, 291, 658

Dunkin S. K., Barlow M. J., Ryan S. G., 1997, MNRAS, 286, 604

Dupret M.-A., Böhm T., Goupil M.-J., Catala C., Grigahcene A., 2006, Communications in Asteroseismology, 147, 72

Eichhorn G., Accomazzi A., Grant C. S., Kurtz M. J., Murray S. S., 2002, Ap&SS, 282, 299

Eisner J. A., Hillenbrand L. A., White R. J., Akeson R. L., Sargent A. I., 2005, ApJ, 623, 952

Feigelson E. D., Lawson W. A., Garmire G. P., 2003, ApJ, 599, 1207

Fernandez M., Ortiz E., Eiroa C., Miranda L. F., 1995, A&AS, 114, 439

Finkenzeller U., Mundt R., 1984, A&AS, 55, 109

Fitzgerald M. P., Jackson P. D., Luiken M., Grayzeck E. J., Moffat A. F. J., 1978, MNRAS, 182, 607

Friedemann C., Hoffrichter J., Reimann H.-G., Gurtler J., 1993a, IBVS, 3866, 1

Friedemann C., Riemann H. G., Gurtler J., Toth V., 1993b, A&A, 277, 184

Fu J. N., Bouzid M. Y., Sterken C., 2005, Astronomische Nachrichten, 326, 349

Fu J. N., Sterken C., Duerbeck H. W., Mennickent R. E., 2003, A&A, 412, 97

Fujii T., Nakada Y., Parthasarathy M., 2002, A&A, 385, 884

Garrison R. F., Schild R. E., 1979, AJ, 84, 1020

Grady C. A. et al., 1996, A&AS, 120, 157

—, 2004, ApJ, 608, 809

Gray R. O., Corbally C. J., 1998, AJ, 116, 2530

Gregorio-Hetem J., Lepine J. R. D., Quast G. R., Torres C. A. O., de La Reza R., 1992, AJ, 103, 549

Grenier S., Burnage R., Faraggiana R., Gerbaldi M., Delmas F., Gómez A. E., Sabas V., Sharif L., 1999, A&AS, 135, 503

Grinin V. P., Kozlova O. V., Natta A., Ilyin I., Tuominen I., Rostopchina A. N., Shakhovskoy D. N., 2001, A&A, 379, 482

Guenther D. B., 1994, ApJ, 422, 400

Guenther D. B., Brown K. I. T., 2004, ApJ, 600, 419

Guenther D. B. et al., 2009, ApJ, 704, 1710

Guenther D. B., Kallinger T., Zwintz K., Weiss W. W., Tanner J., 2007, ApJ, 671, 581

Guetter H. H., 1992, AJ, 103, 197

Harris D. L., Morgan W. W., Roman N. G., 1954, ApJ, 119, 622

Hayashi C., 1961, PASJ, 13, 450

Henize K. G., 1976, ApJS, 30, 491

Herbig G. H., 1960a, ApJ, 131, 632

—, 1960b, ApJS, 4, 337

—, 1998, ApJ, 497, 736

Herbig G. H., Bell K. R., 1988, in Lick Observatory Bulletin, Vol. 1111, Third catalog of emission-line stars of the Orion population, Herbig, G. H. & Bell, K. R., ed., Santa Cruz, Lick Observatory, p. 90

Herbst W., Warner J. W., Miller D. P., Herzog A., 1982, AJ, 87, 98

Hernández J., Calvet N., Briceño C., Hartmann L., Berlind P., 2004, AJ, 127, 1682

Heske A., Wendker H. J., 1985, A&A, 151, 309

Hillenbrand L. A., Strom S. E., Vrba F. J., Keene J., 1992, ApJ, 397, 613

Hoag A. A., Johnson H. L., Iriarte B., Mitchell R. I., Hallam K. L., Sharpless S., 1961, Publications of the U.S. Naval Observatory Second Series, 17, 343

Hoeg E. et al., 1997, A&A, 323, L57

Hoffmeister C., 1934, Astronomische Nachrichten, 253, 195

Høg E. et al., 2000, A&A, 355, L27

Hosokawa T., Offner S. S. R., Krumholz M. R., 2011, ApJ, 738, 140

Houk N., Cowley A. P., 1975, University of Michigan Catalogue of two-dimensional spectral types for the HD stars. Volume I. Declinations -90_ to -53.0 degrees., Houk, N. & Cowley, A. P., ed.

Hu J. Y., The P. S., de Winter D., 1989, A&A, 208, 213

Iben I. J., 1965, ApJ, 141, 993

Iglesias C. A., Rogers F. J., 1996, ApJ, 464, 943

Jacchia L., 1941, Harvard College Observatory Bulletin, 915, 17

Jackson J., Stoy R. H., 1996, VizieR Online Data Catalog, 1116, 0

Jones D. H. P., 1969, Monthly Notes of the Astronomical Society of South Africa, 28, 5

Kallinger T., Matthews J. M., 2010, ApJ, 711, L35

Kallinger T., Zwintz K., Weiss W., 2008, A&A, 488, 279

Kaltcheva N., Kuchera A., Hathaway C., 2010, Astronomische Nachrichten, 331, 384

Kamp I., Paunzen E., 2002, MNRAS, 335, L45

Kaye A. B., 2007, Communications in Asteroseismology, 150, 91

Kazarovets E. V., Samus N. N., 1997, IBVS, 4471, 1

Kazarovets E. V., Samus N. N., Durlevich O. V., Kireeva N. N., Pastukhova E. N., 2011, IBVS, 5969, 1

Kharchenko N. V., 2001, Kinematika i Fizika Nebesnykh Tel, 17, 409

Kukarkin B. V., Kholopov P. N., Kukarkina N. P., Perova N. B., 1972, IBVS, 717, 1

Kurtz D. W., Marang F., 1995, MNRAS, 276, 191

Kurtz D. W., Müller M., 1999, MNRAS, 310, 1071

—, 2001, MNRAS, 325, 1341

Kuznetsov V. I., Boutenko G. Z., Lazorenko G. A., Lazorenko P. F., 2000, A&AS, 142, 389

Lampens P., Rufener F., 1990, A&AS, 83, 145

Lee H., Kim S.-L., Kim H.-J., Jeon Y.-B., Park H.-S., 2005, IBVS, 5656, 1

Lee H.-T., Chen W. P., 2007, ApJ, 657, 884

Lenz P., Breger M., 2005, Communications in Asteroseismology, 146, 53

Lovekin C. C., Deupree R. G., 2008, ApJ, 679, 1499

Maeder A., Meynet G., 1991, A&AS, 89, 451

Makarov V., Bastian U., Hoeg E., Grossmann V., Wicenec A., 1994, IBVS, 4118, 1

Malfait K., Bogaert E., Waelkens C., 1998, A&A, 331, 211

Malkov O. Y., Oblak E., Snegireva E. A., Torra J., 2006, A&A, 446, 785

Mamajek E. E., Lawson W. A., Feigelson E. D., 1999, ApJ, 516, L77

—, 2000, ApJ, 544, 356

Manoj P., Bhatt H. C., Maheswar G., Muneer S., 2006, ApJ, 653, 657

Marconi M., Palla F., 1998, ApJ, 507, L141

Marconi M., Ripepi V., Alcalá J. M., Covino E., Palla F., Terranegra L., 2000, A&A, 355, L35

Marconi M., Ripepi V., Bernabei S., Ruoppo A., Monteiro M. J. P. F. G., Marques J. P., Palla F., Leccia S., 2010, Ap&SS, 328, 109

Massey P., Johnson K. E., Degioia-Eastwood K., 1995, ApJ, 454, 151

Mayne N. J., Naylor T., Littlefair S. P., Saunders E. S., Jeffries R. D., 2007, MNRAS, 375, 1220

McCall M. L., Richer M. G., Visvanathan N., 1990, ApJ, 357, 502

McInally C. J., Austin R. D., 1977, IBVS, 1334, 1

Melnikov S., Woitas J., Eislöffel J., Bacciotti F., Locatelli U., Ray T. P., 2008, A&A, 483, 199

Mendoza V. E. E., Gomez T., 1980, MNRAS, 190, 623

Merín B. et al., 2004, A&A, 419, 301

Miroshnichenko A. S., Bjorkman K. S., Chentsov E. L., Klochkova V. G., Gray R. O., García-Lario P., Perea Calderón J. V., 2001, A&A, 377, 854

Monnier J. D. et al., 2005, ApJ, 624, 832

Mora A. et al., 2001, A&A, 378, 116

Morgenroth O., 1934, Astronomische Nachrichten, 252, 389

Murphy S. J., Lawson W. A., Bessell M. S., 2010, MNRAS, 406, L50

Neri L. J., Chavarria-K. C., de Lara E., 1993, A&AS, 102, 201

Ochsenbein F., Bauer P., Marcout J., 2000, A&AS, 143, 23

Ogura K., Ishida K., 1981, PASJ, 33, 149

Ostlie D. A., Carroll B. W., 1996, An Introduction to Modern Stellar Astrophysics, Ostlie, D. A. & Carroll, B. W., ed.

Palla F., Stahler S. W., 1990, ApJ, 360, L47

—, 1991, ApJ, 375, 288

—, 1992, ApJ, 392, 667

Parenago P. P., 1954, Trudy Gosudarstvennogo Astronomicheskogo Instituta, 25, 1

Paunzen E., 2008, Contributions of the Astronomical Observatory Skalnate Pleso, 38, 435

Perryman M. A. C., ESA, eds., 1997, ESA Special Publication, Vol. 1200, The HIPPARCPOS and TYCHO catalogues. Astrometric and photometric star catalogues derived from the ESA HIPPARCOS Space Astrometry Mission

Phelps R. L., Janes K. A., 1994, ApJS, 90, 31

Pigulski A., Kolaczkowski Z., Kopacki G., 2000, Acta Astron., 50, 113

Pinheiro F. J. G., Folha D. F. M., Marconi M., Ripepi V., Palla F., Monteiro M. J. P. F. G., Bernabei S., 2003, A&A, 399, 271

Popper D. M., 1966, AJ, 71, 175

Pribulla T., Rucinski S. M., Kuschnig R., Ogłoza W., Pilecki B., 2009, MNRAS, 392, 847

Rauw G., Manfroid J., De Becker M., 2010, A&A, 511, A25+

Reegen P., 2007, A&A, 467, 1353

Rhee J. H., Song I., Zuckerman B., 2007, ApJ, 671, 616

Ribas I., Jordi C., Torra J., Giménez Á., 2000, MNRAS, 313, 99

Ripepi V. et al., 2006, A&A, 449, 335

—, 2007, A&A, 462, 1023

—, 2003, A&A, 408, 1047

Ripepi V., Palla F., Marconi M., Bernabei S., Arellano Ferro A., Terranegra L., Alcalá J. M., 2002, A&A, 391, 587

Rogers F. J., 1986, ApJ, 310, 723

Rogers F. J., Swenson F. J., Iglesias C. A., 1996, ApJ, 456, 902

Rostopchina A. N., Grinin V. P., Shakhovskoi D. N., 2001, Astronomy Reports, 45, 51

Rowe J. F. et al., 2006a, Communications in Asteroseismology, 148, 34

—, 2006b, Mem. Soc. Astron. Italiana, 77, 282

Royer F., Gerbaldi M., Faraggiana R., Gómez A. E., 2002a, A&A, 381, 105

Royer F., Grenier S., Baylac M., Gómez A. E., Zorec J., 2002b, A&A, 393, 897

Sartori M. J., Gregorio-Hetem J., Rodrigues C. V., Hetem, Jr. A., Batalha C., 2010, AJ, 139, 27

Schild R. E., Cowley A. P., 1971, A&A, 14, 66

Schild R. E., Neugebauer G., Westphal J. A., 1971, AJ, 76, 237

Schmidt-Kaler T., 1982, in Landolt-Bornstein Numerical Data and Functional Relationships in Science and Technology: Group VI: Astronomy, Vol. 2b, Physical Parameters of the Stars, Springer-Verlag, Berlin

Scholz R.-D. et al., 1999, A&AS, 137, 305

Seggewiss W., 1968, ZAp, 68, 142

Sharpless S., 1952, ApJ, 116, 251

Skrutskie M. F. et al., 2006, AJ, 131, 1163

Stone R. C., 1988, AJ, 96, 1389

Stoy R. H., 1966, Annals of the Cape Observatory, 21, 0

Strohmeier W., 1964, IBVS, 55, 1

Strohmeier W., Knigge R., Ott H., 1964, IBVS, 74, 1

Suárez O., García-Lario P., Manchado A., Manteiga M., Ulla A., Pottasch S. R., 2006, A&A, 458, 173

Sung H., Bessell M. S., Lee S.-W., 1997, AJ, 114, 2644

—, 1998, AJ, 115, 734

Sung H., Chun M.-Y., Bessell M. S., 2000, AJ, 120, 333

Tassoul M., 1980, ApJS, 43, 469

Thé P. S., de Winter D., Perez M. R., 1994, A&AS, 104, 315

The P. S., Hageman T., Tjin A Djie H. R. E., Westerlund B. E., 1985, A&A, 151, 391

Thé P. S., Perez M. R., Voshchinnikov N. V., van den Ancker M. E., 1996, A&A, 314, 233

Turner D. G., 1979, JRASC, 73, 74

—, 1994, Revista Mexicana de Astronomia y Astrofisica, 29, 163

Černis K., Straižys V., 2003, Baltic Astronomy, 12, 301

van den Ancker M. E., Thé P. S., de Winter D., 1996, A&A, 309, 809

van den Ancker M. E., Thé P. S., de Winter D., 2000, A&A, 362, 580

van den Ancker M. E., The P. S., Feinstein A., Vazquez R. A., de Winter D., Perez M. R., 1997, A&AS, 123, 63

van Leeuwen F., 2007, A&A, 474, 653

Verschueren W., 1991, High precision radial velocity determination from CCD Echelle spectra of early type stars in the young cluster NGC 2244, Verschueren, W., ed.

Vieira S. L. A., Corradi W. J. B., Alencar S. H. P., Mendes L. T. S., Torres C. A. O., Quast G. R., Guimarães M. M., da Silva L., 2003, AJ, 126, 2971

Voroshilov V. I., Guseva N. G., Kalandadze N. B., Kolesnik L. N., Kuznetsov V. I., 1985, Catalog of BV magnitudes and spectral classes of 6000 stars, Voroshilov, V. I., Guseva, N. G., Kalandadze, N. B., Kolesnik, L. N., & Kuznetsov, V. I., ed.

Walker G. et al., 2003, PASP, 115, 1023

Walker M. F., 1956, ApJS, 2, 365

—, 1957, ApJ, 125, 636

Wenger M. et al., 2007, in Astronomical Society of the Pacific Conference Series, Vol. 377, Library and Information Services in Astronomy V, Ricketts S., Birdie C., Isaksson E., eds., pp. 197–+

Young A., 1978, PASP, 90, 144

Zwintz K., 2008, ApJ, 673, 1088

Zwintz K., Guenther D. B., Weiss W. W., 2007, ApJ, 655, 342

Zwintz K. et al., 2009a, A&A, 502, 239

—, 2009b, A&A, 494, 1031

—, 2011, ApJ, 729, 20

Zwintz K., Marconi M., Reegen P., Weiss W. W., 2005, MNRAS, 357, 345

Zwintz K., Weiss W. W., 2006, A&A, 457, 237